

Application of Centrifugal Microfluidics and Fluorescence-based Detection for Rapid Biological Analysis

Xin Zhang

B.Eng

A Dissertation submitted in fulfilment of the
requirements for the award of
Doctor of Philosophy (Ph.D.)
to the



Dublin City University
School of Biotechnology

Supervisors:

Professor Richard O' Kennedy

Dr. Caroline Shirley Murphy

August 2017

Declaration

I hereby certify that this material, which I now submit for assessment on the programme of study leading to the award of Doctor of Philosophy is entirely my own work, and that I have exercised reasonable care to ensure that the work is original, and does not to the best of my knowledge breach any law of copyright, and has not been taken from the work of others save and to the extent that such work has been cited and acknowledged within the text of my work.

Signed: Xin Zhang

ID No.: 10114149

Date: 04 Aug 2017

To my dear parents, my husband and my son

Acknowledgement

First of all, I would like to thanks my dear husband, Dr. Zhenhui Yuan. We know each other for nine years and we've learned how to bravely handle the difficulties and how to enjoy our current life. We are both getting stronger than ever. Life is tough sometimes, but it is also colorful. It is your deepest love and greatest encouragements that gave me the strength to successfully finish my PhD. Last, thanks to our cute little one, who helps me went through the most tough period.

I would like to greatly appreciate the significant support of my principal supervisor, Prof. Richard O'Kennedy. I am and will always be very proud of being your student. It would not have been possible to complete this doctoral thesis without your help, support and patience. Five year ago, I barely can't not speak in English. Today, I complete my Ph.D thesis with nine publications. Because you believe that I can do it better. I am so happy I did not disappoint myself and you.

I would like to acknowledge the great help from my co-supervisor, Dr. Caroline Shirley Murphy, who was also my friend. She gave me grateful help at both academic and personal levels. She invited me to her home, her hen's party, her wedding, her baby shower party. She gave me a chance to see Irish culture. This made me love Ireland!

An extra special acknowledgement goes to Dr. Gerard G. Donohoe, who also supervised me during my Ph.D. He showed me how to collaborate with different research groups and showed me how to do research. I till remember he said: sometimes people get confused and emotional, hard work will make you feel better.

My heart-full thanks are given to my lovely colleagues in Applied Biochemistry Group. It was and is a wonderful time working with you.

Also I want to thank to Dr. Dung Trinh-Xuan and Dr. Conor Brennan in the school of Electronic Engineering, Dublin City University, Ireland. You are a professional advisor and a caring and warm-hearted person.

Dublin May 2016

Xin Zhang

Journal papers

1. Kitsara, M., Nwankire, C. E., Walsh, L., Hughes, G., Somers, M., Kurzbuch, D., **Zhang, X.**, Donohoe, G. G., O’Kennedy, R., & Ducreé, J. (2014). Spin coating of hydrophilic polymeric films for enhanced centrifugal flow control by serial siphoning. *Microfluidic. Nanofluid.*, **16**(4), 691-699.

Spin-coating of hydrophilic polymeric films on PMMA was demonstrated. These polymers allowed the successfully implementation of a serial-siphoning- and capillary-valving-based centrifugal platform which could be used for the detection of hIgG, based on our previous study (Nwankire *et al.*, 2013). In this work, XZ prepared the functionalized SAF chip and developed the hIgG immunoassay on the microfluidic platform.

2. Nwankire, C. E., Donohoe, G. G., **Zhang, X.**, Siegrist, J., Somers, M., Kurzbuch, D., Monaghan, R., Kistara, M., Burger, R., Hearty, S., Murrell, J., Martin, C., Rook, M., Barrett, L., Daniels, S., McDonagh, C., O’Kennedy, R., & Murrell, J. (2013). At-line bioprocess monitoring by immunoassay with rotationally controlled serial siphoning and integrated supercritical angle fluorescence optics. *Anal. Chim. Act.*, **781**, 54-62.

In this work, XZ optimized a surfactant (Tween-20) for siphon valving. Titration studies of the immunoassay reagents and Tween-20 concentrations were carried out in order to determine the minimal Tween-20 concentration, which would facilitate sequential delivery of the assay reagents. The Tween-20 concentrations in each assay reagents were optimized by measurement of their contact angles on a plain PMMA substrate, and these were then tested in the serial siphon channels. XZ demonstrated hIgG immunoassays on a microtitre plate and a commercial detector. Subsequently, XZ quantified the integrated hIgG immunoassay using the developed centrifugal microfluidics and a SAF prototype detector. Additionally, she participated in the development of the microfluidic platform.

3. Gorkin, R., Nwankire, C., Gaughran, J., **Zhang, X.**, Donohoe, G. G., Rook, M., O’Kennedy, R., & Ducreé, J. (2012). Centrifugo-pneumatic valving utilizing dissolvable films. *Lab. chip.*, **12**(16), 2894-2902.

In this article, XZ carried out the biologic applications of dissolvable films. It was successfully demonstrated that these films could be used with biological

samples.

Conference paper and posters

1. **Zhang, X.**, Donohoe, G. G., Nwankire, C., Somers, M., Kurzbuch, D., Barrett, L., McDonagh, C., Ducrée, J, & O’Kennedy, R. (2013). Immunoassay on a novel centrifugal microfluidics-based platform. *M6*. Zweibrücken, Germany. July 15-16, 2013.

(This work also was published in Nwankire *et al.*, 2013)

2. **Zhang, X.**, Donohoe, G., Siegrist, J., Somers, M., Kurzbuch, D., Burger, R., Hearty, S., Murrell, J., Martin, C., Barrett, L., McDonagh, C., O’Kennedy, R. and Ducrée, J. (2012). Research on the development of a centrifugal-microfluidic cartridge with integrated detection optical elements for automated at-line bioprocess monitoring of immunoglobulin G. School of Biotechnology Research Day, DCU. Oct. 11, 2011.

(This work also was published in Nwankire *et al.*, 2013)

3. Kitsara, M., Nwankire, C., O’Reilly, A., Siegrist, J., Donohoe, G., **Zhang, X.**, O’Kennedy, R., & Ducree, J. (2012). Hydrophilic polymeric coatings for enhanced, serial-siphon based flow control on centrifugal lab-on-disc platforms. *μTAS*. Okinawa, Japan. Oct. 28 - Nov. 1, 2012.

(This work also was published in Kitsara *et al.*, 2014)

4. Siegrist, J., Donohoe, G.G., Somers, M., Kurzbuch, D., **Zhang, X.**, Burger, R., Hearty, S., Murrell, J., Martin, C., Barrett, L., McDonagh, C., O’Kennedy, R., & Ducrée, J. (2011). A centrifugo-microfluidic cartridge with integrated detection optics towards automated at-line bioprocess monitoring of immunoglobulin G. *μTAS*. 194-196. Seattle, USA. October 2-6, 2011.

In this work, XZ optimized the aminopropyltriethoxysilane (APTES) surface treatment protocol and immobilized Protein A on the SAF chip surface. Subsequently, she developed the IgG immunoassay on the optical chip using the developed cartridge and hardware.

5. Gorkin, R., Burger, R., Kurzbuch, D., Donohoe, G. G., **Zhang, X.**, Czugala, M., Lopez, F. B., O'Driscoll, S., Rook, M., McDonagh, C., Diamond, D., O'Kennedy, R., & Ducrée, J. (2011). Efficient Development Kit for Well-to-Chip Customization and Detection of Colorimetric and Fluorescence Based Microfluidic Immunoassays. *μTAS*. 924-926. Seattle, USA. October 2-6, 2011.

This research reported the development of translational slide-based microfluidic cartridges integrated with SAF/PEDD detection technologies that enable miniaturization/analysis of standard assays. To validate SAF/PEDD detection using the cartridges, XZ designed IgG immunoassay experiments and created standard curves for both fluorescent and colorimetric methods. Additionally, the standard curves generated on the cartridges were compared with the curve generated on the traditional systems (microtitre plate and Tecan analyzer).

Awards

2013- Travel funding from The Institute of Biology of Ireland (IOBI) in conjunction with the Biomedical Diagnostics Institute (BDI), Dublin City University.

2013- Best poster award at the M6 conference, Kaiser Lauternan University, Zweibrücken, Germany.

Abbreviations

2D	Two-dimensional
3D	Three-dimensional
α	Alpha
AP	Antarctic phosphatase
AP-1	Activator protein-1
APC	Antigen-presenting cell
APS	Ammonium persulfate
APTES	3-aminopropyltriethoxysilane
ASC	Apoptosis-associated speck-like protein
β	Beta
BCR	B-cell receptor
BLyS	B lymphocyte stimulator
bp	Base pair
BSA	Bovine serum albumin
BDI	Biomedical Diagnostics Institute
BTG	Bovine thyroglobulin
C	Constant
cAMP	Cyclic adenosine monophosphate
CARD	Caspase activation and recruitment domain
CD14	Cluster of Differentiation 14
cDNA	Complementary DNA
CDRs	Complementarity determining regions
CO ₂	Carbon dioxide
DCU	Dublin City University
δ	Delta
dH ₂ O	Distilled water
DNA	Deoxyribonucleic acid
dNTPs	Deoxynucleotide triphosphates
ϵ	Epsilon
<i>E. coli</i>	<i>Escherichia coli</i>
EDTA	Ethylenediaminetetra acetic acid
ELISA	Enzyme-linked immunosorbent assay
EP	Error prone
Fab	Fragment antigen-binding of antibody

GTX	Gonyatoxin
H	Heavy chain
HCl	Hydrochloric acid
HPLC	High-performance liquid chromatography
HRP	Horseradish peroxidase
Ig	Immunoglobulin
IgA	Immunoglobulin A
IgD	Immunoglobulin D
IgE	Immunoglobulin E
IgG	Immunoglobulin G
IgY	Immunoglobulin Y
IPTG	Isopropyl-beta-D-thiogalactopyranoside
K ⁺	Potassium ion
κ	Kappa
KLH	Keyhole limpet haemocyanin
L	Light chain
λ	Lamda
LOD	Limit of detection
mAb	Monoclonal antibody
MC	Microcystin
MG	Molecular grade
MgCl ₂	Magnesium chloride
mRNA	messenger RNA
MW	Molecular weight
N ₂	Nitrogen
NH ₂	Amino group
NK	Natural killer
oligo(dT)	Oligodeoxythymidylic acid
OVA	Ovalbumin
PAGE	Polyacrylamide gel electrophoresis
PBS	Phosphate buffered saline
PBST	Phosphate buffered saline with Tween 20
PCR	Polymerase chain reaction
PSP	Paralytic shellfish poisoning
PTX	Pectenotoxins

QUB	Queens University Belfast
RNA	Ribonucleic acid
RNase	Ribonuclease
RT	Reverse transcriptase
RTCA	‘Real-time’ cell analysis
SB	Super broth
scFv	Single chain antibody fragment
SDS	Sodium dodecyl sulfate
SOC	Super optimal catabolite
SOE	Splice overlap extension
STX	Saxitoxin
TAE	Tris-acetate-EDTA
TCR	T-cell receptors
TEMED	N,N,N',N'-Tetramethylethylenediamine
TLR	‘Toll-like’ receptor
TMB	3, 3', 5, 5' tetramethylbenzidine
Tris HCl	Tris(hydroxymethyl)aminomethane hydrochloride
V	Variable
VH	Variable heavy
VL	Variable light
WHO	World Health Organisation
γ	Gamma

Units

%	Percent
A	Absorbance
AU	Arbitrary units
cfu	Colony-forming unit
cm	Centimeter
CV	Coefficient of variation
Da	Dalton
EC50	Half-maximal effective concentration
g	Acceleration
hrs	Hours
IC50	Half-maximal inhibitory concentration
kb	Kilobase
kDa	Kilodalton
kg	Kilogram
L	Litre
M	Molar
mg	Milligram
min	Minute
mL	Millilitre
mM	Millimolar
mm	Millimetre
mmol	Millimoles
ng	Nanogram
nm	Nanometre
nM	Nanomolar
pg	Picogram
pH	Negative logarithm of the hydrogen ion concentration
pI	Isoelectric point
pM	Picomolar
U	Units
µg	Microgram
µL	Microlitre
µm	Micrometer
µM	Micromolar

Contents

Acknowledgements

Publications and Presentations

Table of contents

List of Figures

List of Tables

Chapter 1

Introduction	1
1.1 Introduction	1
1.2 The immune system	3
1.2.1 Innate immunity	3
1.2.2 Adaptive immunity	4
1.2.2.1 Cell-mediated immunity	6
1.2.2.2 Humoral immunity	6
1.3 Antibodies	7
1.4 The development of recombinant antibodies using phage display	11
1.5 The antigen-antibody interaction	13
1.5.1 Heidelberger-Kendall curve	13
1.5.2 The Hook effect in an immunoassay	15
1.6 Immunoassays	16
1.6.1 Historical perspective of immunoassays	16
1.6.2 Principles of immunoassays	18
1.6.3 Immunoassay Classifications	18
1.6.3.1 'Label-free' immunoassays	18
1.6.3.2 Labelled immunoassays	19
1.6.3.3 Radioimmunoassay (RIA)	19
1.6.3.4 Enzyme-based immunoassays (EIA/ELISA)	20
1.6.3.5 Fluorescent-based immunoassays (FIA)	20

1.6.3.6 Homogeneous immunoassays	22
1.6.3.7 Heterogeneous immunoassays	23
1.6.3.8 Competitive immunoassays	23
1.6.3.9 Non-competitive immunoassays	24
1.7 Signal amplification strategies for immunoassays	26
1.7.1 The Avidin-Biotin system	26
1.8 Microfluidics	30
1.8.1 Microfluidic platform	32
1.8.2 The development of microfluidic platforms	33
1.9 Application of microfluidic platforms in immunoassay	32
1.9.1 Microfluidic propulsion	35
1.9.2 Valving in centrifugal microfluidics	39
1.9.2.1 Capillary valve (hydrophilic valve)	39
1.9.2.2 Hydrophobic valve	39
1.9.2.3 Siphon valve	40
1.9.3 Substrate materials for microfluidic immunoassays	41
1.9.4 Surface modification	42
1.9.4.1 Plasma treatment	43
1.9.4.2 Chemical vapour deposition (CVD)	43
1.9.4.3 Combination of plasma treatment and silanization	43
1.9.4.4 Silanization	44
1.9.5 Detection methods in microfluidic immunoassays	44
1.10 Simulation of an immunoassay in a microchannel	45
1.11 Thesis aims	46

Chapter 2

Materials and Methods	47
2.1 Materials	48
2.1.1 Reagents	48
2.1.2 Equipment	50
2.1.3 Culture media formulations	52
2.1.4 Buffer preparation	53
2.1.4.1 General buffers	53
2.1.4.2 Buffers for Western blotting	53
2.1.4.3 Buffers for sodium dodecyl sulfate-polyacrylamide gel electrophoresis (SDS-PAGE)	54

2.1.5 Commercial antibodies and antigens.....	56
2.1.6 Commercial kits	56
2.1.7 Bacterial strains	57
2.1.8 Material for fabrication of microfluidic platforms	57
2.2 Methods	59
2.2.1 Production of scFv antibody library.....	59
2.2.1.1 Phenol-chloroform extraction of RNA	59
2.2.1.2 cDNA synthesis by reverse transcription PCR	60
2.2.1.3 PCR amplification of antibody light and heavy chain genes.....	62
2.2.1.4 Splice by overlap extension (SOE) PCR using VELOCITY™ DNA polymerase	65
2.2.1.5 Agarose gel electrophoresis	66
2.2.1.6 Purification of PCR products from agarose Gel using QIAquick™ gel extraction kit.....	66
2.2.1.7 Plasmid DNA purification	66
2.2.1.8 Restriction enzyme digestion of scFv insert and pComb3XSS vector	66
2.2.1.9 Ligation of SOE insert into pComb3XSS vector.....	67
2.2.1.10 Transformation of XL-1 Blue <i>E.coli</i> cells with pComb3XSS vector containing SOE insert	69
2.2.1.11 Enrichment of rabbit phage library via bio-panning against immobilized STX-OVA conjugations	69
2.2.1.12 Polyclonal phage ELISA analysis.....	71
2.2.1.13 Direct monoclonal ELISA of solubly-expressed scFv fragments.....	72
2.2.1.14 Re-infection into Top10F' cells and scFv check via colony-pick PCR.....	73
2.3 Methods for development of microfluidic platforms.....	73
2.3.1 Structures of microfluidic platforms	73
2.3.1.1 Flow-cell	73
2.3.1.2 'Supercritical angle fluorescence' (SAF) element compact-disc	75
2.3.1.3 Reagents delivery CD	77
2.3.2 Fabrication methods for microfluidic platforms	79
2.2.3 Surface modification methods.....	80
2.2.3.1 Amine surface functionalisation by liquid phase.....	80
2.2.3.2 Amine functionalisation by chemical vapour deposition.....	81
2.3.4 Hardware instrumentation	82
2.3.4.1 Supercritical angle fluorescence (SAF) prototype detector	82
2.4 Immunoassay experimental methods.....	84
2.4.1 Procedure for conventional hIgG FIA.....	84
2.4.2 Procedure for FIA on microfluidic flow-cell devices	85

2.4.3 Procedure for FIA analysis on microfluidic CDs.....	86
2.5 Immunoassay data analysis methods.....	87
2.5.1 Fitting of microfluidic FLISA curves and analysis of bioprocess samples using SigmaPlot®	87
2.5.2 Fluorescence image analysis using the Andor camera.....	89
2.6 Computational simulation	90
2.6.1 Theoretical methods	90
2.6.2 Numerical approach	93

Chapter 3

Generation of an Anti-Neosaxitoxin Rabbit scFv Library.....	94
3.1 Introduction	95
3.1.1 Paralytic shellfish poisoning toxin (PST).....	97
3.1.2 Methods for PSTs detection	99
3.1.2.1 Antibody-based methods for PST detection.....	100
3.1.2.2 Leporine host.....	102
3.2 Aim of this chapter	104
3.3 Results	104
3.3.1 Immunisation of rabbit with Neosaxitoxin-KLH	104
3.3.2 Construction and screening of the anti-Neosaxitoxin scFv rabbit library.....	104
3.3.3 Amplification of rabbit antibody heavy and light chains and PCR optimisation.....	104
3.3.4 Cloning the SOE product into the pComb3XSS vector through restriction digestion	113
3.3.5 scFv check via ‘colony-pick’ PCR	116
3.3.6 scFv check via soluble monoclonal ELISA	116
3.4 Discussion.....	118

Chapter 4

Development of Microfluidic System For Rapid HIgG Detection ...	121
4.1 Introduction	122
4.1.1 Manufacturing process of monoclonal antibody	122
4.1.2 Microfluidics	125
4.2 Aims of this chapter	128

4.3 Results.....	128
4.3.1 Components of human IgG (hIgG) immunoassay	129
4.3.2 Optimisation of development of hIgG FLISA on an ELISA plate	129
4.3.2.1 Optimisation of the protein A coating concentration and biotinylated anti-hIgG concentration	130
4.3.2.2 Determination of influence of addition of reagents	133
4.3.2.3 Optimising the ratio between biotinylated-antiIgG and NeutrAvidin Dylight.....	136
4.3.1 Development and optimisation of a hIgG FLISA on a ‘proof-of-concept’ microfluidic platform with flow-cells	138
4.3.3.1 Design of ‘proof-of-concept’ microfluidic platform with flow-cells	138
4.3.3.2 Surface functionalisation.....	140
4.3.3.3 Determination of the influence of removal of the washing step during flow-cell-based hIgG immunoassay	142
4.3.3.4 Comparision of flow-cell based hIgG FLISA with two different APTES solvents	144
4.3.3.5 Stability study of surface chemistry on flow-cells.....	148
4.3.3.6 Generation of a calibration curve for FLISA in flow-cells and quantification of bioprocess sample IgG concentrations	150
4.3.4 Development and optimisation of the first design of microfluidic compact ‘disc-like’ platform (CD) — ‘SAF-element’ CD	152
4.3.4.2 Custom-engineered system for performing microfluidic immunoassays	153
4.3.4.3 Optimisation of microchannel diameters on ‘SAF-element’ CDs	158
4.3.4.4 Generation of hIgG calibration curve using optimal conditions on ‘SAF-element’ CDs	159
4.3.4.5 Stability study of surface chemistry on ‘SAF-element’ CDs	160
4.3.5 Development and optimisation of the second design of microfluidic compact ‘disc-like’ platform (CD) — ‘reagent delivery’ CD	162
4.3.5.1 The design of the microfluidic CD-like platform: ‘reagent delivery’ CD ..	162
4.3.5.2 SAF detector for SAF ring lens	163
4.3.5.3 Optimisation of Tween-20® concentration for siphon valving	165
4.3.5.4 Characterisation of serial siphon valving	167
4.3.5.5 Generation of calibration curve on ‘reagent delivery’ CDs and quantification of bioprocess sample IgG levels	169
4.4 Discussion	171

Chapter 5

Numerical simulation of microfluidic immunoassay	175
5.1 Introduction	176
5.1.1 Numerical simulation of microfluidic immunoassay	176
5.1.2 Simulation conditions	177
5.2 Aims of this chapter	178
5.3 Results	179
5.3.1 Influence of the flow velocity	180
5.3.2 Influence of channel height on assay performance	184
5.3.3 Influence of the sensor area	187
5.3.4 Simulation of the indirect hIgG assay in microchannel	190
5.3 Results	194

Chapter 6

Overall Conclusions	197
----------------------------------	-----

Chapter 7

Appendix

7.1 Introduction	203
------------------------	-----

Chapter 8

Bibliography	208
---------------------------	-----

List of Figures

Figure 1.2.2 An overview of adoptive immunity.	5
Figure 1.3 The basic structure of an antibody (IgG) molecule, Fab and scFv antibody fragments.	10
Figure 1.4 Selection of antibodies from antibody libraries (panning) by phage display.	12
Figure 1.5.1 Representation of the relationship between the amounts of immuno-complex formed when a variable amount of antigen reacts with a constant amount of antibody.	14
Figure 1.6.3.2 The sub-classification of labelled immunoassays.	19
Figure 1.6.3.5 Illustration of the principle of fluorescence measurement	21
Figure 1.6.3.9 Illustration of competitive immunoassay and non-competitive immunoassay formats.	25
Figure 1.7.1 Application of the biotin-avidin complex in sandwich and competitive immunoassays.	29
Figure 1.8 Illustration of laminar flow in a microchannel.	31
Figure 1.9.1 Illustration of three fluid propulsion methods	38
Figure 1.9.2 Illustration of three forms of passive valving in a centrifugal microfluidic platform	40
Figure 2.3.1.1 Schematic of the flow-cell structure.	73
Figure 2.3.1.2 Schematics of 'SAF' (supercritical angel fluorescence) elements of the CD structure at three angles of view.	75
Figure 2.3.1.3 A schematic of reagent delivery CD structure.	77
Figure 2.3.3.1 A schematic of Zeonor slide functionalisation with plasma treatment and liquid-phase APTES deposition.	80
Figure 2.3.4.1 Schematic representation of the SAF-reader.	83
Figure 2.4.2 Illustration of holder for flow-cell immobilisation.	86
Figure 2.5.1 Illustration of the micro panel tabs in the SigmaPlot software.	88
Figure 2.6.1 Schematic diagram of 2D model of the microchannel.	90

Figure 3.1 Outbreaks of PSP toxins in the coastal water in Europe during the years from 1993 to 2002.....	96
Figure 3.3.3.1 PCR optimisation of rabbit variable heavy chain (~400 bp) genes using different primer combinations and increased MgCl ₂ concentrations.....	105
Figure 3.3.3.2 Amplification of rabbit heavy chain genes (~400bp amplicon) using the cDNA from a Neosaxitoxin-immunised rabbit.....	106
Figure 3.3.3.3 PCR amplifications for the variable light (kappa) genes (~400 bp).....	107
Figure 3.3.3.4 PCR optimisation of V _K 7 and V _K 8 variable light regions using Phusion [®] Taq High-Fidelity DNA polymerase with HF and GC buffers.....	108
Figure 3.3.3.5 Large-scale PCR amplification of V _K 7 and V _K 8 variable light regions using <i>Phusion[®] Taq High-Fidelity DNA polymerase</i> with HF buffer.....	109
Figure 3.3.3.6 MgCl ₂ optimisation of rabbit variable light chain lambda (V _λ) (~400 bp) amplification.....	110
Figure 3.3.3.7 Optimised PCR amplification of rabbit variable light chain lambda antibody gene sequences.....	111
Figure 3.3.3.8 Splice by extension overlap PCR (SOE-PCR) of variable heavy and variable light chain fragment to form a complete scFv fragment.....	112
Figure 3.3.4a The pComb3XSS vector map and relevant digestion sites.....	113
Figure 3.3.4b Digestion of the SOE product and the pComb3XSS vector.....	114
Figure 3.3.5 Colony-pick PCR.....	116
Figure 3.3.6 Soluble monoclonal ELISA of phage clones from panning round 4...	117
Figure 4.1 Schematic of the mAb manufacturing process.....	124
Figure 4.1.2 A schematic of the simultaneous function of single and double serial siphon valve channels between chambers.....	127
Figure 4.3.1 Schematic of indirect hIgG immunoassay.....	129
Figure 4.3.2.1a Optimisation of Protein A coating concentration using conventional FLISA	131
Figure 4.3.2.1b Optimisation of conventional FLISA anti-human IgG antibody concentration.....	132
Figure 4.3.2.2 Effect of mixing reagents (biotinylated anti-hIgG and NeutrAvidin	

DyLight-650) on hIgG indirect assay performance	134
Figure 4.3.2.3 Optimisation of ratios in mixing biotinylated-anti-hIgG and NeutrAvidin DyLight	137
Figure 4.3.3.1 Illustration of flow-cell design.....	139
Figure 4.3.3.3 Checkerboard FLISA on flow-cells for determination of the influence of removal of the wash step after BSA blocking.....	143
Figure 4.3.3.4a Comparison of morphology of assay spots between flow-cells prepared using isopropyl alcohol and ethanol prepare.....	146
Figure 4.3.3.4b Checkerboard FLISA for comparison of flow-cells prepared with ethanol and isopropyl alcohol	147
Figure 4.3.3.5 Checkerboard FLISA on flow-cells for stability testing.....	149
Figure 4.3.3.6 Illustration of bioprocess sample quantification based on two formats	151
Figure 4.3.4.1a A schematic cross-section of a ring lens structure.....	153
Figure 4.3.4.1b A schematic of the SAF layer with 20-SAF elements	154
Figure 4.3.4.1c A schematic of the microfluidic unit on the 'SAF-element' CD.....	156
Figure 4.3.4.2 The testing setup for hIgG microfluidic immunoassay on CDs	157
Figure 4.3.4.4 A schematic of calibration curve of hIgG FLISA based on the 'SAF-element' CD	159
Figure 4.3.4.5 Stability of PECVD-APTES surface during prolonged storage.....	161
Figure 4.3.5.1 A schematic of microfluidic unit on 'reagents delivery' CD	162
Figure 4.3.5.2 A schematic of the SAF detector for the SAF chip.....	164
Figure 4.3.5.3 Optimisation of the microfluidic assay conditions by varying Tween-20® (TW-20) concentration in the FLISA reagents	166
Figure 4.3.5.4 Frame sequence of the serial siphons interspersed by 'in-line, capillary valves showing the sequential delivery of four reagents over the sensor spot.....	168
Figure 4.3.5.5 hIgG FLISA calibration curves	170
Figure 5.1.2 Schematic of the hIgG immunoassay	178
Figure 5.3.1 Influence of flow velocity on microfluidic assay performance	183

Figure 5.3.2 Influence of channel height on assay performance.....	186
Figure 5.3.3 Influence of sensor area on assay performance	189
Figure 5.3.4 Influence of reagents' concentration on the assay performance	192

List of Tables

Table 1.2.2 Features of innate and adoptive immunity.	5
Table 1.3 Characteristics and functions of mammalian antibodies.	9
Table 1.5.1 The properties of the Heidelberger-Kendall curve.	15
Table 1.6.1 Immunoassay applications.	17
Table 1.6.3.4 Enzymes and their substrates commonly used in immunoassays.	20
Table 1.6.3.6 Properties of homogeneous and heterogeneous immunoassays.	23
Table 1.7 Comparison of competitive and non-competitive immunoassays.	25
Table 1.7.1 Characteristics of different biotin-binding proteins.	27
Table.1.9.1 Comparison of microfluidic propulsion techniques.	37
Table 1.9.3 Comparing characteristics of various type of material for fabrication of microfluidic platforms	41
Table 2.1.1.2a Reverse transcription of PCR.	60
Table 2.2.1.2b PCR program to synthesize cDNA using thermal cycling.	60
Table 2.2.1.3a Primer combinations for amplification of antibody variable genes. ..	61
Table 2.2.1.3b Standard multiplex mixture for PCR reactions.	62
Table 2.2.1.3c PCR program for GoTaq polymerase.	62
Table 2.2.1.3d The standard multiplex mixture for the PCR reactions using Phusion DNA polymerase.	62
Table 2.2.1.3e The PCR program for using Phusion DNA polymerase.	63
Table 2.2.1.4a Reaction mix for SOE-PCR.	64
Table 2.2.1.4b The PCR program for SOE-PCR.	64
Table 2.2.1.8 The components for restriction enzyme digestion of the SOE products and pComb3XSS.	66
Table 2.2.1.9 Ligation mixtures for cloning rabbit scFv SOE-product into pComb3XSS vector.	67
Table 2.2.1.11 Details of panning strategy used.	70

Table 3.1.1a Structures of PSP toxin components.....	96
Table 3.1.1b Specific toxicity of each component.	97
Table 3.1.2.1 Outline of developed antibodies for PSTs detection.	100
Table 3.3.4a Bio-Panning strategy for the Neo-saxitoxin rabbit scFv library.....	115
Table 3.3.4b Bio-panning inputs and outputs of the rabbit anti-Neosaxitoxin phage library.....	115
Table 4.3.3.2 Optimization of surface modification conditions with different materials.	141
Table 4.3.3.3 Outline of hIgG FLISA procedures on flow-cell.....	143
Table 4.3.4.3 Optimisation of SAF element CD design using various reagents.....	158

Abstract

Application of Centrifugal Microfluidics and Fluorescence-based Detection for Rapid Biological Analysis

Xin Zhang

The goal of this research was to develop and optimise microfluidic systems and assays for rapid detection of selected targets such as marine toxins and human IgG. The measurement of IgG, as the major format of therapeutic antibodies, was used as a prototype to develop a centrifugal-based microfluidic system for effectively monitoring biopharmaceutical production. To achieve this, a sandwich immunoassay for human IgG detection was developed and used to study the implementation of a new microfluidic CD-based cartridge. The centrifugal-based microfluidic CD adopted a serial siphon technique for implementation of automated sequential delivery of the assay reagents. Surface-confined supercritical angel fluorescence (SAF)-based detection was designed to sensitively measure the fluorescence signal from the microfluidic CD-based immunoassay. The CD substrate was functionalized with aminopropyltriethoxysilane (APTES) using plasma enhanced chemical vapour deposition (PECVD) for the immobilization of analyte capture protein. The developed prototype microfluidic system could automatically run a microfluidic assay in less than 30 min, and accurately measure industrial bioprocess samples that contained 10 mg mL^{-1} of human IgG. Additionally, computational simulations were performed to fundamentally understand the kinetics of immunoassays in a microfluidic system. The effects of varying assay parameters on the capture of analytes in microfluidic-based heterogeneous immunoassays under real-world operating conditions, was examined by using theoretical modeling and experimental binding assay results. A marine toxin, saxitoxins (STX), was another potential target for analysis using the developed centrifugal-based microfluidic CD. Work was carried out to generate recombinant antibodies (scFv) to saxitoxin and its derivatives. After successful immunization of the host animal with different STX-conjugates, an scFv antibody phage library against anti-STX was constructed by PCR amplification of scFv genes, cloning the genes library into phagemid vector and transforming into *E. coli* cells. The phages expressing high affinity antibody gene were isolated by “bio-panning”.

CHAPTER 1

Introduction

1.1 Introduction

This thesis mainly focuses on the development of a microfluidic ‘lab-on-chip’ system, which is able to be used for the analysis of hIgG or marine toxins. In addition, studies on the development of a recombinant antibody for marine toxin detection were carried out.

This chapter will initially introduce the immune system, which includes innate and adaptive immunity. Innate immunity describes a general non-specific first line of defence of the body to an infection or a foreign substance, while adaptive immunity is a highly directed response which involves specific cells (cellular response) and antibody generation (humoral response). These concepts will be discussed to provide a basis for the understanding and need for the generation of recombinant antibodies. A successful and specific immune response to a small-molecular weight marine shellfish toxin is necessary for the generation of a recombinant antibody with high affinity. Phage display, one of the most important tools used in the isolation and engineering of recombinant antibodies, will also be outlined.

Immunoassay and its applications will then be introduced. Immunoassay is one of the most widely used analytical tools in medicine and fundamental life-science research. Immunoassays can be classified into several formats, which meet various requirements. However, the core of immunoassay systems is the interaction between the antibody and the antigen, which significantly impacts the sensitivity and specificity of immunoassays. In order to enhance the performance of immunoassays, amplification strategies, such as the use of the avidin-biotin system, are also widely applied. These concepts and applications are introduced to provide a background for the design and development of the specific immunoassay used in the research described in this thesis.

Additionally, advanced microfluidic immunoassay systems and the associated applications are introduced. Microfluidics is an emerging technology that presents significant benefits for miniaturizing immunoassays due to its capacity for parallel analysis of multiple analytes with significantly reduced assay time and sample consumption. The major components required for development of a microfluidic system are propulsion, fluid valving, substrate materials, surface modification strategies, and the requisite detection method. The details of these factors will be discussed to provide

an overview for the development of a novel microfluidic assay system. The concept of computational simulation will be introduced to model key parameters (e.g. reagent flow speed, kinetics etc.) that impact on our understanding of immunoassay in low volume environments. This approach will be applied to define the importance of analyte molecule transport factors including convection and diffusion, binding kinetics, flow velocity and channel height in microfluidic systems. Furthermore, this model will be applied to provide a strategy to optimize microfluidic assays for maximal sensitivity, minimal sample volume requirements and fast performance.

1.2 The immune system

The immune system protects the body against the invasion of foreign bodies and pathogens and maintains an individual's well-being. It consists of two major parts, the innate immune system and the acquired immune system, which interact at several levels to develop a complete defence against invading pathogens (Agarwal, 2010).

1.2.1 Innate immunity

Innate immunity describes the initial defences required to prevent infectious agents from entering the body. As shown in Table 1.2.2, innate immunity is a non-specific but immediate response to foreign bodies, the efficiency of which is not enhanced through repeated exposure to the same foreign object. In addition, innate immunity lacks immunological memory and the response time is short (Agarwal, 2010). The functional components of innate immunity can be divided into anatomical, physiological, and chemical barriers (Turvey & Broide, 2010). Among these barriers the anatomical and physiological barriers are the primary defences against pathogens. These defences include: intact skin, mucosal clearance mechanisms, low stomach pH, and bacteriolytic lysozyme secretions (Turvey & Broide, 2010). If a pathogen penetrates the epithelial surface it can be destroyed by the neutrophils, macrophages and NK cells, and defence elements such as the complement system and interferons (Gomez *et al.*, 2005). Moreover, innate immunity plays a critical role in activating the subsequent adaptive immune response (Akira *et al.*, 2001; Shanker, 2010).

1.2.2 Adaptive immunity

The adaptive immunity consists of cell-mediated immunity and humoral immunity. It defends against the pathogens, which have evolved to resist innate immunity. Additionally, it is involved in the generation of immunological memory. The adaptive immune system is highly specific against a wide range of pathogens due to the participation of extremely diverse types of lymphocytes and other white blood cells. Moreover the extent of the immune response is enhanced through repeated pathogen exposure over days/weeks or even years (Yuan *et al.*, 2012). An overview of the adaptive immunity is illustrated in Fig. 1.2.2. The two types of adaptive immunity, humoral immunity and cell-mediated immunity, involve different cells and molecules. Humoral immunity is mediated by antibodies, which are produced by B lymphocytes. Antibodies neutralize and eliminate microbes and microbial toxins that are present generally outside of host cells. Cell-mediated immunity can defend against intracellular microbes. For example, T lymphocytes destroy microbes by activating phagocytes or directly killing infected cells (Abbas *et al.*, 2012).

Table 1.2.2 Features of innate and adoptive immunity (adapted from Agarwal, 2010).

	Innate	Adaptive
Level of defence	First line	Second line
Antigen specificity	Not specific to antigen	Highly specific
Time to respond	Minutes to hours	Days to weeks
Response on repeated exposure to the antigen	Extent of response remains the same on repeated exposure to the antigen	Improves with repeated exposures
Memory	No memory	Memory
Types of immune Cells	Granulocytes, macrophages, natural killer cells, natural killer T cells	T lymphocytes, B lymphocytes

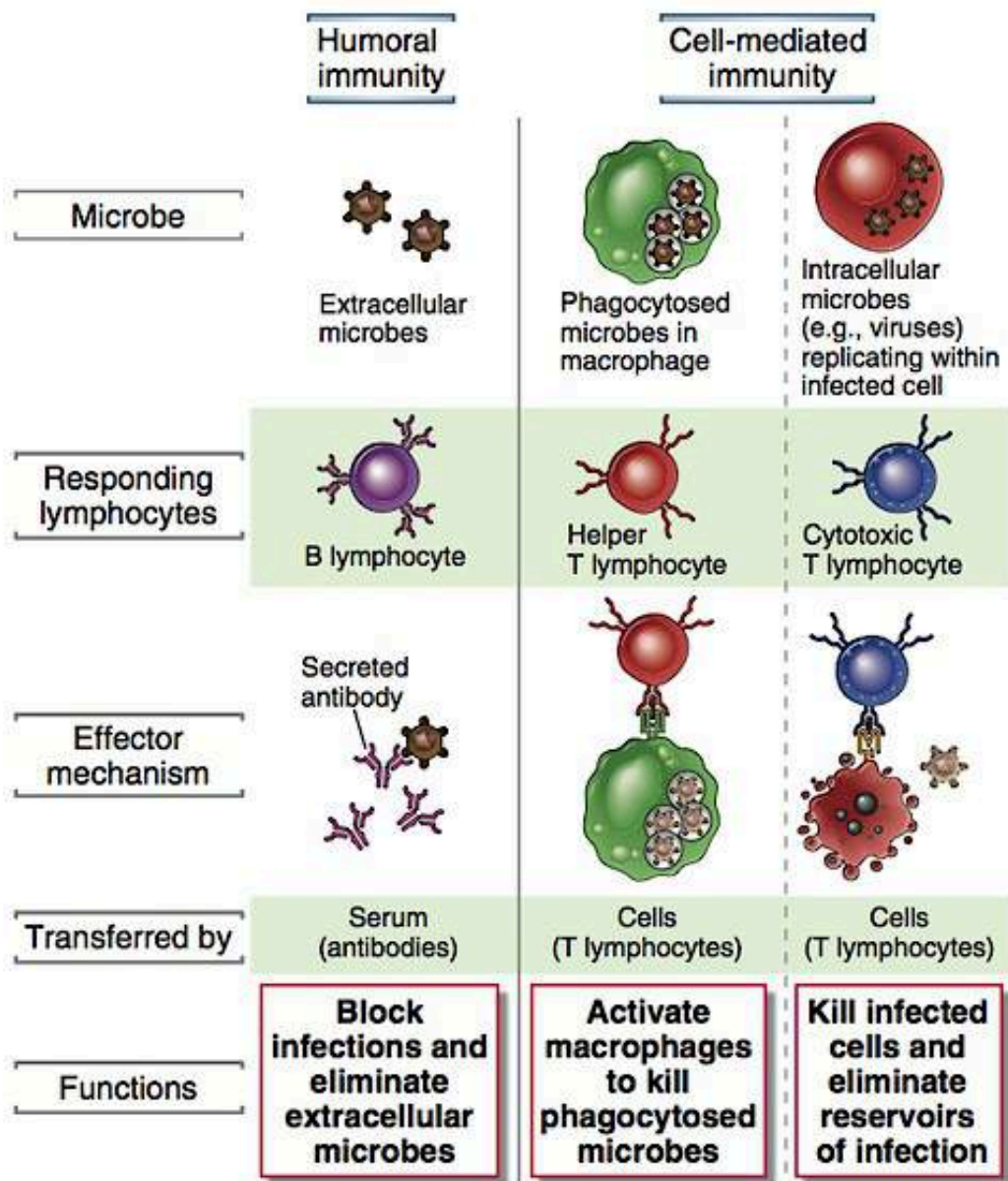


Figure 1.2.2 An overview of adaptive immunity. In humoral immunity, activated B-cells secrete antibodies that eliminate extracellular microbes. In cell-mediated immunity, activated T-cells either activate macrophages to destroy phagocytosed microbes or kill infected cells (adapted from Abbas *et al.*, 2012).

1.2.2.1 Cell-mediated immunity

Cell-mediated immunity has evolved to deal with infections that cannot be reached through humoral antibodies, like intracellular pathogens, such as viruses. T-lymphocytes (T-cells) are the key components of cell-mediated immunity. They originate in the thymus circulate permanently between the blood and lymphatic system (Pancer & Cooper, 2006). The activation of naive T-cells mainly depends on interactions of T-cell receptor (TCR) with major histocompatibility complex (MHC)-associated peptide antigens displayed on antigen-presenting cells (APCs). However, the initiation of T-cell responses for antigens requires participation of some accessory molecules on the T-cells, including CD3, CD4, CD8, CD28, CTLA-4, LFA-1, VLA-4 and ζ . The APCs can be phagocytes containing surviving microbe or microbe-infected non-phagocytic cells (e.g. epithelial cells). The MHC molecules that display peptides to T-cells include class I MHC expressed by all nucleated cells in the body and class II MHC produced mainly by specialised APCs, including dendritic cells, macrophages and B lymphocytes (Reinhardt and Jenkins, 2003; Abbas *et al.*, 2012).

The TCR and CD4 or CD8 co-receptor together recognize the MHC molecules on APCs, providing the initiating signal for T-cell activation. The naïve cytotoxic T-cells (T_C) recognise an antigen in association with a class I MHC. If an infected cell is recognised by a T_C cell, it induces the infected cell to become apoptotic and commit suicide, thus killing that cell along with any intracellular pathogens. In addition, the T_C cells can release interferon- γ to reduce the spread of pathogens in adjacent cells. The naïve helper T-cells (T_H) activated by class II MHCs, differentiate into subsets of effector cells (T_{H1} , T_{H2} and T_{H17} cells) which produced distinct cytokines. The cytokines perform different functions during adaptive immunity. They can activate macrophages and kill phagocytosed microbes. Additionally, they can activate B-cells to produce antibodies in humoral immune responses (Alberts, 2012).

1.2.2.2 Humoral immunity

Humoral immunity relates mainly to the generation of antibodies by B cells. The humoral immunity defends the microbes presenting in the extracellular spaces. As APCs, B-cells can express MHC II proteins on their surface, which are recognised by

T_H2 cells (Zhu *et al.*, 2012). T_H2 cells release interleukin-4, 5, 10 and 13, which results in the activation, proliferation and differentiation of B-cells. The B-cell displays a membrane bound immunoglobulin on its surface that acts as an antigen receptor. Subsequently, antibody-secreting plasma cells, derived from B cells, are produced. These antibodies serve to neutralise the pathogen and promote its elimination before it can establish a significant infection.

Generally, the B-cell mediated immune response involves the activation of multiple B-cells recognizing an antigen with single or multiple identical antigenic determinants (epitopes). Hence, a large number of antibodies are produced with distinct specificity and affinity. Polyclonal immunoglobulins are a heterogeneous mixture of antibodies, which has many different antigen specificities and epitope affinities (Ofek *et al.*, 2010). They are harvested from the serum of immunised animals. Polyclonal antibodies are widely used in antibody-based methods. In contrast, monoclonal antibodies are derived from a single B cell clone and bind to a single epitope. In general monoclonal antibodies have high specificity and low cross-reactivity. The structure and classification of antibodies are discussed in the following section.

1.3 Antibodies

Antibodies, also known as immunoglobulins (Ig), are soluble glycoproteins secreted by B-lymphocytes in response to foreign antigens. Immunoglobulins are the first molecules involved in specific immune recognition and are widely used in clinical and medical applications. They bind specifically to their respective antigen with a high degree of affinity (Murphy, 2011). According to their physical characteristics and biological properties, mammalian immunoglobulins are often grouped into 5 distinct classes: IgA, IgD, IgE, IgG and IgM (Table 1.3). IgG is the smallest antibody and is widely used in assay development and antibody-based therapeutics. In addition, IgG is the major antibody component (80%) of blood; IgG can bind to viruses, bacterial and fungi, and protects the body by activating the complement system to neutralise pathogens (Lee & Andrew, 2009). In contrast, IgM is produced in the early stages of infection (Li, Woo *et al.*, 2004; Muto *et al.*, 2004). Whereas, IgE is present in small amounts in the serum and is responsible for Type I hypersensitivity reactions (e.g. allergy, asthma and anaphylaxis), IgE levels are also greatly increased in response to helminth parasite

infections (Abbas *et al.*, 2012).

IgA is most abundant and most active in secretions at mucosal surfaces where it provides the primary defence. IgA is also abundant in saliva, tears and breast milk, especially colostrum. IgD is found on the surface of B-lymphocytes. However, its exact function still unclear, although it appears that it acts as an antigen receptor and that it is needed for B cell activation (Lee & Andrew, 2009).

Table 1.3 Characteristics and functions of mammalian antibodies.

Characteristics	IgA	IgD	IgE	IgG	IgM
Heavy Chain	α	δ	ϵ	γ	μ
Light Chain	κ or λ	κ or λ	κ or λ	κ or λ	κ or λ
Molecule Weight (KDa)	150-500	180	190	150	950
Molecular formula	$(\alpha 2\kappa 2)_{1-2}$ or $(\alpha 2\lambda 2)_{1-2}$	$\delta 2\kappa 2$ or $\delta 2\lambda 2$	$\epsilon 2\kappa 2$ or $\epsilon 2\lambda 2$	$\gamma 2\kappa 2$ or $\gamma 2\lambda 2$	$(\mu 2\kappa 2)_5$ or $(\mu 2\lambda 2)_5$
<i>In vivo</i> serum half-life (d)	6	3	2.5	16-36	5
Concentration in serum	1-4 mg/ml	10-400 ng/ml	0-0.4 mg/ml	8-16 mg/ml	0.5-2 mg/ml
Functions	Protect the respiratory and gastrointestinal tracts from infection	Binds to the surface of B-lymphocytes	Triggers the allergic response	Neutralise, opsonise and indirectly lyses the pathogen	Neutralise, opsonise and indirectly lyses the pathogen

(Adapted from Abbas *et al.*, 2012).

Although the structure of each specific immunoglobulin is unique, antibodies are built using the same basic structural plan. Typically an antibody molecule consists of two identical heavy chains (50-70 kD) and two identical light chains (23 kD) (David, 2001). Both heavy and light chains contain constant (C) and variable (V) domains based on differences in amino acid sequence. Unlike the C domains, the V domains show great variability in amino acid sequence composition. The two heavy chains are linked to each other by disulphide bonds and each heavy chain is linked to a light chain by a

disulphide bond. Furthermore, the four chains are assembled into a Y-shape molecule (Fig. 1.3). Each variable region contains three hypervariable regions (HR) or complementarity determining regions (CDRs), which are surrounded by a framework region (FR). The CDR regions are located in loops between the anti-parallel β -sheets (Elgert, 2009). The CDR loops of the light and heavy chains form the antigen-binding surface. An additional domain that lies between the constant heavy chain C_{H1} and C_{H2} domains is the hinge region. This area allows flexibility and some degree of freedom for the movement of the two arms of the antibody molecule. Functionally, an antibody can be divided into a Fab region (fragment antigen binding), and a Fc region (fragment crystallisable). In addition, it is possible to create a scFv (single chain fragment variable) by genetic engineering. The Fab region is composed of two constant and variable domains of both light and heavy chains. In contrast, the Fc region contains heavy chain constant domains. This region has a numbers of important biological functions that include, binding complement and binding to cell receptors. The scFv fragment contains both antigen-binding V_L and V_H domains, connected with a short linker peptide of 10-25 amino acids. Generally, this linker can either connect the N-terminus of the V_H with the C-terminus of the V_L or vice versa in a scFv fragment (Elgert, 2009). Additionally, a longer linker can help to increase affinity and decrease the formation of aggregates (Whitlow *et al.*, 2003). Compared to a Fab, an scFv fragment with a small size of approximately 26-27 kDa allows it to be produced efficiently in bacterial expression systems.

The significance of antibodies as diagnostic and analytical reagents has been known and exploited for almost a century. In recent years, antibodies have become increasingly accepted as therapeutic reagents. Recombinant DNA technology has allowed for the creation of new and improved antibody molecules. The following section describes the use of phage display for the selection of recombinant antibody fragments.

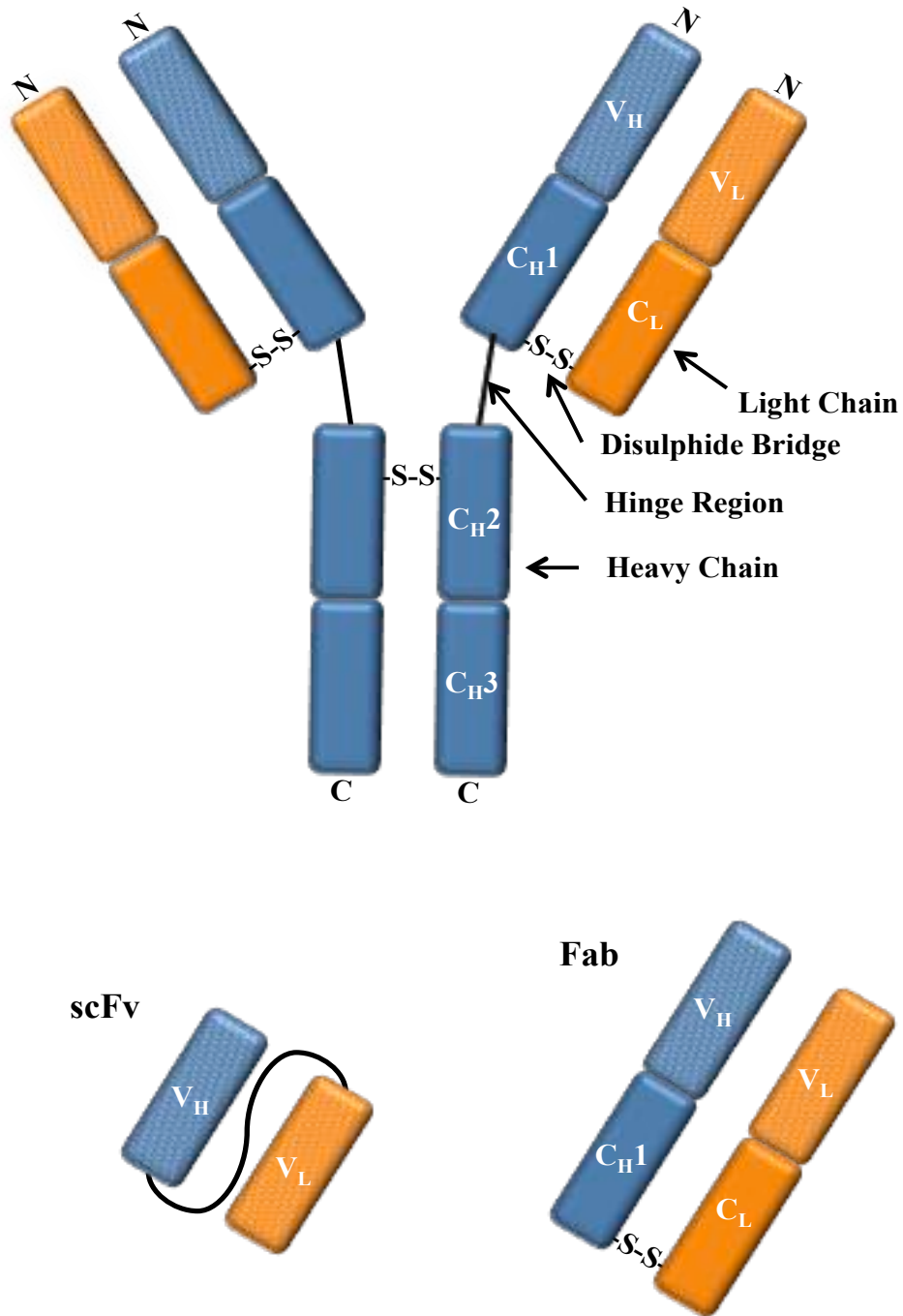


Figure 1.3 The basic structure of an antibody (IgG) molecule, Fab and scFv antibody fragments. Heavy chains are shown in blue and light chains are shown in orange, whereas, the variable regions are outlined with a dashed pattern. The N-terminal end of the antibody molecule is characterised by sequence variability in both the heavy and light chains, which are referred to as the V_H and V_L regions, respectively. The constant portion of the light chains and heavy chains are referred as the C_L and C_H, respectively. Unlike C_L, the constant portion of the heavy chain consists of three structurally discrete regions: C_H1, C_H2 and C_H3. The hinge is a flexible region of the antibody and sits between the C_H1 and C_H2 domains.

1.4 The development of recombinant antibodies using phage display

In contrast to polyclonal antibodies (pAb), recombinant monoclonal antibodies (rAb) have many advantages. These include high specificity and sensitivity, relative short production time, and no variation between antibody batches (Moutel *et al.*, 2009). In addition, unlike pAbs, the affinity and sensitivity of rAbs can be further improved using techniques such as affinity maturation, chain shuffling and error-prone PCR (Hoogenbom, 2002). Recombinant antibody technology involves the amplification of antibody variable genes from the host cDNA by PCR and pairing them at random, creating a library of the antibody genes with different combinations of variable heavy and light chains (Kontermann *et al.*, 2010). This library of antibody genes can be further cloned into an appropriate vector system for expression.

Phage display is one of the most important tools in the isolation and engineering of recombinant antibodies (Rockberg *et al.*, 2008; Tiller *et al.*, 2008; Pansri *et al.*, 2009). This technique involves the use of filamentous bacteriophage for coupling proteins with the genetic information that encodes them and selection of genotypes whose phenotypes interact specifically with the antigen (Pande *et al.*, 2010). This is achieved by cloning the antibody genes into the single stranded phage genome, and coding for surface capsid or coat proteins used for displaying the antibodies as fusion products for target selection on the surface of encapsulated phage particles (Qi *et al.*, 2012). The cloned library is then transformed into *E. coli* cells and grown. This results in the propagation of phage particles in the presence of helper phage. Helper phage provides the necessary proteins for packaging the phage particle (Bradbury *et al.*, 2004). On assembly the phage particles are released from the bacteria and this library of phage particles are selected against the target antigen. Those phage particles with affinity for the antigen bind, whereas, those with no or low affinity are washed away. The selected phage are eluted from the bound antigen, re-infected, re-amplified and reprocessed several times thus enriching for the specific phenotype along with the coding genotype (Hust *et al.*, 2008). This cyclic process of alternating selection and enrichment of phage particles against a specific target is termed “biopanning” (Fig. 1.4). In this thesis the use of this approach for the selection of anti-saxitoxin scFv is described.

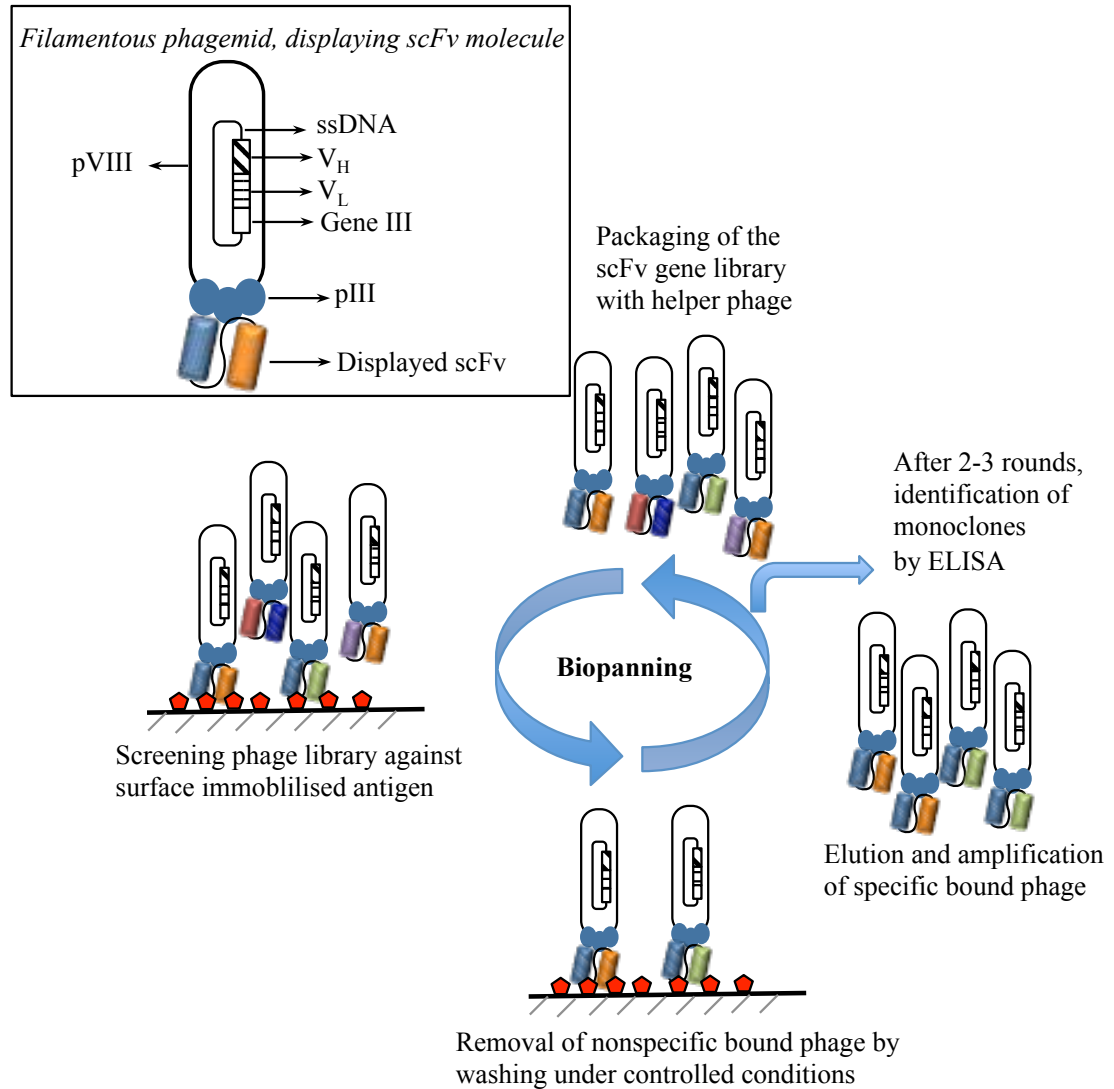
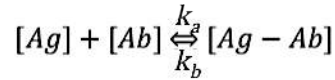


Figure 1.4 Selection of antibodies from antibody libraries (panning) by phage display. Total mRNA was extracted from lymphocytes and then used to synthesise cDNA. Gene fragments encoding for the heavy and the light variable regions of antibodies (V_H, V_L) were amplified and assembled by PCR. The assembled genes are inserted in a phagemid vector in frame with the gene encoding the coat protein pIII. The vector is introduced into *E. coli*. After rescue with helper phage, the library of antibody fragments is displayed on phage (adapted from Hust *et al.*, 2008).

1.5 The antigen-antibody interaction

The antigen-antibody interaction is a typical reversible process with both forward and backward rate constants. This reaction depends on several factors, which includes the concentration of antigen and antibody, temperature, pH, ionic strength (Reverberi *et al.*, 2007). The antigen–antibody complex $[Ag - Ab]$ formation can be described by the Law of Mass Action (Absolom & Van Oss, 1986).



$[Ag]$ = antigen concentration

$[Ab]$ = antibody concentration

$[Ag - Ab]$ = antigen-antibody complex

k_a = association rate constant

k_b = dissociation rate constant

The ratio of the two rate constants gives the equilibrium constant (K_{eq}), which represents the ratio of bound to unbound analyte and antibody.

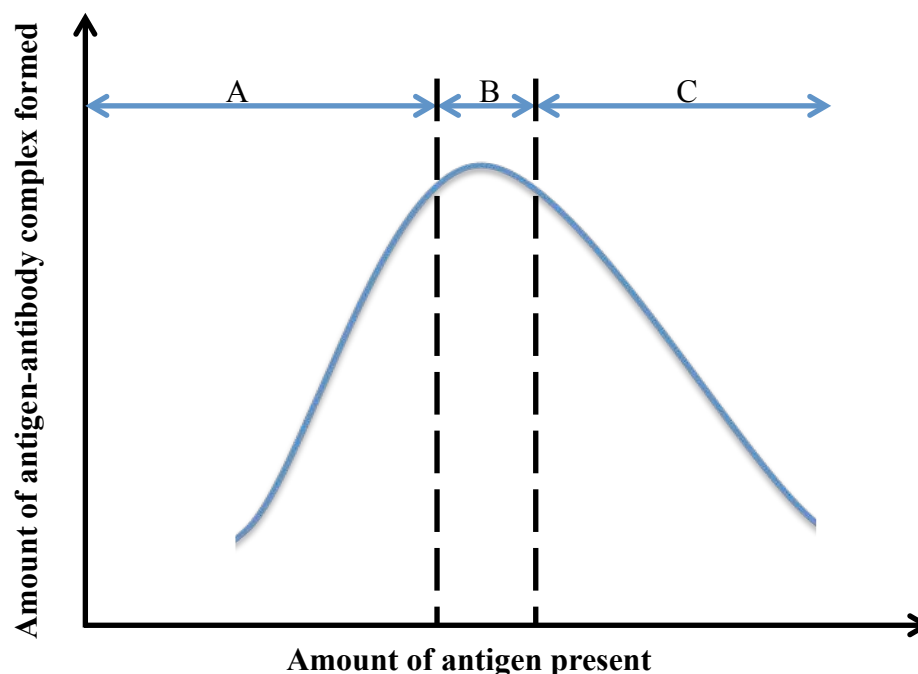
$$K_{eq} = [Ag - Ab]/[Ag][Ab]$$

Principally, the range of K_{eq} is 10^6 L/mol – 10^{12} L/mol. However, K_{eq} less than 10^8 L/mol are not useful in immunoassays. In order to improve antibody detection, the ratio between antigen-antibody complex $[Ag - Ab]$ and free antigen $[Ag]$ should be increased. This can be obtained in two ways: 1) increasing the equilibrium constant; 2) increasing the antibody concentration (Reverberi *et al.*, 2007).

1.5.1 Heidelberger-Kendall curve

The Heidelberger-Kendall curve was used to describe the formation of immunocomplexes in the antigen and antibody reaction (Liu and Huo, 2009; Vercammen *et al.*, 2011). It demonstrated that when an increasing amount of an antigen is added to a fixed amount of corresponding antibody, the amount of formed immunocomplex is described by a bell shaped curve. The Heidelberger-Kendall curve is generated by plotting the amount of antigen against the amount of antibody-antigen

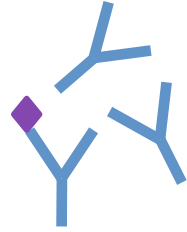
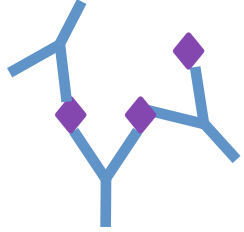
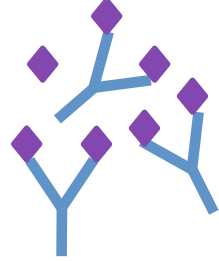
complex formed (Fig. 1.5.1). It is divided into three phases as described in Table 1.5.1. The first phase (A) expresses the type of calibration curve found in an immunometric noncompetitive, excess reagent assay. The following phase (B) describes the reaction when at equilibrium. In the last phase (C), the reaction describes the calibration curve found in a competitive, limited reagent assay (Durner, 2010).



A-antibody excess; B-equilibrium; C-antigen excess

Figure 1.5.1 Representation of the relationship between the amounts of immunocomplex formed when a variable amount of antigen reacts with a constant amount of antibody. The blue curve is known as the Heidelberger-Kendall curve, which is divided into three zones according to immunocomplex formation (modified from Dodig, 2009).

Table 1.5.1 The properties of the Heidelberger-Kendall curve.

Phase	Characteristics	Diagrams
Antibody excess	<p>A large amount of unbound antibody exists.</p> <p>Antigen binding sites tend to be saturated by antibody.</p> <p>Signal increases proportionally to the amount of antigen.</p>	
Equivalence	<p>Cross-linking results in the formation of large immunocomplexes.</p> <p>The binding sites are fully occupied and the reaction has reached saturation.</p> <p>Signal increases with antigen concentration but not proportionally.</p>	
Antigen excess	<p>Most of the binding sites are occupied thus hindering the formation of precipitate due to the high concentration of antigen.</p> <p>Signal decreases with an increasing amount of antigen. This phenomenon is called the Hook effect.</p>	

1.5.2 The Hook effect in an immunoassay

The Hook effect refers to the sharply decreasing signal in the immunoassay even with the addition of more antigens (Buedia *et al.*, 2010) (zone C of Heidelberger-Kendall curve in Fig. 1.5.1). This was reported in many immunoassay formats (Garber, 2008; Liu and Huo, 2009; Al-Mahdili and Jones, 2010). The Hook effect occurs when the amount of antibody in an assay system is not sufficient to bind to excess free antigens. Consequently, excess free antigen can compete for antibody-binding sites with bound antigen. As a result, the readout signal is lower than expected with higher antigen concentrations (Miller, 2004). In this case, the Hook effect leads to an incorrect signal at high concentrations of analyte. The Hook effect can be overcome through the following strategies:

- (1) Adding excess capture antibody into the analyte matrix.
- (2) Removing the excess analyte by a wash step before adding the secondary

antibody.

- (3) Use of a different assay format, such as the sandwich immunoassay.

1.6 Immunoassays

In the last 50 years, the immunoassay technique has made significant contributions to medicine and fundamental life-science research (Ganz *et al.*, 2008; Hachem *et al.*, 2009; Lindsley *et al.*, 2011; Johnson *et al.*, 2013). An immunoassay can be defined as a sensitive analytical assay that employ antibodies to quantitatively and qualitatively measure target analytes in complex biological mixtures (David, 2013). The interaction between the antibody and the antigen is the key point for every immunoassay system, and the level of sensitivity and specificity for antibody determination is at the heart of the immunoassay. Hence, it is critical to select proper immune reagents and assay formats (Bonwick & Smith, 2004; Knopp, 2006).

1.6.1 Historical perspective of immunoassays

In 1959, R.S. Yalow and S.A. Berson developed a new technique, radioimmunoassay (RIA), and used this method to measure insulin in human plasma. This method had a very significant impact on the clinical chemistry laboratory (Yalow, 1959). In 1968, G. Charles Oliver presented the first RIA for the measurement of a drug compound (digitoxin) (Oliver, 1968). Enzyme-labeled immunoassays were first developed in the early 1970s, and this eliminated some of the drawbacks of the RIA method, such as, limited isotope stability, health hazards, and the high equipment costs. Subsequently, the idea of using an enzyme label in an immunoassay was presented. Immunoassay research moved into the area of immunochemical modification, specifically, research focused on how to couple a bulky enzyme molecule to an antibody or antigen without sterically hindering the immunochemical reaction. In 1971, Engvall and Perlmann published their first paper on enzyme-linked immunosorbent assay (ELISA) and demonstrated quantitative measurement of IgG in rabbit serum using alkaline phosphatase as the reporter label (Engvall *et al.*, 1971). In the same year, the first paper on enzyme immunoassay (EIA) was published by van Weemen and Schuurs. In this research work, human chorionic gonadotropin in urine was quantified using an enzyme-coupled to glutaraldehyde as the reporter label (van Weemen *et al.*, 1971). In the following years,

this technology moved from the clinical research laboratory to the mainstream analytical laboratory, where it gradually became a very widely used analytical tool. Examples of different immunoassay applications are listed in the table below.

Table 1.6.1 Immunoassay applications.

Field	Measuring	Authors and Date
Environmental Contamination	Explosives in ground water and soil	Keuchel <i>et al.</i> , 1992
	Herbicides in drinking and river water	McConnell <i>et al.</i> , 1993
	Gibberellin hormones in plant tissue	Yang <i>et al.</i> , 1993
	Determination of mycotoxins in grain	Casale <i>et al.</i> , 1998
Clinical Medicine	Insulin levels in human serum	Hales <i>et al.</i> , 1963
	Detection of cancer biomarkers	Liu <i>et al.</i> , 2008
	Detection of early HIV infection	McFarland <i>et al.</i> , 1999
	Detection of <i>Chlamydia trachomatis</i> infection in human urine sample	Jensen <i>et al.</i> , 2003
	Detection of <i>Helicobacter pylori</i> infection in human body materials	Kabir, 2003
Human Biomonitoring	Human growth hormone in plasma	Schalch <i>et al.</i> , 1964
	Determination of benzene in human blood as an indicator of environmental exposure to volatile aromatic compounds	Angerer <i>et al.</i> , 1991
	Biological monitoring and biochemical effect monitoring of exposure to polycyclic aromatic hydrocarbons	Angerer <i>et al.</i> , 1997
	Monitoring urinary excretion of cannabinoids	Fraser <i>et al.</i> , 2002
	Environmental pollutants in blood of the German population.	Becker <i>et al.</i> , 2002
Food Safety	Determination of the species of origin of milk	Perez <i>et al.</i> , 1992
	Fungicides in potatoes and apples	Brandon <i>et al.</i> , 1993
	Identification of lung tissue in processed meat products	Smith, 1992

1.6.2 Principles of immunoassays

Immunoassays can measure the concentration of a large number of different compounds or analytes (David, 2013). For example these can include: large polymeric proteins, antibodies, nucleic acids or even small molecular-weight haptens, which reside in a complex matrix. This is based on three unique features of antibodies (Zourob *et al.*, 2008):

- a. Antibodies are able to bind to a wide range of antigens. This is because of their unique hypervariable regions at the antigen binding sites.
- b. Antibodies are capable of exceptional specificity, and they can recognise the antigens in the presence of structurally similar compounds. Moreover, antibodies can detect antigen routinely in the picomolar range.
- c. The strong non-covalent bond between an antibody and its target does not breakdown during immunoassay processing.

1.6.3 Immunoassay Classifications

Immunoassays can roughly be divided into two categories distinguished by the use of a label i.e., labelled or 'label-free' (unlabelled) methods. In terms of the labelled immunoassays, they can be classified into several groups as shown in Fig. 1.6.3. Labelled immunoassays can be classified into radioimmunoassay, enzyme immunoassay, fluoroimmunoassay or others according to the type of label. Depending on the requirement for physical separation of antibody-bound antigen from remaining free antigen, labelled immunoassays can be further subdivided into homogeneous and heterogeneous immunoassays. Additionally, labelled immunoassays can be divided into competitive or non-competitive immunoassays formats.

1.6.3.1 'Label-free' immunoassays

In 'label-free' immunoassays, neither antigen nor antibody is labelled. This immunoassay format has many advantages, which includes, direct measurement of antibody-antigen complexes; study of unlabelled and, therefore, unmodified molecules and simple assay setup. 'Label-free' methods include immunonephelometry and immunoturbidimetry. In addition, commercial instruments such as surface plasmon resonance (SPR) and quartz crystal microbalance (QCM) transducers are also used.

1.6.3.2 Labelled immunoassays

In a labelled immunoassay, a molecule is included that will produce a measureable signal, once the antigen-antibody complex is formed. Labelled immunoassays can be classified into many groups as shown in Fig. 1.6.3.2. Examples of immunoassay labels include radioactive compounds, enzymes and fluorescence molecules. Immunoassays are also classified by the different formats used to distinguish the bound antigen-antibody complex from the free unbound label; these formats can be described as competitive and non-competitive. In addition, a further classification is based on the separation of bound antigen-antibody complex. These formats can be described as homogeneous and heterogeneous (Bonwick & Smith, 2004).

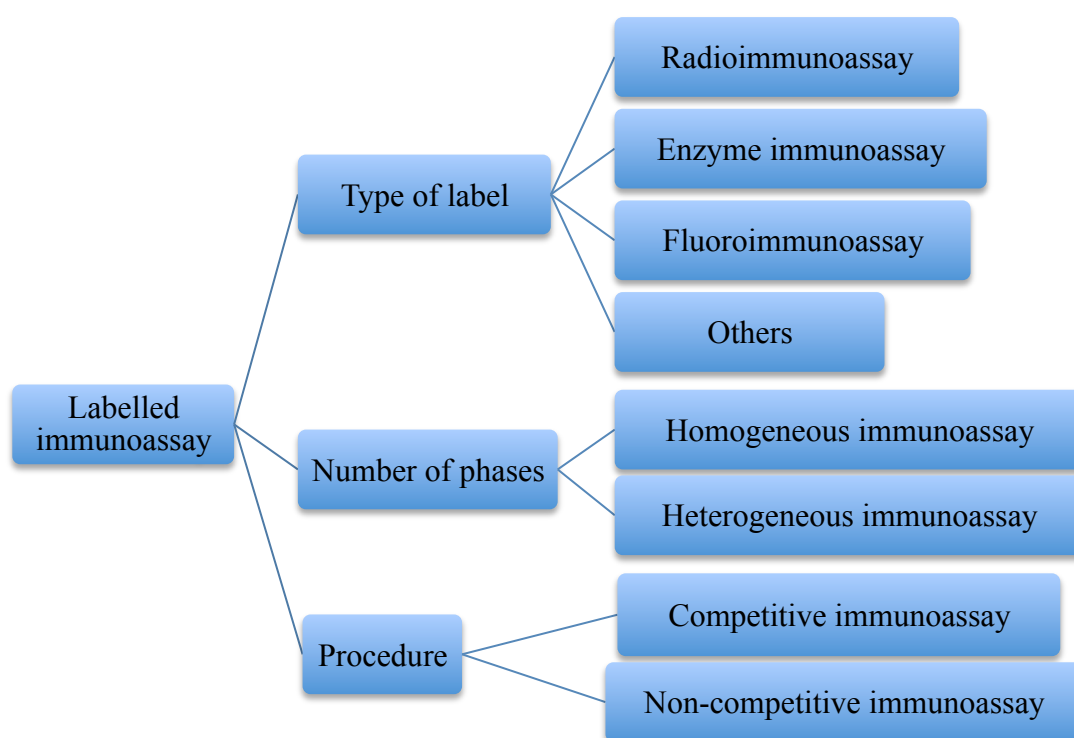


Figure 1.6.3.2 The sub-classification of labelled immunoassays.

1.6.3.3 Radioimmunoassay (RIA)

RIA was first developed by R. S. Yalow, as discussed previously (Section 1.5.1). In this technique a radioactive label is used as the tracer. Although this method has high sensitivity and precision it also has a number of drawbacks. For example, the

radioactive label has limited stability. Furthermore, there are disposal and safety issues which surround the use of radioactive materials. Moreover, there are high costs associated with the detection instrumentation (Gómez-Hens, 2010).

1.6.3.4 Enzyme-based immunoassays (EIA/ELISA)

Enzyme immunoassay, also called enzyme-linked immunosorbent assay (ELISA), has been widely adopted for applications such as diagnostics, quality control, food safety assurance and environmental monitoring. Generally, ELISA can often provide greater versatility in assay designs, higher sensitivity and reproducibility than equivalent RIA methods (Jackson *et al*, 1983; Porstmann *et al*, 1992). Additionally, ELISA is safer as non-toxic enzymes are used as labels instead of harmful radioactive substances. Often enzymes used to label the antigen or antibody in ELISA can convert a colourless substrate to a coloured product. This coloured product can be easily detected using a plate reader and a specific wavelength of light (Gong, 1994). Some of the most commonly used ELISA enzymes are listed below.

Table 1.6.3.4 Enzymes and their substrates commonly used in immunoassays

Enzymes	Substrates	Detection λ_m (nm)
Horseradish peroxidase (HRP)	3,3',5,5'-Tetramethylbenzidine (TMB)	450
Alkaline phosphatase (AP)	<i>p</i> -Nitrophenyl Phosphate (pNPP)	405
β -Galactosidase	<i>o</i> -nitrophenyl- β -D-galactoside (ONPG)	420

1.6.3.5 Fluorescence-based immunoassays (FIA)

Fluorescent molecules are capable of absorbing radiation and emitting it as photons. Instead of an enzyme label, FIA utilises fluorescent labels as the tracer molecule. Importantly, fluorescence-based immunoassays may provide superior performance in terms of assay sensitivity. For example, the utilisation of a fluorophore may increase assay sensitivity by upwards of 10 to 1,000 fold. However, a number of different parameters may affect the performance of the fluorescent complex, such as excitation

and emission wavelengths, fluorescence lifetime, temperature, pH, and concentration. The principle of fluorescence measurement is shown in Fig. 1.6.3.5 (Quentin *et al*, 1984). The fluorophore absorbs light at a specific wavelength and subsequently emits light at a longer wavelength. The application of an appropriate wavelength of light induces the excitation of fluorophores and subsequently, the fluorophores return to the ground state with light emitted at a lower energy (a longer wavelength and slower frequency). The difference between the excitation and emission wavelengths can be described in terms of a Stokes shift. The larger Stokes shift, the easier it is to measure the emitted light without interference from the incident light (Hemmilä, 1985; Diamandis *et al.*, 1996). In addition, an important property of fluorescence is the so called, quantum efficiency, also known as the quantum yield. This fluorescence property is defined as the ratio of the number of photons emitted to the number of photons absorbed (Lakowicz, 1999). It can directly affect the measured fluorescence intensity (Christopoulos *et al.*, 1996). Commonly used immunoassay fluorescent dyes include: Fluorescein, Rhodamine, Alexa, DyLight and ATTO dyes.

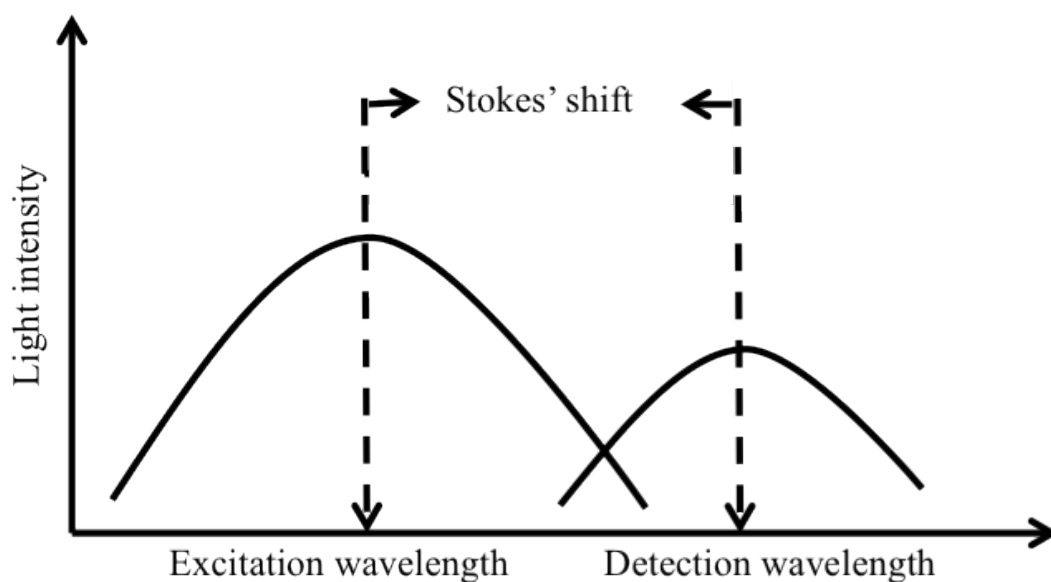


Figure 1.6.3.5 Illustration of the principle of fluorescence measurement (adapted from Demchenko, 2009). The Stokes' shift is the distance between the excitation and detection wavelengths, induced by excitation and emission of the fluorophores. The larger Stokes' shift contributed to a precise detection result without the interference from the emission light.

Theoretically, fluorescence-based methods have upwards of 1,000-fold better sensitivity than absorption-based methods. However, assay sensitivity is often reduced due to the

high background that is often present in the materials and samples used for fluorometric analysis. Specifically, 1) light scattering: scattering of excitation light from solvent molecules or from small particles result in high background signal (Valeur *et al.*, 2012); 2) background fluorescence: the fluorescent components inherent in the assay reagents give rise to background (Tan *et al.*, 2010; Akbari *et al.*, 2014); 3) quenching: the molecules in the antigen matrix (e.g. serum) can often absorb light and thus cause fluorescent quenching (Ramakrishna *et al.*, 2011).

1.6.3.6 Homogeneous immunoassays

Homogeneous immunoassays allow the coexistence of the un-bound and antibody-bound complex of the analyte in the measurement step. Generally, homogeneous immunoassays are faster to perform, as they have no wash steps and a reduced amount of incubation steps (Table 1.6.3.6). The simple experimental setup of a homogeneous immunoassay also allows a robust analysis even when performed by non-laboratory-trained personnel (Kreisig *et al.*, 2011). However, this method has the drawback of low sensitivity and limited dynamic range. One of the major applications of this method is the determination of small molecules (e.g. toxins, pollutants, drugs) using the competitive immunoassay format. For example, Mayilo *et al.* reported on a competitive, homogeneous immunoassay for the successful detection of the hapten digoxigenin (Mayilo *et al.*, 2009).

Table 1.6.3.6 Properties of homogeneous and heterogeneous immunoassays.

Properties	Homogeneous	Heterogeneous
Assay time	Short	Long
Detected limitation	High	Low
Target	Small molecules	Small molecules or proteins
Signal background	High	Low
Sensitivity	Generally low	Generally high

1.6.3.7 Heterogeneous immunoassays

If the antigen–antibody complex is separated from the unbound reactants before measurement, this is referred to as a heterogeneous assay. Heterogeneous assays are widely used to determine the presence of not only small molecules but also macromolecular analytes such as antibodies and proteins, and generally have superior sensitivity and selectivity. The use of either immobilised antibody or antigen has given rise to a wide range of immunoassays, which are implemented using microplates, microbeads (Wheeler *et al.*, 2010), magnetic micro-particles (Ng *et al.*, 2012), or flow-through techniques (Hartwell *et al.*, 2010).

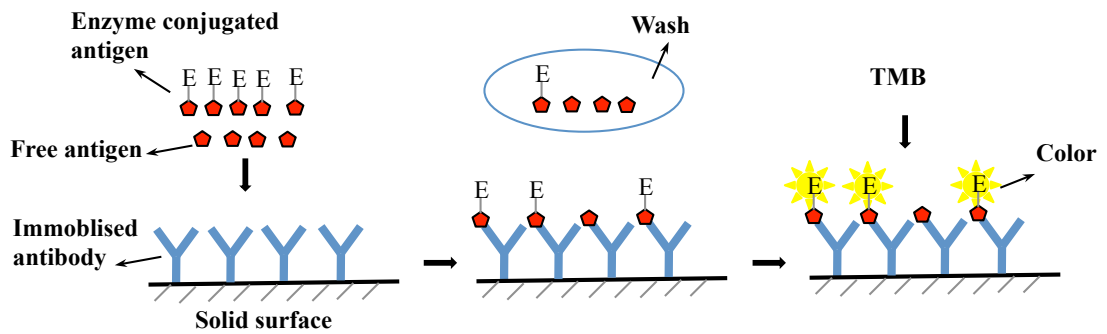
1.6.3.8 Competitive immunoassays

In competitive immunoassay, labelled analyte (usually antigen) and unlabelled analyte present simultaneously compete for the limited number of specific antibody binding sites (Liu *et al.*, 2012; Wang *et al.*, 2014). Generally, the ‘unlabelled’ analyte, or free analyte as the target of quantification, is prepared with the increasing concentrations in order to generate a standard curve, whereas the labelled analyte as the tracer has a constant concentration. After reaching equilibrium unbound analyte is removed by washing with a mild detergent solution. The labelled analyte competes with the free analyte for the antibody binding sites. Thus, an inverse relationship exists between the signal obtained from the tracer and the concentration of the target molecules in the sample, i.e. the more target molecules in the analytical sample the lower the signal. Figure 7A presents the principle of competitive immunoassay. The capture antibodies immobilised on a solid surface, provide a consistent amount of antigen binding sites. Enzyme-labelled antigen and antigen of interest are exposed to the immobilised antibodies and compete for the binding sites. The unbound antigens were removed by a washing step. A substrate solution (e.g. TMB) is added and reacts with the enzyme linked to the antigen, leading to colour generation. The measurement of this change can indicate the amount of free antigen in the sample. Typically the competitive assay is used to detect small molecules, such as haptens, which have only one discrete epitope (Wang *et al.*, 2011; Parra *et al.*, 2012). This assay can provide high specificity.

1.6.3.9 Non-competitive immunoassays

As the name implies, non-competitive immunoassays represent a group of assays, in which the analyte binds to antibody without competition (Bigalke *et al.*, 2011; Mukundan *et al.*, 2012; Liu *et al.*, 2014). The sandwich immunoassay format is one of the widely used non-competitive assay formats, and is illustrated in Fig. 1.6.3.9b. In the sandwich immunoassay, two different antibodies are used for binding the analyte. Generally, one of these two antibodies is immobilised on a solid surface to capture the analyte. The other antibody, with a probe/label added binds to the captured analyte. Therefore, the sandwich assay usually is used to detect relatively large analytes, which allow simultaneous binding of two antibodies with different specificities. In Fig. 1.6.3.9a, the capture antibody is specific to the analyte and will selectively absorb analyte presenting in a sample. After equilibrium is reached, the unbound analyte is removed by washing steps. A second antibody, linked to enzyme, is applied to recognize and bind to a different epitope on the analyte. On application of a substrate solution, the enzyme linked to the second antibody is activated, leading to a color change. The detected signal derived from the color change is directly proportional to the analyte concentration in the sample. Generally, non-competitive immunoassays have high sensitivity and specificity. Typically they are employed in the clinic to measure important disease biomarkers such as Human Immunodeficiency Virus (HIV) (Tang and Hewlett, 2010) and cardiac troponins (Stein *et al.*, 2011).

(a) Competitive immunoassay



(b) Noncompetitive immunoassay

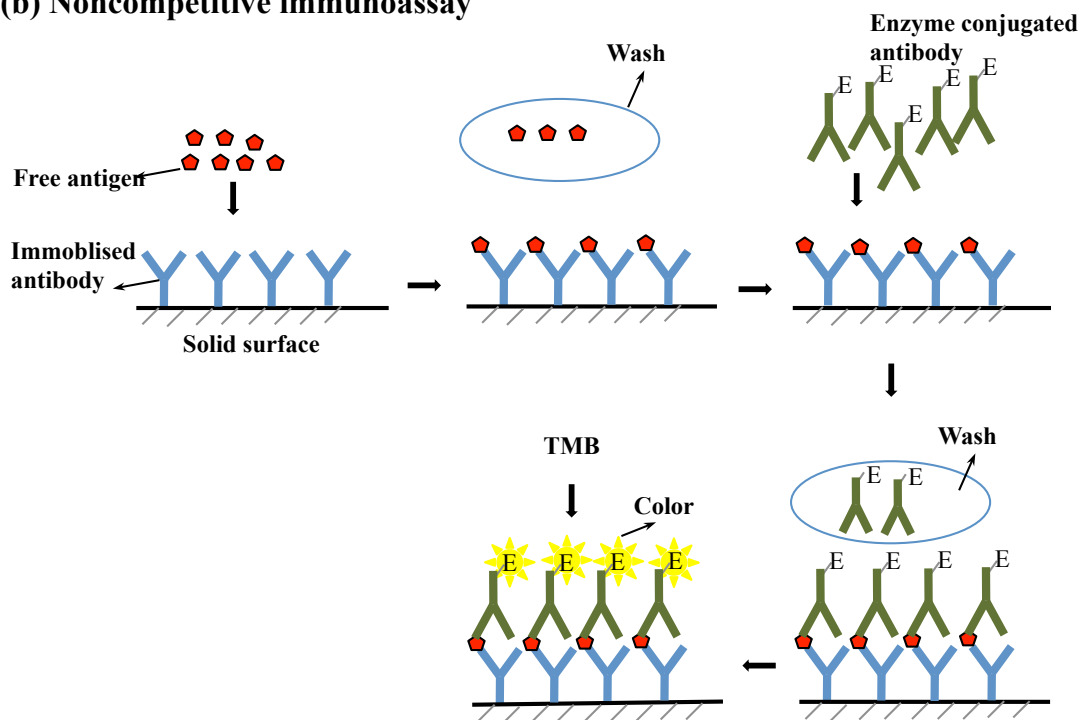


Figure 1.6.3.9 Illustration of competitive immunoassay and non-competitive immunoassay formats. (a) enzyme-labelled and unlabelled analytes competed for binding with surface-immobilised anti-analyte capture antibodies. After the binding reaction reaches equilibrium, the unbound analytes are removed by washing. The signal is generated from measurement of the absorbance, following the reaction between the substrate and the enzyme label, and is indirectly proportional to the amount of free antigen. (b) For the non-competitive immunoassay, antigen is sandwiched between the surface-immobilised capture and the detection antibodies (labelled with enzyme). The absorbance generated is directly proportional to the amount of captured analyte.

1.7 Signal amplification strategies for immunoassays

The sensitivity of an immunoassay can be dramatically enhanced by using a signal amplification system. Immunoassay signal amplification can be achieved by many different methods. However, a widely used method is the biotin-avidin system.

1.7.1 The Avidin-Biotin system

Biotin, also known as vitamin H, is a small and water-soluble molecule that is found in living cells. The biotin molecule contains a valeric acid chain, which reacts with various biotin-affinity proteins through derivatization. Biotin has a high affinity constant ($k_d=10^{-15}$ M) for the egg-white protein – Avidin (Lesch *et al.*, 2010). The avidin – biotin interaction is the strongest known non-covalent bond and is, therefore, employed in the purification of biotin-bonded molecules from complex matrices such as serum (Tomizaki *et al.*, 2010).

Avidin is a basic glycoprotein found in the egg white and tissues of birds, reptiles and amphibians. It is a tetrameric protein having four identical binding sites. The basic isoelectric point of avidin (10-10.5) confers structural stability in a wide range of pH and temperature values. However, disadvantages of avidin is its high nonspecific binding properties due to its high carbohydrate content (10%) and its high charge at neutral pH, due to its isoelectric point (Almonte *et al.*, 2014).

A second biotin binding protein is streptavidin found in *Streptomyces avidinii*. Similar to avidin, streptavidin contains four identical subunits each having one binding site. However, streptavidin has no carbohydrate and has a pI of 5.5 (Chiver *et al.*, 2010). Another biotin binding protein is the commercially available NeutrAvidin™. This protein is also a deglycosylated version of avidin and has a high binding affinity for biotin. Its development was based on research that proved that the carbohydrate portion was not necessary for the biotin-avidin reaction (Wang and Kaplan, 2011). Unlike avidin and streptavidin, NeutrAvidin™ lacks the Arg-Tyr-Asp sequence which can cause non-specific binding particularly in immunohistochemical methods (Nguyen *et al.*, 2011). NeutrAvidin™ has a pI of 6.3 and is widely used to detect biotinylated molecules (Table 1.7.1).

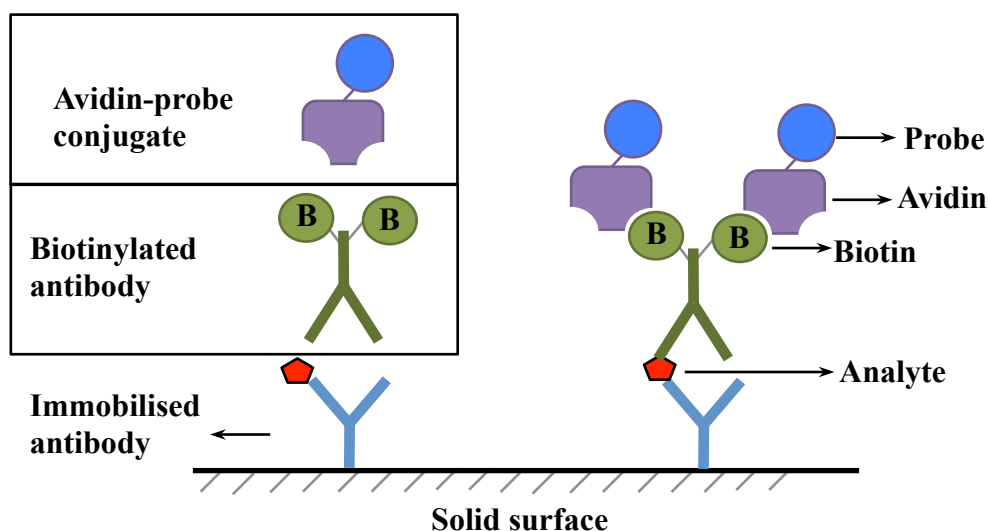
Table 1.7.1 Characteristics of different biotin-binding proteins (adapted from Thermo Scientific avidin-biotin technical Handbook, last accessed on 20th Aug 2014; retrieved from http://www.piercenet.com/files/1601675_AvBi_HB_INTL.pdf).

Characteristics	Avidin	Streptavidin	NeutrAvidin
Molecular Weight	67KDa	53KDa	60KDa
Biotin-binding Sites	4	4	4
Isoelectric Point	10-10.5	5.5	6.3
Affinity for Biotin (M)	10^{-15}	10^{-15}	10^{-15}
Non-specific Binding	High	Low	Very Low
Source	Egg-white, oviducts of birds, etc.	Bacteria e.g. <i>Streptomyces avidinii</i>	<i>In vitro</i> production of genetically modified avidin
Applications	Purification of proteins from complex mixtures	Purification of cell-surface glycoproteins and membrane antigens	Immunoprecipitation capturing biotinylated cell-surface proteins and peptides

The use of the biotin-avidin system in immunoassays can be divided into two main categories (Colburn, 2005). These are: (1) avidin can be used to mediate the interaction between the detector molecule and the primary antibody or antigen (Han *et al.*, 2011), and (2) avidin/biotin can be immobilised onto the solid phase in order to improve the characteristics of the capture system (Liu *et al.*, 2014).

An example of the biotin-amplified detection system (1) using either a sandwich immunoassay format or a competitive immunoassay format is shown in Fig 1.7.1. In the sandwich format (Fig. 1.7.1a), the antigen is bound to the solid phase via a capture antibody and then bound by a biotinylated primary antibody. Once biotin is present in the system, an avidin-conjugated detector can be used to quantify the amount of antigen. In this approach, the avidin molecules are incorporated into the biotin-containing system such that additional free binding sites are available for subsequent interaction with the detector. In contrast, in the competitive format (Fig. 1.7.1b), the biotinylated and non-biotinylated antigen molecules compete for the combining sites of an immobilised capture antibody. The biotinylated antigen, which is bound to the capture antibody, is then determined by the avidin-detector conjugate.

(a) Sandwich immunoassay



(b) Competitive immunoassay

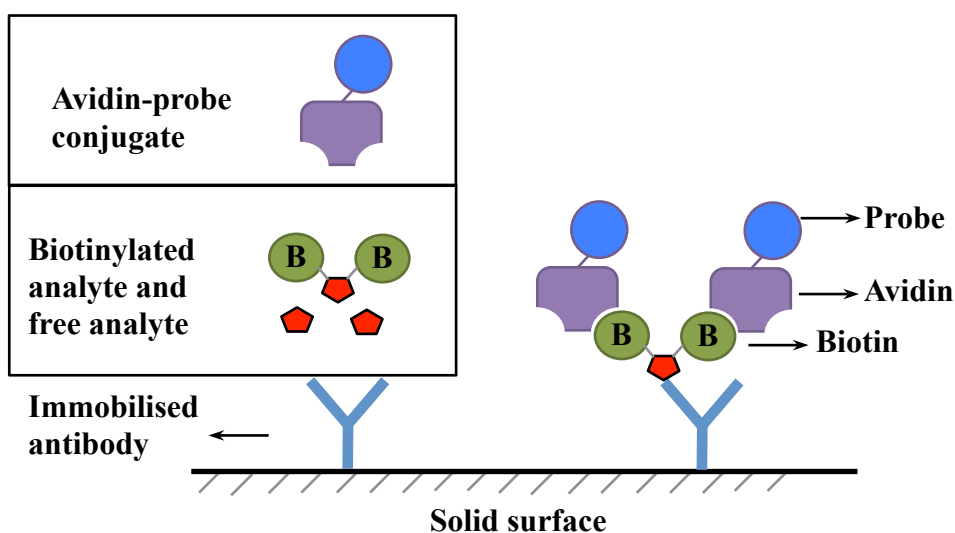


Figure 1.7.1 Application of the biotin-avidin complex in sandwich and competitive immunoassays. (a) The sandwich immunoassay format, in which an antigen from a complex mixture of molecules is selectively bound to solid phase via a capture antibody, and detected subsequently via a biotinylated primary antibody and avidin-conjugated detector. (b) The competitive immunoassay format, wherein a biotinylated antigen competes with the native form of the antigen, prior to quantification by the avidin-conjugated detector.

The major formats of immunoassays were introduced previously. Currently, the format most often applied to perform these various immunoassays is a 96-well microtiter plate,

which possesses a few inherent shortcomings. Firstly, several hours of incubation time are required under static conditions. This is because analyte molecules in the bulk solution must diffuse across a long distances to encounter and interact with antibodies on the surface. Generally, the process of molecular diffusion takes hours. For example, a large protein like IgG (150 kDa) needs more than 3 hours to diffuse 1mm (Lionello *et al.*, 2004). Secondly, large amounts of several assay reagents are required. Generally, a volume of 100 μ L of each reagent is used to perform the microtiter plate-based immunoassay. Additionally, the microtiter plate-based immunoassay involves a labour-intensive protocol, which may lead to large operator errors. After each reagent incubation step, a wash step is carried out manually by pipetting washing solutions in/out. To improve throughput and reproducibility of these processes, robotic systems, such as a microtiter plate washer, can be used for wash solution handling. However, this approach requires high costs for purchase and maintenance. Another solution to circumvent these issues is miniaturization and automation of immunoassays in microfluidic systems. This will be introduced in the following section.

1.8 Microfluidics

Reducing the level of immunoassay reagents to a microscale and the handling of these fluids in a network of microchannels, is called microfluidics. The reduction in scale results in a number of unique features (Fig. 1.8):

- a. Laminar flow. Typically, the fluid flow in microchannel falls into the category of laminar flow, which shows parallel flow layers with no disruption between the layers. For laminar flow the velocity profile in the channel obeys the Hagen-Poiseuille law, with maximum velocity at the geometric center and zero velocity at the walls of the microchannel (Berthier *et al.*, 2010). This laminar flow can contribute to an easily controllable fluid.
- b. Diffusion. Molecules can be transported across layers by diffusion in a typical laminar flow. Different fluids containing miscible fluids and molecules can flow next to each other in a microchannel without any mixing other than by diffusion. Small molecules diffuse faster than larger ones, which facilitate separation of molecules by size (Gossett *et al.*, 2010; Lenshof and Laurell, 2010). It is possible to design microchips to detect small analytes in complex samples such

as blood (Tachi *et al.*, 2009).

- c. Surface tension. Due to scaling down effects, the surface-to-volume ratio dramatically increases. Therefore, surface tension dominates over gravitation forces in the microchannel. For a passive microfluidic system, controlling this force to handle the fluid by simply designing a series of microchannel, can enable a cheap, portable platform (Galusinski and Vigneaux, 2008; Nwankire *et al.*, 2013).

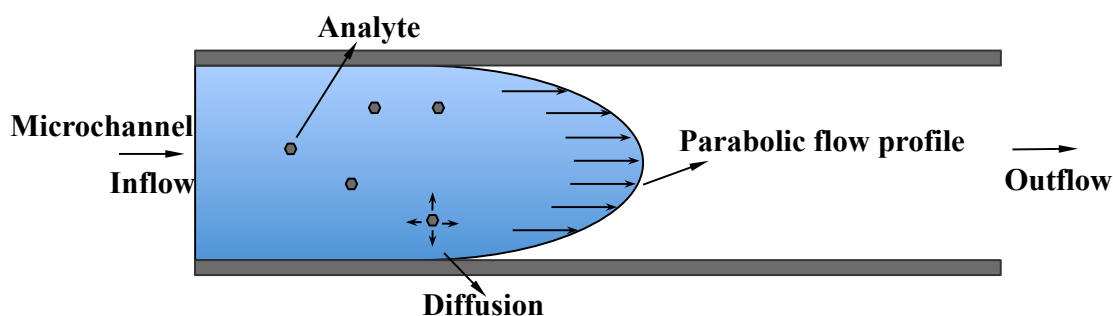


Figure 1.8 Illustration of laminar flow in a microchannel. The fluid with analytes enters the microchannel at the inlet on the left side and flows through the microchannel under laminar conditions with a parabolic flow profile. The analyte molecules can diffuse perpendicularly to the flow direction whenever a concentration gradient exists. (Modified from Zimmermann *et al.*, 2005)

On the basis of these features microfluidics-based technologies have revolutionized the potential for new assay format development and implementation. Compared to conventional immunoassay formats, microfluidic platforms provide remarkable new features. A high ‘surface-to-volume’ ratio with microchannels, for instance, is capable of dramatically influencing interfacial reaction kinetics in solid-phase-based immunoassays and the handling of reagents in the micro and nano-litre range (Bange *et al.*, 2005). Consequently, these features allow a ‘sample-to-answer’ test to be generated with short analysis times, minimal reagent consumption, integration, automation and parallel processing, leading to *in-line*, *at-line* and *in-situ* processing of samples. Furthermore, centrifugal microfluidic platforms inherently possess additional advantages when compared to other ‘lab-on-a-chip’ systems, due to the absence of expensive syringe pumps. Thus, disc platforms enable full integration of multiple liquid

handling and assay processes including pumping, metering, mixing, reagent storage and sequential reagent delivery. To this end, several multi-step and multiplex assays can be integrated onto the platforms, and with further development, they can facilitate the integration of optical sensors on other detections strategies.

1.8.1 Microfluidic platform

Simple microfluidic devices include the capability of automation, miniaturisation, enclosed reactions, cost effectiveness, lower reagent consumption and shortened operation time (Haeberle & Zengerle, 2007; Dungchai *et al.*, 2011; Guo *et al.*, 2012). Details on some of the problems related to immunoassays and how they can be addressed through microfluidics are now presented and discussed.

- a. Reduced amounts of reagent and sample: Most reagents, such as fluorescent labels and enzymes, are integral to immunoassays but are expensive. Therefore, minimisation of both reagent and sample amounts is an effective way to reduce the cost in an immunoassay. Microfabrication technology can be applied to the generation of multiple fluid-handling components, and these can be networked within one simple microfluidic device. Such integrated micro-devices can substantially reduce reagent consumption (Lai *et al.*, 2004).
- b. Decreased analysis time: The widely applied heterogeneous immunoassay requires many incubation and washing steps. The requisite long incubation times are caused by inefficient mass transport of antigen/antibody from solution to the solid surface. If the analysis time can be reduced from days to minutes or even seconds, the immunoassay system would be capable of fast and continuous real-time monitoring. Recent reports from the literature show that, this problem also could be solved by the application of microfluidic devices as it could enhance the reaction efficiency and reduce the incubation times (Miller *et al.*, 2012; Kantak *et al.*, 2012; Xiao *et al.*, 2013; Kim *et al.*, 2014).
- c. Automation. In classical immunoassay procedures, a loss of precision and accuracy can occur due to operator error. In contrast, integrated microfluidic devices reduce the operational errors, and provide automated functions such as: delivery, pumping, valving and mixing of reagents, washing as well as ‘on-chip’ detection (Gorkin, 2010). Automation of the experimented process can often

increase speed, precision, and accuracy.

- d. Integration and portability. Miniaturization has more advantages than the simple ‘scale-down’ of chamber dimensions and volumes. For trace chemical interactions based on surface and solution phases, the ratio of surface area to volume is higher, and, therefore, results in faster interaction time and better molecule transportability. A portable device is necessary to eliminate delay for the delivery in the application of clinical diagnostics. A further benefit of portable microfluidic devices is a reduction in power consumption. Moreover, portability is a key factor for ‘point-of-care’ applications (Bhagat *et al.*, 2011).

1.8.2 The development of microfluidic platforms

Initially, microfluidic devices often had simple channel geometries that allowed for a few chemical reactions on a glass or polymer chip (Haraldsson, 2005). The first and most successful application of microfluidics was the inkjet print head, and it provides the basics for ink-jet technology (Le, 1998). At the end of 1980s, micro-valves and micro-pumps were produced by silicon micromachining. On this premise automation of liquid handling protocols based on microfluidic integration became a reality. A new field of “lab-on-a-chip” (LOC) or “micro total analysis systems” (μ TAS) then emerged (Mark *et al.*, 2010). Current microfluidic devices are far more complex with entire laboratory protocols shrunk down to only a few cm. The dramatic increasing number of publications in these areas demonstrate that microfluidic technology is now firmly established in academia, where it provides a new toolbox for the development of new methods and products in life sciences (Mark *et al.*, 2010).

1.9 Application of microfluidic platforms in immunoassay

In order to transfer an immunoassay to a microfluidic platform, there are some fundamental properties of microchip fabrication and design that need to be considered (Bange *et al.*, 2005). These include:

- a. Materials. The characteristics of the materials are critical for the application of a microfluidic system in immunoassay due to the performances of chemical and physical operations inside the microchip. The ideal material used to fabricate

microfluidic systems possesses chemical resistance, optical transparency, ease of microfabrication and low cost (Henares *et al.*, 2008).

- b. Fluid force. Capillary phenomena are important in micro-channels as adhesion to the walls is stronger than the cohesive forces between the water molecules (Haeberle & Zengerle, 2007). This causes an increase in the flow resistance for a pumped liquid. Thus, both pump and capillary force control the flow of liquid.
- c. Valving. Valve performance is a critical component in microfluidic platforms. It contributes to precise control of the flow of liquid at multiple points throughout the assay process.
- d. Microfluidic design. Design is important with regard to the device performance, specifically, in the case of handling the fluid in micro-scale. An ideal microfluidic system should be portable, self-contained and able to integrate multiple functions, such as reagent preparation, sequential delivery.
- e. Surface modification. Modification of the surface is often essential in order to provide the proper surface chemistry for specific antibody immobilisation. In order to remove the excess reagents and block the unused immobilisation sites, generally, washing and well defined blocking processes are required.
- f. Detection. The detection method can directly affect the sensitivity and accuracy of a microfluidic-based immunoassay. With regard to the micro-scale detection area, however, the conventional detection methods such as a plate-reader or fluorescent microscope are not suited. Therefore, a novel detection method with significantly high sensitivity needs to be considered.

These challenges have been addressed in many publications (Whiteside, 2006; Henares *et al.*, 2008; Mark *et al.*, 2010; Tabeling, 2010; Lee *et al.*, 2011, Giordano *et al.*, 2012). A short review of some techniques and developments are described below.

1.9.1 Microfluidic propulsion

Microfluidic platforms can be classified into different groups according to various principles of liquid propulsion, such as capillary, centrifugal, pressure-driven, electrokinetic, acoustic microfluidic-based, magnetic-driven and syringe systems (Madou *et al.*, 2006). In this section, centrifugal microfluidics is discussed and compared with two other popular fluid propulsion methods, which are syringe pumping and electrophoresis.

A pressure driven flow platform is characterized by liquid transport mechanisms based on pressure gradients. Typically this leads to hydrodynamically stable laminar flow profiles in microchannels. There is a broad range of different implementation strategies in terms of using external or internal pressure sources such as using syringes, pumps or micropumps, gas expansion principles or pneumatic displacement of membranes. In Fig. 1.9.1a, a syringe-driven flow is illustrated for example. The external syringe pump is coupled to microfluidic channel. The samples and reagents are processed by injecting them into the chip inlets either batch-wise or in a continuous mode (Henares *et al.*, 2008; Mark *et al.*, 2010). A pressure driven approach can be used for a wide range of solutions because of the relative ease and insensitivity to surface contamination, ionic strength and pH. It even allows non-electrically conductive fluid flows. However, the flow behaviour using peristaltic pumps is usually non-linear which may cause problems in miniaturisation and multiplexing.

Electrokinetic pumping in microfluidic channels is performed by employing and housing planar microelectrodes on to one or more sides of the microchannel structures (Yang & Kwok, 2004). This method can be principally used for the controlled manipulation, isolation, concentration, separation and characterisation of electrically polarisable particles, such as intact cells, proteins, viruses, bacteria, and micro-organisms (Dalton & Kaler, 2007). In Fig. 1.9.1b, an electrokinetic platform is illustrated. In this system, a pair of coplanar meandering electrodes with an alternating current (ac) voltage is configured in parallel with the channel. The electrically charged particles or molecules in this electric field are attracted by the electrodes. This effect can be used for chromatographic separation (Haeberle & Zengerle, 2007). The electrokinetic system does not require any moving parts and is easily implemented. However, some disadvantages of this method include: (1) the requirement of a high

voltage (1-30 kV) power supply; (2) high sensitivity of the flow rate to the ionic strength and the pH of the solution; and (3) difficulty in valving liquids (Madou *et al.*, 2006).

Centrifugal force is typically performed on ‘compact-disc (CD)-like’ structures containing channels and micro-chambers. Centrifugal force is produced by spinning the CDs using a rotor, as shown in Fig. 10c. The volumetric flow rate is dependent on the speed at which the disc spins, the distance from the centre of the disc, the geometry of the fluidic channels, and the fluidic properties (density, viscosity, and surface tension). The centrifugal approach provides several benefits over the other pumping methods. Firstly, centrifugal forces only need a low-power rotary motor. In addition, fluid flow is dependent upon the intensity and liquid viscosity rather than pH or ionic strength. Furthermore, centrifugal propulsion can work through the entire length of the fluid body. This allows smooth, controlled, and reproducible flow, but reduces the influence of bubbles, as well as enabling transfer of liquid with a high efficiency. Finally, many parallel units can be placed on an individual platform, and this is beneficial for the simplification of multiple operation steps in immunoassays (Siegrist *et al.*, 2009). Currently, a whole range of fluidic functions, including decanting, mixing, metering, and separation, have been implemented with the centrifugal microfluidic platform (Gorkin *et al.*, 2010). In addition, analytical measurements in a centrifugal microfluidic platform can be made by electrochemical (Kim *et al.*, 2013), fluorescence (Chang *et al.*, 2013) or light absorption-based methods (Czugala *et al.*, 2012).

Table 1.9.1 Comparison of microfluidic propulsion techniques (adapted from Madou *et al.*, 2006).

	Centrifuge	Pressure	Electrokinetic
Valving for liquids	Available	Available	Available
Maturity	Products available	Products available	Products available
Influence for propulsion	Density and viscosity	Geometry of channel	pH and ionic strength
Power source	Rotary motor	Pump and mechanical roller	Metal electrode
Materials	Plastic, paper	Plastic, glass, paper	Glass, plastic
Flow rate	From less than 1 nl s^{-1} to greater than $100\text{ }\mu\text{l s}^{-1}$	Very wide range (less than nl s^{-1} to Liter s^{-1})	$0.001 - 1\text{ }\mu\text{l sec}^{-1}$
General remarks	Inexpensive CD drive; mixing is easy; most solutions possible (serum and cells); better for diagnostic platform	Standard technique; difficult to miniaturize and multiplex	Mixing difficult; high voltage source is dangerous and many parameters influence propulsion; better for smallest samples

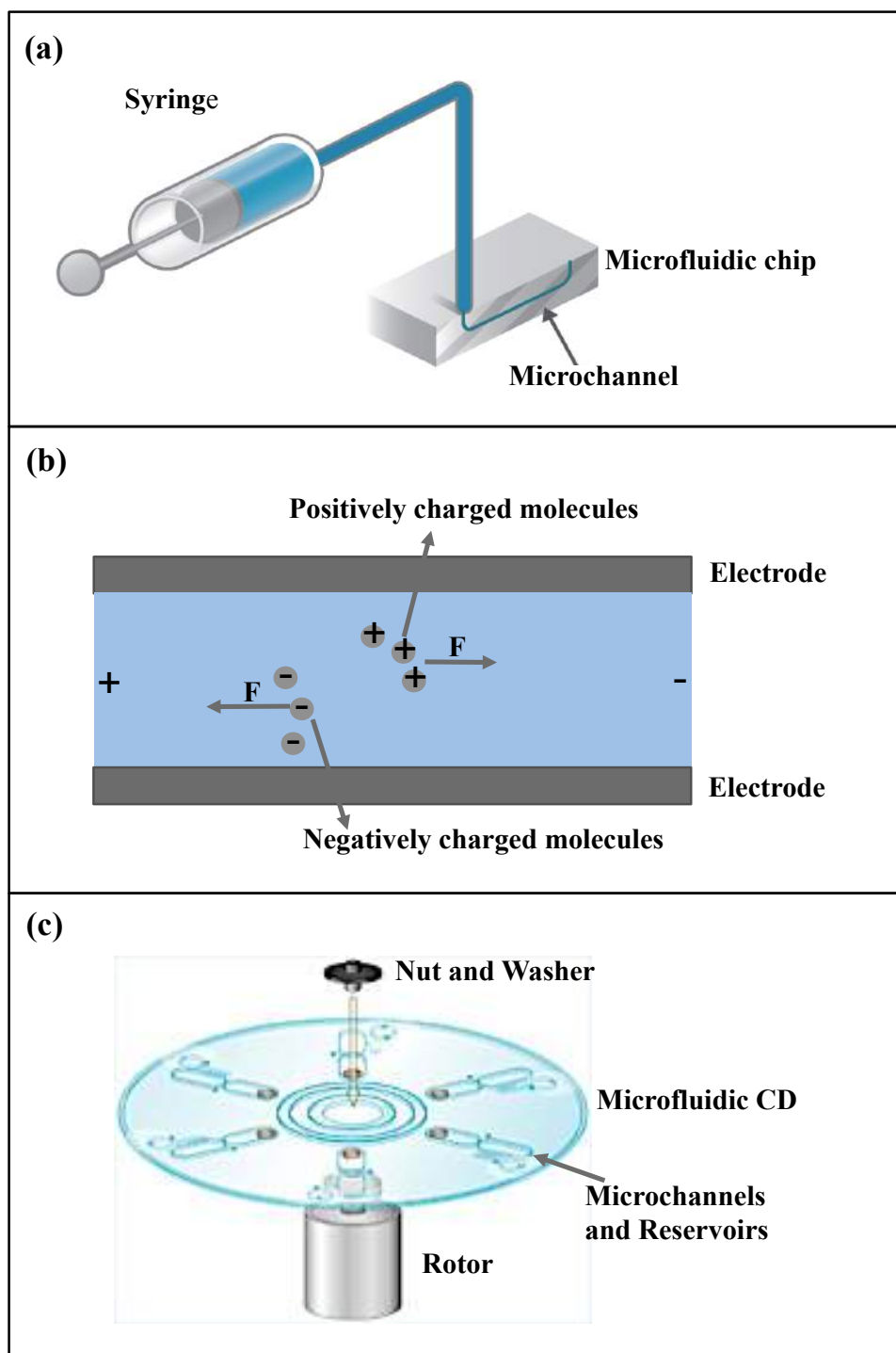


Figure 1.9.1 Illustration of three fluid propulsion methods. (a) Syringe pump. A syringe is coupled to microfluidic channel. The samples in the syringe are injected into the channel by an external force on the syringe. (b) Electrophoresis. A pair of coplanar meandering electrodes with an AC voltage provides a steady electric field to the electrically charged particles or molecules, which can be separated according to charge and size. (c) Centrifugal pump. A rotor is applied to provide a controllable centrifugal pumping force, which depend on the speed at which the disc spins, the distance from the centre of the disc, the geometry of the fluidic channels, and the fluidic properties (density, viscosity, and surface tension).

1.9.2 Valving in centrifugal microfluidics

The most important determining factor in choosing a fluidic system is the ease of implementing valves. In the case of the centrifugal microfluidic CDs, valving is accomplished by varying rotation speed and capillary diameter. A selection of valving formats that can be applied in a centrifugal microfluidic CD is discussed in the following sections.

1.9.2.1 Capillary valve (hydrophilic valve)

The capillary valve is most often used in centrifugal microfluidic systems. This passive valve operates in hydrophilic channels and the movement of fluid is aided by centrifugal force generated by the rotation of the microfluidic disc. However, when a fluid has reached a sudden widening in the microchannel, a large surface tension force will develop. In Fig. 1.9.2a, a schematic operation of a capillary valve is shown. When the surface tension force is higher than that of the centrifugal force, the flow of fluid stops, despite the continued rotation of the CD. However, when a critical burst frequency is reached, the centrifugal forces overpower the surface tension forces, and the fluid will then move down the microchannel.

1.9.2.2 Hydrophobic valve

Two distinct strategies have been used to produce hydrophobic valves: (1) extension in channel geometry, and (2) modification of the local surface property, such as surface tension. Both schemes are illustrated in Fig. 11b. In the channel geometry approach, when fluid experiences a quick change from a wide to narrow channel, the flow of liquid (right) can be blocked. Alternatively, hydrophobic functionalisation of the channel downstream has the same effect (Fig. 1.9.2b, left). In both cases, fluid can be forced past the hydrophobic valve by means of increasing the spin frequency to a threshold value. The most significant disadvantage associated with hydrophobic valving is that the effectiveness of passive fluid control is reduced when surfactant or some organic solvents are present in the solution (Haeberle and Zengerle, 2007; Tsougeni *et al.*, 2010).

1.9.2.3 Siphon valve

The siphon valve relies on a hydrophilic environment and surface tension acts as a pump in this model while centrifugal force acts as resistance. When the cross section of the channel is small enough to provide sufficient surface tension, the liquid in the chamber is able to flow along the channel (Siegrist *et al.*, 2009). In Fig. 1.9.2c, the fluid is pumped out from a loading reservoir into a microchannel and then is stopped in one position under a condition of high-speed rotation. When the rotation speed is reduced to a certain level, capillary forces can pump fluid over the siphon channel crest. Therefore, the functional siphon valve is based on well-controlled rotational speed. Siphons are extremely useful on microfluidic CD platforms where they can serve several functions, often times in combination, such as valving, pumping, metering, and volume definition (Ducrée *et al.* 2007; Kido *et al.* 2007; Gorkin *et al.*, 2012).

Passive valves are controlled by varying the rotational speed of the CD, and require only deliberate geometry designs or surface modifications without extra moving parts. In order to obtain a great accuracy level and avoid errant release of the fluid, the material, position, and dimensions of passive valves must be designed carefully.

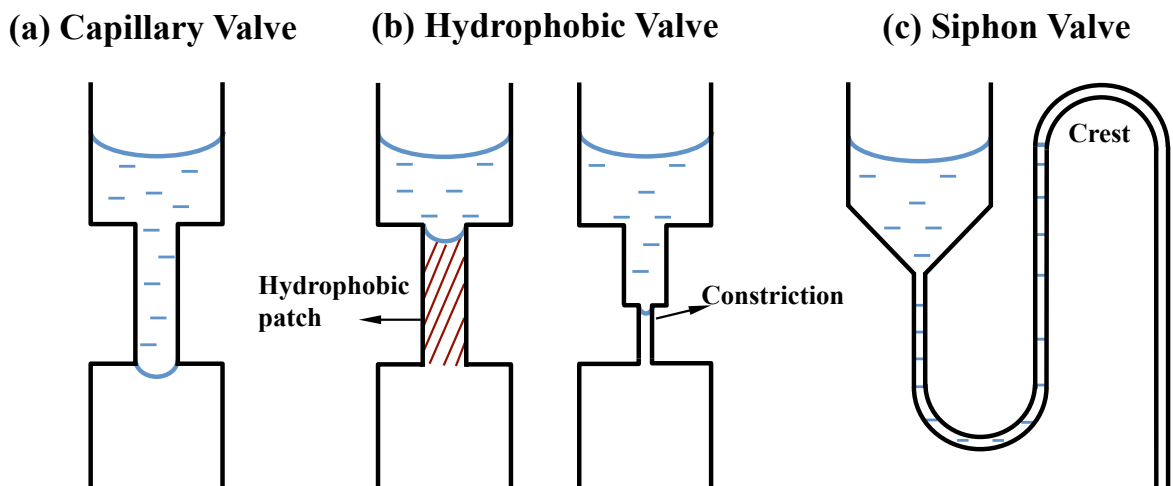


Figure 1.9.2 Illustration of three forms of passive valving in a centrifugal microfluidic platform (modified from Siegrist *et al.*, 2009).

1.9.3 Substrate materials for microfluidic immunoassays

The most widely used materials for fabrication of microfluidic platforms are silicon, glass and polymers (Henares *et al.*, 2008). A comparison of these materials is summarised in Table 1.9.3.

Table 1.9.3 Comparing characteristics of various type of material for fabrication of microfluidic platforms (adapted from Henares *et al.*, 2008)

Materials	Silicon	Glass	Polymers
Cost of raw materials	Expensive (~ 1 dollar cm ⁻²)	Less expensive (20~40 cents cm ⁻²)	Cheap (~ 1 cent cm ⁻²)
Ease in fabrication	Available in the integrated circuit industry; involved in a series of processes and chemicals	Geometry limitation due to the isotropicity (shallow, semicircular cross-section)	High processibility
Mass production	Yes, slow process; high cost	Yes, slow process; high cost	Yes (not well-developed); fast process; low cost
Optical	Opaque	Transparent	Transparent; may absorb the ultraviolet light
Thermal conductivity	1.4 W mK ⁻¹	~ 1 W mK ⁻¹	~ 0.1 W mK ⁻¹
Biocompatibility	Usually need surface modification	Good	Depends on polymers and applications
High temperature sterilisation	Feasible	Feasible	Tend to deform
Electric conductive	Semiconductor	Electric insulator	Electric insulator

Silicon has great thermal conductivity, stable chemical and physical properties. However, silicon is not optically transparent in the UV/visible region, which is normally the detection wavelength range for most bioanalyses (Osterbroek, 2003). Also, microchip construction using silicon requires costly fabrication facilities and this therefore limits the implementation of this material in a commercial environment. Glass substrates possess good chemical resistance and offer excellent optical properties for biomolecular detection. However, microfabrication with glass using a common method of isotropic wet etching is also expensive (Fiorini & Chiu, 2005). Currently, polymers are attracting far more attention for use in microfluidic devices due to the ease of microfabrication. Physical and chemical properties like good chemical resistance, optical transparency, low autofluorescence and absence of UV absorption. The availabilities of various surface chemistries contributing to many choices of immobilisation techniques for different antibodies or antigens are additional advantages (Attia and Marson, 2009). The most typically used polymers include polystyrene, polypropylene, polyvinyl chloride (PVC), polycarbonate, polymethyl methacrylate (PMMA) and polydimethylsiloxane (PDMS). Among these, PMMA and PDMS show unique potential for microfluidic immunoassay systems because of low cost, high transparency and excellent dielectric and mechanical properties.

1.9.4 Surface modification

An ideal substrate for microfluidic immunoassay should have a high binding capacity but also should show outstanding adhesion, stability and resistance against harsh washing and regeneration conditions. For covalent attachment of biomolecules, the polymer surface needs to be functionalised. Many methods for surface modification have been used for enhanced antibody immobilisation and reduction of non-specific binding. Non-specific binding of molecules in a heterogeneous assay impacts the accuracy and precision of the immunoassay. Surface modifications can generate both covalent and non-covalent antibody-substrate interactions by alterations in surface chemistry (Zhou *et al.*, 2010). Many methods for surface modification of PMMA surfaces are available (Brown *et al.*, 2006; Tennico *et al.*, 2010; Chehimi *et al.*, 2014). A description of three widely used surface modification methods follows.

1.9.4.1 Plasma treatment

A plasma refers to a partially ionised state of matter (Flamm and Auciello, 2012). In this state a proportion of electrons and ions are free instead of being bound to an atom or molecule (Zhou & Voelcker, 2010). Plasma surface modification relies on gases (i.e. oxygen, nitrogen and hydrogen), which react with the substrate surface and subsequently create chemical functional groups.

1.9.4.2 Chemical vapour deposition (CVD)

CVD refers to a chemical process used to generate a thin film on a substrate surface by the deposition of gaseous molecules, which chemically react on the surface (Gubala *et al.*, 2010; Zhou *et al.*, 2010). The sequence of events in CVD includes sublimation, pyrolysis and deposition. Chen and Lahann have deposited poly (4-benzoyl-p-xylylene-co-p-xylylene) on PDMS via CVD and, subsequently, wet-chemically patterned the resulting reactive coating of a microchannel with poly (ethylene oxide) (Chen *et al.*, 2005). Chen *et al.*, have demonstrated CVD polymerization of a range of functionalised poly (p-xylylenes) within PDMS microchannels with complete coating of the entire channel length (Chen *et al.*, 2006). In these previous studies, it was demonstrated that the CVD technique could overcome the challenges caused by the conventional liquid-phase technique, which were the requirement of manual intervention to introduce the precursors (e.g. APTES), and poor uniformity of surface coating.

1.9.4.3 Combination of plasma treatment and silanisation

In contrast to the multi-step complexity of the methods described above, a fast and simple route to versatile amine-functionalised surfaces on plastics was demonstrated by Gubala's group (Gubala *et al.*, 2010). In this method oxygen plasma activation was combined with plasma enhanced chemical vapour deposition (PECVD) using an aminated precursor. This technique has a number of advantages over the multistep, wet chemical methods or even CVD. It can be used to coat a large number of substrates in a single batch, it avoids direct contact with the solvent, and thus reduces chemical waste. In addition, the process can be performed at room temperature (Volcke *et al.*, 2010). Moreover, no major limitations have been observed in terms of preparation of

homogeneous coatings on curved or patterned surface and microfluidics channels (Angelini *et al.*, 2006).

1.9.4.4 Silanisation

Surface silanisation can be implemented on different substrates if they have surface hydroxyl groups, which are capable of reacting with alkoxysilanes to form covalent Si-O-Si bonds with the underlying substrate (Howarter & Youngblood, 2006; Raj *et al.*, 2009). (3-Aminopropyl)-triethoxysilane (APTES) is a commonly used aminosilane in the process of silanization. This agent contains an amine terminal and a silane terminal, which can be introduced onto the oxidative surfaces and provides amine-groups for reaction with biomolecules. Additionally, the application of APTES for the immobilization of antibodies on the microchannel surface, has been extensively reported in the literature (Lee, 2006; Lee *et al.*, 2010; Chen *et al.*, 2010).

1.9.5 Detection methods in microfluidic immunoassays

To develop fast, sensitive and portable point-of-care device, it is crucial to choose an appropriate detection method with high sensitivity and portability. The most commonly used detection methodology in microfluidic systems is fluorescence, in which a specific fluorophore is labelled fluorescently. Typically, fluorescence detection system consists of the following components: a light source for emitting light at a suitable wavelength range, an excitation filter to eliminate unwanted light, a dichroic mirror for the optical separation of excitation and emission channels, an emission filter, and a detector with electronics for signal processing (Lin *et al.*, 2011). Integration of fluorescent labels with microfluidics can offer several benefits. The reduction in the sample volume can mitigate background signal noise and improve the sensitivity as well as signal-to-noise ratio (Irawan *et al.*, 2007). However, challenges still exist in using fluorescent labels with microfluidics. Firstly, the chip material needs to be microscopy-compatible, e.g. low auto-fluorescence. Secondly, traditional fluorescent signal acquisition is bulky, which does not facilitate development of fully integrated and portable systems in point-of-care microfluidic systems.

A new polymeric material, cyclic olefin polymer (COP) demonstrated itself to be an

ideal substrate for fluorescence detection in microfluidic system. Outstanding features of COPs, such as high chemical resistance, good optical transparency and low autofluorescence, have been reported (Roy *et al.*, 2010; Jena *et al.*, 2011; Ait-Ali *et al.*, 2012). In addition, COPs present excellent properties for fabrication, allowing integration of optical components on-chip (Skinner *et al.*, 2014). Furthermore, COPs are cost efficient (Nunes *et al.*, 2010).

In recent years, more and more research has focused on improvement of detection technology for lab-on-a-chip systems. Several ‘lab-made’ fluorescence detection systems have been developed with advanced features, such as miniaturization, low background signal and low costs. For example, Yang *et al.* developed a scanning laser induced fluorescence detection system by using optical fibers, which was compatible, low cost and stable (Yang *et al.*, 2012). Tan *et al.* designed and fabricated a microfluidic system, where fluorescence intensity was enhanced by twenty times using a photonic crystal surface embedded in the microfluidic chip (Cunningham, 2015). All of these fluorescence detection technologies can facilitate point-of-care device portability.

Today, although there are numerous novel microfluidic systems generated and widely used, the majority of research still focuses on the stage of demonstrations rather than quick commercialization, as many hurdles exist. Firstly, high initial investment for market entry is required; secondly, the fabrication technologies are too expensive; and finally, application of immunoassays on a chip requires a lot of research for development and optimization.

1.10 Simulation of an immunoassay in microchannels

Microfluidic systems can enhance the kinetics of an immunoassay in comparison with that performed in a microtitre plate. This microfluidic paradigm strongly relies on the micro-dimensional channel. At these small scales fluids exhibit laminar flow, i.e. fluidic streams that flow parallel to each other, and mixing occurs only by diffusion. However, the enhancement effect on the kinetics of microfluidic immunoassay also can be influenced by many other conditions such as the design of microchannel geometry, the flow velocity of reagents in the microchannel and the size of the sensing area. In order to understand how changes in these conditions affect the immunoassay, the technique of computational simulation can be used to predict the trends in assay performance

resulting under different modelled conditions. Furthermore, the predicted data can provide very useful information for the design and optimization of microfluidic systems and assays.

1.11 Thesis Aims

The main purpose of the thesis is the development and optimization of microfluidic system for use with immunoassays for selected targets such as marine toxins and human IgG.

Firstly, Saxitoxins (STX) are potent cyanobacterial neurotoxins that accumulate in water, fish and shellfish which feed upon marine algae. These toxins can cause paralytic shellfish poisoning, blockage of Na^+ ion channels in nerve membranes, and may result in paralysis and respiratory failure. To meet the urgent requirement for reliable detection methods and to reduce the risk of human exposure to potent marine biotoxins, the generation of an anti-STX antibody with high affinity and specificity to a range of saxitoxin derivatives such as neosaxitoxin, gonyuatoxin, decarbamoyl and saxitoxin itself was envisioned.

Secondly, the thesis research aims to develop a prototype microfluidic system for the performance of rapid and sensitive immunoassays. The microfluidic platform should include well-designed microchannel networks, which incorporates sample loading, valving, and sequential delivery. In order to perform the heterogeneous immunoassay in the microfluidic platform, the functionalised substrate should have uniformly deposited amine groups. Additionally, an optical detection method should be developed to meet the requirement of quick, sensitive and accurate measurement. Moreover, this microfluidic immunoassay should detect selected samples in the nanomolar range and the assay time should be significantly shorter than conventional methods (e.g. ELISA based on microtitre plates) and should ideally have potential for automation.

Finally, the developed microfluidic-based immunoassay should be analysed and evaluated by computational simulation. The kinetics of microfluidic-based immunoassay should be studied; furthermore, the effect of varying assay parameters should be verified.

CHAPTER 2

Material and Methods

2.1 Materials

2.1.1 Reagents

All reagents used were of analytical grade and purchased from Sigma-Aldrich Ireland Ltd (Dublin, Ireland), unless otherwise specified.

Reagent	Supplier
Bacteriological Agar Yeast extract Tryptone	Cruinn Diagnostics Ltd., Hume Centre, Parkwest Business Park, Nangor Road, Dublin 12, Ireland.
DNA Ligase Helper phage Restriction enzymes Phusion High-Fidelity DNA polymerase Antarctic Phosphatase	ISIS Ltd., Unit 1 & 2, Ballywaltrim Business Centre, Boghall Road, Bray, Co. Wicklow, Ireland.
dNTPs GoTaq [®] DNA Polymerase	Medical Supply Company Ltd, Damastown, Mulhuddart, Dublin 15, Ireland.
PageRuler [™] Plus Prestained Protein Ladder	AGB Scientific Limited – A VWR International Company, Orion Business Campus, Northwest Business Park, Ballycoolin, Dublin 15, Ireland.
PCR primers	Eurofins MWG Operon, 318 Worple Road, Raynes Park, London, SW20 8QU, UK.
Platinum [®] Taq DNA Polymerase High Fidelity Trizol	Bio-sciences, Crofton Road, Dun Laoghaire, Dublin, Ireland.

RNaseZap™ RNAlater™ Glycogen (5 mg/mL) 3M Sodium acetate	Applied Biosystems/Ambion, 2130 Woodward St., Austin, TX 78744-1832, USA.
Protein A Neutravidin-Dylight 650	Thermo Fisher Scientific Inc., 3747 N Meridian Rd, Rockford, IL., USA.
IgG-free bovine serum albumin (BSA)	Jackson ImmunoResearch Laboratories Inc., 872 West Baltimore Pike, West Grove, PA 19390, USA.
A biotinylated, secondary anti-human-IgG antibody	Gallus Immunotech Inc., 6570 First Line of Westgarafraxa, FERGUS, Ontario N1M 2W4, USA.
Micro-90 concentrated cleaning solution	VWR International LLC. 100 Matsonford Road, Radnor, PA 19087-8660, USA.

2.1.2 Equipment

The equipment used and the suppliers are listed below.

Equipment Name	Supplier
Biometra T-Gradient PCR machine	LABREPCO, 101 Witmer Road, Suite 700, Horsham, PA19044, USA.
Eppendorf™ Centrifuge 5810 R with swing-bucket rotor (A-4-62) and fixed-angle rotor (F-45-30-11)	AGB Scientific Limited – A VWR International Company, Orion Business Campus, Northwest Business Park, Ballycoolin, Dublin 15, Ireland.
Gene Pulser Xcell™ electroporator, Biorad Gel electrophoresis system	Bio-Rad Laboratories, Inc., 2000 Alfred Nobel Drive, Hercules, California 94547, USA.
MSC-Advantage Laminar Flow Cabinet PX2 thermal cycler	Thermo Electron Corporation, 81 Wyman Street, Waltham, Massachusetts (MA), 02454, USA.
Nanodrop™ ND-1000	NanoDrop Technologies, Inc., 3411 Silverside Rd 100BC, Wilmington, DE19810-4803, USA.
Roller mixer SRT1	Science lab, Inc., 14025 Smith Rd, Houston, Texas 77396, USA.
Safire™ 2 plate reader	Tecan™ Group Ltd. Seestrasse 103, CH-8708 Männedorf, Switzerland.
Vibra Cell™ sonicator	Sonics and Materials Inc., 53 Church Hill Road, Newtown, CT 06470-1614, USA.

ANDOR iXon 885 camera	Andor Technology plc., 425 Sullivan Avenue, Suite #3, South Windsor, CT 06074, USA.
Epilog Zing Laser cutter	Epilog Laser, 16371 Table Mountain Parkway, Golden, CO 80403, USA.
Roland MDX-40A Benchtop Milling Machine	Roland DG Corporation, 1-6-4 Shinmiyakoda, Kita-ku, Hamamatsu-shi, Shizuoka-ken, 431-2103, Japan.
Computer-numerical control (CNC) machine (T-Tech, GA, USA-QuickCircuit 5000)	RoutOut CNC Ltd., Unit D5, Capel Hendre Industrial Estate, Ammanford, SA18 3SJ, USA.
Cutter-plotter (Graphtec, Japan-Graphtec CE-2000)	Graphtec America Inc. 17462 Armstrong Avenue Irvine, CA 92614-5724, USA.
Hot Roll Laminator	ChemInstruments International Inc., 9079 Tyler Blvd, Mentor, Ohio 44060, USA.
Harrick Plasma Cleaner PDC-002 Mass flow controller (PDC-FMG)	Henniker Plasma, Cavendish House, Birchwood Park, Warrington, WA3 6BU, England.
Scroll pump (Edwards XDS-5)	Mason Technology, 228 South Circular Road, Dublin 8, Ireland.

Oxford Plasmalab System100 PECVD reactor	Oxford Instruments, Abingdon, Oxfordshire, OX13 5QX, United Kingdom.
--	---

2.1.3 Culture media formulations

All the reagents were prepared in distilled water and autoclaved at 120°C for 20 minutes.

Media	Components
2x Tryptone Yeast extract (2xTY)	Tryptone (16 g/L) Yeast extract (10 g/L) NaCl (5 g/L)
Super Broth (SB)	MOPS (10 g/L) Tryptone (30 g/L) Yeast extract (20 g/L)
Super Optimal Catabolite (SOC)	Tryptone (20 g/L) Yeast extract (5 g/L) NaCl (0.5 g/L) KCl (2.5 mM) MgCl ₂ (20 mM) Glucose (20 mM)

2.1.4 Buffer preparation

2.1.4.1 General buffers

All the reagents were prepared in distilled water and autoclaved at 120°C for 20 minutes.

Buffer Name	Components
Phosphate-buffered saline (PBS) 150 mM (pH 7.4)	NaCl (5.84 g/L) Na ₂ HPO ₄ (4.72 g/L) NaH ₂ PO ₄ (2.64 g/L)
PBS Tween 20 (PBST)	NaCl (5.84 g/L) Na ₂ HPO ₄ (4.72 g/L) NaH ₂ PO ₄ (2.64 g/L) Tween 20 (0.05 %,v/v)

2.1.4.2 Buffers for Western blotting

Transfer Buffer	Volume (1 L)
Tris	3.03 g
Glycine	14.4 g
Methanol	200 mL
	<i>Adjust to 1L with dH₂O</i>

2.1.4.3 Buffers for sodium dodecyl sulfate-polyacrylamide gel electrophoresis (SDS-PAGE)

Preparation of 12.5 % Separation Gel	1 gel/ 6 mL
1 M TrisHCl (pH 8.8)	1.5 mL
30 % (w/v) acrylamide (AcrylaGel)	2.5 mL
2 % (w/v) methylamine bisacrylamide (Bis-AcrylaGel)	1.0 mL
Water	934 μ L
10 % (w/v) sodium dodecyl sulfate (SDS)	30 μ L
10 % (w/v) Ammonium persulfate (APS) (Fresh)	30 μ L
N,N,N',N'-Tetramethylethylenediamine (TEMED)	6 μ L

Preparation of 4.5 % Stacking Gel	1 gel/ 2.5 mL
1 M TrisHCl (pH 6.8)	300 μ L
30 % (w/v) acrylamide (Acrylagel)	375 μ L
2 % (w/v) methylamine bisacrylamide (Bis-Acrylagel)	150 μ L
Water	1.625 mL
10 % (w/v) SDS	24 μ L
10 % (w/v) APS	24 μ L
TEMED	2 μ L

10X Electrophoresis Buffer	Volume (1 L)
196 mM Glycine	144 g
50 mM Tris (pH 8.3)	30 g
0.1 % (w/v) SDS	10 g

4X Loading Dye	Volume (10 mL)
Tris 0.5M (pH 6.8)	2.5 mL
Glycerol	2 mL
2-mercaptoethanol	0.5 mL
20 % (w/v) SDS	2.5 mL
Bromophenol blue	0.01 g
Water	2.5 mL

Coomassie Stain	Volume (500 mL)
0.2 % (w/v) Coomassie blue R-250	1 g
45 % (v/v) Methanol	225 mL
Water	225 mL
10 % (v/v) Acetic acid	50 mL

Coomassie Destain	Volume (1 L)
10 % (v/v) Acetic acid	100 mL
25 % (v/v) Methanol	250 mL
Water	650 mL

2.1.5 Commercial antibodies and antigens

Reagent	Supplier
Horseradish peroxidase-conjugated goat anti-rabbit pAb Horseradish peroxidase-conjugated rabbit anti-mouse pAb	Sigma Aldrich, 3050 Spruce Street, St. Louis, MO 63103, USA.
Mouse anti-haemagglutinin (HA) mAb	Cambridge Bioscience, 24-25 Signet Court, Newmarket Road, Cambridge CB5 8LA, UK.
Horseradish peroxidase-conjugated mouse anti-M13 antibody	GE Healthcare Bio-Sciences AB, SE-751 84 Uppsala, Sweden.

2.1.6 Commercial kits

Reagent	Supplier
Superscript III reverse transcriptase kit	Invitrogen Corporation, 5791 Van Allen Way, Carlsbad, CA 92008, USA.
Wizard Plus SV Miniprep™ kit	Promega, 2800 Woods Hollow Road, Madison, WI 53711, USA.
QIAquick gel extraction Kit	Qiagen, 28159 Avenue Stanford, Valencia, CA 91355, USA.
NucleoSpin® Xtra Midi Plasmid Purification Kit	Macherey-Nagel, Fisher Scientific Ireland Ltd., Suite 3, Plaza 212, Blanchardstown Corporate Park 2, Ballycoolin, Dublin 15.

2.1.7 Bacterial strains

All strains were purchased from Stratagene, La Jolla, California, USA.

<i>E. coli</i> TOP10F' strain: {lacI ^q , Tn10(Tet ^R)} mcrA Δ(mrr-hsdRMS-mcrBC) Φ80lacZΔM15 ΔlacX74 recA1 araD139 Δ(ara-leu)7697 galU galK rpsL (Str ^R) endA1 nupG.
<i>E. coli</i> XL1-Blue strain: recA1 endA1 gyrA96 thi-1 hsdR17 supE44 relA1 lac [F' proAB lacI ^q ZΔM15 Tn10 (Tet ^R)].

2.1.8 Material for fabrication of microfluidic platforms

Material	Supplier
Zeonor™ slide Zeonor™ SAF chip	Zeon Corporation, Shin Marunouchi Center Building, 1-6-2 Marunouchi, Chiyoda-ku, Tokyo 100-8246, Japan.
Poly(methyl methacrylate)	Radionics Ltd., Glenview Industrial Estate, Herberton Road, Rialto, Dublin 12, Ireland.
Pressure-sensitive adhesive	Adhesives Research Ireland Ltd., Raheen Business Park, Limerick, Ireland.

2.2 Methods

2.2.1 Production of scFv antibody library

The approach for recombinant antibody generation is based on a standard protocol (Barbas *et al.*, 2004). The novelty of the work undertaken was to attempt to generate unique scFv antibody fragments against PSP toxins, which have a number of potentially different side-groups and would act as different epitopes. In addition, these fragments would have His and other tags which would be highly valuable for immobilisation and correct orientation of the antibodies to ensure excellent functionality for binding on any sensor surface developed.

Immunisation of a New Zealand white rabbit with paralytic shellfish poisoning (PSP) toxin conjugates (NeoSTX-KLH) was successfully performed by Queen's University Belfast (QUB). Serum samples, bone marrow and spleen were also obtained and transferred to DCU. In order to determine an immune response against NeoSTX-KLH, serum titre analysis was carried out. A NUNC™ 96 well plate was coated with 10 µg/mL NeoSTX-KLH conjugate and 10 µg/mL KLH overnight at 4°C. The antigen solution was flicked out from the overnight plate, wells were blocked with 3 % (w/v) milk powder (Marvel) /PBS (150 mM, pH 7.4) solution, 200 µL per well, at 37°C for 1 hour. Following blocking, the plate was washed three times with PBST (150 mM, pH 7.4) and three times with PBS (150 mM, pH 7.4). The immune serum was serially diluted from 10^{-2} to 10^{-7} in 1 % (w/v) milk powder (Marvel)/0.01 % (v/v) Tween-20/PBS (150 mM, pH 7.4) and added to the plate. This was incubated for 1 hour at 37°C; following this it was washed as above. HRP-labelled anti-rabbit polyclonal antibody (Sigma Aldrich, Ireland), 100 µL, at a 1/2,000 dilution in a 1 % (w/v) milk powder (Marvel) /PBS (150 mM, pH 7.4) solution was added to each well. The plate was incubated at 37°C for 1 hour. Following incubation, the plate was washed as above and 100 µL 3, 3', 5, 5' tetramethylbenzidine (TMB) substrate solution (Sigma Aldrich, Ireland) prepared in 0.05 M phosphate-citrate buffer, pH 5.0, was added to each well. The plate was then incubated for approximately 20 minutes under tin foil to allow for colour development after which the reaction was stopped by addition of 50 µL of 10 % (v/v) HCl. The absorbance was then determined at 450 nm with a Tecan™ Safire II plate reader (Tecan™, UK).

2.2.1.1 Phenol-chloroform extraction of RNA

All tubes and equipment were 'RNase-free' or treated with Presept and RNase Zap in order to remove all contamination resulting from RNase. All of the manipulations were carried out in a laminar flow cabinet. Both the spleen and the bone marrow were stored in RNeasy[®]. Then the RNeasy[®] was normally centrifuged at 2,500 g (Eppendorf 5810R, bucket rotor A-4-62) for 10 minutes. After removal of RNeasy[®], 10mL of cold Trizol[™] was immediately added to the sample and homogenized using a sterile homogeniser (autoclaved and baked O/N at 180°C) at 50% output for 45 seconds followed by 100% output for 15 seconds. A further 20mL of Trizol[™] reagent was added and incubated for 5 minutes at room temperature in order to dissociate nucleoprotein complexes. Subsequently, the samples were centrifuged at 2,500 g (Eppendorf 5810R Rotot A-4-62) for 20 minutes at 4°C. The supernatant containing the genetic material was transferred to a polypropylene Oakridge tube and mixed with 6mL of MG-chloroform by manually shaking for 15 seconds, followed by 15 minutes incubation at room temperature. The centrifugation was carried out at 12,000 g using a SS34 rotor for 25 minutes at 4°C. The RNA solution was concentrated into the upper aqueous layer. This layer was carefully transferred to a polycarbonate tube and mixed with 15mL of MG-isopropanol by manually shaking for 15 seconds. The sample was incubated at room temperature for 10 minutes and was centrifuged at 17,000 g (fixed angle, pre-cooled Sorval SS34 rotor) for 25 minutes at 4°C. An RNA pellet was formed in the bottom of the tube. After carefully removing the supernatant and adding 30mL of cold 75% (v/v) MG ethanol, the final centrifugation was performed at 17,000 g for 20 minutes at 4°C. The supernatant was removed and the air-dried pellet was gently re-suspended in 500uL of MG-water. The RNA solution was quantified using the NanoDrop[™] spectrophotometer ND-1000.

2.2.1.2 cDNA synthesis by reverse transcription PCR

Reverse transcription was carried out using a Superscript III First Strand Synthesis System RT-PCR kit. In this protocol, two mixtures were prepared and each of them contained a 20X reaction mixture. The details are outlined in Table 2.2.1.2a. Mixture 1 was dispensed into 8 X 25 µL aliquots and centrifuged before step 1 of the PCR (Table 2.2.1.2b). The tubes were placed on ice for 1 minute and 25 µL of mixture 2 was added

to each tube before step 2 of the PCR program. The contents of four of the tubes were pooled together and 20 μL of RNase H was added into each tube (1 μL of RNase H into 10 μL of reaction mixture). RNase H was used to digest template RNA from the RNA-cDNA hybrid. This was then followed by step 3 of the PCR program i.e. the synthesis of cDNA. The cDNA obtained was stored at -80°C .

Table 2.2.1.2a Reverse transcription of PCR.

Mixture 1	1x	20x
RNA	X μL (to give 5 μg)	20X μL
Oligo-(dT) ₂₀ (50 μM)	1 μL	20 μL
dNTPs (10 mM)	1 μL	20 μL
MG Water	Y μL (to give final volume of 200 μL)	20X Y μL

Mixture 2	1x	20x
10X RT Buffer	2 μL	40 μL
MgCl ₂ (25mM)	4 μL	80 μL
DTT (0.1 M)	2 μL	40 μL
RNase OUT (40 U/ μL)	1 μL	20 μL
Superscript III RT (200 U/ μL)	1 μL	20 μL

Table 2.2.1.2b PCR program to synthesize cDNA using thermal cycling.

Step	Temperature ($^{\circ}\text{C}$)	Time (minutes)
1	65	5
2	50	50
	85	5
3	37	20
	4	Hold

2.2.1.3 PCR amplification of antibody light and heavy chain genes

Polymerase chain reaction (PCR) was used to amplify the variable heavy and variable light chain antibody genes from the synthesised cDNA. The pComb3XSS series primer sequences were obtained from Barbas *et al.* (2001) and primers were synthesised by Eurofins-MWG-Operon. The various primer combinations used for the heavy and light variable chains were as follows:

Table 2.2.1.3a Primer combinations for amplification of antibody variable genes.

Item	Abbreviation	Forward	Reverse
Variable light chain kappa	VK1	RSCVK1	RKB9J10-BL
	VK2	RSCVK1	RKB9J0-BL
	VK3	RSCVK1	RKB42J0-BL
	VK4	RSCVK2	RKB9J10-BL
	VK5	RSCVK2	RKB9J0-BL
	VK6	RSCVK2	RKB42J0-BL
	VK7	RSCVK3	RKB9J10-BL
	VK8	RSCVK3	RKB9J0-BL
	VK9	RSCVK3	RKB42J0-BL
Variable light chain lambda	VL λ	RSC λ 1	RJ λ o-BL
Variable heavy chain	VH1	RSCVH1	RSCG-B
	VH2	RSCVH2	RSCG-B
	VH3	RSCVH3	RSCG-B
	VH4	RSCVH4	RSCG-B

Table 2.2.1.3b Standard multiplex mixture for PCR reactions.

Component	Concentration	In 50 μ L volume
GoTaq Buffer (5 X)	1X	10.0 μ L
V_L/V_H Forward Primer (100mM)	60 pM	0.5 μ L
V_H/V_L Reverse Primer (100mM)	60 pM	0.5 μ L
MgCl₂	1.5 mM	3.0 μ L
dNTP (50mM)	0.2 mM	1.0 μ L
cDNA	0.5 μ g	1.0 μ L
GoTaq Polymerase	5 U/50 μ L	0.25 μ L
H₂O	-	33.75 μ L

In order to efficiently amplify the antibody genes, optimization of the concentration of MgCl₂ used was essential.

Table 2.2.1.3c PCR program for GoTaq polymerase.

Step	Temperature	Time	Number of Cycles
1	95 °C	2 minutes	1
2	95 °C	15 seconds	30
	60 °C	30 seconds	
	72 °C	60 seconds	
3	72 °C	5 minutes	1
	4 °C	Hold	

For PCR optimisation of variable light chain kappa 7 and 8 regions, the Phusion[®] High-Fidelity DNA polymerase was used. The PCR reaction system was as follows:

Table 2.2.1.3d The standard multiplex mixture for the PCR reactions using Phusion DNA polymerase.

Component	Concentration	In 50 μ L volume
Phusion Buffer HF/GC (5 X)	1X	10.0 μ L
Forward Primer (100mM)	60 pM	0.5 μ L
Reverse Primer (100mM)	60 pM	0.5 μ L
DMSO	3% (v/v)	1.5 μ L
dNTP(50mM)	0.2 mM	1.0 μ L
cDNA	0.5 μ g	1.0 μ L
Phusion DNA Polymerase	1.0 U/50 μ L	0.5 μ L
H₂O	-	Make up reaction to 50 μ L

Table 2.2.1.3e The PCR program for using Phusion DNA polymerase.

Step	Temperature	Time	Number of Cycles
1	94 °C	2 minutes	1
2	94 °C	30 seconds	30
	55 °C	30 seconds	
	68 °C	30 seconds	
3	72 °C	8 minutes	1
	4 °C	Hold	

2.2.1.4 Splice by overlap extension (SOE) PCR using VELOCITY™ DNA polymerase

The primers used in SOE PCR were follows:

RSC-F (sense)	5' GAG GAG GAG GAG GAG GAG GCG GGG CCC AGG CGG CCG AGC TC 3'
RSC-B (reverse)	5' GAG GAG GAG GAG GAG GAG CCT GGC CGG CCT GGC CAC TAG TG 3'

The combined V_H and V_L genes were generated by pooling amplified V_H (V_H1-4) and V_L (V_Lκ and V_Lλ) in equivalent molar concentrations and then linked using SOE-PCR.

Table 2.2.1.4a Reaction mix for SOE-PCR.

Component	Concentration	In 50 µL volume
HiFi Buffer (5 X, contains 10mM Mg²⁺)	1X	10.0 µL
Forward Primer	60 pM	0.5 µL
Reverse Primer	60 pM	0.5 µL
DMSO	3% (v/v)	1.5 µL
dNTP(10mM)	0.2 mM	5.0 µL
Template: V_H	100 µg	0.17 µL
V_L	100 µg	0.2 µL
VELOCITY DNA Polymerase	0.4 U/µL	1.0 µL
H₂O	-	Make up reaction to 50 µL

Table 2.2.1.4b The PCR program for SOE-PCR.

Step	Temperature	Time	Number of Cycles
1	98 °C	2 minutes	1
2	98 °C	40 seconds	30
	48 °C	30 seconds	
	72 °C	2 minutes	
3	72 °C	6 minutes	1
	4 °C	Hold	

2.2.1.5 Agarose gel electrophoresis

Agarose gel electrophoresis was required to analyse the PCR products. A 1% (w/v) agarose gel was made up by heating the acetate-EDTA (TAE) buffer containing agarose powder at 100°C for 3-4 minutes. At high temperatures, the agarose dissolved in TAE. When it was cooled, 5 µL of SYBR[®]Safe DNA gel stain was added and manually mixed and the gel was poured into a prepared gel mold. DNA samples were prepared by mixing with DNA loading dye. A 1kb Plus DNA molecular weight ladder was required for size quantification. Gel electrophoresis was performed at a voltage of 100V until distinct ladder bands were observed.

2.2.1.6 Purification of PCR products from agarose Gel using QIAquick[™] gel extraction kit

Following the agarose gel electrophoresis of all the PCR products, the expected DNA bands were excised from the gel with a sterile, sharp scalpel, using a Darkreader transilluminator. The DNA was purified from the gel using the QIAquick Gel Extraction Kit. Once completed, the DNA products were quantified using the Nanodrop[™] and stored at -20°C.

2.2.1.7 Plasmid DNA purification

Plasmid DNA purification was carried out using a NucleoBond[®] Xtro Midi/Maxi kit. The *Escherichia coli* strain, containing the pComb3XSS plasmid was cultured in SB broth containing carbenicillin (100 µg/mL) at 37°C overnight in an orbital shaker. Subsequently, the harvested bacterial cells were purified using NucleoBond[®] Xtro Midi/Maxi kit. The product was quantified using Nanodrop[™] and stored at -20 °C.

2.2.1.8 Restriction enzyme digestion of scFv insert and pComb3XSS vector

SOE-PCR products were digested with restriction enzyme *Sfi*I, whereas the plasmid DNA used in this recombinant phage display system was digested using restriction enzymes including *Sfi*I, *Xba*I, and *Xho*I. After digestion, the pComb3XSS vector was

treated with Antarctic phosphatase to prevent re-annealing of the vector. Both digested SOE insert and pComb3XSS vector were electrophoresed on a 1.5 % (w/v) agarose gel and subsequently gel-purified, using the QIAquick gel extraction kit. Once complete, they were quantified using the Nanodrop™ and stored at -20 °C.

Table 2.2.1.8 Components for restriction enzyme digestion of the SOE products and pComb3XSS.

	Component	Volume
Digestion of SOE-products	10 X NEB buffer 2	10 µL
	100 X BSA	1 µL
	SfiI (20,000 U/mL)	18 µL
	SOE products	10 µg
	Water	Make up to 100 µL
	Incubation at 50 °C for 5 hours	
Digestion of pComb3XSS	10 X NEB buffer 2	10 µL
	100 X BSA	1 µL
	SfiI (20,000 U/mL)	6 µL
	pComb3XSS	20 µg
	Water	Make up to 100 µL
	Incubation at 50 °C for 5 hours	
	XbaI	3 µL
	XhoI	3 µL
	Incubation at 50 °C for 5 hours	
	10 X Antarctic phosphatase	10 µL
	Incubation at 37 °C for 30 minutes, then 65 °C for 20 minutes	

2.2.1.9 Ligation of SOE insert into pComb3XSS vector

Ligation of the scFv fragment into pComb3XSS was carried out using T4 DNA Ligase. The designed vector pComb3XSS and SOE insert were mixed in a 2:1 (vector/insert) ratio. The samples were incubated at room temperature overnight. Additionally, two ligation controls were set up as well. The Control 1 was prepared to ligate vector DNA

with Stuffer generated from pComb3XSS digestion. The control 2 contained Ligase and vector. The components of the ligation reactions are shown in Table 2.2.1.9. After transforming each ligation samples by electroporation into *E.coli* cells, the ligation control 1 could be used to indicate the ligation efficiency of vector DNA, whereas the ligation control 2 could test the level of background ligation (the detail is discussed in next section).

Table 2.2.1.9 Ligation mixtures for cloning rabbit scFv SOE-product into pComb3XSS vector.

	Component	Volume
Ligation of SOE insert into pComb3XSS vector	pComb3XSS vector	1.4 µg
	SOE insert	700 ng
	10 X ligase buffer	20 µL
	Ligase	10 µL
	Water	Make up to 200 µL

Control 1 was set up to check the ligation efficiency:

	Component	Volume
Control 1	pComb3XSS vector	140 ng
	Stuffer	140 ng
	10 X ligase buffer	2 µL
	Ligase	1 µL
	Water	Make up to 20 µL

Control 2 was set up to check re-annealing of the vector:

	Component	Volume
Control 2	pComb3XSS vector	140 ng
	10 X ligase buffer	2 µL
	Ligase	1 µL
	Water	Make up to 20 µL

2.2.1.10 Transformation of XL-1 Blue *E.coli* cells with pComb3XSS vector containing SOE insert

Transformation of the electrocompetent *E.coli* cells was carried out using the Gene Pulser X-cell electroporation system. After completely thawing *E.coli* cells on ice, 50 μ L of the cells were mixed with each ligation groups which included control and the SOE/vector samples. Three tubes were stored on ice for 1 minute. Each sample was transferred to a pre-chilled electroporation cuvette (2 mm) and electrophoresed at a voltage of 2.5 kV and a capacitance of 25 μ F, a resistance of 200 Ω . A volume of 1 mL of pre-warmed SOC medium was added into each cuvette and the samples were immediately transferred to a sterile tube, which contained 2 mL of pre-warmed SOC medium. The bacterial cultures were incubated at 37°C for 1 hour with shaking at 250rpm before inoculation of serial diluted samples onto 2XTY agar plates, which contained carbenicillin (100 μ g/mL). These plates were incubated overnight at 37°C.

The size of phage library was obtained by counting the colonies on the vector and scFv insert plates and calculating the number of transformants per μ g of vector DNA. Ideally, the final phage library size should be several times 10^8 but at least 5×10^7 total transformants. Additionally, colonies obtained from ligation control 1 were counted. A yield of 10^8 colony-forming units (cfu) per μ g of vector DNA can indicate good vector quality and ligation efficiency. Calculation of cfus per μ g of vector DNA in ligation control 2 was performed to indicate background ligation, where the vectors were self-ligated. Ideally, the colony number from control 2 should be less than 10% from control 1.

The ligated transformant colonies on the plates were scraped off and resuspended in 20% (v/v) glycerol, then immediately stored at -80 °C after snap-freezing in liquid nitrogen. At this stage the phage library of anti-NeoSTX-KLH was ready for bio-panning.

2.2.1.11 Enrichment of rabbit phage library via bio-panning against immobilized STX-OVA conjugations

The phage library was rescued using a stock of commercial M13K07 helper phage. Stored phage library (1mL) was inoculated into 400 mL of 2xTY medium,

complemented with 100 µg/mL carbenicillin. The culture was propagated at 37°C in an orbital incubator until an OD₆₀₀ of 0.4 was reached. Helper phage (1mL) was added and incubated statically at 37°C for 30 minutes before being transferred to a 37°C orbital shaker for 2 hours. A final concentration of 50 µg/mL of kanamycin was added to the culture, and incubated overnight at 37°C.

The STX-OVA conjugate was immobilised on NUNCTM immunotubes. The protocol was as follows: 500 µL of 50 µg STX-OVA in sterile-filtered PBS solution was added into an immunotube, and then left overnight at 4°C. It is crucial to keep the immunotube standing upright to ensure the bottom of immunotube was completely coated with antigen. The immunotube was blocked with 5% (w/v) milk powder (Marvel) in PBS for 2 hours. Meanwhile, the phage library that was incubated overnight was harvested by PEG-NaCl precipitation. Firstly, the phage library was centrifuged at 3,220 g in a GSM rotor (brake-on) for 15 minutes at 4°C. The phage library was precipitated with 4 % (w/v) PEG and 3 % (w/v) NaCl by centrifugation on 18,514 g in a GSM rotor (brake-off) for 20 minutes at 4°C. The supernatant was poured off and the pellet was allowed to drain for 10 minutes before being resuspended in 1mL of KLH-PBS (1mg/mL). A further centrifugation step was carried out to precipitate excess bacterial pellet at 8603 g in an Eppendorf centrifuge (5018R) for 5 minutes at 4°C. Subsequently, 500 µL of this supernatant was added to the immunotube, which has been washed with PBST (150 mM, pH 7.4) and PBS (150 mM, pH 7.4). The immunotube was washed with PBST (150 mM, pH 7.4) and PBS (150 mM, pH 7.4) after incubation at 37°C for 2 hours. This procedure ensures the removal of the weak-binding phage. To elute the bound phage library, a 500 µL of 10 mg/mL Trypsin-PBS was added to the washed immunotube and incubated at 37°C for 20 minutes. Trypsin, one of the most widely used enzyme in proteomics, can cleave peptides on the C-terminal side of amino acid, a lysine and arginine. The eluted solution was transferred into new clean tube and labeled as 'output from the first round of panning'. For re-infection, 200 µL of output from the first round of panning was added to 4 mL of XL1-Blue cells (OD₆₀₀ of approximately 0.5) and allowed to infect for 30 minutes at 37°C. This was plated onto 2xTY plates containing 100 µg/mL carbenicillin and incubated overnight at 37°C. Input and output titres were determined by counting the number of colonies and calculating the number of transformants or colony forming units/mL (cfu/mL). The four rounds of bio-panning used are shown in Table 2.2.1.11.

Table 2.2.1.11 Details of panning strategy used.

	Pan 1	Pan 2	Pan 3	Pan 4
Coating conc. (STX-OVA)	50µg/mL	25µg/mL	5µg/mL	2.5µg/mL
Number of wash	5x PBST/PBS	10x PBST/PBS	15x PBST/PBS	15x PBST/PBS
Culture volume	400mL	100mL	100mL	100mL
Helper phage volume	1000µL	200µL	500µL	500µL

For soluble expression, the output phage from Pan 4 were re-infected into *E. coli* Top10F'. A volume of 200 µL of Pan 4 output was added into 4 mL of Top10F' cells (OD₆₀₀ of approximately 0.5) and allowed to incubate for 30 minutes at 37°C. This was plated onto 2xTY plates with 100 µg/mL carbenicillin and incubated overnight at 37°C.

2.2.1.12 Polyclonal phage ELISA analysis

A polyclonal phage ELISA was carried out with the output phage from Pan 1, Pan 2, Pan 3 and Pan 4. A 96-well plate was coated with 1 µg/mL of STX-OVA and 1 µg/mL of Neo-STX-KLH in PBS (150 mM, pH 7.4), and incubated overnight at 4°C. The following day, the plate was blocked with 200 µL of 3 % (w/v) milk powder (Marvel) in PBS (150 mM, pH 7.4) and incubated for 1 hour at 37°C. After washing 3 times with PBST (150 mM, pH 7.4) and PBS (150 mM, pH 7.4), 100 µL of outputs (1:10 diluted in PBS) from each round of panning was added to the plate and incubated at 37°C for 1 hour. A further wash step was carried out to remove the weakly bound phage and then 100µL of horse-radish peroxidase (HRP)-labelled anti-M13 antibody (diluted 1/1,000 in a 1 % (w/v) milk-powder/PBS) was added to each well. After incubation for 1 hour at 37°C, the final wash step was performed as above. A 100 µL volume of TMB substrate solution was prepared in 0.05M phosphate-citrate buffer, pH 5.0, and then added to the plate. The plate was then covered in tinfoil and left for 20 minutes incubation at 37°C. The reaction was stopped by addition of 50 µL per well of 10 % (v/v) HCl. Subsequently, the absorbance was determined at 450 nm with a Tecan™ Safire plate reader.

2.2.1.13 Direct monoclonal ELISA of solubly-expressed scFv fragments

Single colonies were picked from pan 4 Top10F' re-infection plates and transferred into sterile non-absorbent 96 well plates, contained 100 μ L of SB broth and 100 μ g/mL carbenicillin. These single clones were incubated at 37°C overnight in an orbital incubator and labeled as "stock plates". Subsequently, 25 μ L of each colony was transferred into new sterile non-absorbent 96 well plates, which contained 175 μ L of SB broth and 100 μ g/mL carbenicillin. The plates were incubated at 37°C in an orbital incubator until an OD600 of 0.6-0.8 was reached. Meanwhile, the stock plates were mixed with 80% (v/v) glycerol to give a final concentration of 20 % (v/v). These plates were stored at -80 °C. To induce expression of the scFv fragments, a final concentration of 1mM IPTG was added into each transferred colony culture and incubated at 37°C overnight in an orbital incubator. The plates were then centrifuged at 3,220 g (Eppendorf centrifuge 5018R) for 40 minutes. The supernatant was carefully removed and the pellets were resuspended in 200 μ L sterile PBS (150 mM, pH 7.4). In order to extract the periplasmic scFv from the precipitated cells, the plates were freeze-thawed three times. After the final thaw, the plates were centrifuged at 3,220 g (Eppendorf centrifuge 5018R) for 5 minutes and the supernatant containing the scFv fragment, was used for ELISA analysis.

The 96 well ELISA plates (Maxisorp™, NUNC™) were prepared by coating wells with 1 μ g/mL of STX-OVA and 1 μ g/mL Neo-STX-KLH in PBS (150 mM, pH 7.4), and incubating overnight at 4°C. The next day, 200 μ L of 3 % (w/v) milk powder (Marvel) in PBS was added to each well and incubated for 1 hour at 37°C. After 3 washes with PBST (150 mM, pH 7.4) and PBS (150 mM, pH 7.4), the plates were incubated with 100 μ L per well of scFv-containing supernatant for 1 hour at 37°C. A further wash step was carried out to remove the weakly bound scFv fragments and a 1:2,000 dilution of HRP-labelled anti-rabbit polyclonal antibody was added to each well. After 1 hour incubation at 37°C, a final wash step was performed. A 100 μ L volume of TMB was directly added to the plates followed to 20 minutes incubation in the dark. The reaction was stopped using 50 μ L per well of 10 % (v/v) HCl, after which the absorbance was measured at 450 nm on a Tecan™ plate reader.

2.2.1.14 Re-infection into Top10F' cells and scFv check via colony-pick PCR

Individual colonies, which were re-infected into Top10F', were picked from pan 4 agar plates and inoculated into 50 μ L sterile water for 10 minutes at 95°C to induce cell lysis. These lysed samples were PCR amplified, as described in Section 2.3.3. The PCR products were analysed by electrophoresis on a 1 % (w/v) agarose gel.

2.3 Methods for development of microfluidic platforms

In the following sections all methods applied for the preparation, processing and readout of the immunoassay cartridges are discussed. Initially the structures of the microfluidic platforms developed are illustrated. Fabrication methods for the microfluidic platforms are then presented. Subsequently, experimental setups for fluorescence-based microfluidic investigations are described. Finally, microfluidic immunoassay analysis methods are explained.

2.3.1 Structures of microfluidic platforms

In this study, three microfluidic platforms with different complexity of microchannel networks were developed. All of the microfluidic platforms were designed using the CAD software package Pro/Engineer (PTC, US). These three microfluidic platforms had a common feature, which is they consisted of laminated layers, including a Poly-(methyl methacrylate) (PMMA), a pressure sensitive adhesive (PSA), and a cyclic olefin polymer (COP) slide (Zeonor[®]), or Zeonor slide. The PMMA layers were applied to provide big chambers for reagents, such as reservoirs, waste chambers. The PSA layers with a 50 μ m thickness generally were used to provide microchannels, whereas, the COP layers were used as the substrate for solid-phase microfluidic assays.

2.3.1.1 Flow-cell

The flow-cell was a 'proof-of-concept' microfluidic platform with a relatively simple microchannel network. As shown in Fig. 2.3.1.1, it consists of five laminated layers. The first and the third layer were made from PMMA. The former provided loading and

venting holes whereas the latter provided reservoirs, valves and venting holes. The second and fourth layers of flow-cell were made from PSA, whose role was to provide microchannels and stick to the PMMA layers. On these four layers of the flow-cell, holes lying at same position provided a pin hole for the flow-cell assembly. The bottom layer was Zeonor slide made from COP (Zeonor[®]), on which the protein A was immobilized. The assembled five layers with different patterns constituted the flow-cell, which allowed three parallel assays.

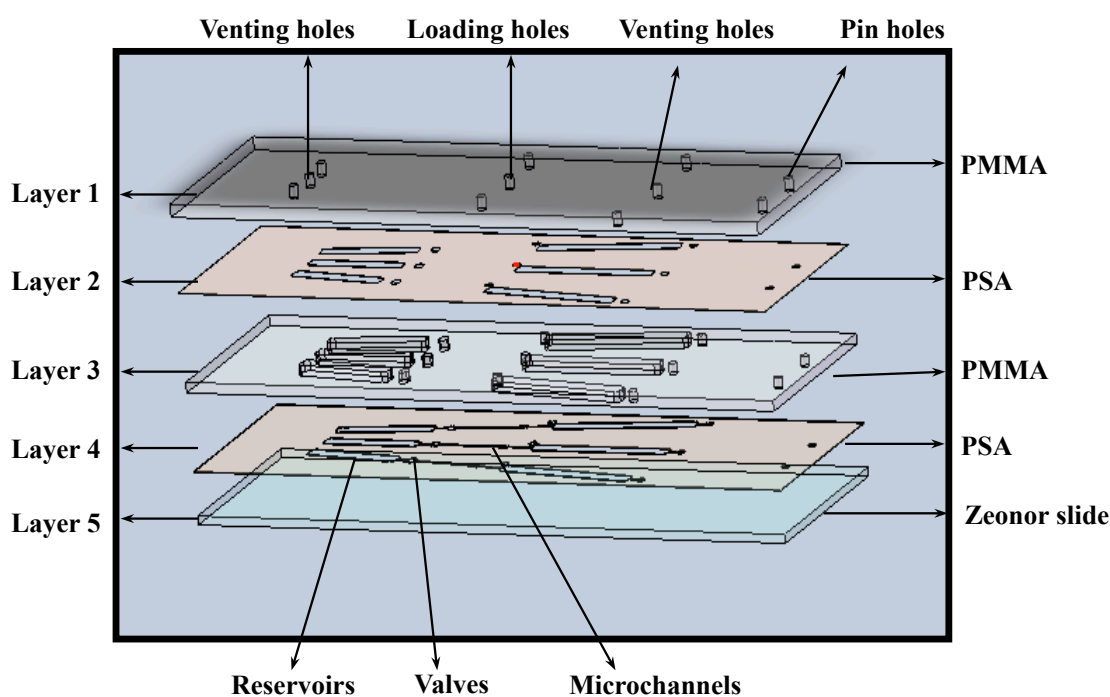


Figure 2.3.1.1 Schematic of flow-cell structure. The flow-cell contains five layers with different patterns: two PMMA layers, two PSA (pressure sensitive adhesive) layers and one Zeonor slide. The first PMMA layer acts as a cover of assay system, providing various holes. The second PMMA layer provides reservoirs and valves. The main functions of the two PSA layers are to adhere the PMMA layers and the Zeonor slide together and to provide the microchannels.

2.3.1.2 ‘Supercritical angle fluorescence’ (SAF) element compact-disc

This microfluidic platform was also developed in a compact-disc (CD) format in our study. It was named a ‘SAF’ element CD due to the application of the supercritical angle fluorescence-based optical detection method, which is described in section 2.3.4. The ‘SAF’ element CD consisted of laminated layers of PMMA, PSA and injection-moulded COP SAF (Zeonor[®] 1060R chips). The five different layers of the ‘SAF’ element CD were shown in Fig. 2.3.1.2. Additionally, the structure of ‘SAF’ element CD was illustrated in various perspectives. Fig. 2.3.1.2A shows the top view of the different layers, including the top disc, top PSA, middle disc, middle PSA and SAF disc. The top and the middle disc were made from PMMA. The former (1.5 mm thick) provided loading and venting holes whereas the latter (2.0 mm thick) provided reservoirs, and valves. The top and middle PSA (50 μ m thick) provided microchannels and sticks the PMMA discs together. The bottom disc was an injection-moulded Zeonor slide (1.7 mm thick), with SAF optical structures. On these five discs, the extra three holes on the edges provided pin holes for the CD assembly. Fig. 2.3.1.2B illustrates the 3D layers of the ‘SAF’ element CD. The spatial sequence of CD layers is clearly exhibited. Fig. 2.3.1.2C shows the top view of an assembled ‘SAF’ element CD. It contained 20 microfluidic units, which allow 20 parallel assays. This element was carried out in conjunction with researchers from the School of Physical Sciences at DCU.

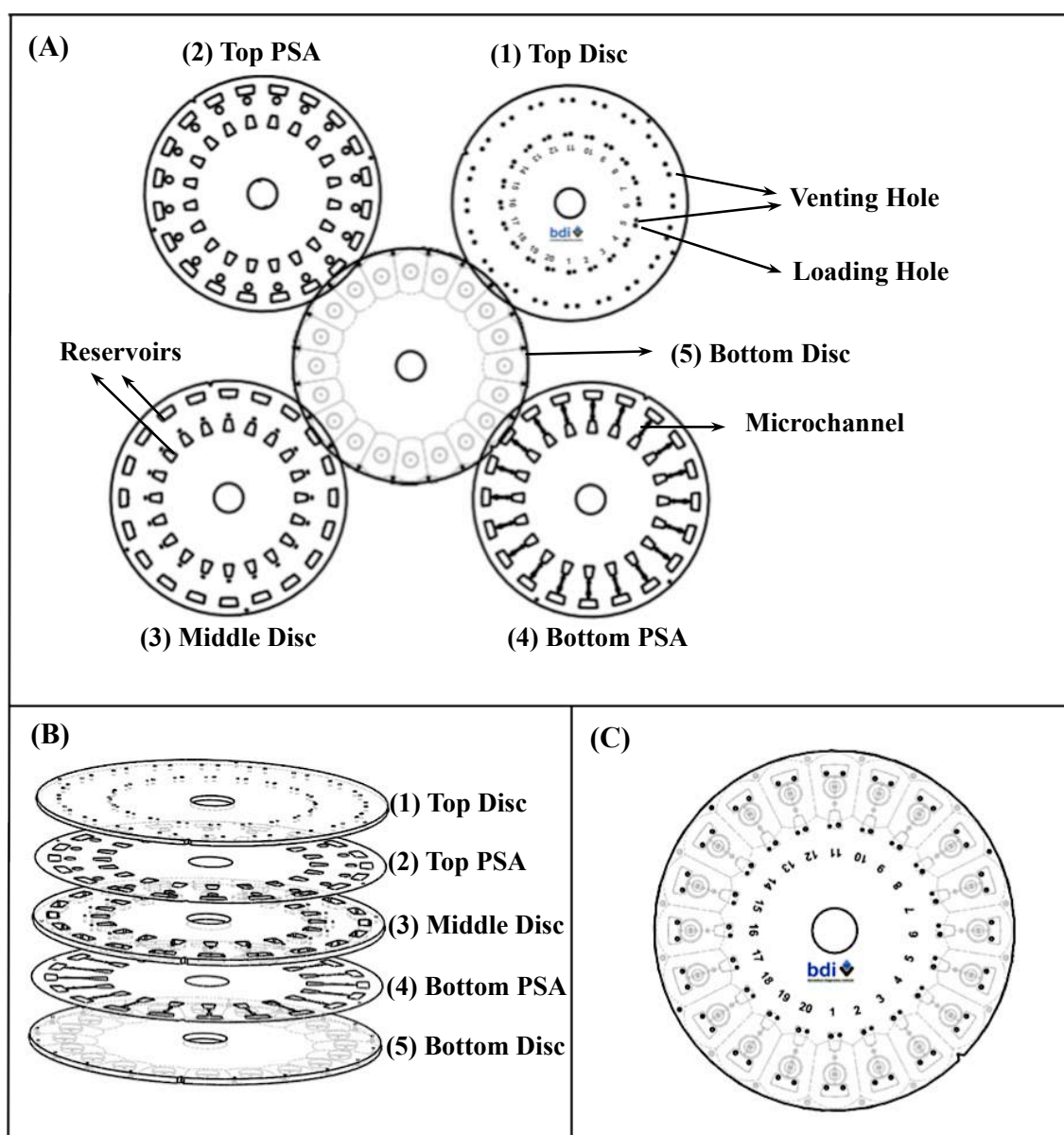


Figure 2.3.1.2 Schematics of 'SAF' (supercritical angel fluorescence) elements of the CD structure at three angles of view. Fig. A shows the top view of the five different layers, including: (1) Top disc (1.5mm thick PMMA) with sample loading and air venting holes, (2) Pressure sensitive adhesive (50 μ m thick) with chamber features, (3) Middle disc (2.0 mm thick PMMA) with chamber features, (4) Pressure sensitive adhesive (50 μ m thick) with microchannel, (5) Bottom disc (1.7mm thick) with 20 SAF ring lens on the lower side. A schematic of the spatial sequence of these five discs is given in Fig. B. The top view of assembled 'SAF' element CD is illustrated in Fig. C.

2.3.1.3 Reagents delivery CD

In the last section, the structure of ‘SAF’ element CD was introduced. In this section, another generation of CD which is designed with a combination of SAF detection and serial siphon will be described. This new generation of CD possesses advanced features of reagents sequential delivery, therefore; it is also named as ‘reagents delivery CD’.

The 3D structure of reagents delivery CD was illustrated in Fig. 2.3.1.3. The reagents delivery CD contained four SAF chips and five layers with different patterns. Both layer 1 and layer 5 were made from 1.5 mm thick PMMA. Layer 1 worked as the cover and provided loading and venting holes whereas layer 5 worked as the holder for SAF chips. Layer 3 was made from 2.0 mm thick PMMA, containing reservoirs and reagent delivery microchannels. Layers 2 and 4 were made from PSA with 50 μm thick provided microchannels. In addition, the PSA between PMMA layers worked as adhesives. . The four SAF chips with amine groups and optical ring lens, were adhered to the CD by a middle layer of PSA. Additionally, two pin holes on the edges were designed to assist the CD assembly. The reagent delivery CD contained four parallel functional areas. For each of the assay areas, all four reagent chambers and the centre straight chamber were connected with designed serial siphons respectively. A waste chamber was designed for collecting reagents.

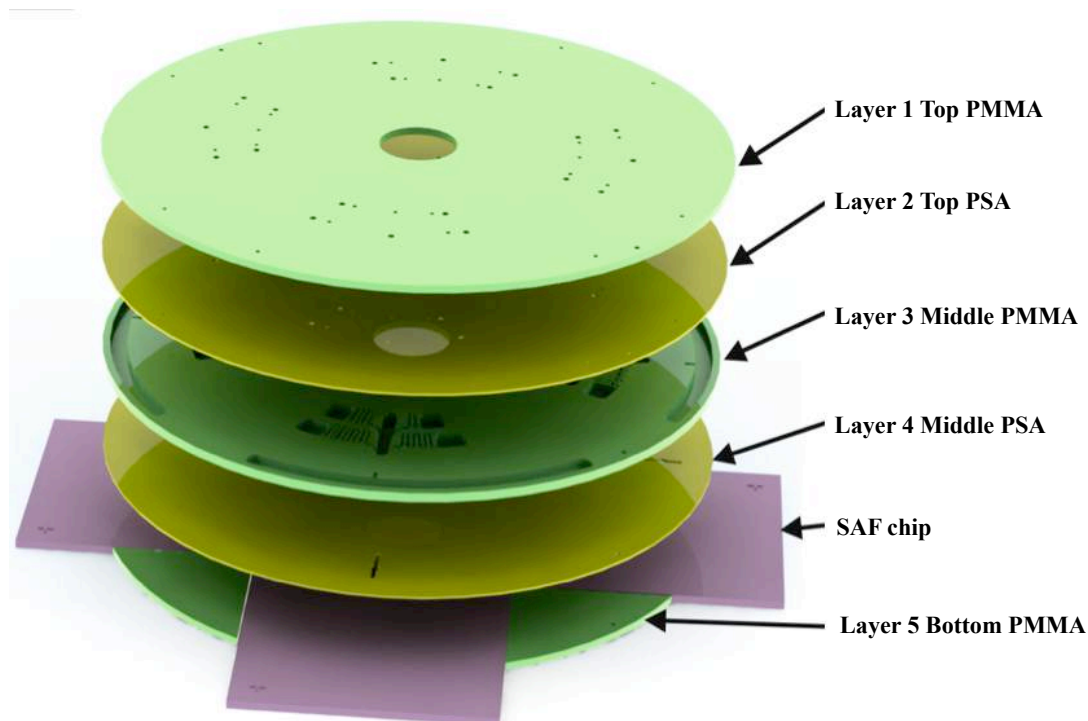


Figure 2.3.1.3 A schematic of reagent delivery CD structure. It shows the six different layers, including (1) top disc (1.5mm thick PMMA) with sample loading and air venting holes, (2) PSA (50 μ m thick) with loading and venting holes, (3) middle disc (2.0 mm thick PMMA) with reagent chambers and serial siphon features, (4) PBS (50 μ m thick) with assay channel, (5) SAF chips (1.7mm thick) with an amine surface for protein immobilization, (6) Bottom disc (1.5mm thick) to seal off the SAF chips.

2.3.2 Fabrication methods for microfluidic platforms

The microfluidic platforms in this study contain different layers with various materials and various sizes of channels, as introduced in the previous section. Therefore, different fabrication methods and tools were required to manufacture the micro-components. In this section, three machines used in this study are discussed, including a computer numerically controlled (CNC) laser cutting machine (Zing 16 Laser, Epilog, USA), a CNC milling machine (MDX-40A, Roland, Japan) and a knife-cutter plotter (Graphtec, Graphtec CE-2000, Japan).

This laser cutting system was widely applied in manufacturing micro-components

whose feature size is larger than 50 μm (Godino *et al.*, 2012; Gubala *et al.*, 2013; Nwankire *et al.*, 2013;) due to the relatively low-cost, quick processing and ease of operation. In this study, it was used to mechanically manufacture the relatively large components in PMMA, including the outline of the flow-cell and disc, reservoirs, chambers and holes on the top layers.

The CNC milling system shows significant potential for the manufacture of small micro-components with greater precision and a better surface finish (Karle *et al.*, 2010; Mark *et al.*, 2011). In this study, the Roland MSX-40A CNC machine with a powerful 3D milling device, was applied to precisely manufacture the siphons and capillary valves on the middle PMMA layer of the reagents delivery CD.

The cutter plotter was used to cut channels widths as narrow as 200 μm in thinner materials such as 50 μm PSA (Bartholomeusz *et al.*, 2005; Siegrist *et al.*, 2010). A cutter-plotter (Graphtec, Graphtec CE-2000, Japan) was used to cut PSA patterned with micro-components, such as microchannels.

Once the design and machining of the microfluidic flow cells/CDs were completed the patterned layers of microfluidic platform were aligned and assembled with a temperature controlled roll laminator (Hot Roll Laminator, ChemInstruments, USA). Each of the microfluidic structures was inspected for faults and imperfections when assembled before they were used for testing.

2.3.3 Surface modification methods

In this study, COP ZeonorTM was integrated into microfluidic platforms and was used as the substrate for solid phase assays. Although COPs have excellent properties for many applications, they are lacking in active groups to facilitate covalent functionalisation. Additionally, COPs are hydrophobic, and therefore need to be modified to provide hydrophilic properties. This can be achieved in several ways: e.g. photografting (Stachowiak *et al.*, 2007) ozonolysis (Diaz-Quijada *et al.*, 2007) or using oxygen plasmas (Larsson *et al.*, 2007). Surface activation of COPs by use of oxygen plasmas was been demonstrated extensively (Borcia *et al.*, 2006; Riyadh *et al.*, 2007; Yu *et al.*,

2015). The process of oxygen plasma-based surface modification is commonly applied because it is fast and homogeneous and no hazardous chemicals are required. After activation by oxygen plasma, the surface of the COP Zeonor™ was cross-linked with aminosilanes. APTES is one of the most commonly used aminosilanes due to its simple structure and minimal cost. There are two general APTES-based deposition methods i.e. liquid-phase and vapor phase deposition. Liquid-phase treatments with aminosilanes to create surfaces that are reactive towards antibodies and other specific binding molecules have been extensively investigated (Yakovleva *et al.*, 2002; Bange *et al.*, 2005; Kim *et al.*, 2011; Nwankire *et al.*, 2014). This method contains multiple steps and therefore is not suitable for large-scale production. In contrast to liquid-phase treatment, PECVD treatment is a fast and simple route to versatile amine-functionalized surfaces on COP plastics by a combination of the oxygen plasma activation method with plasma enhanced chemical vapour deposition from an aminated precursor (Volcke *et al.*, 2010). It is a single step high throughput process, and is a versatile surface engineering technique which has proven to be an excellent tool for surface modification and large-scale production that does not leave behind liquid waste (Gandhiraman *et al.*, 2010; Gandhiraman *et al.*, 2012).

Both surface modification methods were applied and developed in this study. The developments involved in the research described in this thesis, such as selection of concentrations of APTES applied and the curing times, are discussed in Chapter 4. Descriptions of two surface modification methods developed and used in this study follow.

Before the surface modification step, the COP Zeonor™ slides/chips needed to be completely cleaned by ultrasonication to allow effective functionalisation of the surface. Hence, a 2% (v/v) solution of Micro-90™ was used to remove oil, grease, resin and any biological material by sonication at 50 °C for 30 minutes. Subsequently, the COP Zeonor™ slides were rinsed three times with deionised (DI) water and a 100% (v/v) solution of isopropyl alcohol. The slides were then rinsed again with DI water and dried with a stream of nitrogen. After cleaning, the COP Zeonor™ slides were placed in plastic bags and stored in a desiccator.

2.3.3.1 Amine surface functionalisation by liquid phase

For the liquid phase-based amine slide functionalisation, a multi-step procedure was performed. In this process the surface of the slides were activated by an oxygen plasma stream, which promote surface oxidation and hydroxylation (-OH groups). After that, the slides were coated with a solution of 3-aminopropyltriethoxysilane (APTES). The full procedure is outlined as below.

A microwave-induced plasma was generated by a Harrick plasma cleaner. The operating pressure of the chamber was set using a scroll pump and a mass flow controller. The oxygen was applied as a gas stream, regulated by the integrated mass flow controller and adjusted to approximate 1000 mT. The Zeonor™ chips were exposed to the oxygen plasma for 10 minutes. The surface-activated slides were immediately placed into a solution of APTES as plasma treatment is highly unstable and decays rapidly. A 3% (v/v) solution of APTES that contained 5% (v/v) 2-propanol was used to amine functionalise the Zeonor™ slides. The slides were incubated in this solution at room temperature for 2 hours (Fig. 2.3.3.1). After functionalisation, the slides were ultrasonically cleaned for 15 minutes (2x) using a 100% (v/v) solution of isopropyl alcohol. The slides were then baked in an oven at 80 °C for 1 hour.

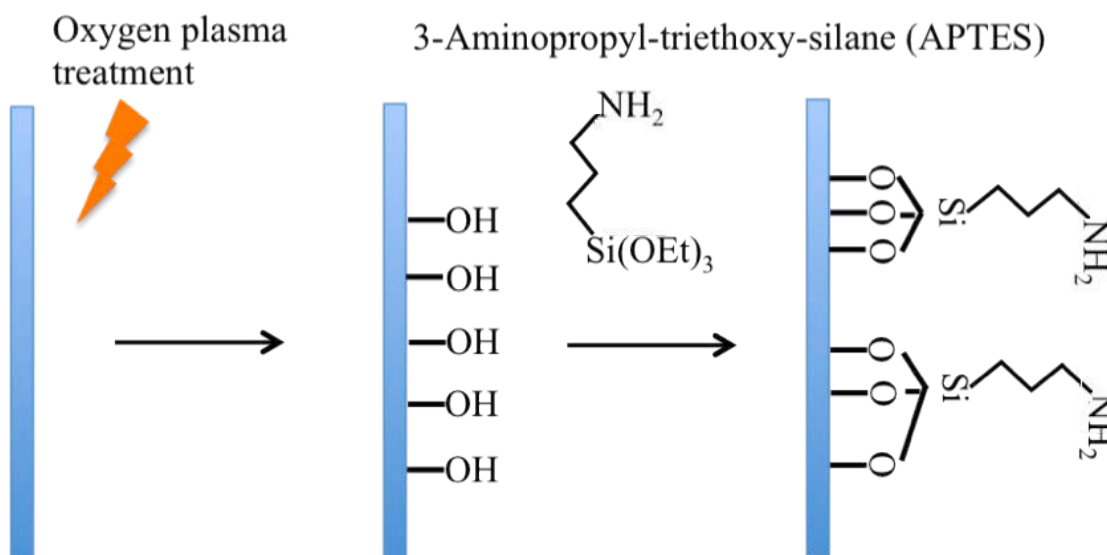


Figure 2.3.3.1 A schematic of Zeonor slide functionalisation with plasma treatment and liquid-phase APTES deposition. A Zeonor slide was first hydroxylated through oxygen plasma treatment, followed by silanization with APTES solution. The -NH₂ groups on the factionalised Zeonor surface were able to react with proteins.

2.3.3.2 Amine functionalisation by chemical vapour deposition

In addition, to the liquid phase APTES surface functionalisation, a second method, plasma enhanced chemical vapour deposition (PECVD), was used to amine-functionalise the surface of the Zeonor slides and the SAF ring lens chips. In contrast to liquid phase depositions described above, PECVD treatments tend to produce a more homogeneous and denser surface coating (Gandhiraman *et al.*, 2011; Le *et al.*, 2011;).

An Oxford Plasmalab System100 PECVD reactor was used to carry out the deposition experiments. The process chamber is configured as a capacitance coupled system with an operating frequency of 13.56 MHz. This reactor was capable of distributing gas and APTES vapour uniformly in the chamber due to a combination of an electrically isolated gas spreader and a radio-frequency (RF) powered showerhead.

Zeonor slides were placed in the chamber, which maintained at a pressure of 200 mTorr during all process phases. Prior to APTES deposition, plasma pre-treatment was performed to oxidise the surface of Zeonor slide, using a mixture of argon and oxygen, and input power was set to 150 W for 3 minutes. After this pre-treatment, oxygen flow was stopped; the process power reduced to 5 W, and then APTES vapour was introduced to the chamber. The liquid APTES was supplied to the chamber through a heated stainless steel canister. There was a tendency of the APTES vapour to polymerise between the canister and chamber due to the thermal contours within the gas lines. In order to suppress this condensation, which could lead to blockages or loss of flow to the chamber, the gas lines used were maintained at an elevated temperature.

After either liquid phase or PECVD APTES treatments, the SAF chips were manually spotted with 30 μL of Protein A at a concentration of 10 $\mu\text{g mL}^{-1}$ and incubated at 4 °C overnight. Subsequently, the chips were blocked for 1 hour at 37 °C with a 30 μL of a 1% (v/v) solution of 'IgG-free' BSA. The chips were then washed 3 times with PBST and PBS, after which they were dried using either a stream of nitrogen or incubation at 37 °C for 20 minutes.

2.3.4 Hardware instrumentation

2.3.4.1 Supercritical angle fluorescence (SAF) prototype detector

For fluoroimmunoassays, a fluorescence binding protein (NeutrAvidin-Dylight 650) was used to detect human IgG. In order to efficiently detect the fluorescence signal, an "in house" prototype SAF optical reader system designed by Dr. Dirk Kurzbuch and Mr. Martin Sommers (DCU, BDI), was applied. A diagram of the prototype instrument is shown in Fig. 2.3.4.1. This prototype instrument allows the detection of low levels of analyte in small volumes. The system utilises a SAF signal enhancement element known as a SAF lens. Due to its high collection efficiency optics, this device can collect a large amount of fluorescent light. Furthermore, SAF detection allows the collection of fluorescence only from molecules that are in close proximity to the interface of the substrate and the sample solution and not from the bulk solution (Kurzbuch *et al.*, 2009 & 2013). This important aspect of SAF leads to substantial reductions in background signal and can be a substantial advantage over other methods especially in turbid media and autofluorescent environments.

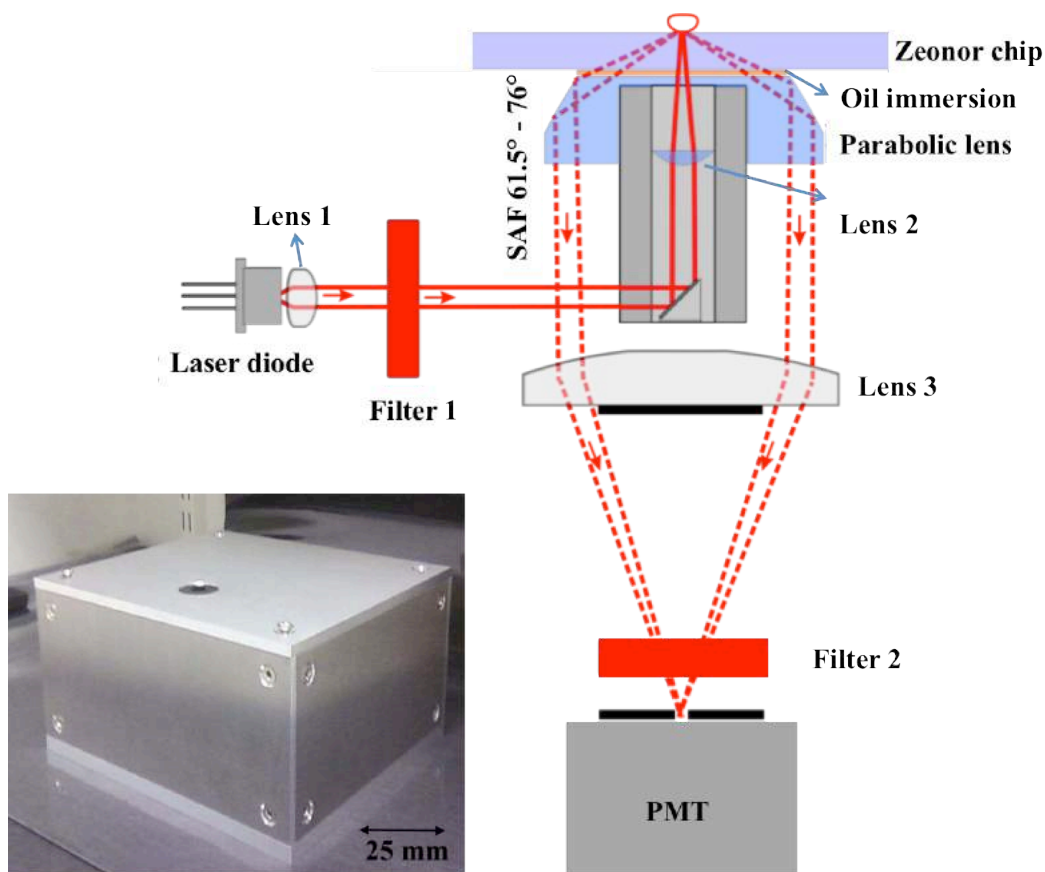


Figure 2.3.4.1 Schematic representation of the SAF-reader.

A laser diode (Roithner Lasertechnik, Austria) with a wavelength of 635 nm is used to excite the chip through a filter (FF01- 625/26-25, Semrock Inc., USA). The parabolic collector is made of Zeonex 480R, a high transmission, mouldable plastic, and features a diameter of 16 mm and a focal length of 100 mm. An aspheric lens (*lens 2*, $f_1 = 5$ mm) focuses excitation light onto the top surface of the biochip. In the presence of oil immersion, supercritical angle fluorescence emitted between 61.5° and 76.0° is collected and collimated by total internal reflection at the parabolic surface. A planoconvex lens (*lens 3* = 30 mm, diameter = 30 mm) is used to focus the emitted fluorescence through a detection aperture onto the photomultiplier (H8259-02 PMT module, Hamamatsu, Japan). A combination of an emission filter (FF01-676/29-25, Semrock Inc.) and detection aperture (diameter = 800 nm) is used to block excitation light. In this device, the minimum angle of collection is limited to 61.5° by the outer radius of the parabolic element, and maximum angle is limited to 76.0° due to geometric reasons. However, 98% of SAF signal was collected between these two angles.

2.4 Immunoassay experimental methods

Initially optimisation of the hIgG fluorescence-immunoassay (FIA) was carried out using conventional 96-well microtitre plates. At this stage no surface modifications were necessary as microtitre plates are commercially manufactured with high capacity protein binding surfaces.

2.4.1 Procedure for conventional hIgG FIA.

Protein A

Protein A, the IgG capture protein was diluted to 5 µg / mL in PBS (150 mM, pH 7.4) and 100 µL was added to the microtitre plate. The plate was covered and incubated at 4°C overnight. After coating, the plate was washed 3 times with PBST (150 mM, pH 7.4) and PBS (150 mM, pH 7.4), the plate was emptied and tapped to remove excess liquid after each wash cycle.

Blocking

A volume of 300 µL of 3% (v/v) BSA 'IgG-free' in PBS (150 mM, pH 7.4) was added to each protein A-coated well. After 1 hour of incubation at 37°C, the plate was then washed 3 times with both PBST and PBS.

hIgG samples

A series of dilutions of hIgG was prepared in PBS (150 mM, pH 7.4) and 100 µL of each sample was added to the plate. In addition, a negative control with no hIgG (100 µL PBS) was also set up. The hIgG samples and the negative controls were then incubated at 37°C for 1 hour. Subsequently, the plate was washed 3 times with both PBST and PBS.

Secondary antibody

A biotinylated, secondary anti-human-IgG antibody was diluted to 1:500 in PBS (containing 1% (w/v) BSA). One hundred µL of the diluted solution was added to each well and incubated at 37°C for 1 hour. After the incubation, the plate was then washed 3 times with both PBST and PBS.

The detector antibody

A biotin-binding fluorescent protein conjugate, Neutravidin-Dylight 650, was diluted to 1:500 in PBS and 100 μ L of the diluted solution was added to each well. This was followed by incubation at 37°C for 1 hour, the plate was washed 3 times with both PBST and PBS.

Fluorescence detection

After addition of 100 μ L of PBS to each well, detection was carried out on a Tecan Microplate ReaderTM with excitation at 654 nm and emission at 673 nm. The raw fluorescence signal values from each well were saved in an excelTM file.

2.4.2 Procedure for FIA on microfluidic flow-cell devices

Once the surface modification was complete, 30 μ L of a solution of 10 μ g/mL Protein A was spotted onto the Zeonor slide. After overnight incubation at 4 °C, the slide was blocked with 3 % (v/v) BSA in PBS. Following incubation at 37°C for 30 minutes, the slide was carefully rinsed with 1XPBST and PBS, and then carefully dried with nitrogen. Subsequently, the five layers of the flow-cell device were manually assembled in a clean room.

The flow-cells were fitted into a ‘CD-like’ holder (Fig. 2.4.2). This holder was then placed onto an instrument which allows for centrifugal spinning, i.e. on the spin test stand. In total 30 μ L of each of the assay reagents (BSA, PBS, hIgG, anti-human IgG and Neutravidin-DyLight) were sequentially loaded into a loading hole on the microfluidic flow cell. Centrifugal force was used to flow each solution over the protein A spot. The spin rate was adjusted manually to ensure that each liquid flowed at roughly the same speed. Each solution was removed from the microfluidic flow cell waste chamber before the addition of the next solution. After the addition of each solution the microfluidic flow cell was incubated at room temperature for 5 minutes. Fluorescence was measured immediately after the last wash step using the prototype SAF reader system. The excitation and emission wavelengths were 652 nm and 672 nm, respectively.

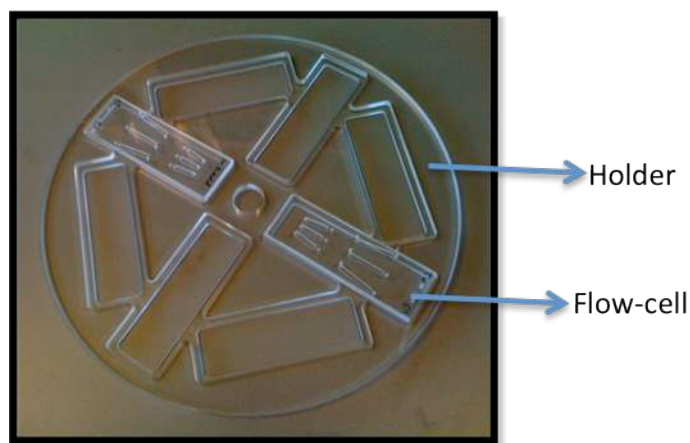


Figure 2.4.2 Illustration of holder for flow-cell immobilisation.

2.4.3 Procedure for FIA analysis on microfluidic CDs

In this section a description is given of the microfluidic FIA analysis, which utilises two different types of microfluidic CDs, shown in Fig 2.3.1.2 and Fig. 2.3.1.3.

FIA analysis using SAF elements CD

Prior to performing hIgG FIA analysis reagents were diluted with PBS (150 mM, pH 7.4). In addition, a biotinylated anti-human-IgG antibody, and a Neutravidin-Dylight 650 were diluted in PBS (150 mM, pH 7.4) at a ratio of 3:1. This mixed solution was covered with tinfoil and incubated at 37°C for 20 minutes. The FIA reagents (30 µL) were sequentially added in the reagent chambers through the loading hole, and centrifugally propelled across the ‘protein A’ capture spot. The loading sequence was as follows: BSA (3% (v/v) in PBS), hIgG standards, PBS (150 mM, pH 7.4), fluorescent detector reagent, and PBS (150 mM, pH 7.4). Fluorescence was measured immediately after the last wash step using our prototype SAF reader system.

FIA analysis using reagents delivery CD

Prior to microfluidic FIA testing, reagents were diluted with PBS and Tween[®] 20 (TW-20) (PBST). In addition, a biotinylated secondary anti-human-IgG antibody, and a Neutravidin-Dylight 650 were diluted in PBS (150 mM, pH 7.4) at a ratio of 3:1. The fluorescent detection reagent was subsequently incubated in the dark at 37°C for 20 minutes. FIA reagents (30 µL) were added in their designated chambers, and propelled

across the 'protein A' capture spot. The delivery sequence and TW-20 concentrations of the FIA reagents were as follows: BSA (1 % (w/v) in PBST with 0.6 % (v/v) TW-20), hIgG standards (0.16, 0.8, 2, 4, 20, 50, 100 $\mu\text{g mL}^{-1}$) and diluted bioprocess sample (PBST with 0.6 % (v/v) TW-20), wash solution 1 (PBST with 0.4 % (v/v) TW-20), fluorescent detector reagent (PBST with 0.7 % (v/v) TW-20) and wash solution 2 (PBST with 0.4 %v/v TW-20). Fluorescence was measured immediately after the last wash step using the prototype SAF reader system. The excitation and emission wavelengths were 652 nm and 672 nm, respectively.

2.5 Immunoassay data analysis methods

2.5.1 Fitting of microfluidic FIA curves and analysis of bioprocess samples using SigmaPlot®

Quantitative immunoassay relies on a calibration curve to determine the analyte concentration in samples from the intensity of signal produced. The calibration curve is a plot of calibrator concentration against signal level. The SigmaPlot® software was used in this research to fit data generated by the microfluidic hIgG FIA curves. In addition, industrial bioprocess samples were also analysed. The macro panel in Fig. 2.5.1 shows the various standard curve options. Analysis was performed as follows:

- (1) Select the 4-PL equation from the equation list and use this function to fit the curve
- (2) Select the columns to use for the X and Y data from the X data column and Y data column drop list boxes.
- (3) Use the *Log format X data* checkbox to select whether or not to plot the X-axis using a common log-scale.
- (4) Select the '*Predict unknowns*' option to compute results using the solution to the fit. Also select the *Plot predicted values* checkbox to plot the predicted values on standard curve.
- (5) When finished, click *OK*. A standard curve is created with plotted drop lines to indicate the unknown values.

A sample of a plotted standard curve with indicated unknown is shown in Fig.

2.5.1 For the standard curve, the concentration values were plotted against the response (with error bars), and the lines of dashes indicated the X and Y values of the unknowns.

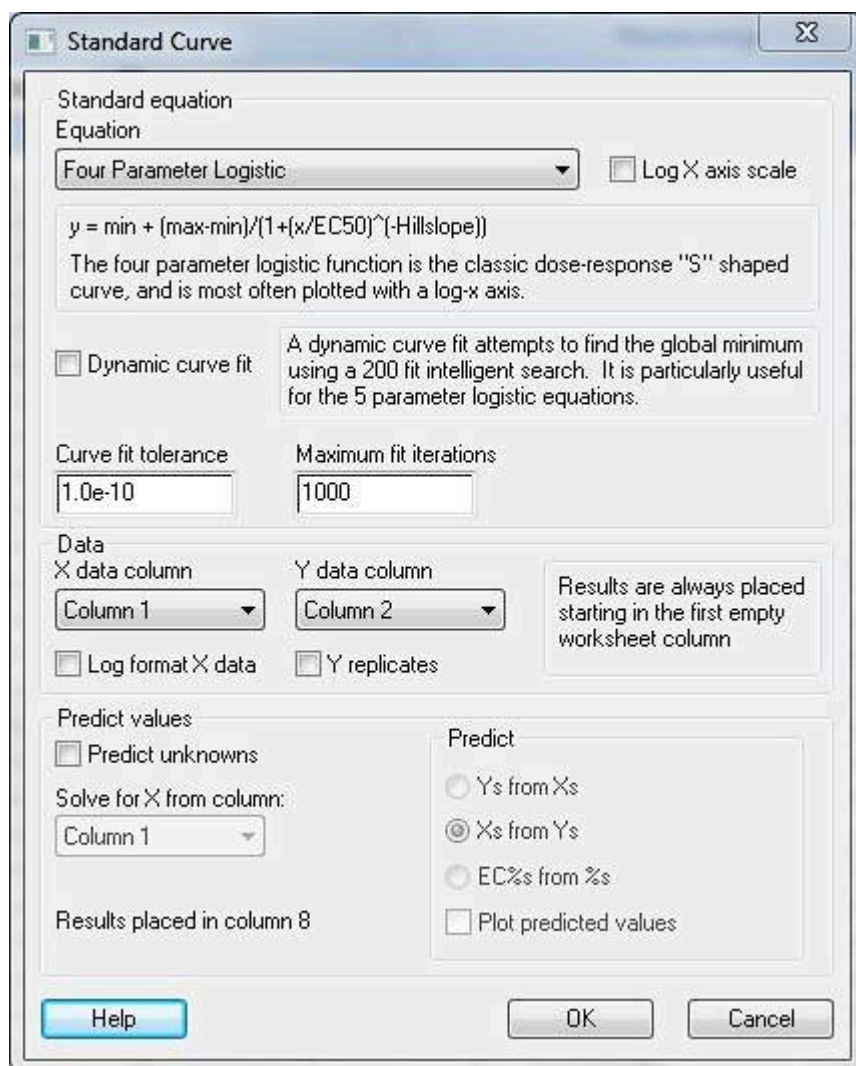


Figure 2.5.1 Illustration of the micro panel tabs in the Sigma Plot software.

2.5.2 Fluorescence image analysis using the Andor camera

Fluorescence assay spots from microfluidic CD/slides were imaged using a (Olympus IX71) microscope that incorporated a unique camera (ANDOR iXon 885). The Andor camera was chosen as it has extreme sensitivity, rapid frame rates and high resolution. In this fluorescence microscope, polychrome V (PV) was used as the excitation light because 1) it provided the user with the ability to adjust the excitation wavelength and 2) it shows over 60% quantum efficiency (QE) at 652nm, which is the wavelength of light needed to excite the NeutrAvidin DyLight-650 fluorophore. In addition, this highly sensitive microscope also contains advance image analysis software.

Each of the SAF ring lens chips was cut out of the CD using the CNC milling machine. Each ring lens chip was then analysed using the 4X objective lens on the Andor camera. A green filter was used for FLISA spot image generation as this offered better image clarity than the corresponding red filter. The image of emission light of the NeutrAvidin DyLight-650 fluorophore at a wavelength of 672nm was collected and then analysed using the microscope's image analysis software.

2.6 Computational simulation

Microfluidic networks offer several advantages over conventional microtitre plates where the assays are performed using much larger volumes and longer times. However, to take full advantage of microfluidic networks, it is important to understand the influence of factors (such as flow velocity, channel height and capture area length) on binding kinetics and to identify the major parameters affecting assay performance in microfluidics. In this section, theoretical models applied to investigate the effect of these factors are introduced.

2.6.1 Theoretical models

As shown in Fig. 2.3.1.3, the microfluidic networks are complicated due to the sequential delivery of reagents. However, the characteristics of assay related microchannels are simple as illustrated in Fig. 2.6.1.

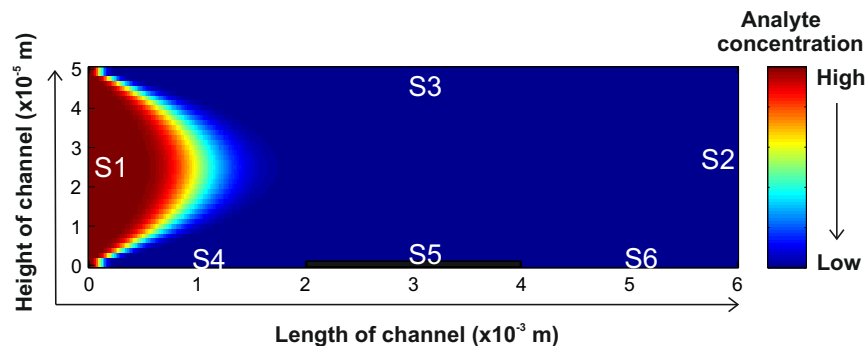


Figure 2.6.1 Schematic diagram of 2D model of the microchannel. The analyte molecules flow into this microchannel with a velocity which shows a parabolic profile. Then they will be transported to the capture area (functionalized and located between 2×10^{-3} to 3×10^{-3} m on the wall), through convection and diffusion. The boundaries of this model were divided into six different surfaces with distinct conditions.

This microchannel has a length of $6000 \mu\text{m}$ and height of $50 \mu\text{m}$. The capture area had a length of $2000 \mu\text{m}$. In the application, Protein A was immobilized on the capture area to bind IgG molecules. When the IgG in bulk solution flowed into the microchannel with a

certain velocity, there are three processes involved: (1) convection along the x-axis of the microchannel; (2) diffusion from the bulk solution to the capture area and (3) adsorption on the surface by binding to Protein A (Gulliver *et al.*, 2007; Parsa *et al.*, 2008). These three processes are described by the convection-diffusion equation of the form

$$\frac{\partial C}{\partial t} = D\Delta C - \vec{u}\nabla C + R \quad \text{Equation (1)}$$

where C is the concentration of analytes in bulk solution, D is the diffusion coefficient of analyte, \vec{u} is the value of local velocity of bulk solution in the microchannel, and R is the source term (Berthier *et al.*, 2010). This partial differential equation obeys the law of conservation of mass, where the changes of analyte concentration in bulk (the left-hand side) equal the sum of replenishment of analyte by transport (diffusion and convection) and the consumption due to adsorption (the right-hand side). Inside a rectangular microchannel with micrometer height, the fluid is typically laminar (Reynolds number $Re \ll 1$). Hence, the velocity profile is a Hagen-Poiseuille flow profile (parabolic flow profile), with maximum velocity at the geometric center of the microchannel and zero velocity at the wall of microchannel (Berthier *et al.*, 2010). Therefore, \vec{u} in the microchannel is inconsistent. In the 2D case of a rectangular microchannel, the value of \vec{u} along vertical axis is

$$v(y) = \frac{3}{2}\bar{v}[1 - (\frac{y}{d/2})^2] \quad \text{Equation (2)}$$

where \bar{v} is the average velocity of fluid, d is the height of microchannel (Berthier *et al.*, 2010). The value of y is the distance from random point to center of cross section of the microchannel. The source term R , in Eq. 1, represents the process of molecular adsorption from bulk to surface in our application. It can be described by a Langmuir equation

$$\frac{d\Gamma_t}{dt} = k_{on}C_w(\Gamma_{max} - \Gamma_t) - k_{off}\Gamma_t \quad \text{Equation (3)}$$

where k_{on} and k_{off} represent the association constant and dissociation constants, respectively. Γ is the concentration of adsorbed analyte on the surface by the capture molecule. Γ_{max} is the maximum surface density of binding sites on the wall. C_w is the analyte concentration in a solution layer adjacent to the capture area.

The relationship between the rate of analyte adsorption and the concentration gradient of analyte in solution layer on the wall is described by Fick's law (Equation 4),

$$\frac{d\Gamma}{dt} = -D \frac{\partial C}{\partial y'} = -D \nabla C \quad \text{Equation (4)}$$

To simulate the adsorption products concentration field, the Eq. 1 can be coupled to Eq. 3 via Eq.4. The derivative equation is

$$\Gamma = \frac{D \nabla C + k_{on} C_w \Gamma_{max}}{k_{on} C_w + k_{off}} \quad \text{Equation (5)}$$

In order to solve equations (1, 3 and 5) and simulate the behavior of analyte convection-diffusion-adsorption in this particle microchannel, a set of additional restraints at the boundary domains (called the boundary conditions) were defined. These are based on the accurate modeling study by Squires's group (Squires *et al.*, 2008). The numerical approach applied to solve the ordinary differential equations (ODEs) was a finite difference approach based on the Crank-Nicholson semi-implicit scheme (Berthier *et al.*, 2010). \vec{n} is the unit normal vector directed out of a surface.

$$\text{Surface (1)} \rightarrow 0 \leq y' \leq H, x = 0, C = C_0 \quad (6)$$

$$\text{Surface (2)} \rightarrow 0 \leq y' \leq H, x = L, \vec{n} D \nabla C = 0 \quad (7)$$

$$\text{Surface (3)} \rightarrow 0 \leq x \leq L, y' = 0, \vec{n} D \nabla C = 0 \quad (8)$$

$$\text{Surface (4)} \rightarrow 0 \leq x \leq \frac{L-S}{2}, y' = 0, \vec{n} D \nabla C = 0 \quad (9)$$

$$\text{Surface (5)} \rightarrow \frac{L-S}{2} \leq x \leq \frac{L+S}{2}, 0 \leq y' \leq H, \frac{\partial \Gamma}{\partial t} = -D \frac{\partial C}{\partial y'} \quad (10)$$

$$\text{Surface (6)} \rightarrow \frac{L+S}{2} \leq x \leq L, y' = 0, \vec{n} D \nabla C = 0 \quad (11)$$

Boundary condition (6) ensures that the input analyte solution has a consistent concentration, C_0 . Boundary conditions (7) (8) (9) and (11) define that no analyte diffuses out through the microchannel. The 'Boundary condition' (10) infers that the

analytes adsorption only happened at surface (5) and the adsorption kinetics of analyte at this functionalised capture surface (5) obeys Fick's law.

2.6.2 Numerical approach

The numerical approach applied to solve the ordinary differential equations (ODEs) was the Crank-Nicholson semi-implicit scheme (Press *et al.*, 1987). The details are included in Appendix chapter.

CHAPTER 3

Generation of an Anti- Neosaxitoxin Rabbit scFv Library

3.1 Introduction

With the frequent worldwide occurrence of red tides, marine toxins have recently received a lot of attention. Paralytic shellfish poisoning (PSP) toxins are among the most deleterious marine neurotoxins, because of the severe effects these toxins can induce on humans. PSP are produced mainly by planktonic dinoflagellates, which belong to the genera *Alexandrium* and *Gymnodinium*. PSPs are ingested by plankton feeders such as bivalves and the toxin leaves appreciable amounts of PSP in their digestive glands. Although the toxin does not harm the bivalves, it can cause serious illness or death for people who consume the contaminated bivalves. No visible difference in appearance can be observed between harmless and toxic shellfish or water. Furthermore, PSP toxins are stable under high temperature. Therefore, they cannot be killed by cooking or freezing (Campbell *et al.*, 2010). Symptoms of PSP can set in almost immediately or within hours. They include a tingling sensation that starts in the lips and tongue and moves to the hands and feet. This can be followed loss of control of the limbs, difficulty breathing. Depending on the amount of toxin ingested, PSP can paralyze breathing function and cause death in as little as 15 minutes. Currently, medical treatment for PSP is to provide respiratory support for patients and there is no antidote for PSP as the palliative care (Humpage *et al.*, 2010).

Fig. 3.1 shows that outbreaks of PSP found in Europe from 1993 to 2002 (<http://oceanworld.tamu.edu/resources/oceanography-book/harmfulalgalblooms.htm>).

During the 10 years period, PSP toxin was presented in a significant high frequency in these coastal states, including Norway, Ireland, United Kingdom, France, Portugal and Spain. In the last decade, the presence of high levels of PSP toxins were reported continuously all over the world. For example, many PSP cases were discovered near Puget Sound, California and Northern Channel Islands in 2012, and Alaska in 2014, according reports by Food Poisoning Bulletin (<http://foodpoisoningbulletin.com/tag/paralytic-shellfish-poison-bsp/>). The frequently outbreaks of PSP seriously threaten human health. Additionally, it causes economic losses in coastal communities and aquaculture industries worldwide.

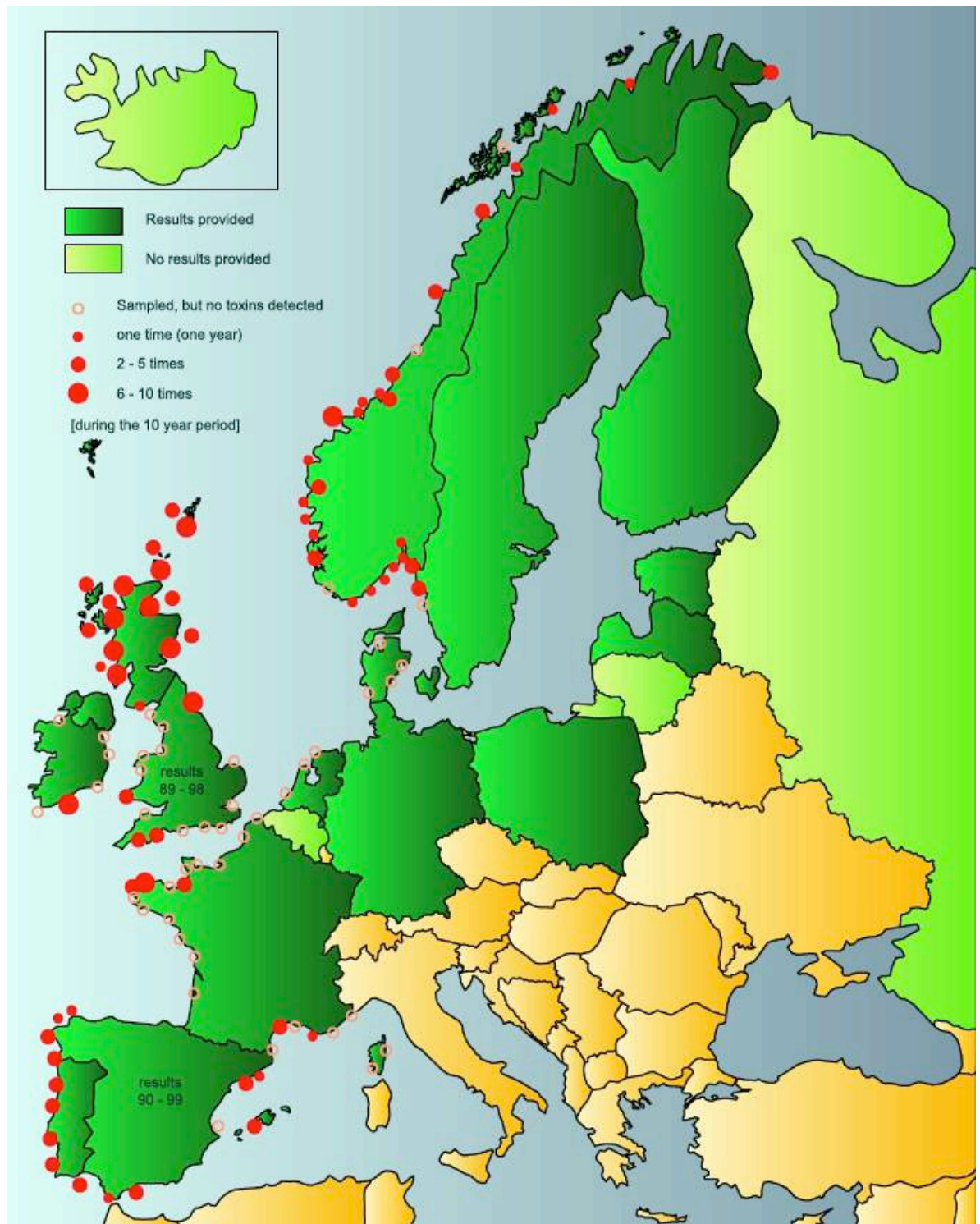


Figure 3.1 Outbreaks of PSP toxins in the coastal water in Europe during the year from 1993 to 2002 (adapted from Harmful Algal Blooms, last accessed on 1st Sep 2014, retrieved from <http://oceanworld.tamu.edu/resources/oceanography-book/harmfulalgalblooms.htm>).

3.1.1 Paralytic shellfish poisoning toxin (PST)

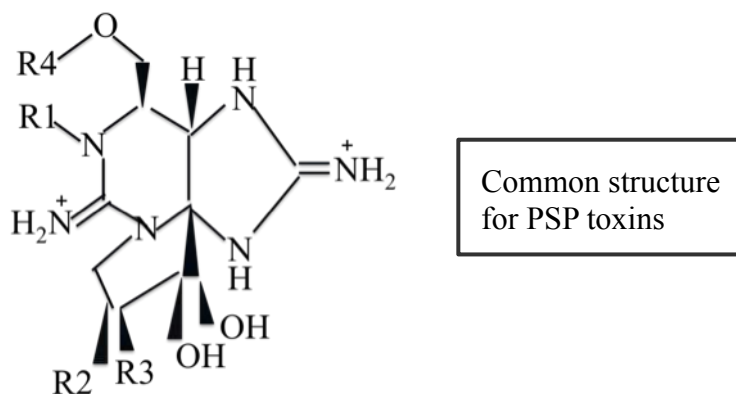
Paralytic shellfish poisoning can cause respiratory-related death. The mode of action of PSP toxicity is that it can block sodium channels in excitable membranes, which leads to the stoppage of the propagation of neuronal impulses (Maria *et al.*, 2014). The PSP toxins cover a group of toxins components whose structures are similar but with different groups (hydroxyl, carboxyl and sulfate moieties) at four sites on the backbone structure. Table 3.1.1a illustrates the isoform structures commonly observed in toxic dinoflagellates and toxin-contaminated shellfish, and it shows that these components are derivatives of Saxitoxin (STX) (Andrew *et al.*, 2014).

PSP toxins are generally water-soluble and heat stable. However, stability can change significantly depending on the pH and the toxins' structure (Etheridge, 2010). For instance, toxin components degrade quickly at an alkaline pH. In most cases, toxins are stable under acidic conditions. Nevertheless, the stability of each PSP toxin depends on characteristics of the structure e.g. STX is very stable.

Importantly, the potency of each toxin is dependent on its structure (Campbell *et al.*, 2011). Table 3.1.1b shows the specific toxicity of each toxin component expressed as mouse units (MU) per μmole of toxin, in which 1 MU is a dose of toxin that can kill a male mouse (ddY strain) in 15 min. The carbamate toxins are the most potent and they include STX, Neo and GTX1/4. The decarbamoyl toxins (dcSTX, dcNEO, dcGTX1/2) have intermediate toxicity and are reported in certain bivalves, but are not commonly found in toxic dinoflagellates. The N-sulfocarbamoyl toxins (GTX5 and C1/4) are less potent (Tatters *et al.*, 2013).

Bioconversion of PSP toxins components in shellfish has been demonstrated (Jeon *et al.*, 2008). Accumulated ciguatoxins (CTX) in shellfish gradually transform to STXs, and this transformation can occurred widely in many ecosystems. In addition, the rate of transformation is reported to be very slow, suggesting that the reaction is not enzymatic. However, this activity is not stable, and could be promoted by thiol compounds, especially glutathione (GSH), a biological reductant that is distributed widely in different organisms.

Table 3.1.1a Structures of PSP toxins components (adapted from Andrew *et al.*, 2014).



Component	R1	R2	R3	R4
Saxitoxin	H	H	H	CONH ₂
Neosaxitoxin	OH	H	H	CONH ₂
Decarbamoyl saxitoxin	H	H	H	H
Decarbamoyl neosaxitoxin	OH	H	H	H
Gonyautoxin 1	OH	OSO ₃ ⁻	H	CONH ₂
Gonyautoxin 2	H	OSO ₃ ⁻	H	CONH ₂
Gonyautoxin 3	H	H	OSO ₃ ⁻	CONH ₂
Gonyautoxin 4	OH	H	OSO ₃ ⁻	CONH ₂
Gonyautoxin 5	H	H	H	CONHSO ₃ ⁻
Gonyautoxin 6	OH	H	H	CONHSO ₃ ⁻
Decarbamoyl gonyautoxin 1	OH	OSO ₃ ⁻	H	H
Decarbamoyl gonyautoxin 2	H	OSO ₃ ⁻	H	H
Decarbamoyl gonyautoxin 3	H	H	OSO ₃ ⁻	H
Decarbamoyl gonyautoxin 4	OH	H	OSO ₃ ⁻	H
C1	H	OSO ₃ ⁻	H	CONHSO ₃ ⁻
C2	H	H	OSO ₃ ⁻	CONHSO ₃ ⁻
C3	OH	OSO ₃ ⁻	H	CONHSO ₃ ⁻
C4	OH	H	OSO ₃ ⁻	CONHSO ₃ ⁻

Table 3.1.1b Specific toxicity of each component (adapted from Tatters *et al.*, 2013).

Component	Specific Toxicity (MU)
STX	2483
neoSTX	2295
deSTX	1274
GTX1	2468
GTX2	892
CTX3	1584
GTX4	1803
dcGTX2	1617
dcGTX3	1872
GTX5	160
C1	15
C2	239
C3	33
C4	143

1MU is a dose of toxin that can kill a male mouse in 15 minutes

3.1.2 Methods for PSTs detection

To date, several methods for detecting PSP toxins are available. The mouse bioassay is the most commonly used method to determine the presence of PSP toxins. It is accredited by the Association of Analytical Communities (AOAC) and accepted internationally as the official method in most countries for the quantitative measurement of the PSP toxins in shellfish (Horwitz, 2000). The mouse bioassay is performed by the application of potentially contaminated samples on mice or rats, and then monitoring of the symptoms and time to death. The toxicity of sample can be directly analysed through this method. However, ethical issues due to the utilization of animals exist. Additionally, this assay shows many technical limitations, including: poor specificity with low sensitivity, low sample throughput, high cost and it is labor-intensive (Humpage *et al.*, 2010; Turner *et al.*, 2012).

Chemical methods used for the determination of PSP toxins include high performance liquid chromatography (HPLC) methods with fluorescence detection (Asp *et al.*, 2004; Lawrence *et al.*, 2005), liquid chromatography/mass spectrometry (LC/MS) (Song *et al.*, 2013), and capillary electrophoresis (CE) (Juan-Garcia *et al.*, 2005). Some chemical methods are non-quantitative, and do not enable identification of the different components of PSP toxins in the sample but yield an overall estimate of total toxin content. Additionally, these methods are time-consuming, costly, and labor-intensive.

Immunochemical-based techniques, like ELISA, are developed for analytical detection of PSP toxins. In the last decade, this approach was increasingly established in their use for toxicology screening (Wong *et al.*, 2010; Garet *et al.*, 2010; Fraga *et al.*, 2013; Szkola *et al.*, 2013; Kawatsu *et al.*, 2014), because it provided a rapid and effective way to detect toxins in complex biological matrices without major purification by utilization of antibodies.

3.1.2.1 Antibody-based methods for PST detection

Many heterologous assay formats have been developed to detect PSTs. Generally, the assays show high sensitivity, but inaccurate results as a result of the antibody specificity (Dubois *et al.*, 2010). Several developed antibodies for detecting PSTs are outlined in Table 3.1.2.1. These antibodies show cross-reactivity to the different components of PSTs, which causing specificity issues relating to the analysis of sample with diverse components. For example, the monoclonal antibody raised to GTX 2/3 illustrated 100% cross-reactivity to GTX 2/3 but less cross-reactivity to the other toxin analogues (Campbell *et al.*, 2007). Therefore, it can be applied to quantitatively analyse the amount of GTX 2/3 in samples lacking other toxins. However, it could induce underestimation and overestimation issues when applied to screen real unknown samples. For regulatory purposes, underestimation could have severe health implications to the consumer whereby contaminated material is declared safe for consumption, whereas overestimation could cause detrimental economic losses to the industry through the unnecessary closure of harvesting beds.

A novel approach to alleviate the problem of underestimation of results is to combine two or more antibodies of varying reactivity into the test format. Several assays have

been investigated (Jellett *et al.*, 2002; Campbell *et al.*, 2009; Bratcher *et al.*, 2011; Campbell *et al.*, 2011; Zhang *et al.*, 2014). In these assays, cocktails of antibodies raised to different PSPs analogues were employed. Therefore, the overall PSPs can be quantified in a sample. Additionally, these assays were simple, rapid, sensitive and gave high output. Compared with the mouse bioassay and the chemical methods, they are more suitable for PSP toxin screening, but are incapable of indicating exact toxicity of samples.

Ideal antibodies applied to detect PSP toxins in samples should possess a similar cross-reactivity to a full range of PSP toxins. This is because an antibody with different cross-reactivity to various components of PSP toxins is incapable of accurate detection of various components of PSP toxins in samples. However, the ideal antibody is not available. Currently, the accuracy of these developed assays depends heavily on the toxin profile. Therefore, these methods have the limitation in determination of overall PSP toxicity in the samples containing several PSPs.

It was reported that antibodies raised against STX groups had low cross-reactivity to NeoSTX groups, and *vice versa*, if PSPs were subdivided into STX (non-hydroxylated) and NeoSTX (hydroxylated) groups from an immunological point of view. Therefore, to incorporate the full spectra of PSP toxins to an equivalent extent, antibodies produced to both the non-hydroxylated (STX) or hydroxylated toxins (NEO) will have to be utilized (Usleber *et al.*, 2001).

Thus, Chu *et al.* found poor correlation between assays based on either anti-STX antibodies or anti- neoSTX antibodies, but combining the results from the two assays markedly improved the detection rate, to the extent that these authors concluded that their combined use could screen out 80–85% of MBAs that produce negative or low positive results. Continuing the theme of multiple assays to improve specificity, Kawatsu *et al.* raised monoclonal antibodies (designated GT-13A) to GTX2/3 to complement those previously raised against STX and neoSTX. These antibodies retained the STX/neoSTX lineage discrimination found in other antibodies, but did have a near equal affinity for GTX2/3, dcGTX2/3, and C1/2. This multiple assay approach was taken even further by Garthwaite *et al.*, who recommended the use of a suite of ELISAs to screen shellfish samples for not only PSTs, but also amnesic, diarrhoeic, and neurotoxic shellfish poisons.

Table 3.1.2.1 Outline of developed antibodies for PSTs detection.

	Antibody Type		Immunogen	Specificity (from high to low)	Ref.
STX	Polyclonal (Rabbit)	Ab	STX-FA-BSA	STX, GTX 1/4	Chu and Fan, 1985
STX	Polyclonal (Rabbit)	Ab	STX-FA-KLH	STX, dc-STX, GTX 2/3, NeoSTX, B1, C1/2, GTX 1/4	Renz, 1988
STX	Polyclonal (Rabbit)	Ab	STX-GA-poly-alanine lysine	STX, NeoSTX, GTX 2/3	Cembella <i>et al.</i> , 1990
STX	Monoclonal	Ab	STX-PJ-Gox	STX, GTX2/3, dc-STX, B1, NeoSTX, GTX1/4, C1/2	Dietrich <i>et al.</i> , 1996
Neo-STX	Polyclonal (Rabbit)	Ab	Neo-FA-KLH	NeoSTX, GTX	Chu <i>et al.</i> , 1992
Neo-STX	Polyclonal (Rabbit)	Ab	Neo-PJ-GOx	NeoSTX, GTX 1/4, STX, GTX 1/4	Burk <i>et al.</i> , 1995
GTX 2/3	Monoclonal	Ab	GTX 2/3-KLH	GTX2/3, dc-GTX2/3, C1/2, GTX 1/4, STX, NeoSTX	Kawatsu <i>et al.</i> , 2002

3.1.2.2 Leporine host

Immunoglobulin (Ig) rearrangements are a major contributor to the generation of a diverse primary antibody repertoire. During the Ig rearrangement, heavy and light chain variable region are assembled in developing B lymphocytes (Sehgal *et al.*, 1999). The heavy chain variable region is composed by variable (V), diversity (D) and joining (J) gene segments, while light chain variable region consists of V and J gene segments. Unlike rodents and other primates, the antibody diversity generated by $V_H(D)J_H$ rearrangement in rabbits does not depend on the use of many variable gene segments. In rabbits, one out of >50 functional V_H gene segments, V_{H1} , is predominantly used (Becker *et al.*, 1990; Bassing *et al.*, 2002). The advantage of this for recombinant antibody work is that a relatively small number of primer sets are required, compared to mice and other primates.

In contrast to V_H , the rabbit light kappa chain (V_KJ_K) rearrangements are much more diverse. Rabbits have two κ chain isotypes, $\kappa 1$ and $\kappa 2$. Normally, ~70-90% of the serum antibodies are the $\kappa 1$ isotype in rabbit. In the mutant Besilea strain, $\kappa 2$ isotype is predominantly expressed. $\kappa 1$ includes four different allotypes, b4, b5, b6 and b9 (Popkov *et al.*, 2003). After rearrangement, diversity of the rearranged $V_H(D)J_H$ and V_KJ_K are further developed by of somatic hypermutation and gene conversion-like changes in B-cells, which migrate to the appendix and other gut-associated lymphoid tissues (GALT) in young rabbits. Thus, the κ light chain appears to be a major contributor toward the generation of the antibody diversity of the rabbit immune repertoire. Although, antibody diversity generated by V_HDJ_H rearrangements in rabbits is much more restricted than in mice or humans, a significant amount of diversity is obtained from V_KJ_K rearrangements.

The unique diversification and gene rearrangement features of the rabbit make it an ideal choice for recombinant antibody development as it combines high specificity with high avidity and affinity (Rader *et al.*, 2000).

3.2 Aim of this chapter

The objective of the research discussed in this chapter was to generate and isolate antibodies that would recognise a range of saxitoxin derivatives such as neosaxitoxin, gonyautoxin, decarbamoyl and saxitoxin itself.

3.3 Results

3.3.1 Immunisation of rabbit with Neosaxitoxin-KLH

Immunisation of a rabbit with NeoSTX-KLH conjugation was successfully performed by Queen's University Belfast (QUB). Serum samples, bone marrow and spleen were also obtained and transferred to DCU for use. The serum was tested by direct ELISA using three conjugates: Neo-STX-BTG, GTX1-4-PER and STX-OVA, which were synthesized at QUB. The serum from the NeoSTX-KLH-immunised rabbit also showed cross reactivity to STX-OVA.

3.3.2 Isolation of RNA from bone marrow and spleen and first-strand DNA synthesis

Bone marrow and spleen were extracted from the immunised rabbit and phenol-chloroform extraction was carried out for isolation of RNA. The cDNA from both the bone marrow and spleen were synthesised by reverse transcription. Subsequently they were quantified and pooled in a 1:1 ratio.

3.3.3 Amplification of rabbit antibody heavy and light chains and PCR optimisation

In order to obtain a sufficient quantity of genetic material for antibody gene library construction, magnesium chloride (MgCl_2) concentration gradient from 0.5mM to 6mM was employed in the PCR (Fig 3.3.3.1). In addition, Go Taq[®] DNA polymerase was used. The condition of 100pmol primer combinations and 2mM MgCl_2 provided the clearest target band (~400bp) with the least non-specific amplification (~700bp), as shown in Fig 3.3.3.1.

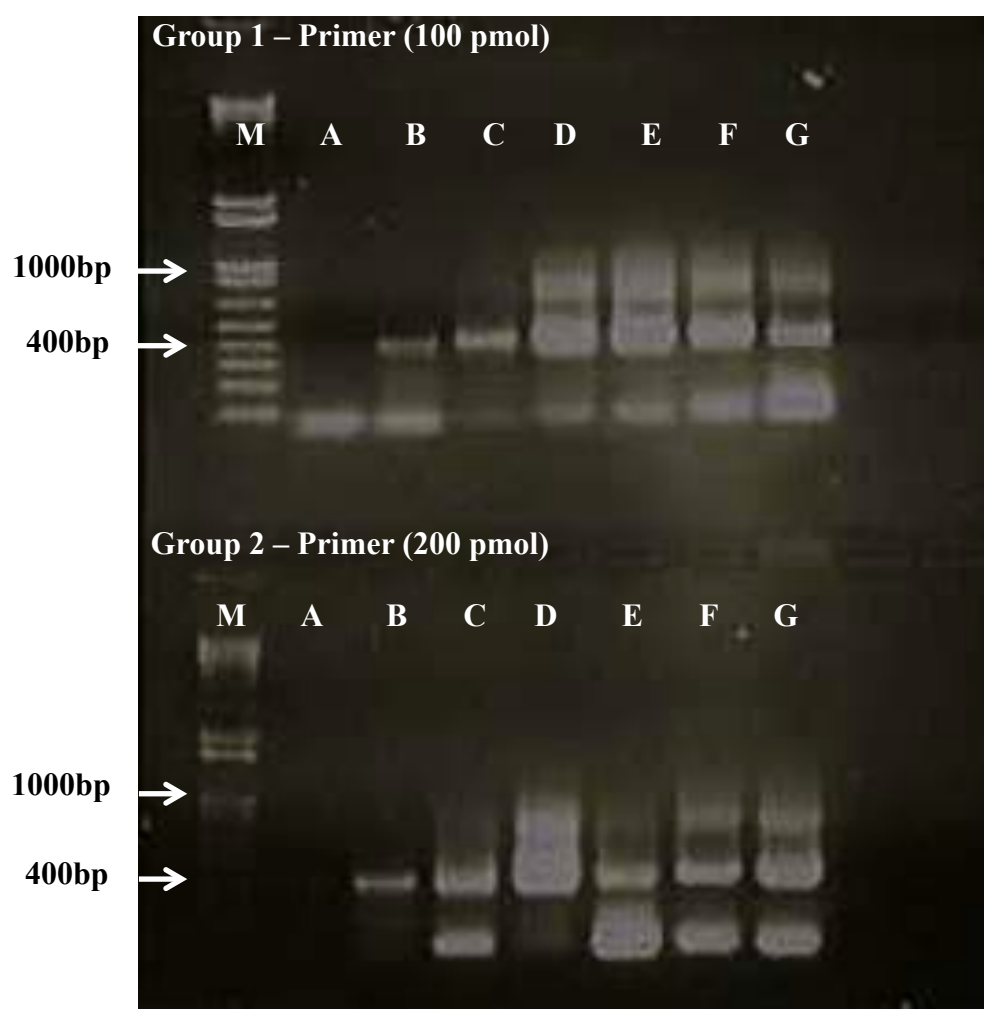


Figure 3.3.3.1 PCR optimisation of rabbit variable heavy chain (~400 bp) genes using different primer combinations and increased MgCl₂ concentrations. In the group 1, primer combination with a concentration of 100 pmol was applied in the PCR reaction system. In the group 2, 200 pmol of primer combination was used. In each groups, the concentrations of MgCl₂ from lane A to lane G were 0, 1, 2, 3, 4, 5 and 6 mM, respectively. Lane M represents a 1KB plus DNA ladder.

Large-scale PCR amplification of the variable heavy chains was carried out using the optimised conditions. These were shown to be a 100 pmol primer combination and 2mM MgCl₂. The correct band of 400 bp was isolated using gel electrophoresis and purified using QIAquick gel extraction.

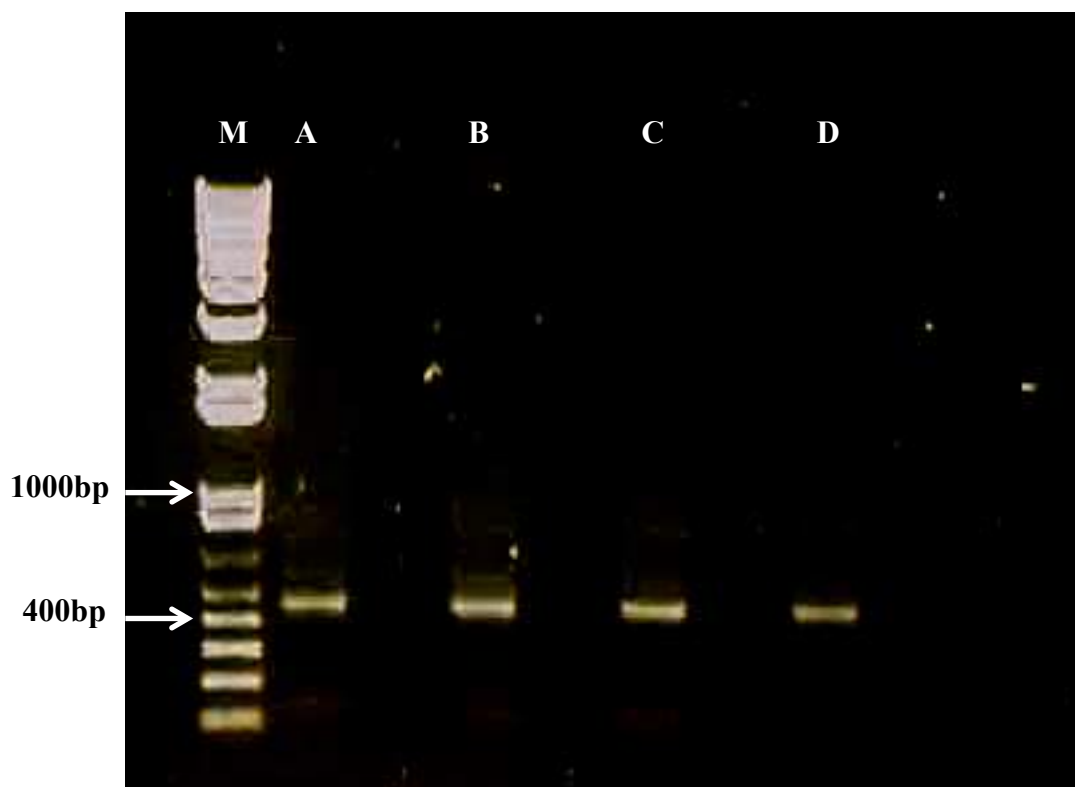


Figure 3.3.3.2 Amplification of rabbit heavy chain genes (~400bp amplicon) using the cDNA from a Neosaxitoxin-immunised rabbit. The 4 combinations for the heavy chain regions were amplified successfully, utilising the primer combinations; RSCVH1 and RSCG-B (VH1), RCSVH2 and RSCG-B (VH2), RSCVH3 and RSCG-B (VH3), and RSCVH4 and RSCG-B (VH4). Lane M represents a 1 KB plus DNA ladder. Lanes A to D represent VH1, VH2, VH3, and VH4, respectively.

In the next stage, PCR amplifications were carried out for the variable light (kappa) regions, using the primers sets RSCVK1 and RKB9J10-BL (V_K1), RSCVK1 and RKB9Jo-BL (V_K2), RSCVK1 and RKB42Jo-BL (V_K3), RSCVK2 and RKB9J10-BL (V_K4), RSCVK2 and RKB9Jo-BL (V_K5), RSCVK2 and RKB42Jo-BL (V_K6), RSCVK3 and RKB9J10-BL (V_K7), RSCVK3 and RKB9Jo-BL (V_K8), RSCVK3 and RKB42Jo-BL (V_K9). All the variable kappa chains amplified successfully at 400 bp with GoTaq™ polymerase, except for the V_K7 and V_K8 primer sets. Subsequently, the correct band of 400 bp was isolated using gel electrophoresis and purified using QIAquick gel extraction.



Figure 3.3.3.3 PCR amplifications for the variable light (kappa) genes (~400 bp). Lane M represents the 1 kb Plus DNA ladder. Lanes A to I represents the V_K1 to V_K9 .

Further optimisation was carried out on the V_K7 and V_K8 variable light kappa primer combination, for the purpose of obtaining a sufficient quantity of DNA material for library construction. Phusion® Taq High-Fidelity DNA polymerase was utilised instead of Go Taq, with two different buffers. There are two possible reaction buffers for PCR reactions using *Phusion*® Taq polymerase, i.e. 5X *Phusion*® GC buffer and 5X *Phusion*® HF buffer. The error rate of HF buffer (4.4×10^{-7}) is lower than that in GC buffer (9.5×10^{-7}). The GC buffer can improve performance on difficult or longer templates. A hot start reaction was carried out for this PCR to aid in amplification efficiency. As illustrated in Fig. 3.3.3d, the correct band was obtained for amplification of V_K7 and

V_K8 with the inclusion of HF buffer. A weaker band was obtained for V_K7 and V_K8 with the inclusion of GC buffer.

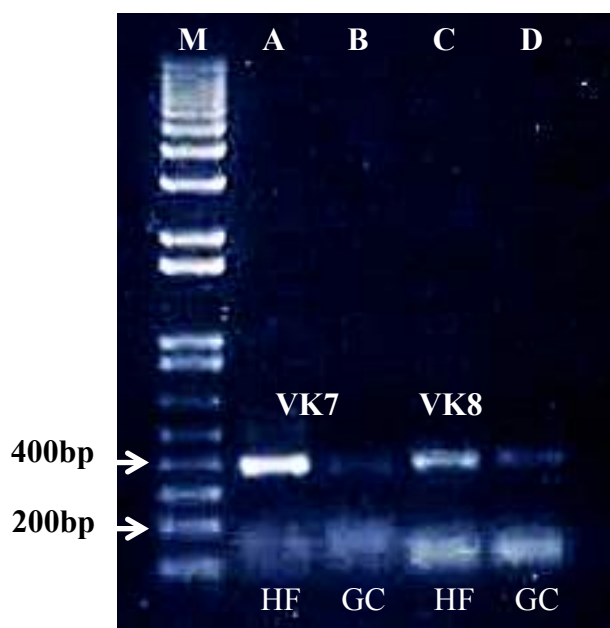


Figure 3.3.3.4 PCR optimization of V_K7 and V_K8 variable light regions using Phusion[®] Taq High-Fidelity DNA polymerase with HF and GC buffers. Lane M represents the 1 kb Plus DNA ladder. Lane A and lane B represent V_K7 using HF and GC buffers. Lane C and lane D represent V_K8 using HF and GC buffers.

Using the optimised conditions, a large-scale PCR amplification of V_K7 and V_K8 was performed (Fig 3.3.3.5).

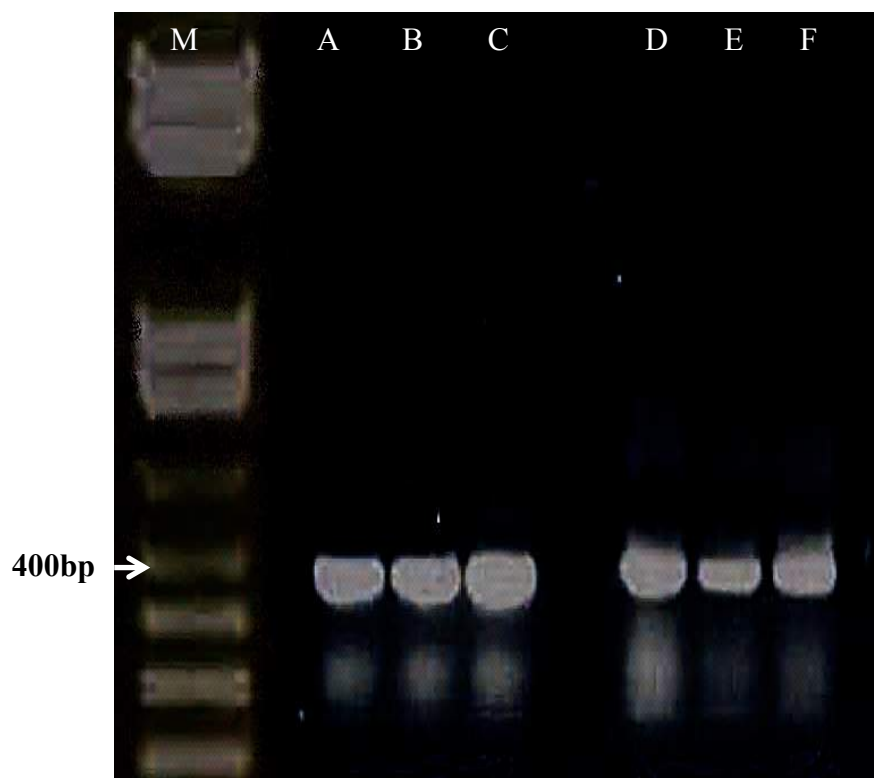


Figure 3.3.3.5 Large-scale PCR amplification of V_K7 and V_K8 variable light regions using *Phusion[®] Taq High-Fidelity DNA polymerase* with HF buffer. Lane M represents the 1 kb Plus DNA ladder. Lanes A to C represents V_K7. Lanes D and F represent V_K8.

For PCR optimization of the variable light lambda (V_λ) regions, a $MgCl_2$ concentration gradient from 0 to 4 mM was prepared. In addition, Go Taq® DNA polymerase was utilised in the PCR reaction. The clearest band with the least amount of smearing was obtained with a $MgCl_2$ concentration of 1 mM. An additional band at 250 bp was also obtained due to non-specific amplification (Fig 3.3.3.5). PCR amplification of V_λ was then performed (Fig 3.3.3.6). The correct band of 400 bp was isolated using gel electrophoresis and purified using QIAquick gel extraction.

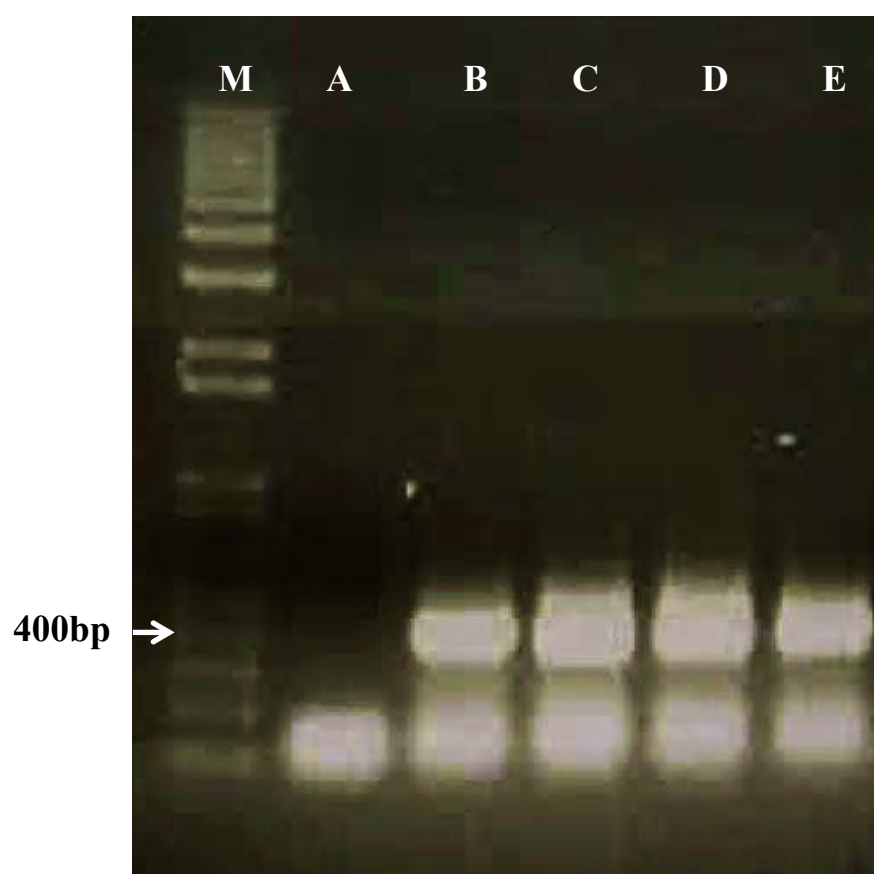


Figure 3.3.3.6 $MgCl_2$ optimisation of rabbit variable light chain lambda (V_λ) (~400 bp) amplification. Lane M represents a 1 kb plus DNA ladder, lane A to lane E, respectively, represent amplicons with increased concentration of $MgCl_2$ (0, 1, 2, 3 and 4 mM).

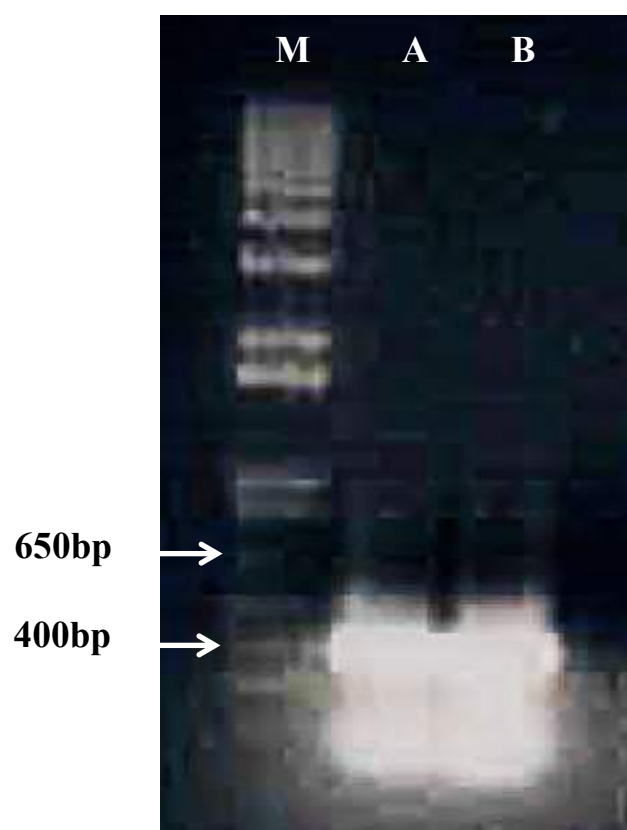


Figure 3.3.3.7 Optimised PCR amplification of rabbit variable light chain lambda antibody gene sequences. Lane M represents a 1 kb plus DNA ladder, and lanes A and B represent VL_{λ} genes.

After the successful large-scale PCR amplification of variable heavy and light chain antibody gene sequences, each of the variable heavy chains (VH1-4) and light chain (V_{K1-9} , $V_{K\lambda}$) were quantified and pooled in a 1:1 ratio. In the next stage a PCR splice overlap extension of variable rabbit heavy and light chains was performed.

SOE-PCR of the rabbit variable heavy and light chain antibody genes

Construction of the rabbit scFv library proceeded by fusing equimolar concentrations of the variable heavy and variable light chain mixtures using the overlap primers, RSC-F and RSC-B. These primers were utilised to amplify a fusion product with a short serine-glycine linker (GGSSRSS). Velocity DNA polymerase was employed for this amplification reaction as it possesses high thermostability combined with its 5'-3' DNA polymerase and 3'-5' proofreading exonuclease activities. This ensures a low PCR error-rate, and enhanced DNA processivity. The reaction was carried out in the presence of 3% (v/v) DMSO. No optimisation of the PCR was required. The target DNA of approximately 750 bp was then purified by gel extraction.

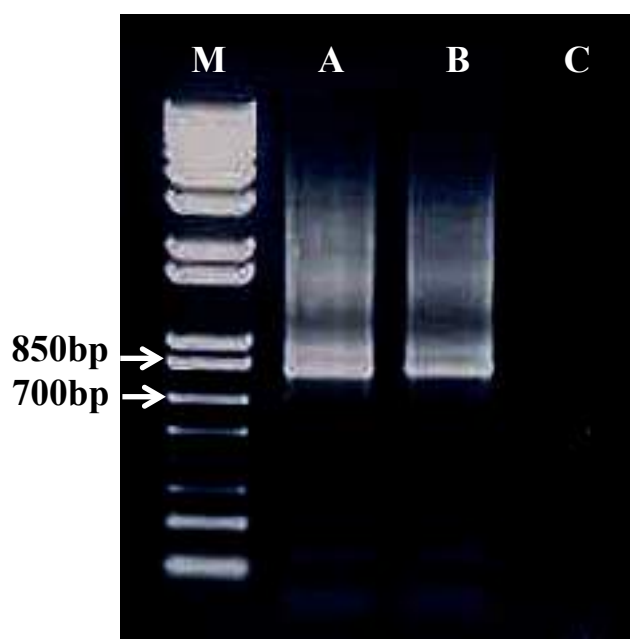


Figure 3.3.3.8 Splice by extension overlap PCR (SOE-PCR) of variable heavy and variable light chain fragment to form complete scFv fragment. The expected molecular weight of this amplicon was 750 base pairs. Lane M represents a 1 kb plus DNA ladder, lanes A and B represent scFv genes, and lane C represents a negative control with absence of DNA template.

3.3.4 Cloning the SOE product into the pComb3XSS vector through restriction digestion

The scFv SOE product was cloned into the pComb3XSS vector using a *Sfi*I restriction enzyme. The pComb3XSS was employed as a vector as it contains a double Stuffer fragment between the two *Sfi*I cloning sites in the heavy and light chain regions, which allows for efficient cloning. Culture of pComb3XSS was performed, as described previously in Chapter 2. The plasmid DNA was purified using a NucleoBond® Xtra Midi/Max kit. The digestion of purified SOE product and vector was carried out using *Sfi*I, *Xba*I, and *Xho*I. The digestion sites are illustrated in Fig 3.3.4a. Before the ligation step the digested pComb3XSS vector was treated with the enzyme, Antarctic phosphatase, which prevents self-ligation of the vector.

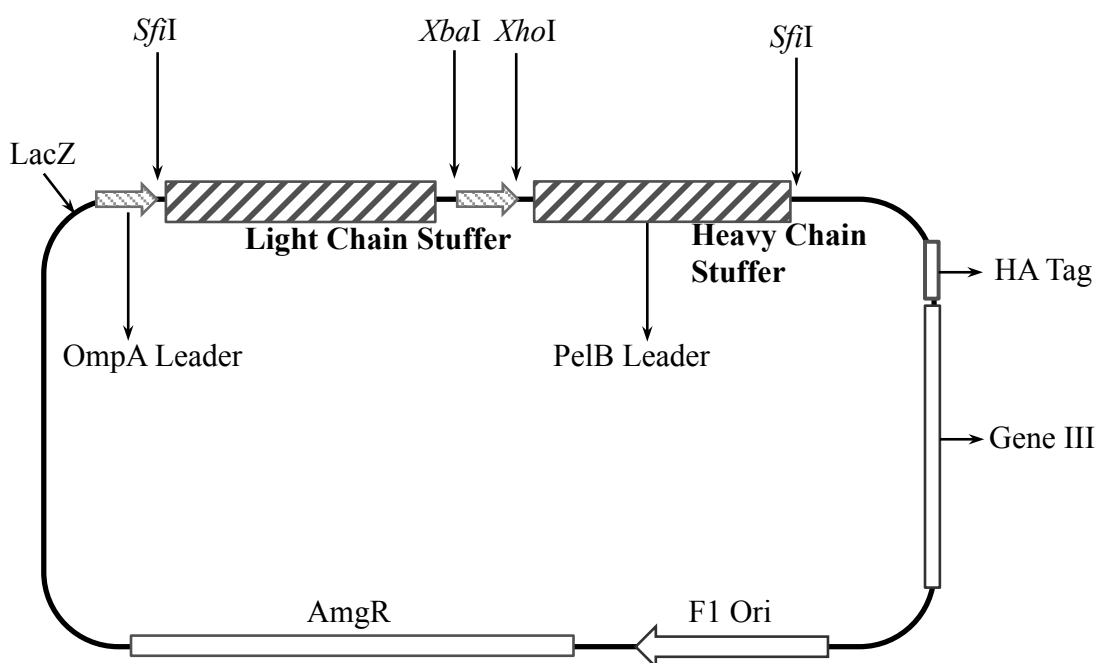


Figure 3.3.4a The pComb3XSS phagemid vector map and relevant digestion sites.

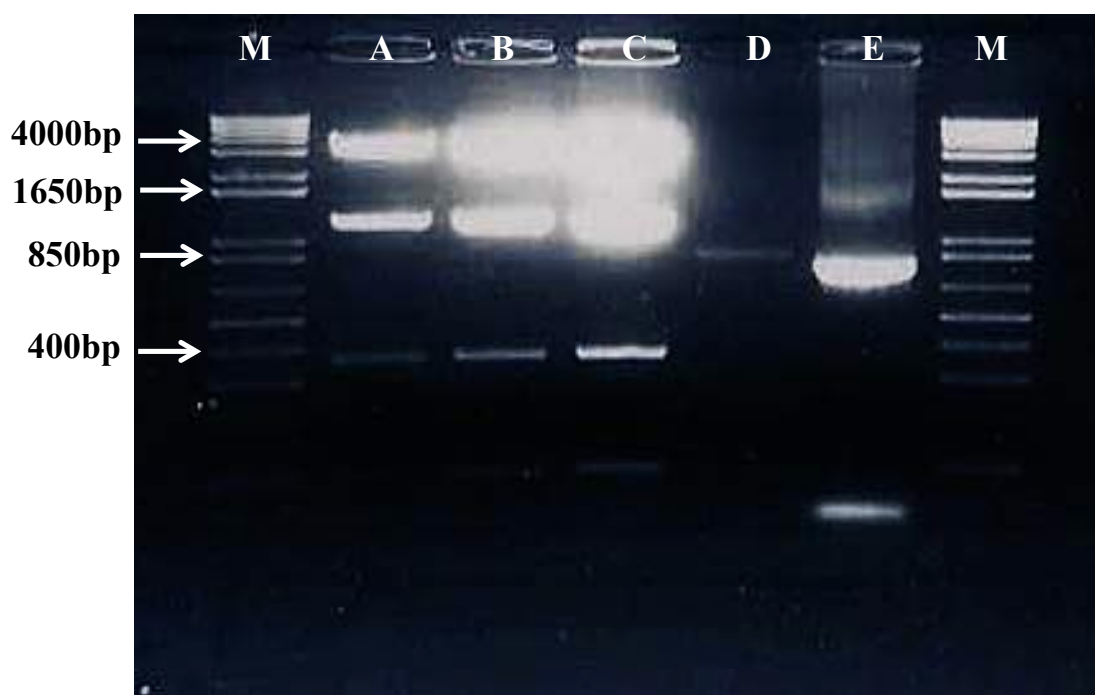


Figure 3.3.4b Digestion of the SOE product and the pComb3XSS vector. Lane M represents a 1 kb plus DNA ladder, lanes A to C represents the digestion of the pComb3XSS vector to produce a heavy chain Stuffer fragment (~1200 bp), a light chain Stuffer fragment (~300bp), the double-cut vector (~3400bp), and the PelB leader (~100bp). Lane D and E are SOE products (~750) and digested SOE products (~700bp).

Both digested vector and SOE genes were extracted from an Agrose/TAE gel and concentrated and purified using ethanol precipitation. Subsequently, a ligation procedure was performed to clone the scFv fragment genes into pComb3XSS vector. Following the ligation, the ligated products were transformed into electrocompetent XL1-Blue cells by electroporation (Section 2.3.10). The transformed rabbit scFv library had a size of 9.2×10^6 cfu/mL. The library was enriched via phage display-panning using immobilised STX-OVA on immunotubes. The M13K07 helper phage was applied in the bio-panning process. Four rounds of bio-panning were performed using decreasing concentrations of STX-OVA conjugate from 50 to $2.5 \mu\text{g/mL}$, and an increasing the number of wash steps and reducing the culture volume (Table 3.3.4a). This strategy was designed to enhance the selection of binding clones that have high affinity. Table 3.3.4b presents the inputs and outputs form each bio-panning round.

Table 3.3.4a Bio-Panning strategy for the Neo-saxitoxin rabbit scFv library.

	Pan 1	Pan 2	Pan 3	Pan 4
Coating conc. (STX-OVA)	50µg/mL	25µg/mL	5µg/mL	2.5µg/mL
Number of washes	5x PBST/PBS	10x PBST/PBS	15x PBST/PBS	15x PBST/PBS
Culture volume	400mL	100mL	100mL	100mL
Helper phage volume	1000µL	500µL	500µL	500µL

Table 3.3.4b Bio-panning inputs and outputs of the rabbit anti-Neosaxitoxin phage library.

	Input (cfu/mL)	Output (cfu/mL)
Pan 1	9.8×10^8	1.3×10^5
Pan 2	9.1×10^9	2.4×10^5
Pan 3	7.1×10^{10}	4.7×10^6
Pan 4	6.9×10^9	9.2×10^6

3.3.5 scFv check via 'colony-pick' PCR

Following bio-panning, a soluble monoclonal ELISA was performed on clones from round 4 outputs. However, no positive clones were observed. To ensure that the antibody library contained scFv inserts, a colony-pick PCR was performed. Colonies were picked from the pan 4 output and the SOE insert were amplified by PCR. The SOE primers, RSC-F and RSC-B, as well as Go Taq DNA polymerase were used for SOE PCR amplification. The PCR products were subsequently analysed using a 1% (w/v) agarose gel.

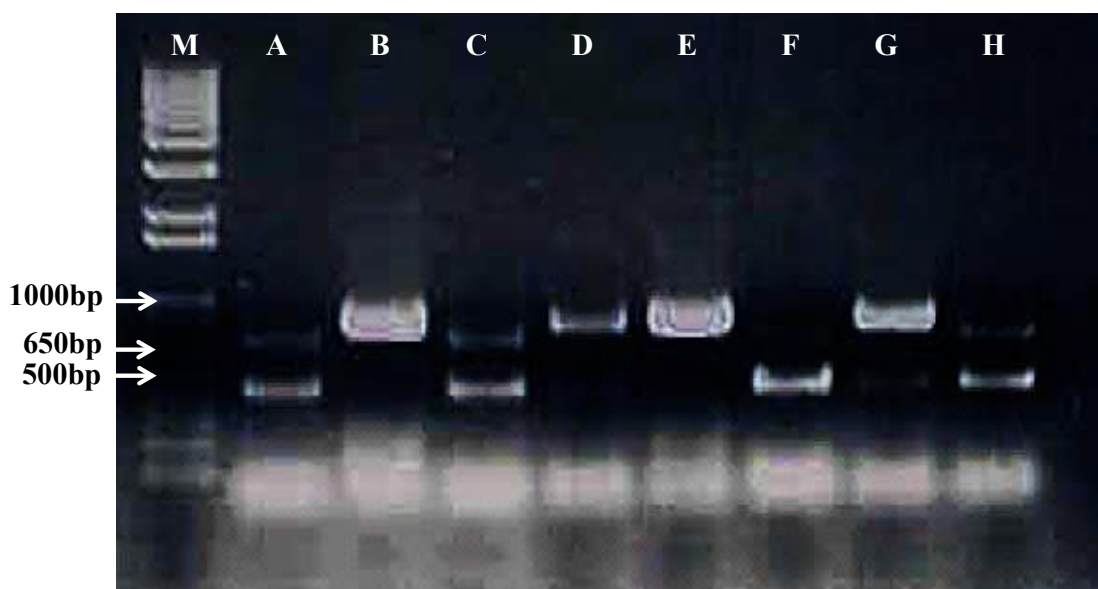


Figure 3.3.5 Colony-pick PCR. Lane M represents a 1 kb plus DNA ladder, lane A to lane H represent the amplified SOE products (~750bp) from panning 4 output colonies. In total the 4 of 8 colonies contained the inserted scFv gene.

3.3.6 scFv check via soluble monoclonal ELISA

A total of 96 colonies were picked from the pan 4 output and tested by monoclonal ELISA. However none of the clones tested showed any significant binding to either STX-OVA or NeoSTX-KLH. Positive clones were identified. However, the signal was very low (Fig. 3.3.6). After repeating this monoclonal ELISA analysis using the same 96 clones, it was observed that the results were not reproducible and no STX-OVA or NeoSTX-KLH-binding clones were isolated.

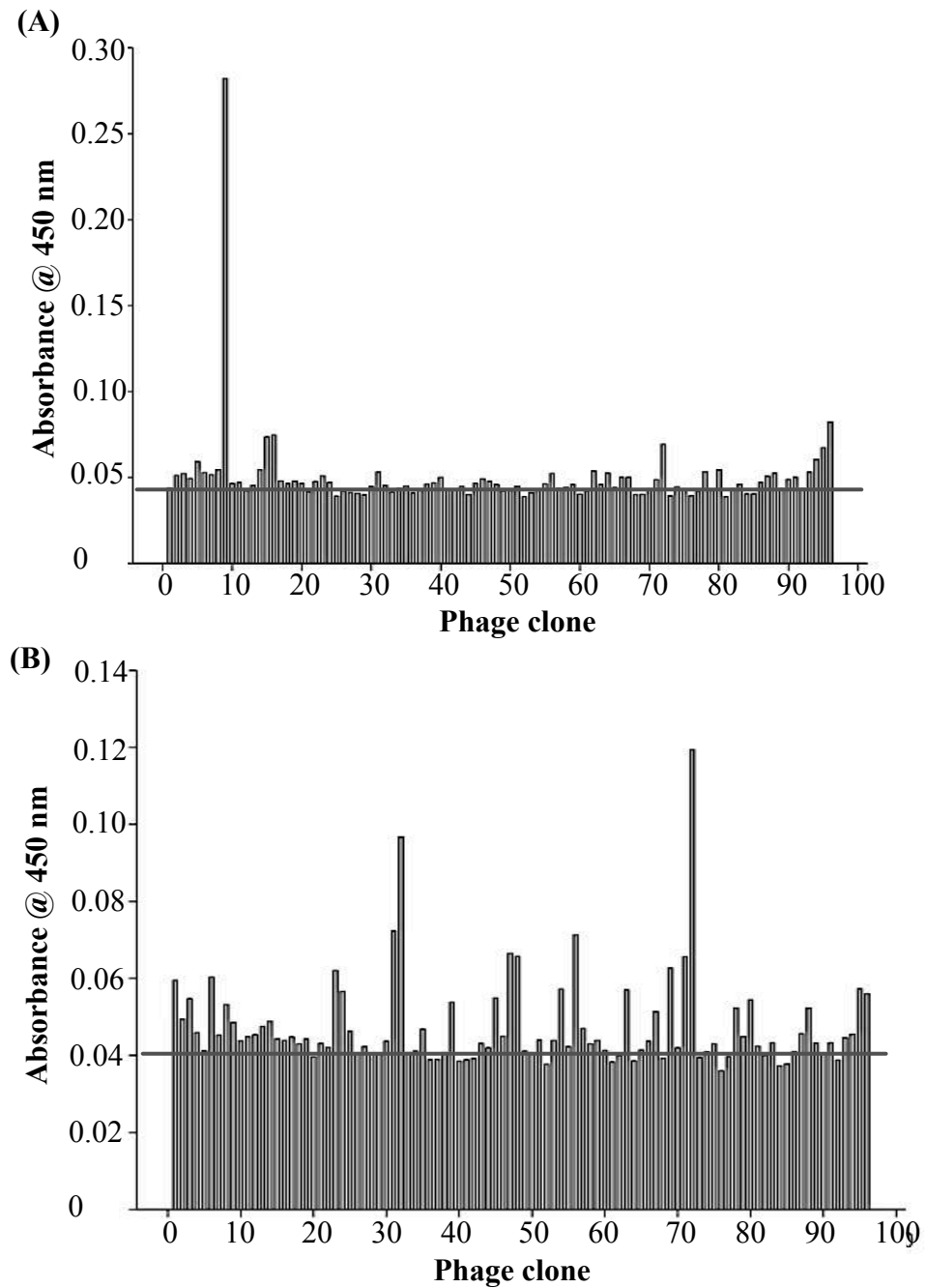


Figure 3.3.6 Soluble monoclonal ELISA of phage clones from panning round 4. In (A), each ELISA well was coated with 1 μ g/mL STX-OVA conjugation. A 1:2,000 (v/v) dilution of a peroxidase- conjugated rat anti-HA monoclonal antibody conjugated with peroxidase (1:2000) was used to detect scFvs. In (B), the same protocol was performed except that 1 μ g/mL NeoSTX-KLH was coated on the wells. In both cases, the blank horizontal lines represent the background signal.

3.4 Discussion

PSTs has previously been identified as a key target for establishment of alternative detection methodologies to animal toxicity assays and analytical techniques. Development of rapid testing methodologies, such as those incorporating immune recognition elements, would serve to support existing techniques, such as HPLC and mass spectral analysis, by providing a rapid warning mechanism for toxin outbreaks. Both monoclonal and polyclonal antibodies have been generated to date, but no reported recombinant antibodies exists to PSTs. Having a recombinant source of antibody would provide the advantage of superior affinity, stability and specificity. Recombinant antibodies have potential for incorporation of tags for functionalisation, immobilisation, purification and detection.

In this work, an immune AZA single chain antibody fragment (scFv) library was constructed from an immunised rabbit host. A rabbit was chosen as the host animal because of its suitability for antibody generation to small-molecular weight targets and because of its unique diversification and gene rearrangement capabilities (See Section 4.1.3). This chapter describes the construction of a rabbit anti-Neo-STX-KLH scFv library. A rabbit was chosen as the host animal and it was immunized by injection with Neo-STX-KLH. The rabbit antibody library was constructed by PCR amplification of V_H and V_L genes, as well as linking V_H and V_L fragments. A scFv fragment phage library was generated by cloning the gene fragment library into the pComb3XSS phagemid vector and transforming into *E. coli* cells. The phage library was rescued by infection with helper phage and screened against immobilised STX-OVA conjugate.

There are many reasons to hinder the isolation of a recombinant antibody. Firstly, immunization problems caused by the toxic nature of the immunogen and the size of the hapten and the quality of conjugation, may lead to poor immune response of an animal. PSPs possess small molecular weights. For such hapten targets, there are limited functional groups to conjugate to a protein carrier for antibody production. Only a few chemical reactions can be used to synthesise immunogen. The formation of the toxin protein conjugate must also reduce the toxicity of the toxin before animal immunisation (Campbell *et al.*, 2011). In an ideal situation, conjugates would be fully characterised with comprehensive analytical techniques before immunisation or screening. The analysis would provide invaluable information regarding molecular mass of the

conjugate and hapten incorporation ratios. However, in this project the analytical systems were not available and the large size of the protein carriers would have made the analysis extremely complex and difficult.

Secondly, the amplification problems during the construction of the antibody library may lead to inefficient variable gene assembly and a poor diversity of scFv library. Due to the diverse V_KJ_K rearrangements, the generation of a rabbit antibody repertoire requires many V-specific oligonucleotide primers. This in turn, can require extensive optimisation to amplify the various light chain and heavy chain sequences and capture a good representation of the repertoire (Barbas *et al.*, 2004). Furthermore, if the overlap PCR product of the variable heavy and variable light chains is not highly efficient, sequence frame shifts may occur resulting in poor quality of the library (Koohapitagtam *et al.*, 2010). These factors may have contributed to the production of an inferior scFv library, with minimal specificity for PSPs.

A further problem is that the elimination of useful clone during selection of target-binding phage. The selection of target-binding clones from phage display libraries is driven by two processes: (1) the panning step. Clones that bind to the desired target or any other physical moieties present during the panning step, such as walls of the vessels, are enriched (Menendez *et al.*, 2005). (2) the amplification step. Infection of bacteria by a single phage particle and the secretion of ~1,000 copies of phage (Barbas *et al.*, 2001). The undesired loss in target-binding clones after the amplification step was commonly present in the past, when researchers could only isolate and characterise a small sub-population of phage clones. Derda and coworkers demonstrated that a library of phage-displayed peptides contains clones that bind to a target better than other clones and clones that amplify faster than other clones. Herein, the amplification of a library leads to loss of diversity of clones. It was reported that the simplest strategy to bypass this problem is to skip the amplification steps altogether. The method has been used successfully in several instances (Arap *et al.*, 2002; Krag *et al.*, 2006; Brown *et al.*, 2010). An alternative strategy is to provide uniform amplification for selected clones which can be achieved by: (1) isolating clones from one another; (2) supplying each clone with an equal number of bacteria.

The main limitation of this project work was the scarcity and high price of purified toxin material. If a reliable, purified source of toxin material becomes available in the

future, it may be possible to isolate the recombinant antibody to PSPs from the existing immune libraries.

CHAPTER 4

Development of Microfluidic System for Rapid HIgG Detection

4.1 Introduction

4.1.1 Manufacturing process of monoclonal antibody

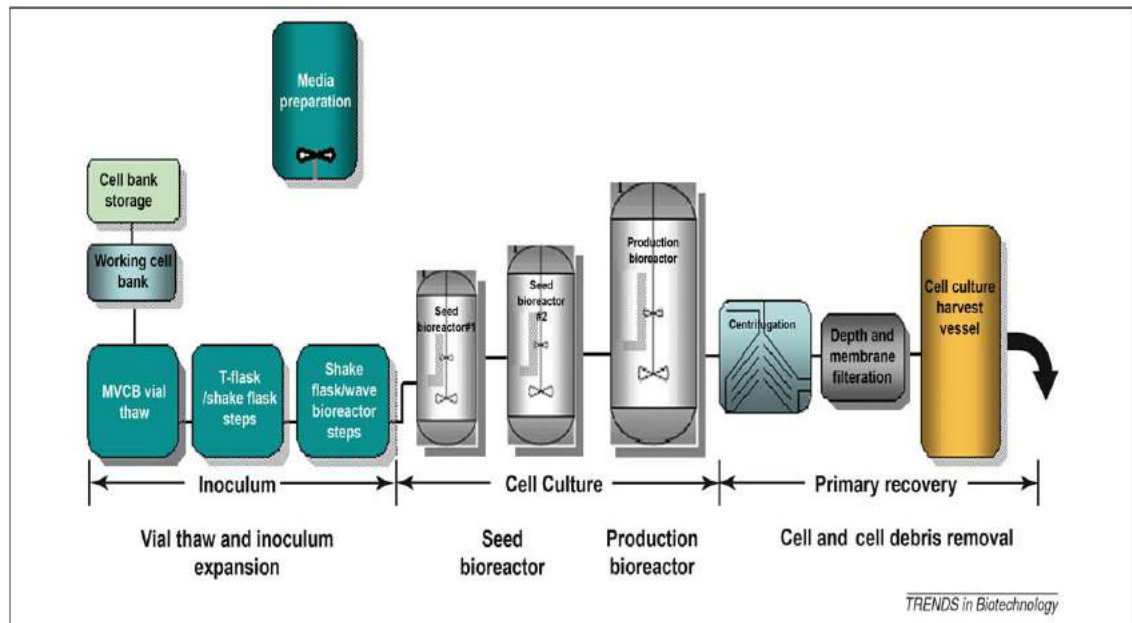
Monoclonal antibodies (mAbs) are a major class of human therapeutics and have been widely used for the treatment of cancer, autoimmune, cardiovascular and inflammatory diseases, as well as organ transplantation. These glycosylated proteins have many strengths that include their specificity and strong affinity, effector functions and other biological activities (Booy *et al.*, 2006). One of the greatest advantages is the potential ease of generating mAbs with high affinity and specificity to virtually any target of therapeutic interest (Carter, 2011). So far, over 30 mAbs have been licensed by the United States Food and Drug Administration (FDA) for clinical application meanwhile hundreds of candidate molecules are in clinical and pre-clinical stages of testing. A substantial proportion of these approved and candidate antibody therapeutics are in an IgG format (Li & Zhu, 2010; Boonsopon *et al.*, 2015). Worldwide sales of therapeutic mAbs have risen dramatically and the market for therapeutic mAb derivatives is one of the fastest growing sectors in the pharmaceutical industry.

Typical mAb production is carried out on an industrial scale using very large bioreactor vessels. This process can be broken down into two major stages: the upstream processes and the downstream processes. An overview of these manufacturing processes is illustrated in Fig. 4.1. The upstream process includes the culture of the hybridomas or cell lines for generation of therapeutic antibodies or their derivatives and primary recovery (Jain & Kumar, 2008) (Fig. 4.1A), whereas the downstream processes ensure the removal of process-related impurities (e.g. Protein A) to safe levels in the final drug product (Fig 4.1B) (Shukla & Thömmes, 2010). The potential for product failure or issues with quality control is high, as these procedures are complex and involve multiple steps as well as long production times. Therefore, efficient controlling and monitoring of the manufacturing process is a critical issue.

An ideal process monitoring system should be non-invasive by providing detailed process information without interference with the process itself. ‘On-line’ bioprocess monitoring is important for early detection of problems such as infections, to provide the opportunity to react immediately. Optical sensors are now applied for ‘on-line’ bioprocess monitoring. They are ideal for monitoring cultivation processes because the testing can be performed within the process (*in situ*), with living cells (*in vivo*), and ‘on-

line' and can be very sensitive. Optical, noninvasive measurements do not interfere with the growth of the cells and no analyte is consumed. Measurements in 'real-time', with no time delay, allow effective control and early detection of problems (Werner, 2004).

(A) Upstream processing



(B) Downstream processing

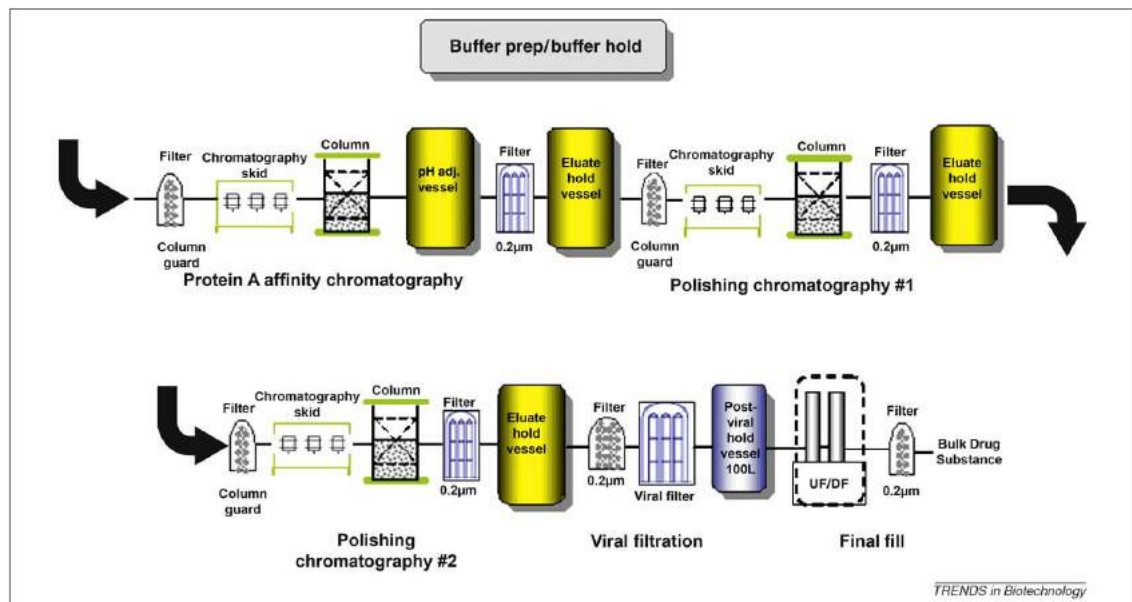


Figure 4.1 Schematic of the mAb manufacturing process (adapted from Shukla & Thömmes, 2010). (A) The upstream process started with vial thawing and expansion of cells via a series of inoculum steps. The cells were then expanded in a series of seed bioreactors before being transferred to the production bioreactor, where the mAb was expressed into the medium. Centrifugation and a series of filtration steps were used to harvest the cell culture broth from cells and cell debris. (B) The downstream process started with Protein A chromatographic capture and includes two subsequent polishing chromatographic steps for impurity removal. The process also included two dedicated orthogonal steps for viral clearance: low pH viral inactivation after protein A chromatography and viral filtration. The final process step was

ultrafiltration/diafiltration (UF/DF) to formulate and concentrate the product.

4.1.2 Microfluidics

Microfluidics-based technologies have revolutionized the possibility for new assay format development and implementation (Beebe *et al.*, 2002; Vilkner *et al.*, 2004). Compared to conventional immunoassay formats, microfluidic platforms possess remarkable features such as high surface-to-volume ratios and nanoliter microchannel volumes which, in turn, can dramatically impact interfacial reaction kinetics in solid-phase-based immunoassays. Consequently, these features allow a ‘sample-to-answer’ test to be generated with short analysis times, small samples volumes, integrated fluidic handling, and ‘at-line’ processing (Bange *et al.*, 2005). In a recent report, sales of advanced microfluidics devices are estimated to be up to 23% annual compound growth until 2016, expanding the sector to almost \$4 billion. Microfluidics technologies in the Life Science fields include different applications such as drug delivery, industrial and environmental testing, analytical devices, pharmaceutical science uses, point-of-care testing and clinical diagnostics. During such applications, immunoassay is the most widely applied analytical technique (<http://www.i-micronews.com/>). In addition, the relative increase in associated publications reveals that microfluidic techniques have been employed extensively in many immunoassay systems (Becker *et al.*, 2003; Henares *et al.*, 2007; Mark *et al.*, 2010; Yeo *et al.*, 2011; Yetisen *et al.*, 2013; Tam *et al.*, 2014).

Currently, the focus of microfluidic platforms for diagnostics or bioprocess monitoring is on the integration of several analytical steps leading to direct ‘sample-to-answer’ systems. One of the main challenges of integration is the requirement for serial valving to allow the sequential release of fluids in a temporally and spatially controlled manner. In this work, the experimental serial siphon was shown to be robust and reproducible. However, there can be variability in the fluidic release from siphon valves due to dependence on contact angle, rotation velocity, and fluidic properties (e.g. surface tension). To date, liquids with different properties (e.g., surface tension and viscosity) are required to be released at the appropriate time and to the appropriate location. Serial siphons and capillary valves in centrifugal microfluidic platforms have been demonstrated to meet this need (Jia *et al.*, 2006; Bergeron *et al.*, 2008; Siegrist *et al.*, 2010; Nwankire *et al.*, 2013; Kitsara *et al.*, 2014).

The working mechanisms and features of the simplest double siphon device on a microfluidic CD are illustrated in Fig. 4.1.2. Siphon valving required a hydrophilic surface to allow capillary pumping (Siegrist *et al.*, 2010). After fluid was loaded into the upper reservoir chambers, the CD was spun at a high speed to trap the fluid into the siphon channels. The fluid in the siphon channel is static when its position is radially equivalent to the reservoir fluid height. At this stage, capillary forces are equal to the centrifugal forces (Fig. 4.1.2a). If the rotation velocity is reduced to a lower speed, thus allowing capillary force to overcome the centrifugal force, the fluid in the siphon channels are pushed over the first siphon crest and are then detained by the next in-line capillary valve (Fig. 4.1.2b). The capillary valve is formed by an abrupt widening in the siphon channel. This provides higher surface tension forces than centrifugal and capillary forces. A high spin speed causes an increase in the centrifugal force which can burst the capillary valve. When the fluid is in a channel which contains one siphon component, the fluid will completely flow into the lower chamber. However, the fluid in the channels comprised of two siphons, flows into the next siphon and stops at the position radially equivalent to the reservoir fluid height (Fig. 4.1.2c). When the rotation speed is reduced, the fluid is primed over the crest of the following siphon loop (Fig. 4.1.2d). The fluid bursts the capillary valve under a high rotation speed and then the fluid flows into the lower chamber (Fig. 4.1.2e). In this manner, the different fluids are sequentially delivered into one chamber through controlling the CD spin speed.

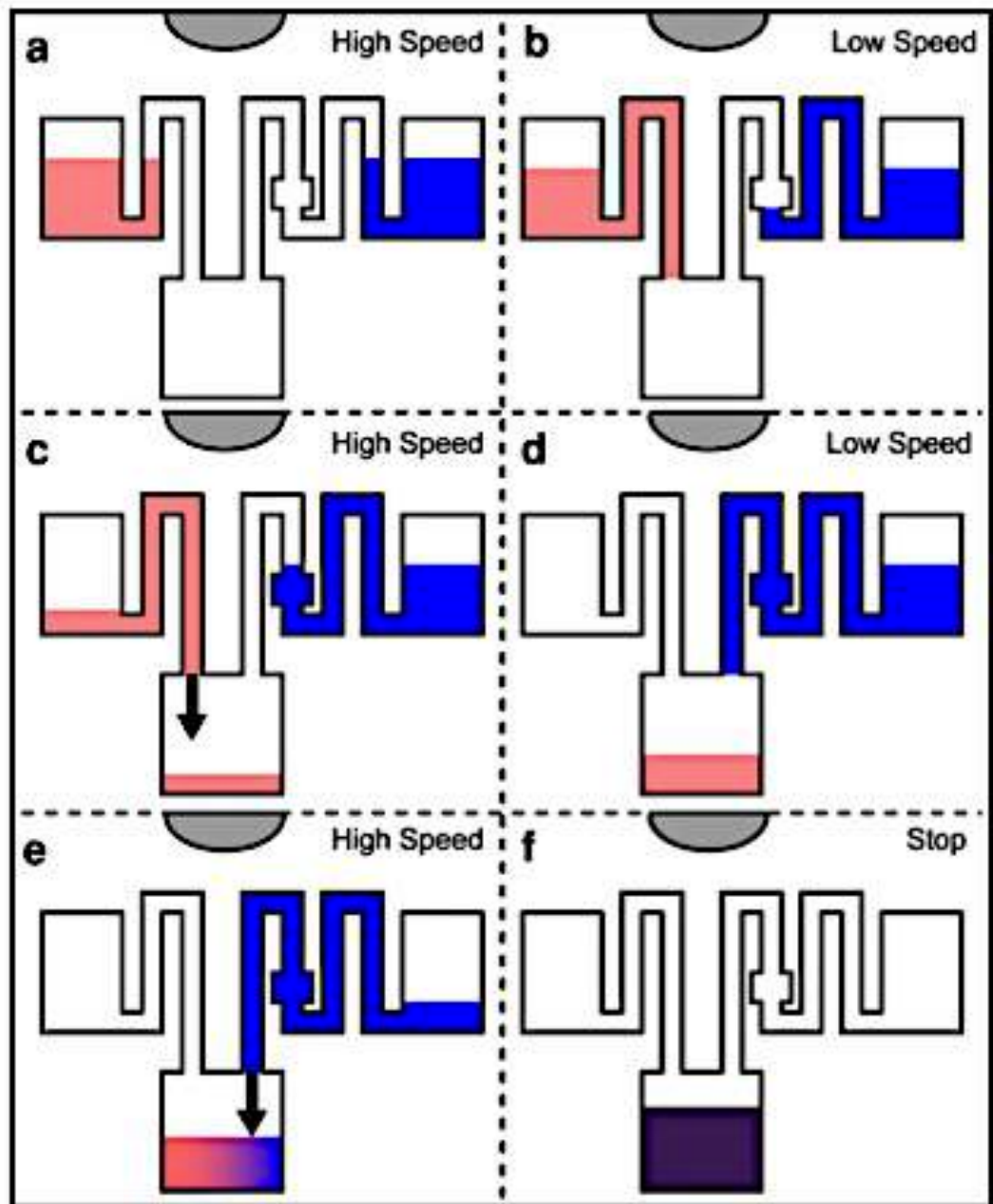


Figure 4.1.2 A schematic of the simultaneous function of single (left, red) and double serial (right, blue) siphon valve channels between chambers (adapted from Jia *et al.*, 2006).

4.2 Aims of this chapter

The aim of the research described in this chapter is the application of microfluidic technology for bioprocess sample analysis. To achieve this goal, an immunoassay possessing high sensitivity and specificity for detecting IgG needed to be designed and developed. Meanwhile, development of an advanced detection system with high sensitivity was also essential. In addition, microfluidic cartridges with advanced fluid handling functions needed to be developed.

4.3 Results

4.3.1 Components of the human IgG (hIgG) immunoassay

An indirect fluorescence-labeled immunoassay (FLISA) was initially designed to detect hIgG molecules by Dr. Gerard Donohoe. The components of this hIgG indirect FLISA included: a capture protein i.e. protein A; the target analyte, hIgG; biotinylated anti-hIgG antibody and the detector complex consisting of NeutrAvidin Dylight 650 (Fig. 4.3.1). Protein A was coated on the solid phase (microtitre plate), and then binds to the Fc region of hIgG with a high affinity. The biotinylated anti-hIgG is added and specifically binds with bound hIgG. Finally, NeutrAvidin with a conjugated fluorescent label, binds with biotin which is conjugated to the anti-hIgG antibody. The utilisation of the 'biotin-neutravidin' system in this assay can provide high signal amplification with associated high sensitivity, often significantly greater than achieved with other labelling approaches.

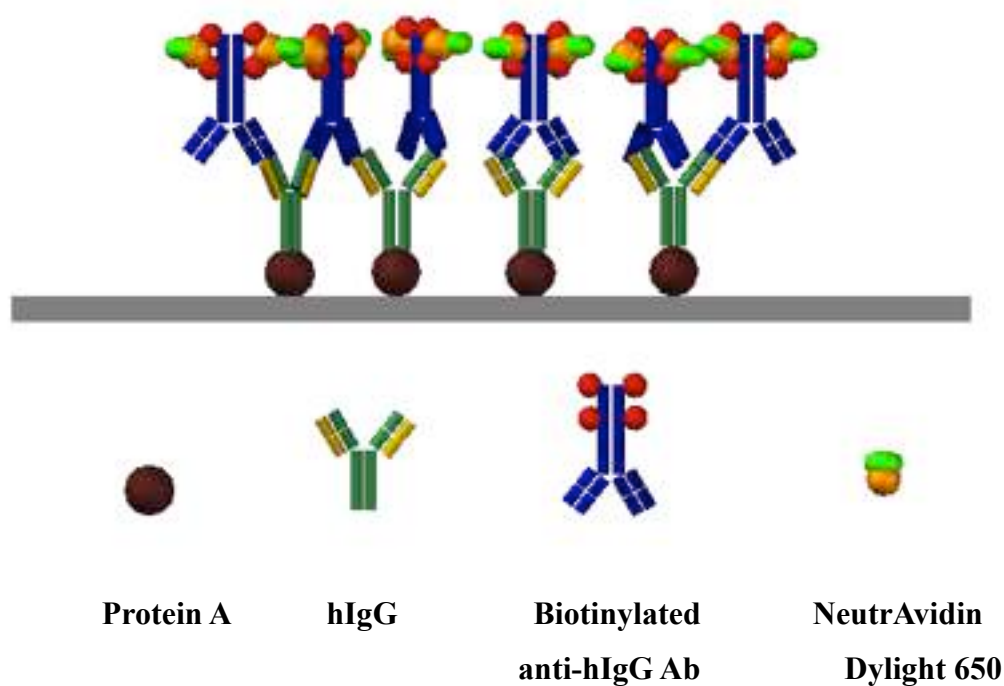


Figure 4.3.1 Schematic of an indirect hIgG immunoassay.

4.3.2 Optimisation and development of hIgG FLISA on an ELISA plate

The designed hIgG FLISA was further optimised on an ELISA plate. After optimisation the concentrations of protein A, biotinylated anti-hIgG and standards (hIgG), a standard curve with optimal performance was developed on an ELISA plate. Additionally, some other aspects of the development of hIgG indirect immunoassay were carried out, such as the timing of the sequence of addition of reagents and the influence of incubation time.

4.3.2.1 Optimisation of the protein A coating concentration and biotinylated anti-hIgG concentration

The optimal ELISA plate coating concentration of protein A was determined. The coating concentrations of protein A (0.2 µg/mL, 1 µg/mL, 5 µg/mL and 25 µg/mL) were compared with utilisation of a 1:250 dilution of mouse anti-hIgG antibody and a 1:2,000 dilution of NeutrAvidin Dylight 650 in PBS. The fluorescence intensity was plotted against hIgG concentration in Fig.4.3.2.1a. The data showed that protein A concentrations below 5 µg/mL generated low fluorescence intensity. In contrast, the 25 µg/mL concentration of protein A generated the highest fluorescence intensity with hIgG concentrations ranging from 10^{-2} to 10^1 µg/mL and generated satisfactory dose-response curves (approx dynamic range of 2.5 logs).

Subsequently, a checkerboard ELISA was performed to determine the optimal concentration of the biotinylated anti-human IgG antibody. Several dilutions of this antibody were prepared (1:250, 1:500, 1:1,000, and 1:2,000). In addition, the Neutravidin Dylight 650 conjugate was diluted to 1 in 2,000 in PBS and the protein A coating concentration was 25 µg/mL. After detection, hIgG concentrations were plotted against fluorescence intensity with a 4-PL model (Fig. 4.3.2.1b). A 1:250 dilution of the biotinylated anti-human IgG antibody yielded the highest fluorescence intensity with a hIgG concentration ranging from 10^{-2} to 10^1 µg/mL and gave the best dose-response curve.

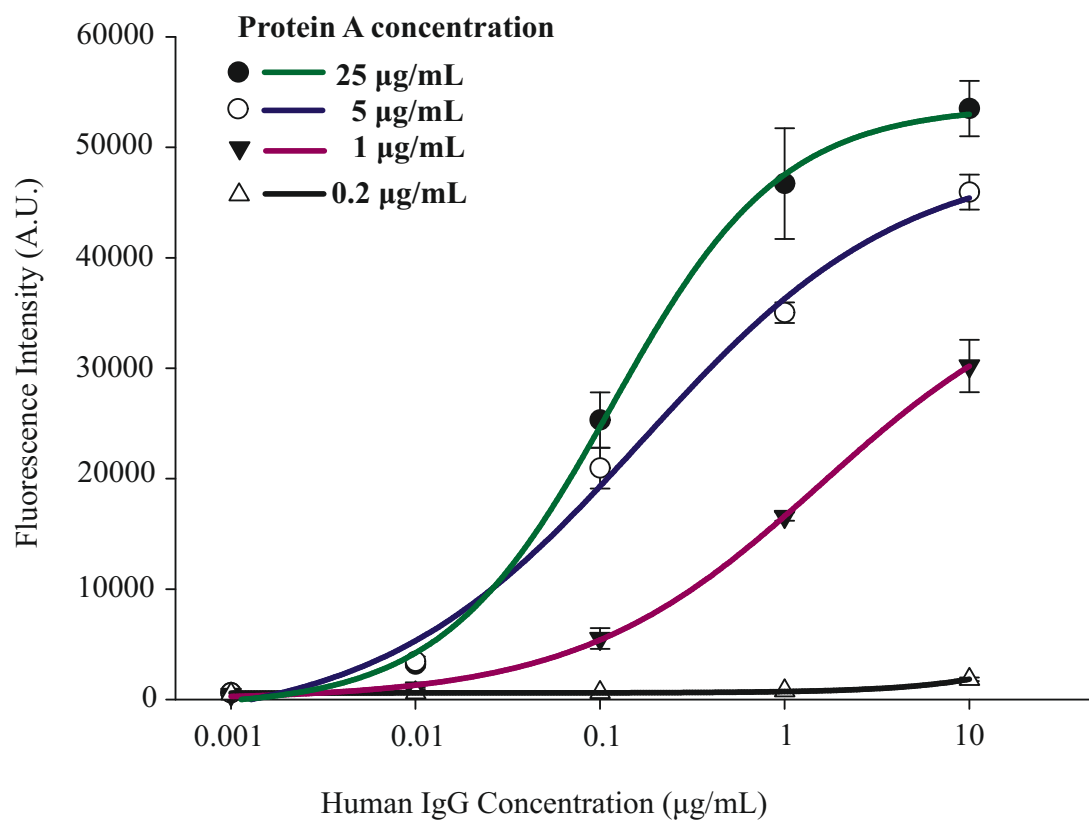


Figure 4.3.2.1a Optimisation of Protein A coating concentration using conventional FLISA . Each sample was tested in triplicate and the error bars represent the standard deviation.

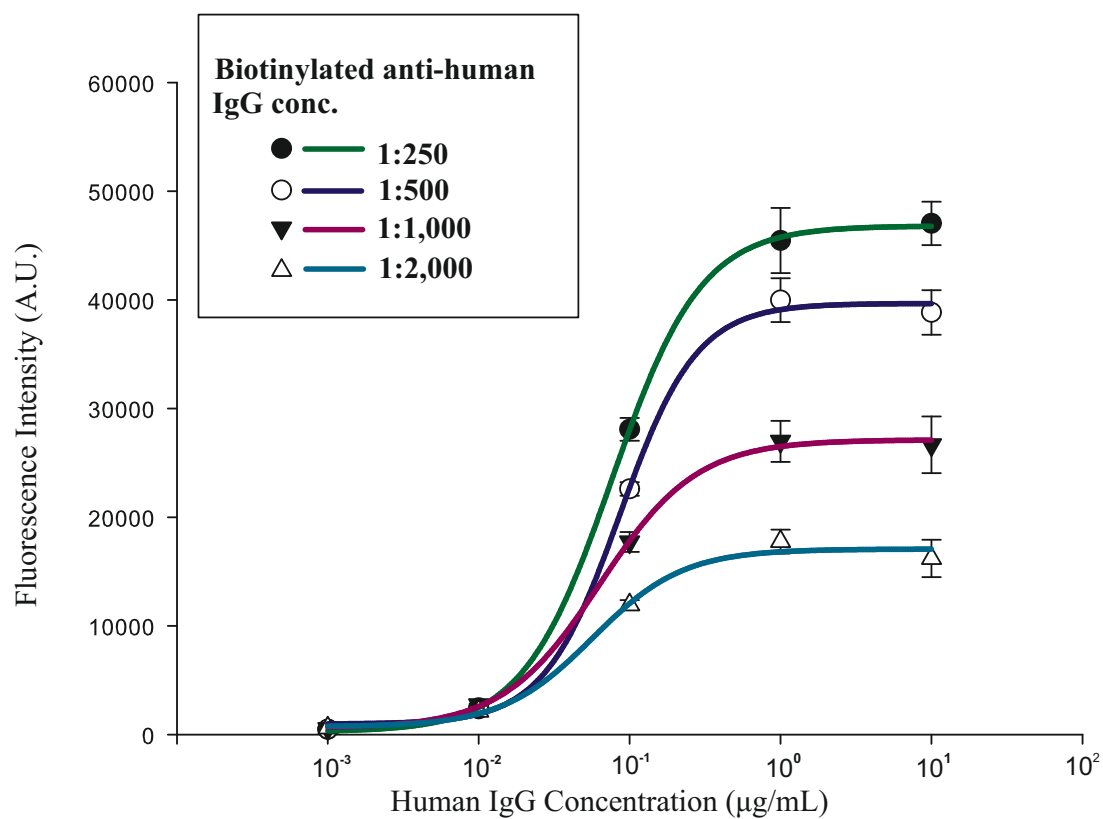


Figure 4.3.2.1b Optimisation of conventional FLISA anti-human IgG antibody concentration. Each sample was tested in triplicate and the error bars represent the standard deviation.

4.3.2.2 Determination of influence of addition of reagents

Although a number of centrifugal microfluidic platforms were successfully demonstrated for immunoassays (Honda *et al.*, 2005; Ukita *et al.*, 2012; Kinahan *et al.*, 2014; Hasegawa *et al.*, 2014), most of these platforms were designed with complex microchannel networks, which were required for a multi-step immunoassay. The complex microchannel networks hindered the generation of a high-performance device enabling easier operation, short analysis times and full automation. Therefore, this study was carried out to simplify assay steps and then obtain a rapid assay.

To this end, further development of the hIgG indirect immunoassay were carried out by analysis of the influence of the sequence of addition of reagents and incubation times. In order to reduce the number of steps of indirect hIgG immunoassay, the effect of the use of a mixture consisting of biotinylated anti-hIgG and NeutrAvidin DyLight 650 was tested in a 96-well plate. The hIgG indirect assay was carried out by using a mixture of biotinylated anti-hIgG and NeutrAvidin DyLight 650 instead of using separate additions (Fig. 4.3.2.2A). On comparison with the initial assay results, the assay using the reagent mixture shows greatly enhanced sensitivity, which is demonstrated by the curve obtained. Additionally, utilisation of a reagent mixture contributes a simpler and faster assay.

In addition, another study was carried out to determine the influence of incubation time on the stability of the reagent mixture (Fig. 4.3.2.2B). The reagent mixture prepared by pre-incubation at 37°C for 20 minutes was compared with the reagent mixture prepared immediately before analysis without incubation. The data shows that such an incubation step provides a more sensitive and robust assay by reducing reagent-induced variations. Furthermore, it indicates that the incubation for 20 minutes at 37°C is sufficient for equilibration of the biotinylated anti-hIgG and NeutrAvidin DyLight 650 reaction. This result suggests that mixing and incubation of the anti-hIgG and NeutrAvidin DyLight-650 molecules prior to addition to the assay surface, can reduce steric hindrance and enhance binding.

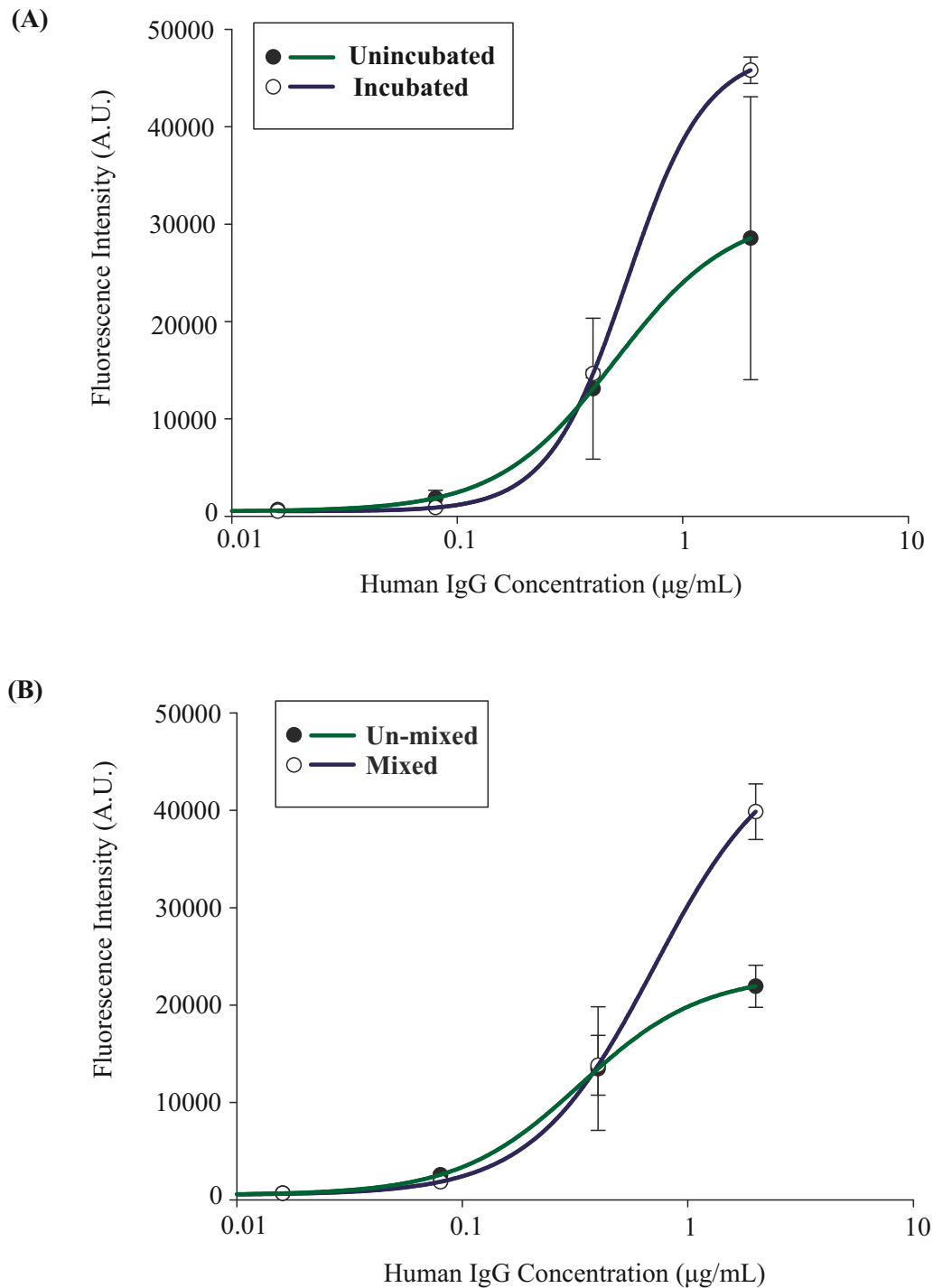


Figure 4.3.2.2 Effect of mixing reagents (biotinylated anti-hIgG and NeutrAvidin DyLight-650) on the hIgG indirect assay performance. (A) comparison of hIgG assay results with or without mixing of reagents. The green curve represents the assay without the application of mixed reagents, In contrast, the blue curve represents the assay adopt the mixing of reagents. (B) Comparison of

hIgG assay results with/without incubation during mixture preparation. The green curve represents the assay using the mixed reagents without incubation at 37°C for 20 minutes. The blue curve represents the assay adopting the mixed reagents prepared with incubation at 37°C for 20 minutes. Each sample was tested in triplicate and the error bars represent the standard deviation.

4.3.2.3 Optimising the ratio between biotinylated-antiIgG and NeutrAvidin DyLight

In order to establish whether or not the ratio of biotinylated anti-hIgG and NeutrAvidin DyLight-650 in a mixture was a critical parameter, numerous assays were performed using different ratios of biotinylated anti-hIgG and NeutrAvidin DyLight in mixtures. The mixtures were prepared by mixing biotinylated anti-hIgG and NeutrAvidin DyLight-650 in 1:1, 2:1, 3:1, and 1:2 ratios, followed by incubation for 20 minutes at 37°C prior to addition to the plate. After detection of the fluorescence signal from assay plates, data were analysed by plotting the fluorescence signal against the human IgG concentrations. Under the condition of using mixing of biotinylated anti-hIgG and NeutrAvidin DyLight-650 in 1:2 and 1:3 ratios, the assays were negatively affected (data not shown). Fig. 4.3.2.3 shows the dose-response curves of the assays with application of the mixing biotinylated anti-hIgG and NeutrAvidin DyLight-650 in 1:1, 2:1 and 3:1 ratios. Comparison of different ratios of biotinylated anti-hIgG and NeutrAvidin DyLight-650 indicated that the 3:1 ratio was superior since the curve was saturated at higher human IgG concentrations and has a larger dynamic range.

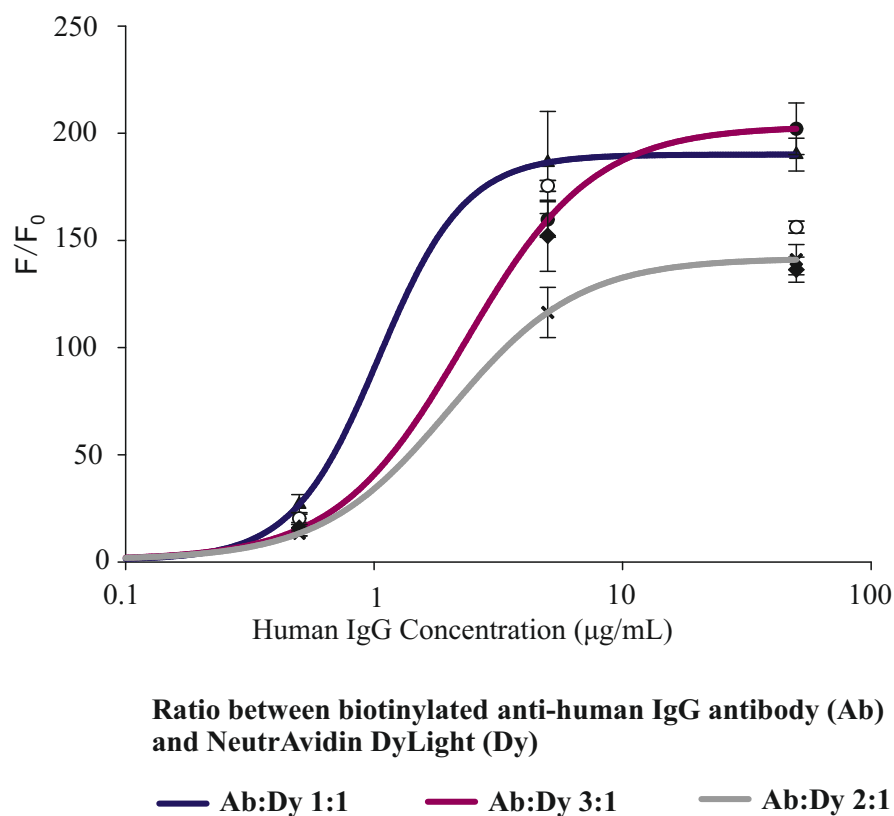


Figure 4.3.2.3 Optimisation of ratios in mixing biotinylated-anti-hIgG and NeutrAvidin DyLight. The mixtures were prepared with different ratios of biotinylated-anti-hIgG and NeutrAvidin DyLight-650 (1:1, 1:2, 1:3, 2:1 and 3:1). Each samples was tested in triplicate and the error bars represent the standard deviation of the mean of three measurements. The fluorescent signal was normalised (F/F_0) before plotting against hIgG concentration.

4.3.3 Development and optimisation of a hIgG FLISA on a ‘proof-of-concept’ microfluidic platform with flow-cells

4.3.3.1 Design of ‘proof-of-concept’ microfluidic platform with flow-cells

The next stage of assay development involved the design, production and testing of simple microfluidic flow-cells. These devices are composed of multilayered materials as previously described (section 2.3.1.1). Each flow-cell contains 3 individual microfluidic units. In addition, a spin holder was designed to accommodate four separate flow-cells (Fig. 4.3.3.1). This structure allows the processing of 12 assays simultaneously. Each reagent is manually loaded into the flow-cell using a pipette via a loading hole. Reagent delivery is achieved by a combination of centrifugal and capillary forces. For each microfluidic unit a microchannel spans the loading hole and the reagent waste chamber. The protein A capture spot is located near the end of the microchannel close to the waste chamber. When a reagent is loaded into the top chamber through a loading hole, it will be held in this chamber due to capillary forces. It is only after the application of centrifugal force, which overcomes weaker capillary forces, that the reagent is pumped through the microchannel. As hIgG flows through the microchannel it encounters the protein A assay spot and binds to it. Excess reagent is subsequently collected in the waste chamber. This simple microfluidic design has several advantages: (1) assay time can be dramatically shortened due to the rapid transport of reagents ; (2) reagent volume can be reduced; (3) assay steps can be simplified; (4) flow-cell design allows for testing of different surface materials; and (5) a closed microfluidic system with disposable cartridges can increase operator safety especially when used for testing of hazardous biological materials.

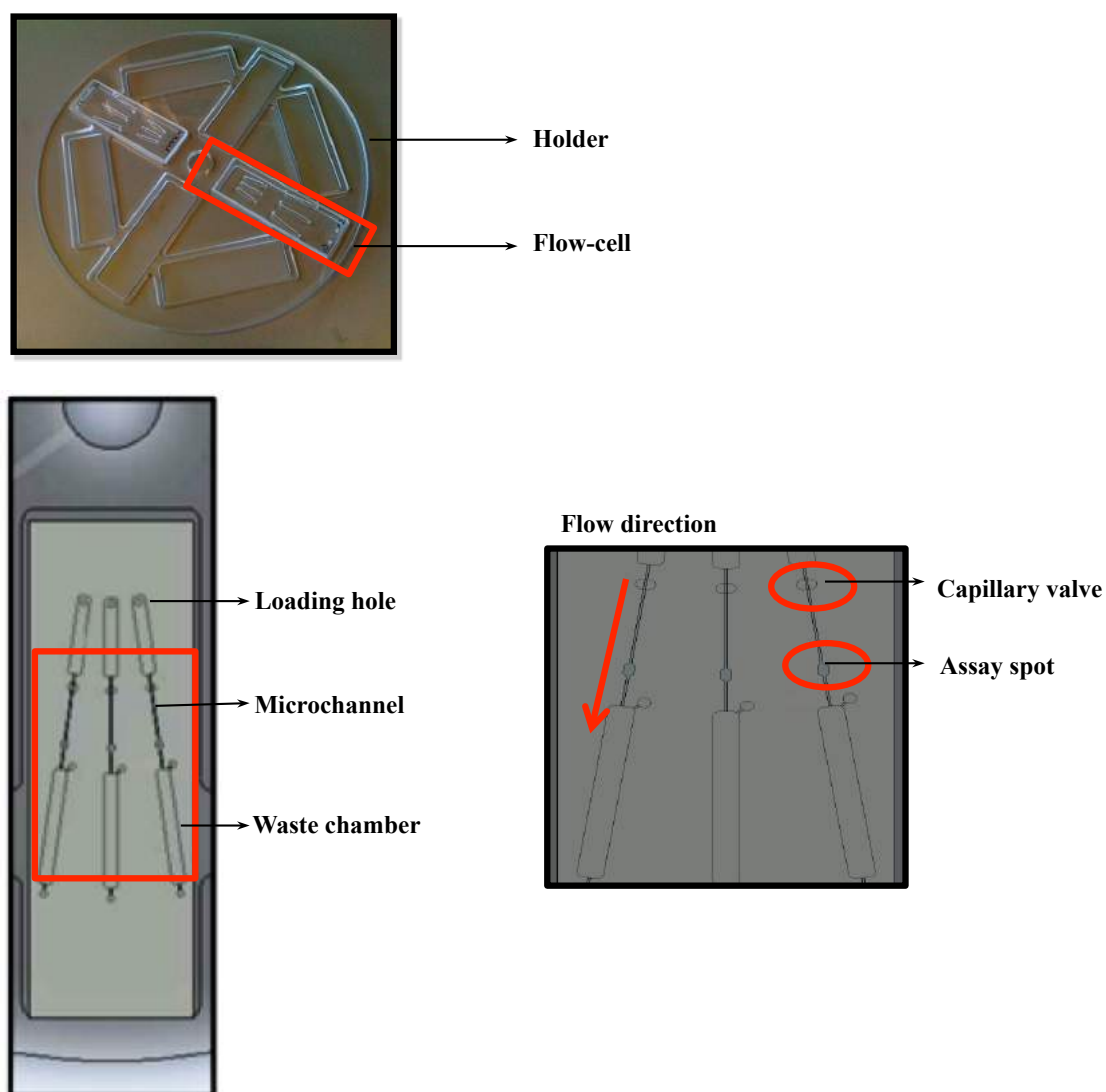


Figure 4.3.3.1 Illustration of flow-cell designs. The spin holder with two flow-cells is illustrated on the top. A whole flow-cell structure is also shown. The flow-cell contains 3 individual microfluidic units, on which two reagent-chambers is connected by a microchannel. The figure on the right shows an enlargement of microchannel which provides a capillary valve and an assay spot.

4.3.3.2 Surface functionalisation

Before the hIgG immunoassay could be applied to the microfluidic flow-cells, a variety of surface materials and immobilisation methods were analysed (Table 4.3.3.2). In total, three different substrates were tested: Zeonor[®], Nunc[™] and glass. In addition, several surface modification methods were compared i.e. PECVD, TEOS/AA, EDC/NHS, and use of an oxygen plasma. Furthermore, curing (baking) times, temperatures and Protein A concentrations were also evaluated. The results showed that three experimental arrangements gave homogenous fluorescent hIgG spots. These groups were: (1) commercial Nunc[™] slides, coated with 500 µg/mL protein A; (2) Zeonor[®] slides treated with an oxygen plasma for 10 minutes and subsequently treated with APTES. The zeonor slides were then baked at 80°C for 1hr and coated with 50 µg/mL protein A; (3) Glass slides treated with plasma for 5 minutes and coated with an APTES solution. Curing was performed at 60°C for 1hr and the slides were coated with 5 µg/mL of protein A. Zeonor[®] was chosen as the substrate for the microfluidic devices. This material is optically clear and has low autofluorescence. Glass was not used as it would have proved cumbersome in device manufacture. Although the commercial Nunc[™] substrate performed as well as the Zeonor[®] polymer it was not used in device manufacture due to its high cost.

Table 4.3.3.2 Optimization of surface modification conditions with different materials.

Slide	Surface Activation	Chemistry	Curing	Pr A conc. (µg/mL)	Outcome
Zeonor[®]	None	None	None	200	X
Zeonor[®]	PEVCD/TEOS/ AA	EDC/NHS	None	200	X
Zeonor[®]	PEVCD/TEOS / AA	EDC/NHS	None	500	X
Nunc[™]	None	None	None	500	GOOD
Zeonor[®]	Plasma (1min)	EDC	None	500	X
Zeonor[®]	Plasma (5min)	APTES	2hrs 80°C	400	X
Zeonor[®]	Plasma (5min)	APTES	1hr 80°C	500	X
Zeonor[®]	Plasma (10min)	APTES	1hr 80°C	50	GOOD
Glass	Plasma (5min)	APTES	1hr 60°C	5	GOOD

(X represents a poor outcome)

4.3.3.3 Determination of the influence of removal of the washing step during flow-cell-based hIgG immunoassay

As outlined in Table 4.3.3.3, flow-cell-based hIgG FLISA has six steps, consisting of (1) BSA blocking, (2) PBS wash, (3) addition of hIgG sample, (3) PBS wash, and (4) addition of mixed biotinylated anti-hIgG and Neutravidin DyLight 650 (anti-IgG/Dylight) followed by (5) a PBS wash. In order to generate a quick immunoassay on a flow-cell, further development was carried out by evaluating the influence of removing wash steps from the assay protocol. To this end, several hIgG FLISAs were performed on a flow-cell removing different wash steps. It included the removal of the wash step after BSA blocking, the wash step after loading hIgG, the wash step before and after loading the mixture of anti-IgG/Dylight. The results were analysed and compared with the established hIgG FLISA (performed with the standard procedure in Table 4.3.3.3). It demonstrated that the assay result can be dramatically affected by the removal of wash steps, with the exception of the wash step after BSA blocking (Table 4.3.3.3). Fig. 4.3.3.3, compares the assay data from a standard procedure with all wash steps against procedures without the wash step after BSA blocking. The checkerboard result of assays under different conditions is illustrated in Fig. 4.3.3.3. Three hIgG samples with concentrations of 0.5, 5 and 50 $\mu\text{g/mL}$ were tested to analyse the trend in the fluorescence signals. The fluorescence intensity (F) for each concentration was normalised by transformation to F/F_0 . The F/F_0 values from standard procedure were lower than the procedure, in which the wash step after BSA blocking was removed. However, a lower F_0 was obtained from the assay without wash step after BSA blocking. The result indicates that, without a wash step, extra BSA molecules adsorbing on the channel walls, can dramatically reduce unspecific binding on the inside of the channel. Additionally, the extra adsorbed BSA induced a signal decline on both background (F_0) and fluorescence intensity (F). In our study, the signal decline on F_0 was more remarkable than F and the F/F_0 values were increased. Additionally, the reduced F values were still above the detection limitation of a designed fluorescence detection system. Therefore, it is possible to remove a wash step after BSA blocking in this flow-cell based hIgG FLISA.

Table 4.3.3.3 Outline of hIgG FLISA procedures on flow-cell.

	Reagents addition sequence
Standard procedure	1. BSA, 2. PBS, 3. hIgG, 4. PBS, 5. Anti-hIgG/Dylight, 6. PBS
BSA wash removed procedure	1.BSA, 2.hIgG, 3.PBS, 4.Anti-hIgG/Dylight, 5.PBS

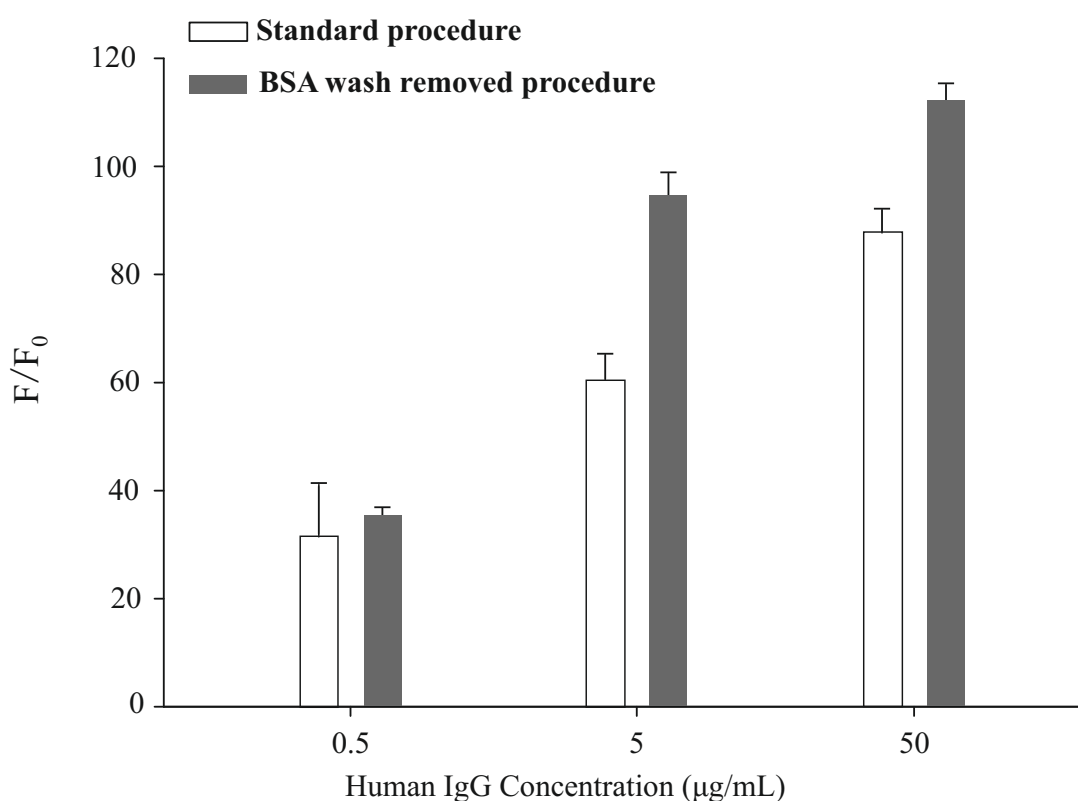


Figure 4.3.3.3 Checkerboard FLISA on flow-cells for determination of the influence of removal of the wash step after BSA blocking. Black bars represent the nomilised fluorescence intensity generated by the assay using the standard optimised procedure. Gray bars represent the normalised fluorescence intensity generated from the assay without the wash step after BSA blocking. Three hIgG samples with concentrations of 0.5, 5 and 50 $\mu\text{g/mL}$ were tested in both procedures. The error bars represent the standard deviation of the mean of three measurements.

Hence, the developed flow-cell-based hIgG FLISA has five steps, consisting of (1) BSA blocking, (2) addition of hIgG sample, (3) PBS wash, (4) addition of mixed anti-hIgG/Dylight followed by (5) a PBS wash. To run this hIgG FLISA in flow-cells, these reagents were added sequentially into the reagent chamber and delivered to the sensor area of the flow-cell under centrifugal force (Fig. 4.3.3.1). By utilization of the developed procedure, the assay time was reduced from more than 6 hours (using 96-well microtitre plates) to approximately 20 minutes (using flow-cells).

4.3.3.4 Comparison of results of flow-cell-based hIgG FLISA with two different APTES solvents

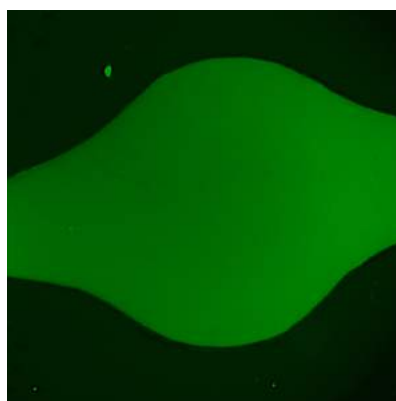
An ideal microfluidic system for diagnostic or monitoring should be disposable and low cost. However, a large amount of ethanol was required during process of convenient liquid APTES deposition. Herein, the study was carried out to investigate an ethanol substitute.

As described in Fig 4.3.3.1, the flow-cell was composed of plastic (PMMA and COP) and PSA. These substrates do not possess native functional groups for specifically interacting with biomolecules and need to be pretreated before fabrication. In our study, the pretreatment includes a wash step to eliminate adsorbed unknown biomolecules and a liquid APTES-deposition step to enhance target biomolecular adsorption. This pretreatment process consumes a large amount of ethanol as solvent. It dramatically increases the cost to produce flow-cells. Therefore, a new solvent with low cost and good performance was considered. Isopropyl alcohol was tested as the APTES solvent and wash solution instead of ethanol in the surface pretreatment stage. The effect of using isopropyl alcohol on surface functionalisation was shown by comparing with the assay results on ethanol pretreated flow-cells (Fig. 4.3.3.4a). In addition, two hIgG samples with the concentrations of 0.5 and 5 $\mu\text{g/mL}$ were tested, respectively.

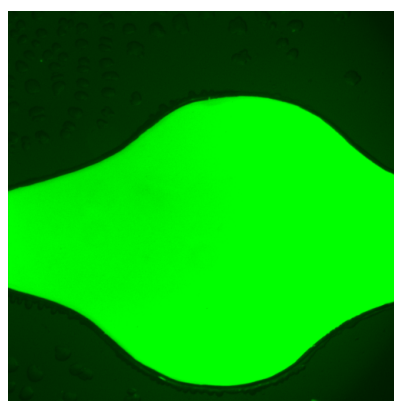
After analysis of these two hIgG samples on the flow-cells with two distinct solvents, the image data was measured from assay spots on flow-cells using an ANDOR iXon 885 camera coupled fluorescence microscope. The image data can directly reveal the distribution of fluorescence on the assay spot and can be used to assess the surface functionalisation method. Herein, a uniform fluorescence distribution on the image data represents a well functionalised surface; and an increased fluorescence from a hIgG sample with high concentrations represents an efficient surface functionalization. Several conclusions can be obtained from the image data in Fig. 4.3.3.4a. They are (1) all image data show relatively uniform morphology for the assay spot; (2) a high concentration of hIgG gave the highest fluorescence signal; (3) for the same hIgG sample, brightness of image data from the two functionalized surfaces is similar. These results indicated that isopropyl alcohol shows good utility for surface modification and can be a potential ethanol substitute during substrate pretreatment.

Image data from fluorescence microscopic analysis

(A) Isopropyl alcohol

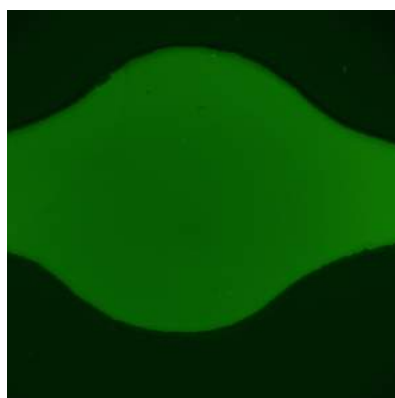


0.5 µg/mL

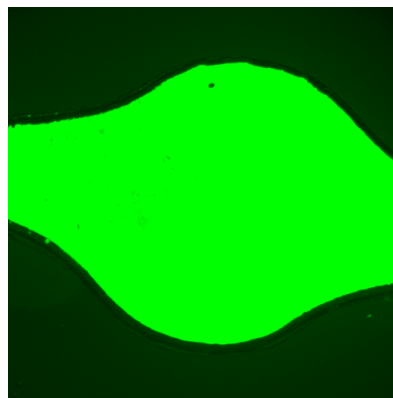


5 µg/mL

(B) Ethanol



0.5 µg/mL



5 µg/mL

Figure 4.3.3.4a Comparison of morphology of assay spots between flow-cells prepared using isopropyl alcohol and ethanol. The image data exhibited by the assay spot with associated fluorescence signal, was measured using an ANDOR iXon 885 camera coupled to a fluorescence microscope.

Additionally, the fluorescence intensity of assay spots was analysed by a SAF detector. The fluorescence intensity detected was plotted against hIgG concentrations in Fig. 4.3.3.4b. The error bars represent the standard deviation from triplicate measurement on each sample. Furthermore, the intra-day coefficient of variation (CV) was analysed from duplicate samples. Compared with the ethanol group, isopropyl alcohol gave a slightly lower fluorescence signal for same concentration of hIgG. However, the CV percentages for each concentration, using isopropyl alcohol, were less than 3%, whereas those using ethanol were up to 11%. All of the results indicate that isopropyl alcohol could be applied instead of ethanol during surface modification of the flow-cells.

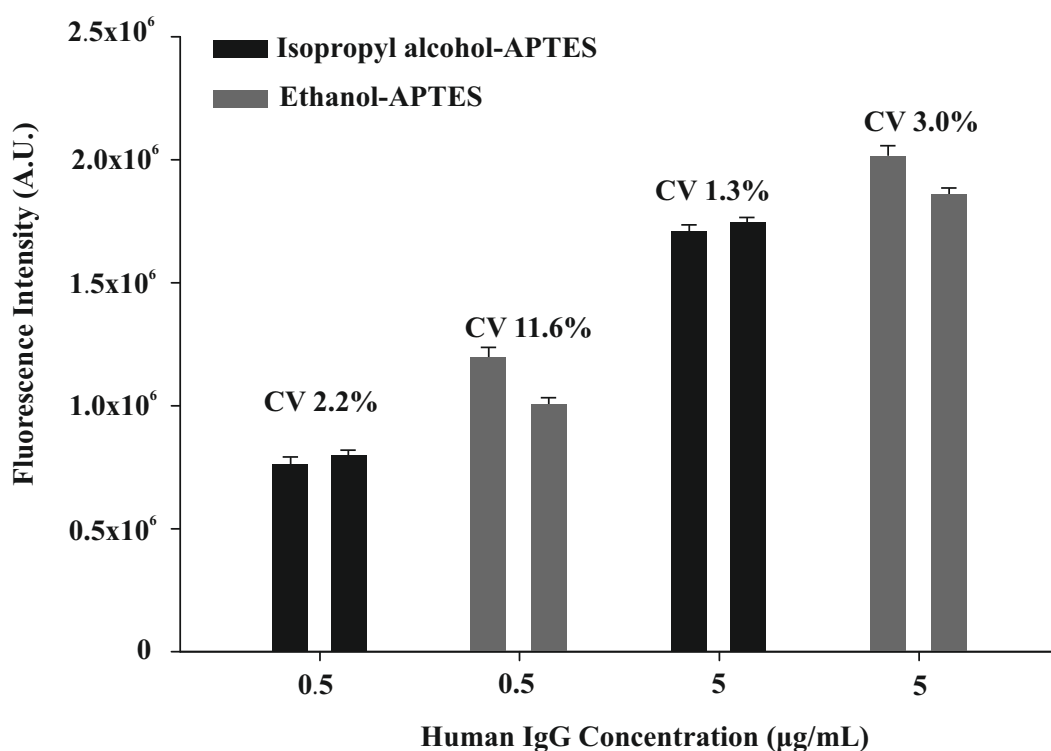


Figure 4.3.3.4b Checkerboard FLISA for comparison of flow-cells prepared with ethanol and isopropyl alcohol. The error bars indicate the standard deviation from triplicate measurements on each sample. The CV percentage illustrated the intra-day coefficient of variation from duplicate samples.

4.3.3.5 Stability study of surface chemistry on flow-cells

The liquid-APTES deposition process was widely used for surface modification of microfluidic systems (Howarter *et al.*, 2006; Lapin *et al.*, 2009; Zhao *et al.*, 2012; Liang *et al.*, 2014). During this process, the amine groups of APTES were introduced on the surface and could bind to target proteins. The existing methods of APTES deposition were modified to produce a stable layer of APTES film for uniform immobilization of biomolecules. The stability of deposited APTES can directly influence the shelf-life of a developed microfluidic system. This study was carried out to evaluate the stability of APTES film on a PMMA substrate and predict the shelf-life of a flow-cell with a deposited APTES film.

In this study, the stability of the liquid-APTES deposition surface was assessed by comparison of hIgG immunoassays performed on flow-cells stored in a desiccator for zero days, two weeks and one month, respectively. Three hIgG samples with concentrations of 0.5, 5 and 50 µg/mL were tested on each of the flow-cells. The fluorescence intensity data from each flow-cell was normalised and compared in Fig. 4.3.3.5. An increase in fluorescence response with increased hIgG concentration was observed on the flow-cell stored for zero days (Fig. 4.3.3.5). The fluorescence response generated on a flow-cell stored for two weeks are similar to the one with zero days storage time. In contrast, the fluorescence response detected from the flow-cell stored for one month showed a decreasing response with increasing hIgG concentrations. This result indicated that the liquid APTES is stable for two weeks in a desiccator. However, they should not be used if stored for one month.

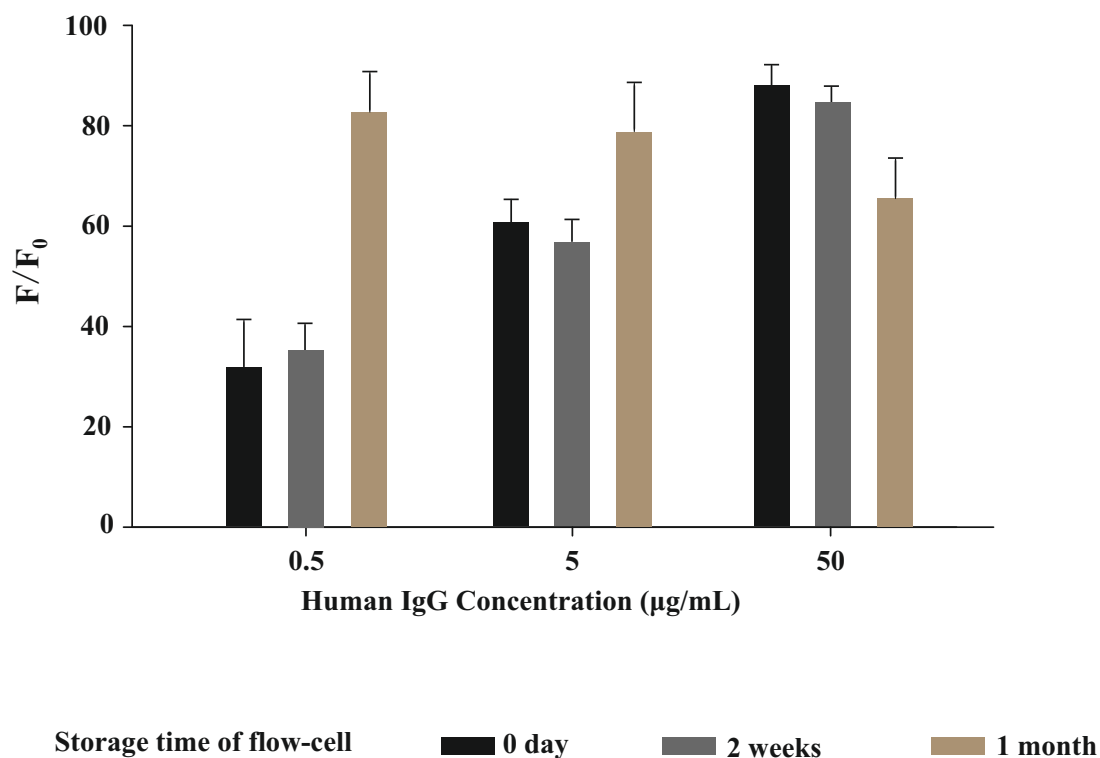
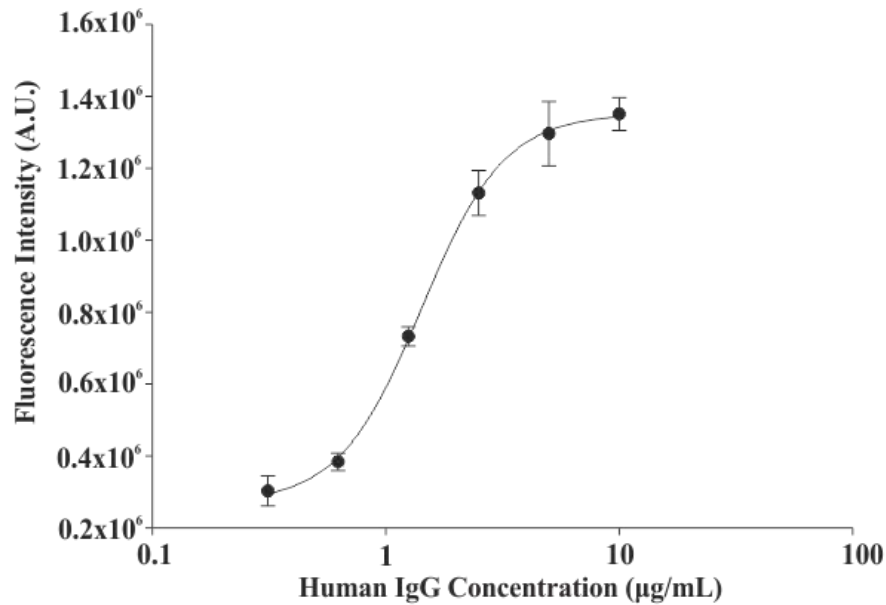


Figure 4.3.3.5 Checkerboard FLISA on flow-cells for stability testing. Protein A (10 µg/mL) was spotted on the modified assay spot surface. Before the test, the flow-cells were stored in a desiccator for zero days, two weeks and one month, respectively. The mixture of biotinylated anti-human-IgG antibody and Neutravidin-Dylight 650, diluted in PBS (150 mM, pH 7.4) at a ratio of 3:1, was pre-incubated at 37°C for 20 minutes. Each sample was tested in triplicate and the error bars represent the standard deviation.

4.3.3.6 Generation of a calibration curve for FLISA in flow-cells and quantification of IgG concentrations in a sample from a bioprocess run

A calibration curve for an IgG immunoassay was successfully generated in the flow-cells. In order to generate the optimal calibration curve, functional groups for biomolecule adsorption were first introduced on the surface by using an oxygen plasma and liquid-APTES deposition methods. Protein A with a concentration of 10 $\mu\text{g/mL}$ was adsorbed on the surface-modified assay spot. Serial dilutions of hIgG, ranging from 0.3 to 10 $\mu\text{g/mL}$, were prepared as the standard samples. The mixture of biotinylated anti-human-IgG antibody and Neutravidin-Dylight 650, diluted in PBS (150 mM, pH 7.4) at a ratio of 3:1, was pre-incubated at 37°C for 20 minutes. The procedure for running FLIA on flow-cells was previously described in section 2.4.3. In total, seven hIgG standards were measured in triplicate using the SAF detection system. In Fig. 4.3.3.6 (A), the inter-day hIgG calibration curve in a flow-cell exhibited a CV of 6.3 to 12.6 % across the entire hIgG concentration range, and the working range from 0.5 to 5 $\mu\text{g/mL}$. Meanwhile, a calibration curve for IgG immunoassay was established on a microtitre plate. The protocol for a microtitre plate-based hIgG FLISA was described in section 2.4.1. Analysis of each sample required 100 μL of the following reagents: protein A (5 $\mu\text{g} / \text{mL}$), hIgG samples, biotinylated anti-human-IgG antibody (1:500 in PBS) and Neutravidin-Dylight 650 (1:500 in PBS). The fluorescence intensity was measured using a Tecan Microplate ReaderTM. In Fig. 4.3.3.6 (B), the inter-day hIgG calibration curve on a microtitre plate exhibited a CV of 5.9 to 18.9 % across the entire hIgG concentration range, and the assay working range was from 0.1 to 10 $\mu\text{g/mL}$. An unknown bioprocess sample, was quantified using calibration curves from the microtitre plate and flow-cell formats. The concentration prediction of the bioprocess sample was determined using the results to generate a curve drawn using SigmaPlot. The concentration of the sample determined using both methods was similar, as conventional FLISA analysis yielded an unknown concentration of approximately 9.3 mg/mL, whereas, the flow-cell-based calibration curve yielded an unknown concentration of approximately 10.1 mg/mL.

(A) hIgG FLISA on a flow-cell



(B) hIgG FLISA on a microtitre plate

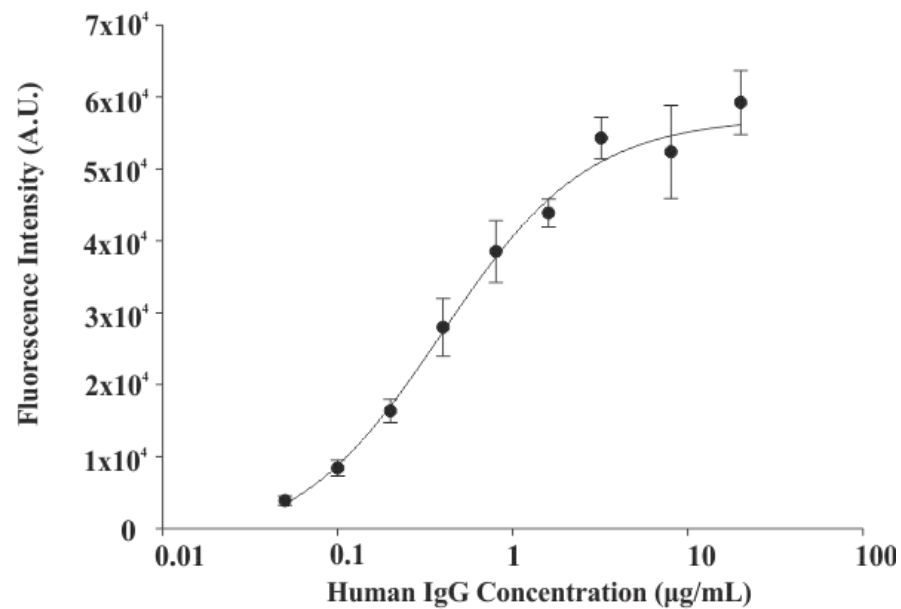


Figure 4.3.3.6 Illustration of bioprocess sample quantification based on two formats. (A) shows the assay performed using a flow-cell and the developed assay format. The predicted hIgG concentration of the bioprocess sample is 10.1mg/mL. (B) This shows the assay carried out on a microliter plate. The predicted hIgG concentration of the bioprocess sample is 9.3 mg/mL.

4.3.4 Development and optimisation of the first design of microfluidic compact ‘disc-like’ platform (CD) – ‘SAF-element’ CD

4.3.4.1 The design of SAF-element CD

The actual overall design of ‘SAF-element’ CD was led by Dr. Charles E. Nwankire in DCU but virtually all of the development work and production was performed by the candidate. The design of the ‘SAF-element’ CD was based on the previous microfluidic flow-cell structure. This new structure was superior due to the utilisation of the SAF ring lens and integrated ‘CD-like’ design. The major features of the SAF-element CD were outlined below:

Centrifugal force

Centrifugal force was employed in the ‘SAF element’ CD due to advantages such as miniaturisation, parallelisation, high-throughput, and low-cost (Duff *et al.*, 1999; Madou, 2002; Madou *et al.*, 2006). A drawback of centrifugal pumping was that it was unidirectional — fluids flow only from the centre of the CD and radiates outward. However, this shortcoming was eliminated by the radially design of flow channels on the ‘SAF-element’ CD.

Capillary valves

Capillary valves were utilised in this CD to efficiently deliver fluids. The capillary valving was achieved by an abrupt widening in a narrow hydrophilic channel, where a larger surface tension force was formed. It can be opened and closed by controlling the spin frequency. When a certain higher frequency, known as the burst frequency, was reached, the centrifugal forces overcame the surface tension forces and push the fluid down the channel (Johnson *et al.*, 2001; Badr *et al.*, 2002; Lai *et al.*, 2004; Cho *et al.*, 2007).

SAF element layer

In addition, a ring lens optical component (supercritical angle fluorescence (SAF)) was designed to achieve highly efficient fluorescence collection with bound substrates. This system consisted of a spherical ring lens for SAF collection and an

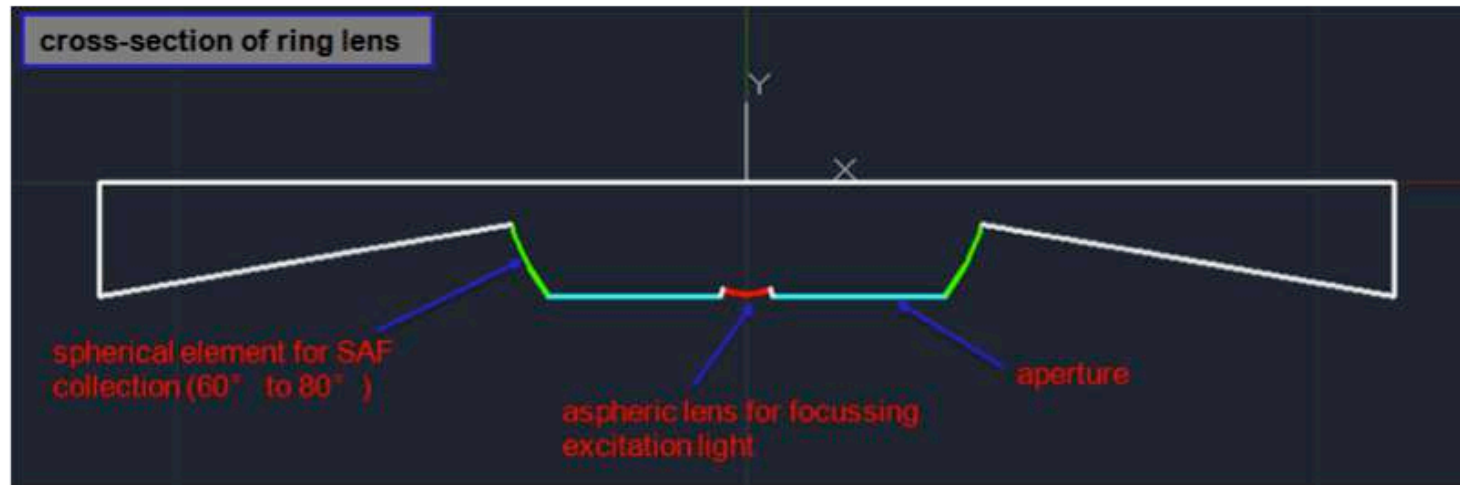


Figure 4.3.4.1a A schematic cross-section of a ring lens structure. SAF light typically propagates within the substrate at angles within the range of $\sim 61.5^\circ$ - 80° . The spherical lens shape (highlighted with green lines) was designed to allow the collection of fluorescence in the above range. The aspheric lens (red line) and aperture (blue line) were designed to focus the excited fluorescence light.

aspherically shaped focusing lens (Fig. 4.3.4.1a). SAF light typically propagates within the substrate at angles within the range of $\sim 61.5^\circ - 80^\circ$. The lens shape was designed to allow optimal fluorescence collection. Zeonor[®] was used as the material of choice, since (1) it had better optical properties than most other moldable plastics, and (2) it was previously used as the substrate in the analysis of proteins and nucleic acids (Lutz *et al.*, 2011).

The first design of a 'SAF-element' CD employed a 20-SAF elements layer (Fig. 4.3.4.1b). Importantly, the availability of more SAF-elements provided more flexibility for microfluidic design on a CD and furthermore allowed for the possibility of multiplex analysis.

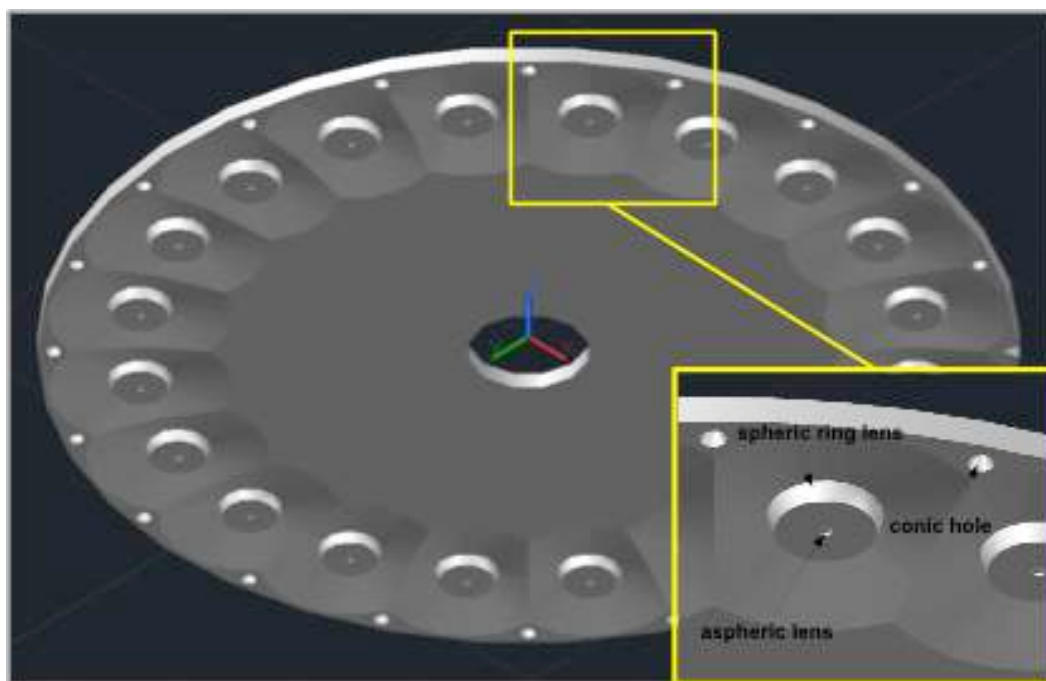


Figure 4.3.4.1b A schematic of the SAF layer with 20-SAF elements. Each SAF layer contained 20 SAF elements. The conic holes facilitated the assembly of the SAF layer with other CD layers.

Each SAF element CD contained 20 microfluidic units, which allows for 20 parallel assays (Fig. 4.3.4.1c). This multiple unit structure provided the possibility to reduce the coefficient of variation created by CD manufacture and manipulation. Similar to the structure of the flow-cell, each microfluidic unit had two chambers (loading chamber and waste chamber), which was connected by a microchannel. In addition, a capillary valve and assay spot was contained in the microchannel. However, a SAF ring lens was used as the bottom layer in the 'SAF-element' CD instead of a Zeonor[®] slide. Furthermore, the vent on each chamber could prevent accumulation of dead fluid in the microchannel. The delivery of fluid in the SAF element CD was achieved by the balancing of centrifugal force and capillary valving. When a reagent was loaded into the top chamber through a loading hole, it was held in this chamber by the capillary force. However, the centrifugal force produced by rotation can overcome the capillary barriers and pump the reagent into the microchannel. In addition, when the reagent flowed through the assay spot, the immune complex is formed. The excess reagent was then collected in the waste chamber under continuous centrifugal force.

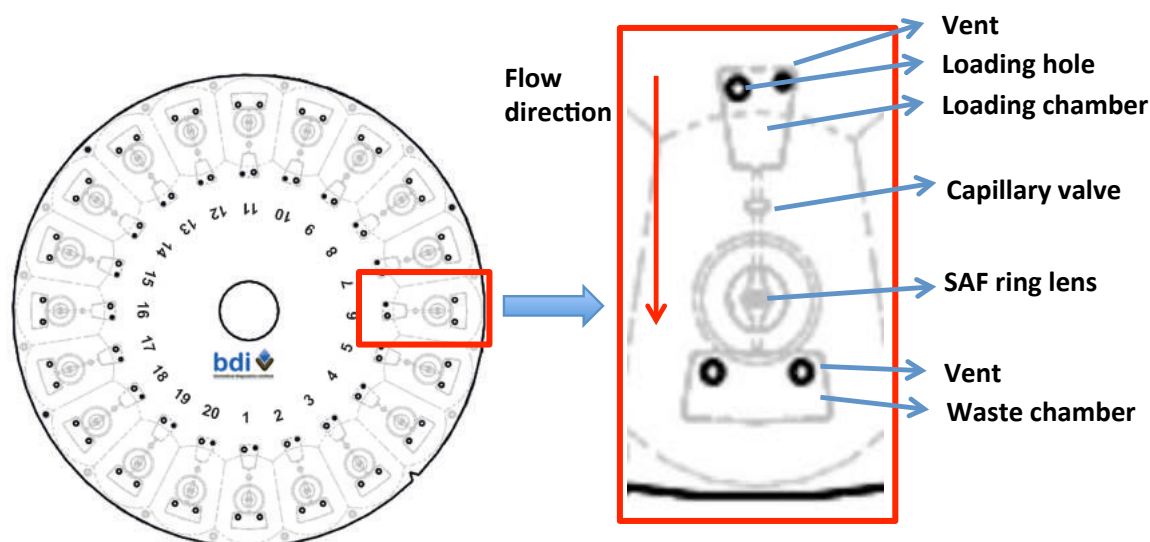


Figure 4.3.4.1c A schematic of the microfluidic unit on the ‘SAF-element’ CD. The design of the ‘SAF-element’ CD was shown on the left. It contains 20 microfluidic units and one of them was enlarged on the right. Each microfluidic unit has two chambers (loading chamber and waste chamber), which was spanned by a microchannel. A capillary valve was located before the assay spot to control the fluid in the microchannel. In addition, the vents designed on chambers can prevent accumulation of dead fluid in the microchannel.

4.3.4.2 Custom-engineered system for performing microfluidic immunoassays

A custom-engineered system, which can provide centrifugal force and monitor the liquid flow in the microchannel, was built in the BDI (Fig. 4.3.4.2). This system played a very important role in the development of microfluidic immunoassays on CDs before the generation of the automotive spin cycle protocol. The whole microfluidic CD testing setup includes two major parts: the test stand is comprised of a computer-controlled motor and a stroboscopic light for imaging a chosen area on the disc during rotation; the control of the motor using a custom LabVIEW program interfaced with a data acquisition system.

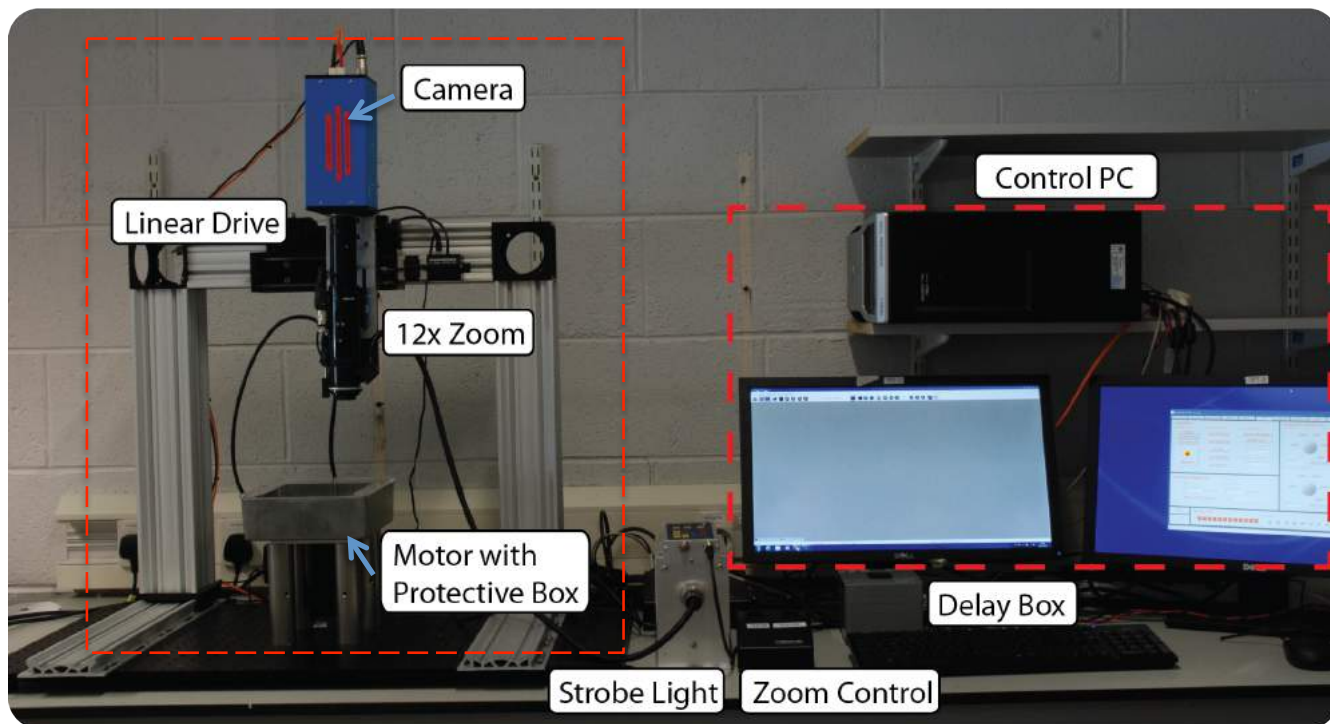


Figure 4.3.4.2 The testing setup for hIgG microfluidic immunoassay on CDs.

The whole testing setup includes two major parts (separated with red lines): (1) the test stand is comprised of a motor and a stroboscopic light, and (2) the control of PC and other control components (zoom control, delay box).

4.3.4.3 Optimisation of microchannel diameters on ‘SAF-element’ CDs

The flow rate can dramatically influence the result of flow-based assays. Therefore, a variety of immunoassay experiments were performed using various reagents and microchannel diameters. The reagents used include: 3% (w/v) BSA (a standard immunoassay blocking reagent) in hIgG FLISA, 3% (w/v) BSA containing 0.25% (v/v) Tween-20[®], and PBS. In addition, the ‘SAF-element’ CDs were manufactured with different microchannel designs that included 0.5 μm , and 0.8 μm with and without capillary valves. A 30 μL volume of each reagent was added into the loading chambers of the ‘SAF-element’ CDs, and then flow was tested and monitored using

the test stand setup. The results are listed Table 4.3.4.3. Compared with the 0.8 μm diameter microchannel, the 0.5 μm microchannel diameter was too narrow to allow reagents to flow, even when the reagent tested was PBS. Furthermore, the 0.8 μm diameter microchannel without valves had the required flow-rate and significantly reduced bubble formation with addition of Tween-20[®].

Table 4.3.4.3. Optimisation of SAF element CD design using various reagents.

Items	0.5 micrometer diameter	0.8 micrometer diameter valve	0.8 micrometer diameter without valve
3% (w/v) BSA with 0.25% (v/v) Tween-20[®]	Bubbles produced	Bubbles produced	Good
3% (w/v) BSA	Dead flow	High spin speed required	Good
PBS	High spin speed required	Good	Good

4.3.4.4 Generation of hIgG calibration curve using optimal conditions on ‘SAF-element’ CDs

After numerous optimisations were carried out, a calibration curve for hIgG detection was successfully generated with on the ‘SAF-element’ CD. In this assay, 10 $\mu\text{g/mL}$ of protein A and 6% (v/v) Ab&Dy was used. In addition, the concentration of hIgG standards ranged from 0.16 to 100 $\mu\text{g/mL}$. Data was plotted using a 4-PL model. Error bars were generated by analysing samples in triplicate (Fig. 4.3.4.5). The developed calibration curve had a dynamic range of quantification of approximately 2 logs, intra- coefficients of variation of approximately 10%, and can detect concentrations of hIgG in the nanogram range.

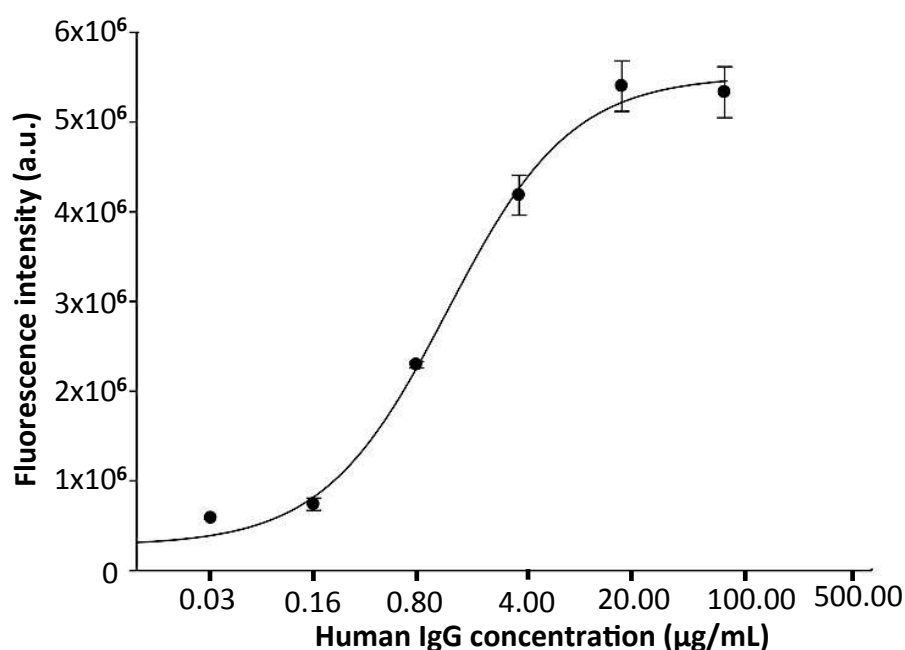


Figure 4.3.4.4 A schematic of calibration curve of hIgG FLISA based on the ‘SAF-element’ CD. The vertical bars indicate the SD from triplicate samples.

4.3.4.5 Stability study of surface chemistry on ‘SAF-element’ CDs

In the hope of improved reproducibility and reduced processing time, the advanced PECVD method was introduced for APTES deposition during the surface functionalisation period. The previous liquid phase deposition method required manual intervention during the process to introduce the precursors (e.g. APTES), resulting in unpredictable variations and low reproducibility. Also, in the plasma treatment step, the oxygen was introduced from the side of the chamber inducing poor uniformity of surface coating. In contrast, in the new PECVD strategy had the ability to automate the whole deposition process. Additionally, a showerhead was used to distribute a uniform coating with good repeatability. Furthermore, processing time was reduced by processing multiple samples simultaneously.

A stability study on the PECVD-APTES-treated chips was also performed. The PECVD-APTES-treated chips were stored in a desiccator to prevent further oxidization. Then the results obtained with chips prepared freshly and stored for one month were compared. Human IgG samples, with concentrations of 0.5 $\mu\text{g/mL}$ and 5 $\mu\text{g/mL}$, were tested on these two differently stored chips. After performing hIgG FLISA, the assay spots were analysed using the ANDOR iXon 885 camera-coupled fluorescence microscope. In Fig. 4.3.4.5, the image data illustrated shows that the morphology properties of both chips, with different storage times, is similar. The one month storage time did not affect the fluorescence intensity. Experimental analysis found that the PECVD-APTES-treated chips can be stored for at least one month without any significant deterioration in surface performance. Importantly, prolonged storage of the PECVD-APTES-treated chips does not negatively impact the surface capture of protein A. This allows for greater flexibility in the scheduling and running of the hIgG immunoassay. In addition, a significant workload in relation to the manual APTES liquid phase treatment of chips was eliminated.

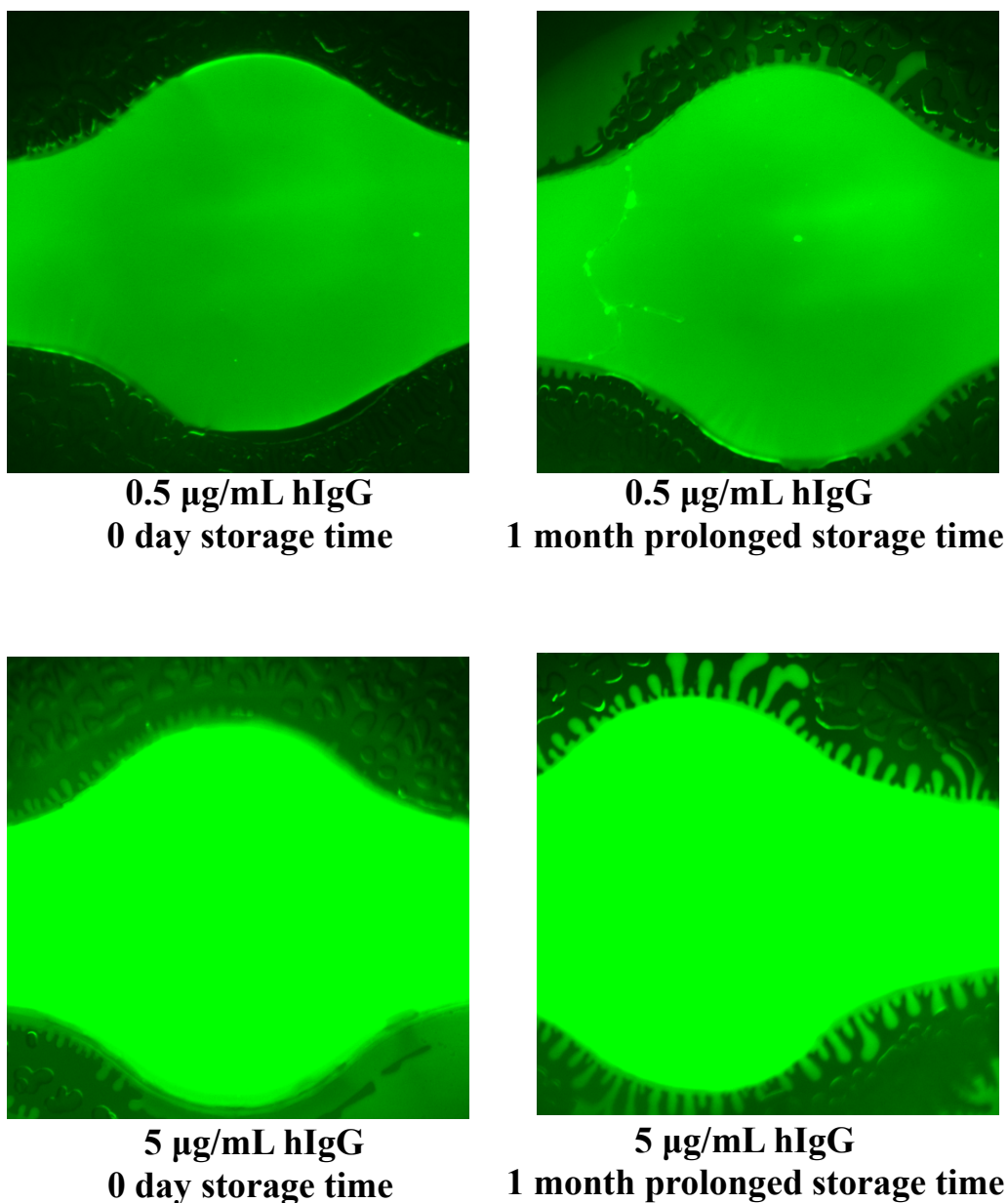


Figure 4.3.4.5 Stability of PECVD-APTES surface during prolonged storage. After APTES-deposition, protein A with a concentration of 10 µg/mL was spotted on the assay spots. Mixtures of biotinylated anti-hIgG antibody and Neutravidin-Dylight 650 were diluted in PBS (150 mM, pH 7.4) at a ratio of 3:1, followed by incubation at 37°C for 20 minutes. The loading sequence of reagents for the hIgG assay on ‘SAF-element’ CD was as follows: BSA (3% (v/v) in PBS), hIgG standards, PBS (150 mM, pH 7.4), the mixture, and PBS (150 mM, pH 7.4).

4.3.5 Development and optimisation of the second design of a microfluidic compact ‘disc-like’ platform (CD) – ‘reagent delivery’ CD

4.3.5.1 The design of the microfluidic CD-like platform – ‘reagent delivery’ CD

Based on the study of the ‘SAF-element’ CD, a new design of the microfluidic CD was generated by the incorporation of serial siphon valves with a SAF ring lens. In addition, centrifugal force was also applied as the fluid delivery force. Other features of the ‘reagents delivery’ CD were as follows:

Serial siphons imbedded with capillary valves

The working mechanisms and features of a simple double siphon device on a microfluidic CD were illustrated previously in section 4.1.2. In this work, the siphon device was expanded by combining serial siphons with capillary valves. In addition, the application of four siphons with an increasing number of loops allows the sequential release of four reagents. One of the microfluidic units on the ‘reagents delivery’ CD is shown in Fig. 4.3.5.1. Four reservoir chambers are linked with increasing numbers of serial siphon components. The reagents in these reservoir chambers can be sequentially released during each high-low cycle of CD spinning:

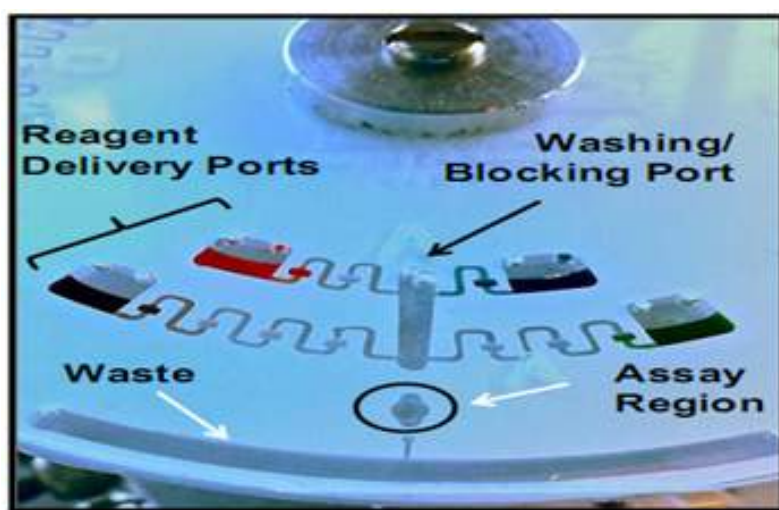


Figure 4.3.5.1 A schematic of a microfluidic unit on a ‘reagents delivery’ CD. Each microfluidic unit contains the following components: four reagent delivery ports, serial siphons, washing/blocking port, assay region and waste chamber.

4.3.5.2 SAF detector for SAF ring lens

Normally, fluorescence signals obtained from microfluidic chips are quantified by analysis of images obtained with a commercial fluorescence microscope. This method is unnecessarily expensive, time consuming, and requires significant operator training, particularly when considering future clinical translation of the technology (Wang *et al.*, 2014). In this study, an ‘in-house’ detector system used to scan fluorescent spots deposited on SAF ring-lens chip was designed and is illustrated in Fig. 4.3.5.2. This SAF detector includes a 635-nm laser diode for excitation, optical elements such as filters, lenses, and detector aperture for collimation and focusing and a photomultiplier (PMT) for detection. In addition, the system contained the following: a parabolic mirror was used to collect SAF emission light; a baffle below the parabolic mirror was used to hold the mirror element and block SAF from lower angles; lens 2 in the former device which was used to focus emitted light was replaced due to the use of the SAF ring lens. The entire system was run using a standard laptop computer. This detector can precisely position the on-disc SAF chips and selectively collect SAF fluorescence above 61.5°. This prototype instrument allows the detection of low levels of analyte in small volumes and the collection of fluorescence only from molecules that are in close proximity to the interface of the substrate and the sample solution and not from the bulk solution.

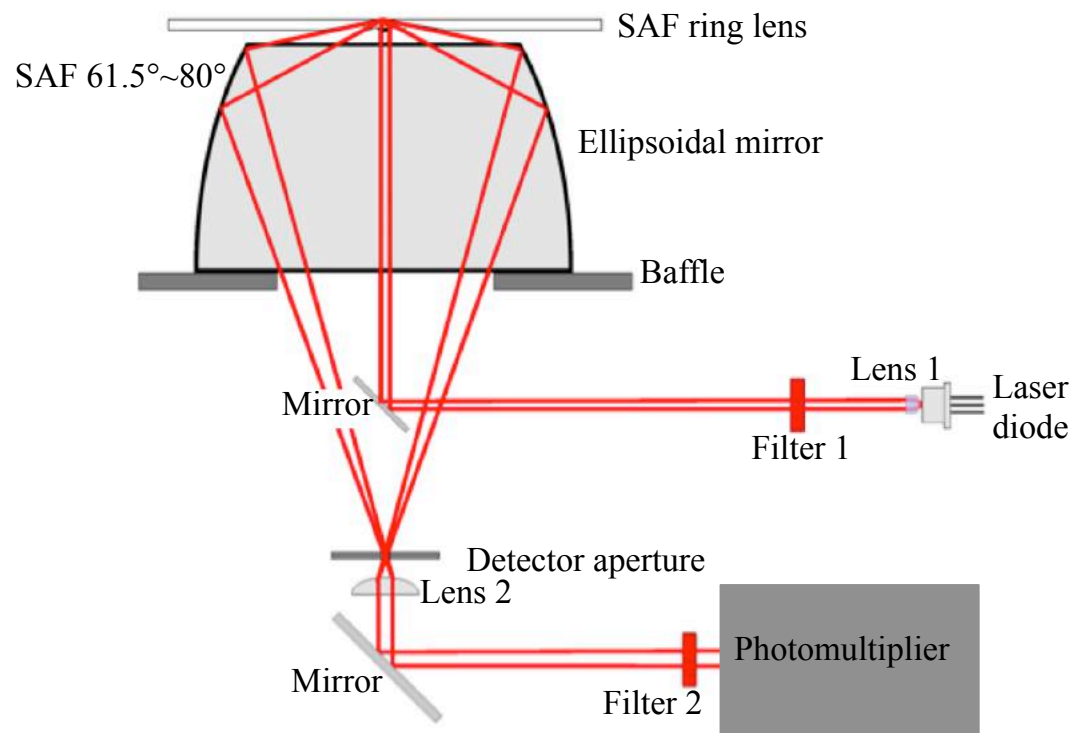


Figure 4.3.5.2 A schematic of the SAF detector for the SAF chip.

4.3.5.3 Optimisation of Tween-20[®] concentration for siphon valving

Due to the hydrophobic nature of the PMMA substrate (water contact angle $\sim 60^\circ$), and the increased surface roughness due to micro-milling of the channels, priming of the siphons was extremely difficult. In previous work, the polymer and adhesive layers of the disc platform were plasma treated before assembly in order to facilitate the priming of the siphons. However, hydrophobic recovery of plasma-treated polymer substrates is well documented in the literature (Nwankire *et al.*, 2011), making this technique highly unreliable.

In order to reduce the surface tension and making it easier to prime the siphons, a titration study of the assay reagents and surfactant-Tween-20[®] concentrations were carried out. Fig. 4.3.5.4 demonstrates that it was critical to specifically optimise the Tween-20[®] concentration for each assay reagent. Therefore, following a series of empirical optimisations, the range for the ideal and absolute working contact angle were determined.

The ideal working range (33° – 37°) is the preferred contact angle, while the absolute working range (30° – 40°) constitutes the limit of the upper and the lower contact angle, outside of which the siphons do not function reliably, e.g. they are either very hydrophobic (reagent does not prime the siphons) or very hydrophilic (reagent primes the siphons uncontrollably, that the inline capillary valves are unable to function properly). Therefore, prior to testing the microfluidic platform, the contact angle of the reagents is measured to ensure that they at least fall within the absolute working range.

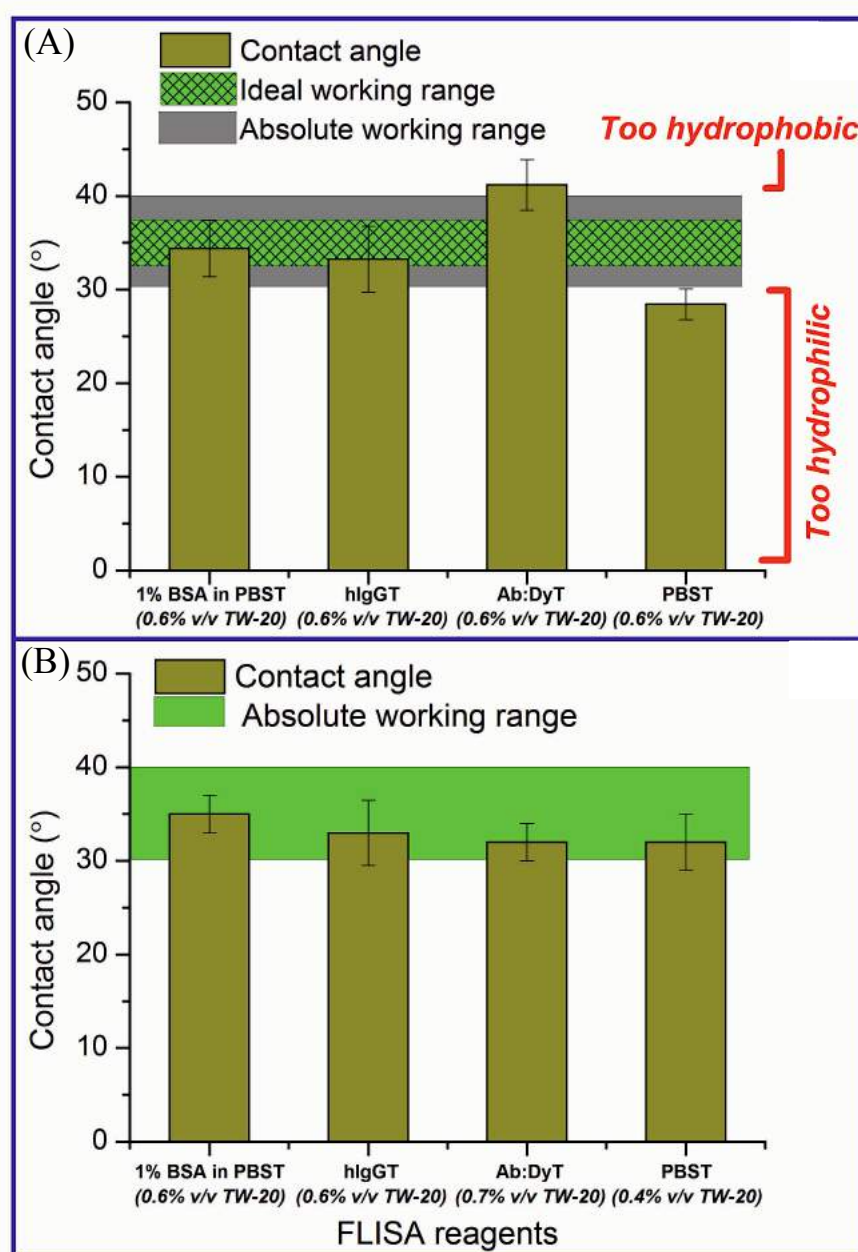


Figure 4.3.5.3 Optimisation of the microfluidic assay conditions by varying Tween-20[®] (TW-20) concentration in the FLISA reagents. (A) Contact angle measurements of similar concentrations of Tween-20[®] in the four FLISA reagents on an untreated PMMA substrate. (B) Contact angle measurements of the different optimized concentrations of Tween-20[®] in the reagents on untreated PMMA substrates. The ideal working range corresponds to the preferred contact angle for proper functioning of the siphons, while the absolute working range is the upper and lower limits, outside of which the siphons will not operate.

4.3.5.4 Characterisation of serial siphon valving

Although serial siphoning on centrifugal microfluidic platforms has previously been reported (Siegrist *et al.*, 2010), this valving scheme has not been implemented to automate the controlled, sequential release of multiple reagents for a heterogeneous, flow-based immunoassay (Fig. 4.3.5.4).

To characterise the microfluidic platform and siphon valves, contrast agent (< 1% v/v) was added to PBS (pH 7.2) and loaded onto the disc. Aliquots (30 μ L) that included the sample, wash 1, label, and wash 2 were first manually pipetted onto the disc. The appropriate spin protocol was then initiated, consisting of four consecutive repeats of \sim 975 revolutions-per-minute (RPM) to burst the inline capillary valves (< 30 s), followed by 30 s at \sim 75 RPM to prime the siphon(s) via capillary action, and a final 4 min at \sim 375 RPM to flow the reagent across the active assay area on the SAF chip. An incubation step of 2 minutes was observed in-between each assay reagent flowing over the active assay spot. The design of the serial siphons, inline capillary valves and the spin profile were specifically optimized for this application. Visualization and monitoring of the on-disc fluidics was realized using a servo-motor coupled to a stroboscope imaging system, similar to systems previously reported in the literature (Grumann *et al.*, 2005).

The entire siphon valving sequence for all reagents was completed in less than 30 minutes, without the need for operator intervention. The micro-milled channels exhibit a cross section of 250 μ m \times 250 μ m. Overall, the serial siphons proved their ability to provide adequate flow control capability for the liquid handling when implementing the IgG assay.

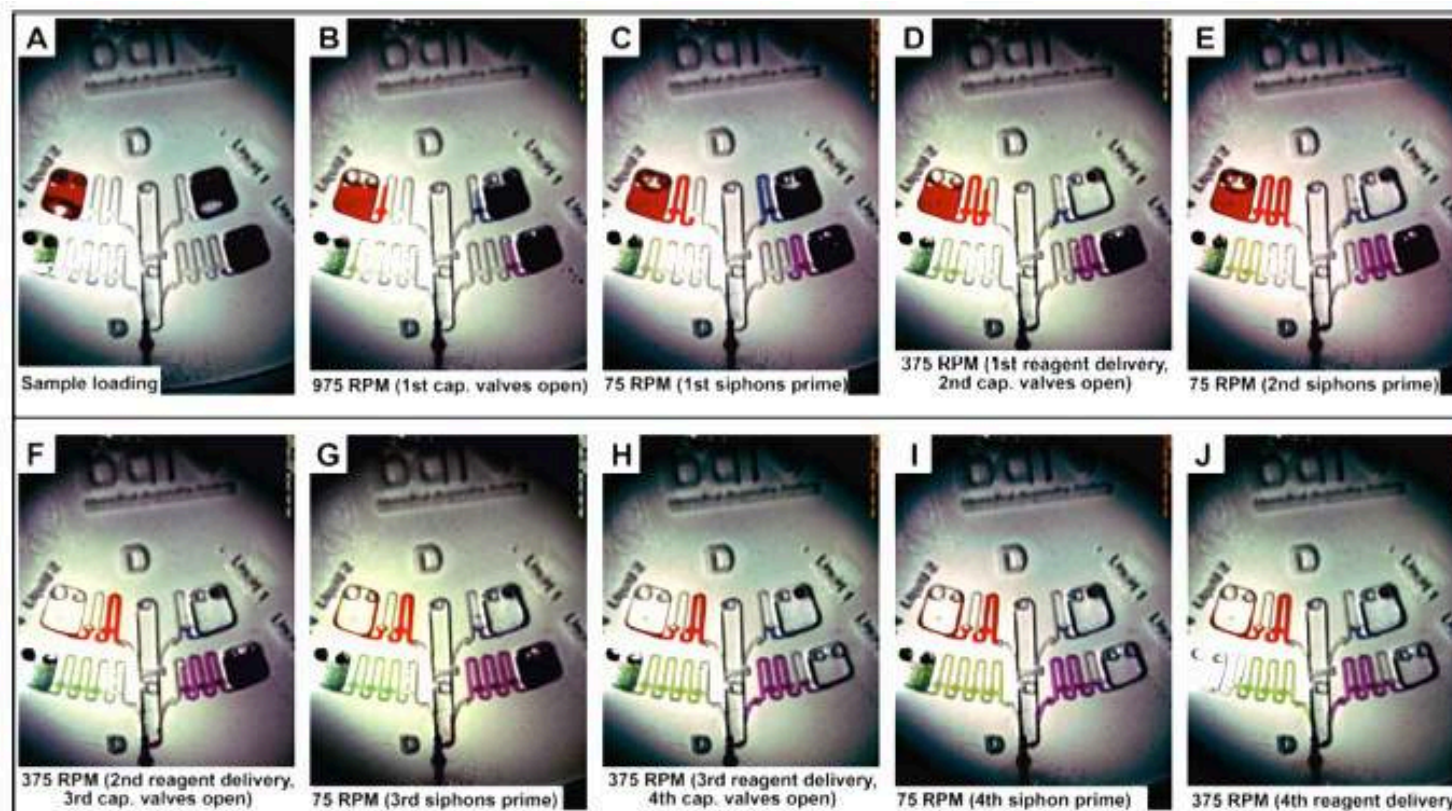


Figure 4.3.5.4 Frame sequence of the serial siphons interspersed by inline capillary valves showing the sequential delivery of four reagents over the sensor spot. (A) At high spinning frequencies ~ 975 RPM, the capillary valves burst, and the centrifugal force holds back the liquid in the siphon channels. (B) At low frequencies ~ 75 RPM, liquid reagent primes the siphon channel by capillary action, and stops at the next inline capillary valve. (C) At ~ 375 RPM, liquid reagent is delivered to the sensor spot. This spin protocol is repeated (D-J) to sequentially deliver all four reagents to the sensor spot.

4.3.5.5 Generation of calibration curve on ‘reagents delivery’ CDs and quantification of bioprocess sample

A calibration curve for an IgG immunoassay was successfully demonstrated using centrifugal microfluidics and a SAF prototype detector. In total, seven hIgG standards, a bioprocess sample and a blank sample were measured in triplicate using microfluidic serial siphon valves and the SAF detection system. Analysis was performed on two different days. Fig. 4.3.5.5B shows an inter-day hIgG calibration curve exhibiting an inter-day CV of 2.2 % to 12.6 % across the entire hIgG concentration range. In contrast, the conventional FLISA (Fig. 4.3.5.5A) displayed greater imprecision as the within-day CV range was 5.9 % to 18.9 %.

Calibration curves from both analyses were used to quantify an “in-house” bioprocess sample which had an IgG concentration of ~10 mg/mL. There was good agreement between both methods as conventional FLISA analysis yielded an IgG concentration of 9.6 to 10.1 mg/mL, whereas, the serial siphon-based centrifugal microfluidic platform yielded an IgG concentration range of 9.6 to 9.9 mg/mL.

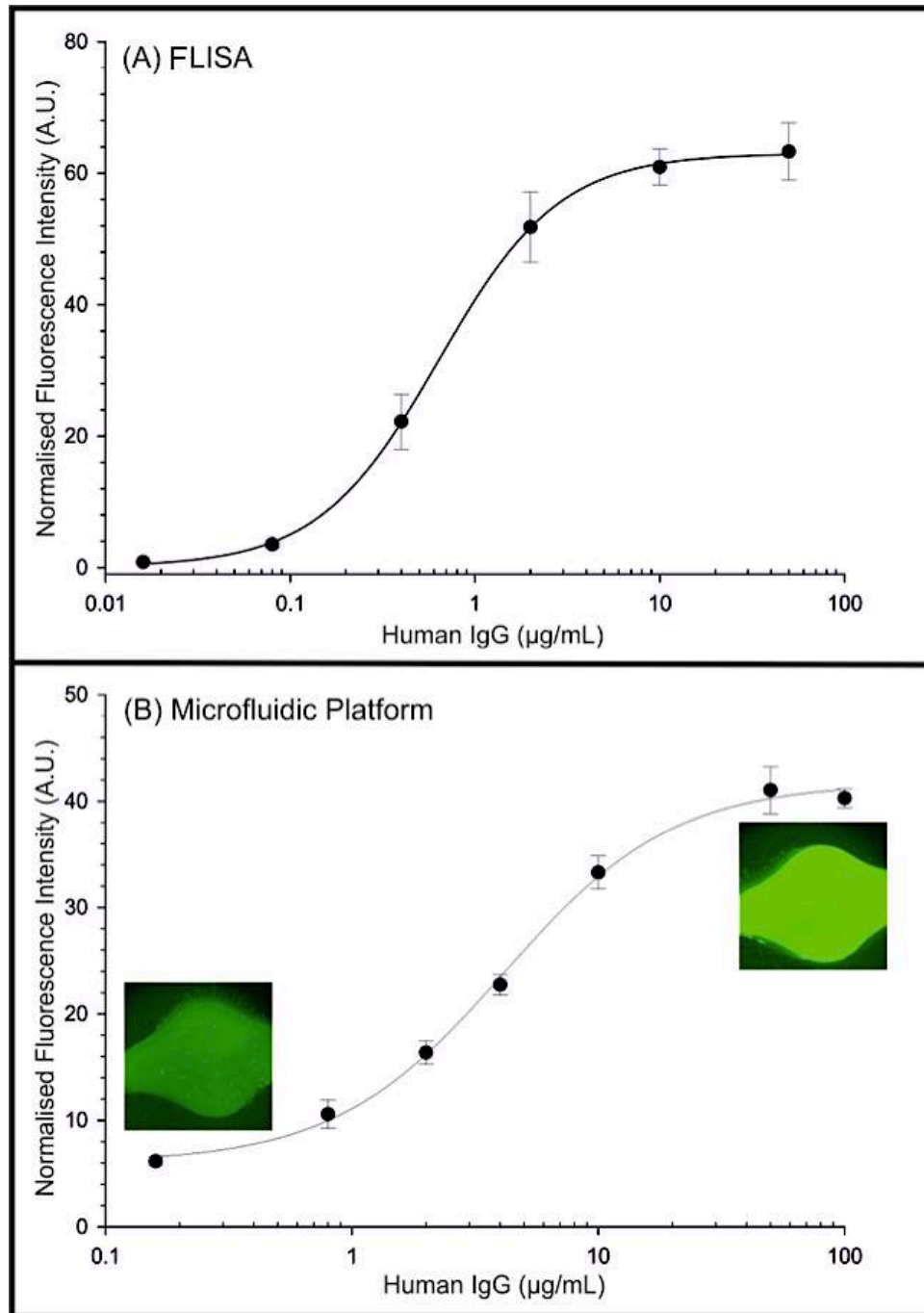


Figure 4.3.5.5 hIgG FLISA calibration curves. A) Conventional FLISA performed with high protein binding well plates and a commercial fluorescent detector. B) Microfluidic FLISA performed with an experimental PECVD-APTES-treated Zeonor[®] surface, microfluidic serial siphon valving system and a prototype SAF detector. Each sample was tested in triplicate and the error bars represent the standard deviation.

4.4 Discussion

Microfluidic systems are expected to play an important role in the achievement of the next generation of diagnostic systems, based on small sample volume consumption, high-speed of reaction, large-scale and parallel assays, and compactness (Lee *et al.*, 2010; Sin *et al.*, 2011; Hugo *et al.*, 2014). However, some important and challenging issues are yet to be resolved. In particular, the development of automatic systems that can sequentially release and deliver assay reagents is necessary for their wider applications. The concept of centrifugal microfluidics can be applied in realising fully automated microfluidic systems without external syringe pumping systems by using single motor control (Amasia *et al.*, 2010; Noroozi *et al.*, 2010; Mark *et al.*, 2012). In this work, centrifugal force-based microfluidics was developed for bioprocess sample analysis with high-speed, parallel operations and automatic reagents delivery.

In the first part of this chapter, a ‘proof-of-concept’ microfluidic system for rapid quantification of hIgG in a bioprocessing matrix was initially demonstrated. The development can be broken down into the following stages. As a first step toward a microfluidic platform for rapid FLISA in ‘flow-through’ conditions, the hIgG indirect FLISA was optimised on a microtitre plate, in relation to assay components and concentrations. In particular, the addition sequence of assay reagents was analysed. It was demonstrated that premixing and preincubating of secondary antibody and detector reagents was superior to sequentially adding reagents. The similar study was carried out on a competitive lateral flow immunoassay by Geertruida (Geertruida *et al.*, 2008). In their study, a quick competitive immunoassay was achieved by the immediate addition of all reagents in the cartridge. These studies show that the investigation of the addition sequence of assay reagents is important for transition to the development of convenient FLISA.

Secondly, the "in house" prototype SAF optical reader system designed by Dr. Dirk Kurzbuch and Mr. Martin Sommers (DCU, BDI), was successfully developed for efficient detection of fluorescence signals. On the one hand, this prototype

instrument allows the detection of low levels of analyte in small volumes, and collection of fluorescence only from molecules in close proximity to the interface of the substrate by utilisation of the SAF signal enhancement element known as a SAF lens (Kurzbuch *et al.*, 2009 & 2013). This important aspect of SAF leads to substantial reductions in background signal. On the other hand this SAF prototype instrument provides outstanding properties in contrast to fluorescence microscopy, which is unnecessarily expensive, time consuming, and requires significant operator training (Wang *et al.*, 2014).

In addition, a ‘proof-of-concept’ system featuring micro-channels molded in PMMA and PSA, with manipulation of SAF optical detection, was achieved. This initial microfluidic design enables 12 parallel FLISAs to be performed by manually loading assay reagents after each flow and incubation. The Zeonor[®] slide, used both as a solid phase to support the formation of the reactive immune complex and as an essential optical component in SAF detection, needs to be functionalised and protein A coated before its assembly into a microfluidic flow-cell. The SAF optical instrument can specifically collect the fluorescence signal inside the microfluidic system from the immune complex, not the bulk solution above. In addition, a standard curve for the quantification of hIgG using a flow-cell was demonstrated, exhibiting nanomolar sensitivity, a dynamic range of quantification of 2 logs, and intra- coefficients of variation of about 10%.

The development and optimization of two generations of microfluidic CDs for hIgG immunoassay was described i.e. the ‘SAF-element’ CD and ‘reagents delivery’ CD. These two CDs were designed with three-dimensional (3D) microstructure and 3D microchannel networks. The 3D microstructure and 3D microchannel networks are one of the key technologies for achieving the high-density integration of multiple microreactors and in realising highly functionalized microsystems (Kikutani *et al.*, 2002; Xia *et al.*, 2005; Yoshiaki *et al.*, 2012).

The ‘SAF-element’ CD was built based on the study of flow-cells, that have a straight flow microchannel. This new CD provides more microfluidic units on each

platform which allows analysis of 20 samples simultaneously. This design can reduce the assay variations from different batches of CDs. In addition, another development was that the SAF optical element was initially incorporated onto the microfluidic disc itself, which enhanced the sensitivity of fluorescence detection. The successful incorporation of an optical component onto a microfluidic platform can facilitate the miniaturization of the fluorescence detection system. A new strategy for surface functionalization, which is PECVD-APTES, was introduced in surface preparation and compared with the liquid-APTES method. It was demonstrated that the PECVD-APTES could provide assay spots with better morphology and a more stable functionalised surface, which can effectively reduce the inter- and intra coefficients of variation.

One of the main challenges to realise automatic operation on microfluidic systems is the sequential release of fluids in a temporally and spatially controlled manner. The serial siphon valve has great potential to sequentially release fluids on centrifugal force-based platforms (Siegrist *et al.*, 2010). The ‘reagents delivery’ CD was designed by incorporating serial siphon valves with the SAF technique on centrifugal microfluidic platforms. The automatic hIgG FLISA on this ‘reagents delivery’ CD was achieved by analysis of the best surface contact angle, determination of the concentration of Tween-20[®] in each of the assay reagents and characterisation of rotation protocol for the serial siphon valving. A calibration curve for the hIgG FLISA was optimised on ‘reagents delivery’ CDs, and a bioprocess sample was then quantified. Interestingly, comparison of both calibration curves revealed that the microfluidic FLISA provides less inter-day CV. However, a shift in the range of the IgG assay was also observed. The conventional FLISA had a range of 0.08 – 10 µg/mL, in contrast, the microfluidic FLISA had a range of 0.8 – 50 µg/mL. This result was not unexpected as our device is a prototype system that contains not only an experimental protein capture surface but also experimental signal detection and reagent delivery systems. In contrast, conventional hIgG FLISA analysis was carried out with standard microtitre plates that have excellent protein binding properties as well as low autofluorescence levels. In addition, a commercially available microplate reader with high fluorescent sensitivity was used for sample analysis. To date, very

few microfluidic platforms were developed to detect hIgG using ELISA/FLISA technique (Pereira *et al.*, 2011; Kim *et al.*, 2011; Seia *et al.*, 2012; Li *et al.*, 2016). One of the microfluidic platform demonstrated by Li's group, provided a lower limited detection of 0.03 ng/mL. However, multiple loading of assay reagents was required during assay procedure in the reported microfluidic platforms. A real automatic microfluidic system for hIgG detection was not demonstrated. An easy-to-use microfluidic system for human IgG detection with high sensitivity was demonstrated with amperometric and fluorescence detection methods by Pereira's group and Seia's group, respectively. This microfluidic chip processes very simple microchannel network, only containing two straight channels. However, the size of the whole system was relatively large due to the application of a syringe pump system. Additionally, seven different assay reagents were required to sequentially pump into the chip in this immunoassay. As a result, this system cannot meet the requirement of a portable and 'sample-to-answer' system. Kim's group developed an automated microfluidic system for the complete performance of magnetic bead-based immunoassay for mouse IgG detection. The assay on the chip is easily parallelized for high-throughput analysis and easily interfaced with various assay substrates by using an APTES micro-patterning method. However, a compact portable external instrument was not reported in this work. Whereas, the research described in this thesis, when compared with the work described above, has many advantages including the provision of a 'sample-to-answer' system with an automated hIgG immunoassay, with acceptable sensitivity and on a portable instrument.

Further optimisation of the microfluidic design, surface chemistry and the fluorescence detector has the potential to yield a lower IgG working range for the SAF-based microfluidic method. However, for our particular application the target analyte is in relative abundance. For example, bioprocess samples typically contain milligram amounts of IgG (Schepter *et al.*, 1999). Therefore, the shift in assay range was not undesirable, as it reduced the dilution needed to allow the sample to fall within the linear range of the calibration curve.

CHAPTER 5

Numerical Simulation of HIgG Immunoassay in Microchannels

5.1 Introduction

5.1.1 Numerical simulation of microfluidic immunoassay

Microfluidics-based technologies have revolutionized the possibilities for new assay format development and implementation. Compared to conventional immunoassay formats, microfluidic platforms provide remarkable new features. A high ‘surface-to-volume’ ratio within microchannels, for instance, is capable of dramatically influencing interfacial reaction kinetics in solid-phase-based immunoassays and handling of reagents in the micro and nano-litre range (Whitesides, 2006; Janasek *et al.*, 2006; Hartman *et al.*, 2009; Konry *et al.*, 2011). Consequently, these features allow a ‘sample-to-answer’ test to be generated with short analysis times, minimal reagent consumption, integration, automation and parallel processing, leading to ‘in-line’, ‘at-line’ and in-situ processing of samples (Lee *et al.*, 2009; Ko *et al.*, 2011). Furthermore, centrifugal microfluidic platforms inherently possess additional advantages when compared to other lab-on-a-chip systems, due to the absence of expensive syringe pumps. Thus, disc platforms enable full integration of multiple liquid handling and assay processes including pumping, metering, mixing, reagent storage and sequential reagent delivery (He *et al.*, 2008; Martinez-Duarte *et al.*, 2010; Amasia *et al.*, 2012; Wang *et al.*, 2013). To this end, several multi-step and multiplex assays can be integrated onto the platforms, and with further development, they can facilitate the integration of optical sensors or other detections strategies.

In the last decade, the modeling of microfluidic assays has received considerable attention. Numerical studies on the kinetics of binding in a heterogeneous microfluidic bioreactor by using a simple 2D model were extensively reported (Zimmermann *et al.*, 2005; Gervais *et al.*, 2006; Friedrich *et al.*, 2008; Fu *et al.*, 2009; Hansen *et al.*, 2012; Selmi *et al.*, 2016). Zimmermann *et al.* investigated the key parameters of a direct immunoassay such as flow rate, surface feature size, and binding constants in a capillary-driven system (Zimmermann *et al.*, 2005). Gervais and Jensen investigated the different regimes for diffusion-limited transport in microfluidic devices with respect to two key parameters i.e. the capture fraction of the bulk analyte at the surface and the saturation time-scale of the reactive surface (Gervais & Jensen, 2006). Fu *et al.* analyzed the fractional sensitivity of a competitive heterogeneous assay in a

microchannel with respect to analyte concentration, flow rate, initial surface density of binding sites, and antibody concentration (Fu *et al.*, 2009). Friedrich *et al.*, used a theoretical model to demonstrate three approaches to optimize analyte transport in microchannels (Friedrich *et al.*, 2008). Hansen and co-workers studied the transport dynamics in a model geometry of a surface plasmon resonance sensor (Hansen *et al.*, 2012) while Selmi *et al.* investigated the electrothermal effect on a binding reaction by performing a 2D simulation on the immunoassay in a microchannel with asymmetrical interdigitated electrodes using the finite element method (Selmi *et al.*, 2016).

To date, most of the literature cited focused on investigating the binding kinetics of analyte in a microchannel. The computational modeling was applied to investigate the influence of critical factors of the binding kinetics of analyte, by predicting the amount of bounded analytes at one specific concentration of analyte reagent as a function of time. These simulated results can reveal how a change in a critical factor affects the binding kinetics with regard to one specific concentration of analyte reagent. However, these data cannot intuitively and accurately reflect the influence of a critical factor on the entire working range of analyte concentrations or the features of a standard curve, which is more essential and valuable for the design of a microfluidic sensor. Generally, the effect caused by a critical factor varies for different concentrations of analyte and analysis of a calibration curve is an essential method to evaluate any developed microfluidic systems (Wakayama *et al.*, 2013; Krause *et al.*, 2013; Shamsi *et al.*, 2014). Unfortunately, there is no study dealing with the influence of the critical factors (such as flow velocity, channel height, capture area length and concentration of assay components) on the standard curve under microfluidic conditions. Hence, this study was carried out to fill this gap.

5.1.2 Simulation conditions

We have previously developed a prototype system for ‘at-line’ and ‘sample-to-answer’ bioprocess monitoring (Nwankire *et al.*, 2013). In this system, microfluidic networks were developed for a surface-based immunoassay for IgG. The antibodies that were immobilized on one wall of a microchannel captured analytes flowing in the microchannel. This technology is capable of detecting analytes from sub-microliter volumes of sample within 30 min, whilst, achieving reasonable sensitivity. In this

system, the heterogeneous indirect assay for hIgG detection included four reagents, which are the capture molecule, Protein A, analyte molecules such as hIgG, the anti-hIgG (biotinylated, chicken IgY) antibody and the detection molecule, NeutrAvidin-DyLight 650 conjugate (Fig. 5.1.2). Protein A is immobilized on the functionalized solid surface, which contains amine groups. It can capture the hIgG molecule in the fluid by binding to the Fc region of hIgG with a high affinity. The biotinylated anti-hIgG is added and specifically binds with captured hIgG on the surface. The NeutrAvidin, conjugated with the fluorescent molecule, specifically binds with biotin, which is conjugated to anti-hIgG. The fluorescence signal produced by DyLight-650 responds to the amount of hIgG in the samples. The utilisation of the ‘biotin-avidin’ system in this assay can provide high signal amplification effects and associated high sensitivity. In the following sections, these reagents are denoted as Protein A, hIgG, anti-hIgG and NeutrAvidin, respectively. This assay involves three heterogeneous binding reactions, which are the reaction between initial capture molecules (Protein A) and analytes (hIgG), hIgG molecules and anti-hIgG and, anti-hIgG and the final detector reagent (DyLight-labelled Neutravidin).

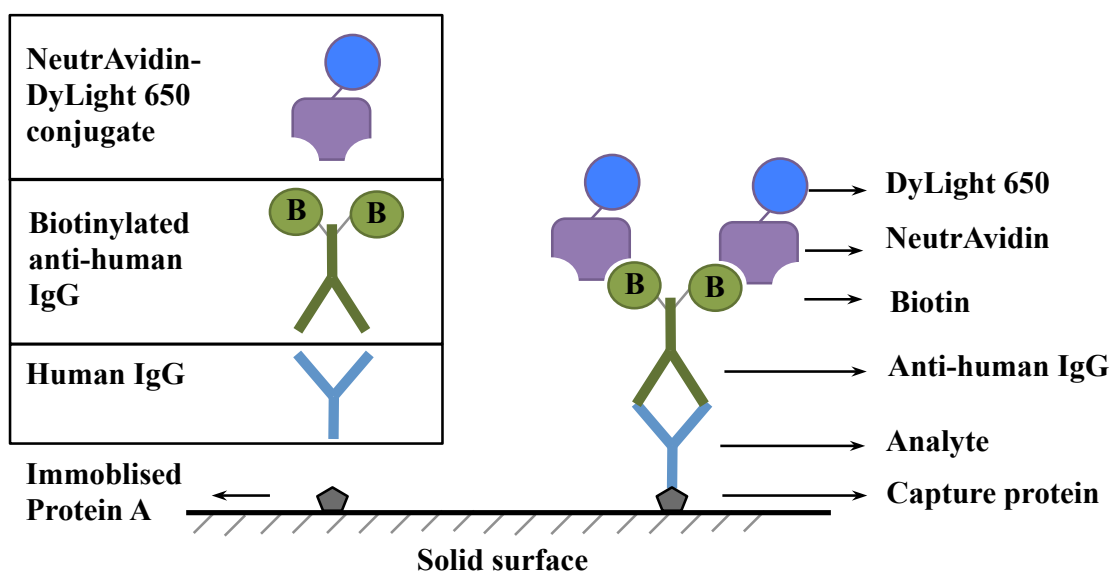


Figure 5.1.2 Schematic of the hIgG immunoassay.

5.2 Aims of this chapter

In this paper, the theoretical modeling focuses on an investigation of the impact of some critical factors (such as flow velocity, channel height, capture area length and concentration of assay components) on the performance of the previously developed

microfluidics-based immunoassay. Additionally, the investigation of the impact of the critical factors on the standard curves is presented from two different aspects. On the one hand, ideal conditions (such as no constraints on reagent availability and assay time) were assumed by most papers in the literature reporting studies of a microfluidic-based immunoassay. The predicted data under ideal conditions can reveal how a change in conditions like velocity and channel height, would affect the binding kinetics during the entire assay working range without any change in the volume of reagents. However, additional studies were performed under conditions with finite volumes of reagents and specific assay times. Under experimental conditions, however, the microfluidic assays are performed under many constraints. For example, the microfluidics for analytical applications (e.g., ‘point-of-care’ assay or ‘time-to-result assay’), were designed to reduce sample consumption and assay time. This is important as it is not possible to use large amounts/volumes of reagent and hour-long assay times in a microfluidic system. Therefore, it may be beneficial to predict the standard curves within the ‘real-world’ constraints, which can really contribute to the design and optimization of microfluidic systems in practical experiments.

5.3 Results

In order to solve the system of ODEs, a number of experimentally derived parameters were used. Protein A was immobilized on the sensor area with an available binding site density of 2×10^{-8} site/m². The diffusivity of hIgG molecules is 3.89×10^{-11} m²/s (Chang *et al.*, 2012). The k_{on} and k_{off} for Protein A and hIgG binding is 8.02×10^3 m³/mol·s and 2.7×10^{-4} s⁻¹ (Saha *et al.*, 2003), respectively. The diffusivity of anti-hIgG molecules is 1×10^{-10} m²/s (Lionello *et al.*, 2005). In this simulation, the binding reaction between hIgG and biotin conjugated anti-hIgG was assumed as the binding between hIgG and anti-hIgG molecule. Additionally, the k_{on} and k_{off} for hIgG and anti-hIgG binding is 2.5×10^5 m³/mol·s and 3×10^{-4} s⁻¹ (Hu *et al.*, 2007), respectively. The hIgG samples with concentrations of 1, 5, 12.5, 25, 62.5, 125, 312.5, 625 and 1250 nM were used which was consistent with the previously developed microfluidic-based immunoassay (Nwankire *et al.*, 2013). The flow velocity is 3.75×10^{-4} ms⁻¹, which is obtained from our experimental data. The cross-section area of the microchannel in our developed microfluidic system was 4×10^{-8} m² with dimensions of 8×10^{-4} m in width and 5×10^{-5} m in height.

5.3.1 Influence of the flow velocity

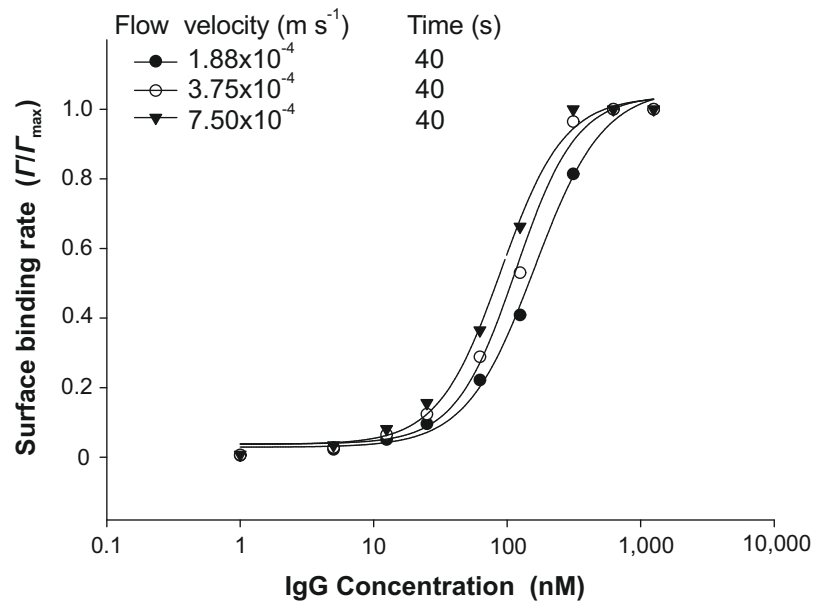
One of the most important parameters in the simulation was the flow velocity. In this study, the way in which a change in flow velocity would affect the assay performance, was examined under the conditions of infinite and finite volumes of reagents, respectively. For the investigation of the binding reaction between Protein A and hIgG under infinite volume conditions, hIgG and its residence time was not limited. The standard curve of hIgG adsorption under these non-limited conditions was obtained by plotting the binding rate (Γ/Γ_{\max}) at one defined moment against the corresponding analyte concentrations. However, the time selected to plot and analyse the standard curve had to be considered carefully. According the equation 5 described in previous section 2.6.1, Γ is not related to flow velocity, but depends on the concentration of bulk solution (C_w). For one defined concentration of hIgG reagent (C_w), although the velocity is different, the Protein A surfaces are ultimately saturated and reach the maximum binding density (Γ_{\max}) at infinite time. The velocity of hIgG reagents only affects the saturation time of the Protein A surface or equilibrium time of hIgG adsorption, except the Γ_{\max} . The lower velocity needs a longer saturation time. Therefore, in this scenario, flow velocity cannot affect the Γ/Γ_{\max} if the residence time is adequately long. In other words, the curves predicted with varying flow velocity would be coincident when the residence time is infinite.

In order to prevent this problem, 40s is applied as a moderate residence time for each velocity. In Fig. 5.3.1a, the simulated surface-binding rate (Γ/Γ_{\max}) at 40s was plotted against the hIgG concentrations. The standard curves of Protein A and hIgG reactions with varying flow velocity and the same residence time, were compared. With increasing hIgG concentrations from 10 to 1000 nM, it can be observed clearly that a higher velocity provides more binding. The utilisation of higher velocity can shift standard curves to the left along the x-axis, where the assay is more sensitive to measure the analyte at lower concentrations. This phenomenon was explained by the profiles of free hIgG concentration above the sensor surface. Fig. 5.3.1b shows the hIgG concentration gradient of the reaction at the same time but with varying velocities. The red color represents high concentrations of hIgG. The blue color represents low concentrations of hIgG. In Fig. 5.3.1b, the free hIgG concentration gradient above the capture surface can be observed. The hIgG concentration gradient was formed above the

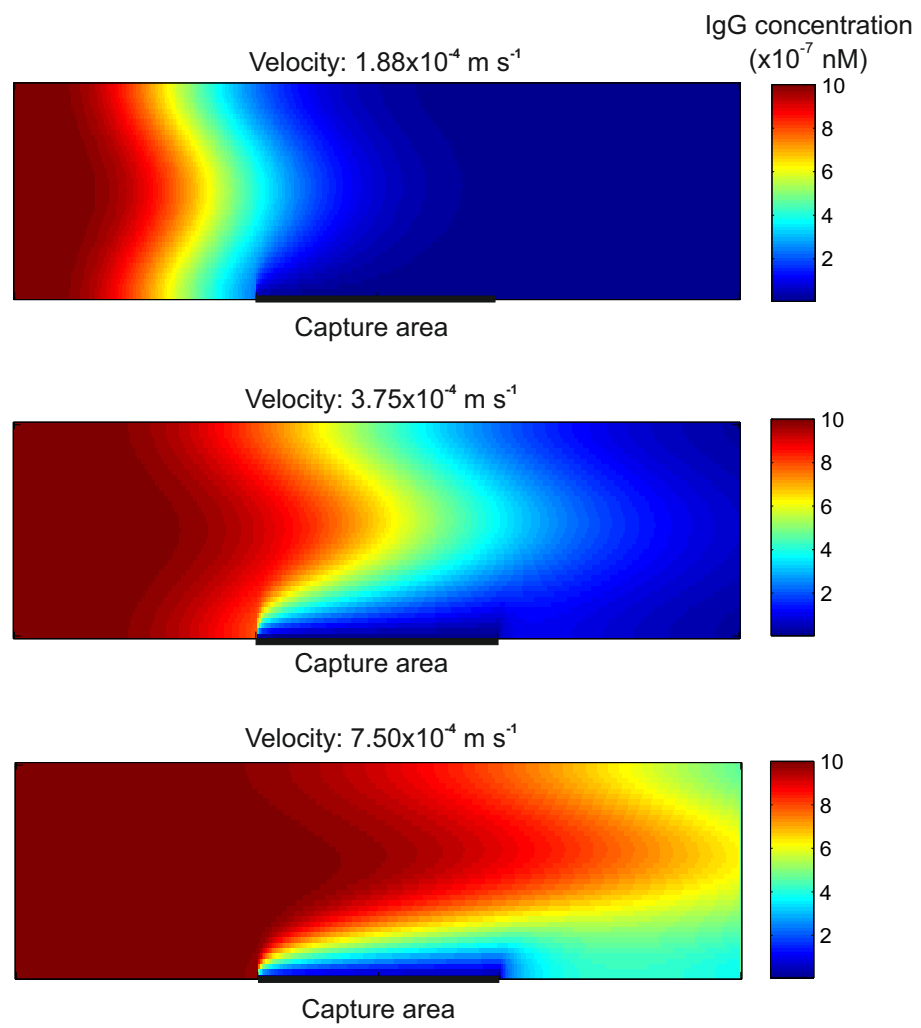
capture surface if the hIgG adsorption on the capture surface was quicker than the hIgG transport from bulk to the surface. In this context, the hIgG concentration near the capture surface is now much lower than the initial input hIgG concentration. This low hIgG concentration area is called the depletion area. As a result, the analyte adsorption process is retarded by the existing depletion area. Therefore, in order to accelerate the adsorption process, reducing the depletion area thickness was considered. Additionally, it can be clearly observed that the blue area shrunk above the capture surface with increase of flow velocity. Fig. 5.3.1b reveals the depletion area can be reduced due to the rapid delivery of hIgG as a result of the higher velocity.

However, finite assay time and a large volume of reagent are not expected for the development of an ideal microfluidic system in practice. For a certain volume of reagent (e.g. 30 μL) and channel geometry (e.g. 8×10^{-4} m (W) + 5×10^{-5} m (H)) in our previously developed system, the residence times for velocities of 1.88×10^{-4} ms^{-1} , 3.75×10^{-4} ms^{-1} and 7.50×10^{-4} ms^{-1} were 40s, 20s and 10s, respectively. As a result of the change in residence time, the benefit on assay performance introduced by the high flow velocity would be reduced. In order to investigate the effect of flow velocity in the practical situation, the simulations were carried out with the constraint conditions shown in Fig. 5.3.1c. The predicted standard curves of Protein A and hIgG reactions were obtained by plotting the binding rate ($\Gamma/\Gamma_{\text{max}}$) with various velocities and residence times against the corresponding analyte concentrations. According to the data in Fig 5.3.1c, with the higher velocity of 7.50×10^{-4} ms^{-1} , there was less binding due to the short residence time (10s). Conversely, the lower velocity of 1.88×10^{-4} ms^{-1} demonstrated more binding as a result of longer residence time (40s). Additionally, the assay with velocity of 1.88×10^{-4} ms^{-1} generated a better sensitivity at a concentration of 100 nM hIgG, but required longer assay time, whereas, in contrast, the assay with a velocity of 3.75×10^{-4} ms^{-1} had a similar working range and relatively short assay time. For the conditions of the higher velocity e.g. 7.50×10^{-4} ms^{-1} , the curve was shifted to the right, where it is not sensitive for detection of hIgG at low concentrations.

(a)



(b)



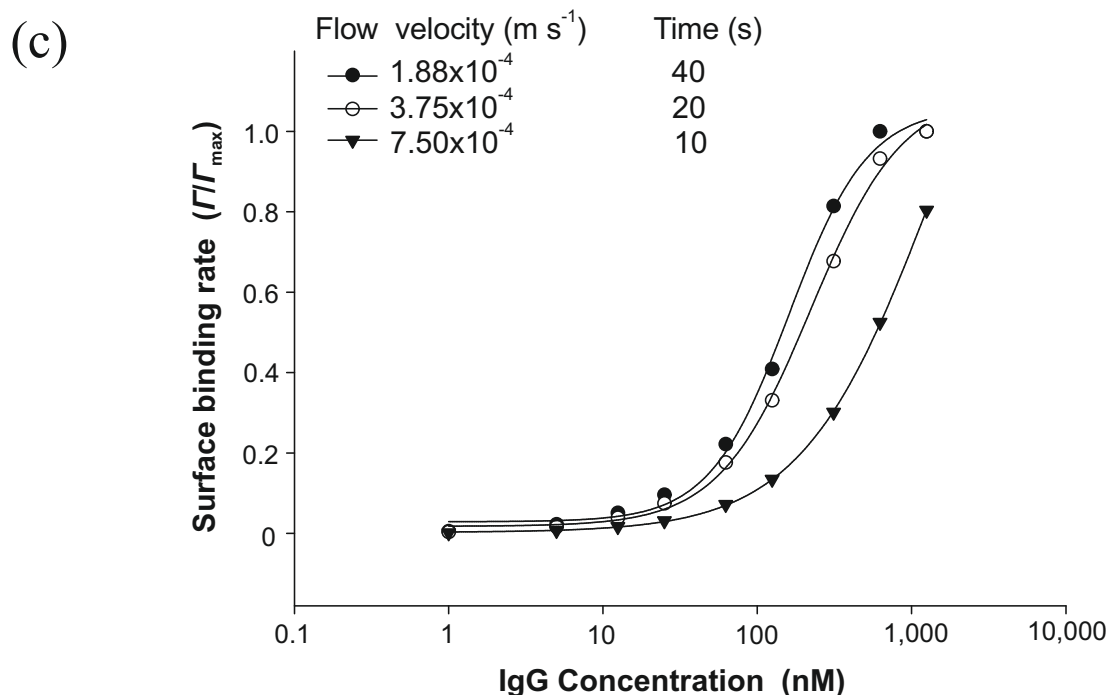


Figure 5.3.1 Influence of flow velocity on microfluidic assay performance. (a) Predicted standard curves without constraint on reagent at 40s. The flow velocities were $1.88 \times 10^{-4} \text{ ms}^{-1}$, $3.75 \times 10^{-4} \text{ ms}^{-1}$ and $7.50 \times 10^{-4} \text{ ms}^{-1}$ respectively. (b) The profiles of hIgG concentration in the microchannel. They showed the hIgG distribution at 100s with velocities of $1.88 \times 10^{-4} \text{ ms}^{-1}$, $3.75 \times 10^{-4} \text{ ms}^{-1}$ and $7.50 \times 10^{-4} \text{ ms}^{-1}$. (c) Predicted standard curves with same volumes of reagents. In the designed microchannel with a specific geometry, 30 μL of each reagent flowing with varying velocities ($1.88 \times 10^{-4} \text{ ms}^{-1}$, $3.75 \times 10^{-4} \text{ ms}^{-1}$ and $7.50 \times 10^{-4} \text{ ms}^{-1}$) had different residence times (i.e. 40s, 20s and 10s).

5.3.2 Influence of channel height on assay performance

With the aim of reducing analyte depletion and accelerating analyte adsorption, the impact of a change in channel height on the binding process was investigated. Simulations were carried out by comparing the predicted standard curves with the application of the different channel heights, which had the values of 1×10^{-5} , 5×10^{-5} and 20×10^{-5} m, respectively. The fluids had a constant velocity of 3.75×10^{-4} ms⁻¹.

According to the equation 5 described in section 2.6.1, Γ is not related to channel height. For one defined concentration of IgG reagent (C_w), although the channel heights are different, the Protein A surfaces are ultimately saturated and reach the maximum binding density (Γ_{\max}) at infinite time. Therefore, without the constraints on reagent and residence time, the influence of channel height on the predicted standard curves would be rarely observed when the residence time is adequately long. This similar problem was discussed in the last section. In this scenario, a moderate time of 20s is applied as the residence time for each simulation. The simulations of a standard curves under these non-limited conditions were obtained by plotting the binding rate (Γ / Γ_{\max}) at 20s against the corresponding analyte concentrations in Fig. 5.3.2a. At 20s, a channel height of 5×10^{-5} m provided a higher binding rate, whereas the values of channel height larger or smaller than 5×10^{-5} m induced a declining trend in binding rate. It revealed that the binding rate did not increase continuously with the increasing height of channel. Therefore, it was essential for development of an efficient fluidic sensor that optimization of the channel height occur. The assay with a channel height of 5×10^{-5} m possesses a working range from 25 nM to 1,000 nM. In contrast, the assays with heights of 1×10^{-5} and 20×10^{-5} m, showed a small working range.

In order to investigate the influence of channel height on the microfluidic assay performance, the simulations had to be carried out with the real-world constraints. We assumed a fluid, with volume of 30 μ L, flowing into microchannels with different heights, which were 1×10^{-5} , 5×10^{-5} , and 20×10^{-5} m, respectively. As a result of the infinite reagent availability, the residence time for a 30 μ L fluid volume varied. In this case, the fluids had a constant velocity of 3.75×10^{-4} ms⁻¹. Therefore, the residence time corresponding to the increasing channel heights (1×10^{-5} , 5×10^{-5} , and 20×10^{-5} m) were 100s, 20s, and 5s, respectively. The effects of channel height are different between the

conditions of finite volumes (Fig. 5.3.2b) and infinite volumes (Fig. 5.3.2a) of reagent availability. From Fig. 5.3.2b it can be observed that the surface-binding rate for each hIgG concentration was obviously increased with the microchannel height of 1×10^{-5} m, especially for hIgG concentrations above 10 nM. Corresponding to the increasing surface binding rate, these three curves were significantly different with respect to working range. With a volume of 30 μ L of hIgG, the height of 1×10^{-5} m provided a sensitive assay in a working range from 0.8 to 125 nM, but needs a relatively longer assay time (100s). The height of 5×10^{-5} m provided an assay with good sensitivity in a working range from 25 to 625 nM, and a 20s assay time, whereas, the height of 20×10^{-5} m showed a working range of high concentration of hIgG, which cannot effectively be applied for our application.

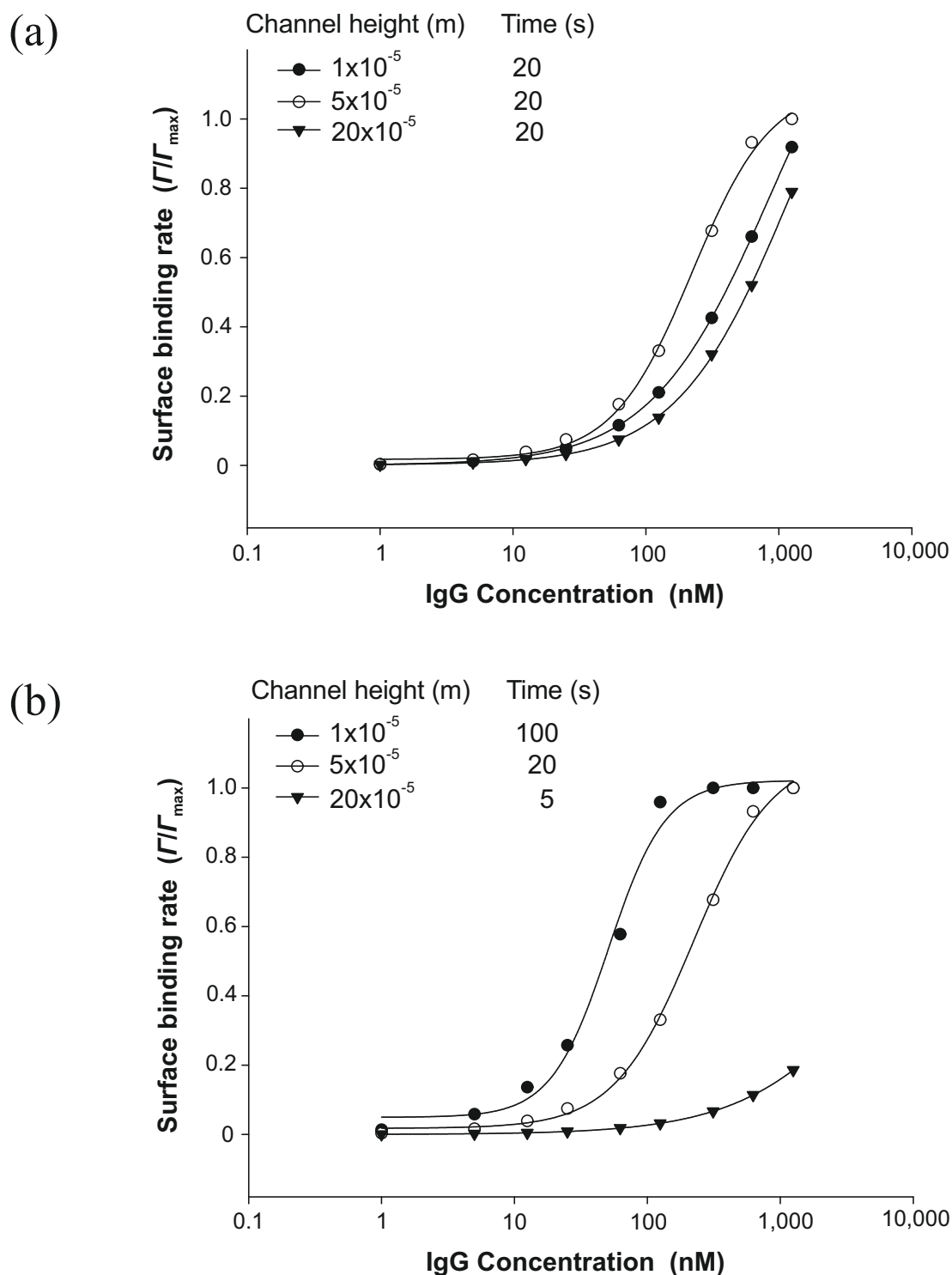


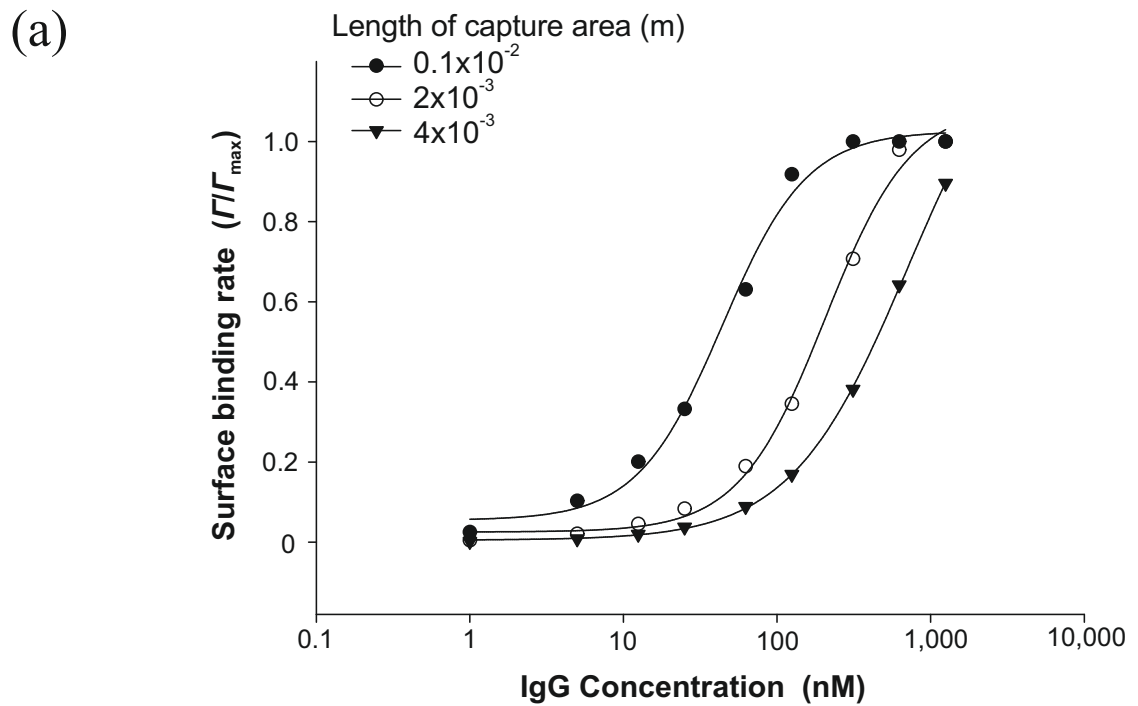
Figure 5.3.2 Influence of channel height on assay performance. (a) Predicted standard curves without constraint on reagent at 20s. The flow channel heights were 1×10^{-5} m, 5×10^{-5} m and 20×10^{-5} m, respectively. (b) Predicted standard curves with same volume of reagents. In the microchannels with heights of 1×10^{-5} m, 5×10^{-5} m and 20×10^{-5} m, $30 \mu\text{L}$ of each reagent with the velocity of $3.75 \times 10^{-4} \text{ ms}^{-1}$ had residence times of 100s, 20s and 5s.

5.3.3 Influence of the sensor area

In the 2D simulation (Fig. 2.6.1), the microchannel, including the capture area on the wall, was defined with two dimensions, which are length and height. The width of capture area was not considered because the mass transport in this direction did not contribute to binding kinetics. In this section, the influence of capture area length on microfluidic assay performance was determined by using different capture area lengths, which were 0.1×10^{-3} , 2×10^{-3} and 4×10^{-3} m. For a fluid with a constant volume in the microchannel, the change in capture area length would not affect the residence time. Hence, the influence of capture area length on the assay performance is consistent under finite or infinite reagent availability. In Fig. 5.3.3a, the predicted standard curves were produced by plotting the surface binding rate at 20s against the hIgG concentrations. The surface binding rates are dramatically increased by using a shorter capture area length. The curve generated with a capture area length of 0.1×10^{-3} m shows an enhanced sensitivity with a working range from 5 to 125 nM, whereas the curves with large capture area length shows working ranges with higher hIgG concentrations. Alternatively, the influence of the analyte-capture area length was verified by simulating distributions of the free hIgG concentration at 20s in the modeled channel, where the capture area lengths were 0.1×10^{-3} , 2×10^{-3} and 4×10^{-3} m, respectively (Fig. 5.3.3b). In the simulation above, the capture areas with increasing length started from the same position (1×10^{-3} m) along the x-axis of the microchannel. Additionally, a fluid that contains 625 nM of hIgG flows over the capture areas with a velocity of 3.75×10^{-4} ms^{-1} .

At 20s, the capture area with a length of 0.1×10^{-3} m was fully covered by the red color without any blue color (depletion area). It revealed that the binding sites on this capture area have been saturated and the value of the surface binding rate ($\Gamma / \Gamma_{\text{max}}$) was 1, which was consistent with the data in Fig. 5.3.3a. However, the capture area with a length of 2×10^{-3} m was partly covered by the red color, which occupies approximately 25% of the length of this capture area. This revealed that the capture area was partly saturated, and the remaining part of the capture area was also covered by a depletion area. Meanwhile, the capture area with a length of 4×10^{-3} m located from 1×10^{-3} to 5×10^{-3} m on the wall, has a large blue area, which occupies more than 75% of the whole capture area. In conclusion, the capture area with a length of 0.1×10^{-3} m had the largest

proportion of saturated area and the one with a length of 4×10^{-3} m had the smallest proportion. The proportion of the saturated area indicated the surface binding rate (Γ/Γ_{\max}). Hence, a smaller sensor can provide a higher surface binding rate in a microchannel as deduced from this simulation. Additionally, it was shown that the present of surface saturation started from one end of the capture area to the other end along the x-axis of the microchannel.



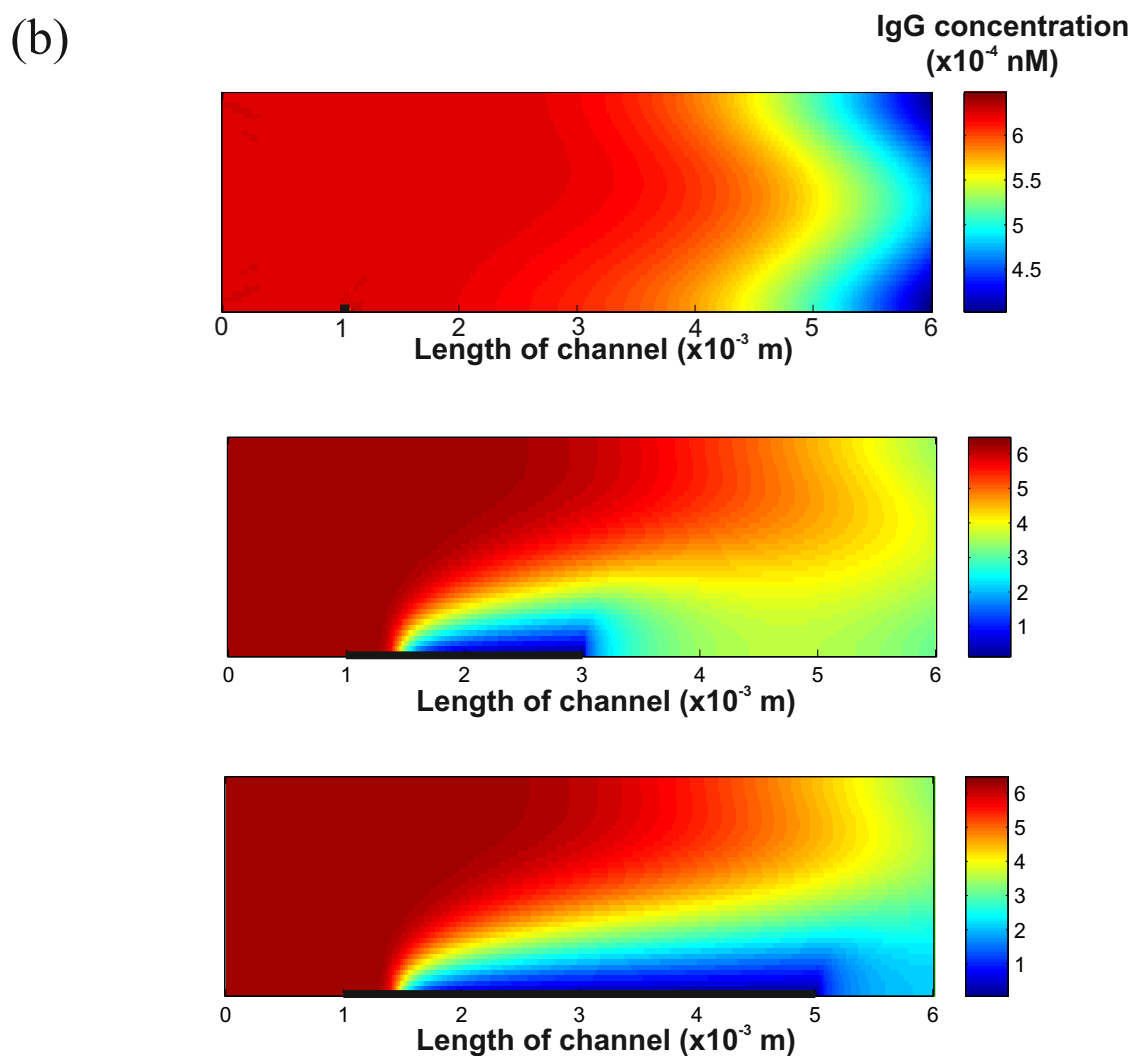


Figure 5.3.3 Influence of sensor area on assay performance. (a) Predicted standard curves with same volume of reagents ($30 \mu\text{L}$), residence time (20s) and flow velocity ($3.75 \times 10^{-4} \text{ ms}^{-1}$). The three curves were generated by using different sensor lengths, which were 0.1×10^{-3} , 2×10^{-3} and 4×10^{-3} m. (b) Predicted profiles of free IgG concentration at 20s in microchannels, where the sensor lengths were 0.1×10^{-3} , 2×10^{-3} and 4×10^{-3} m.

5.3.4 Simulation of the indirect hIgG assay in microchannel

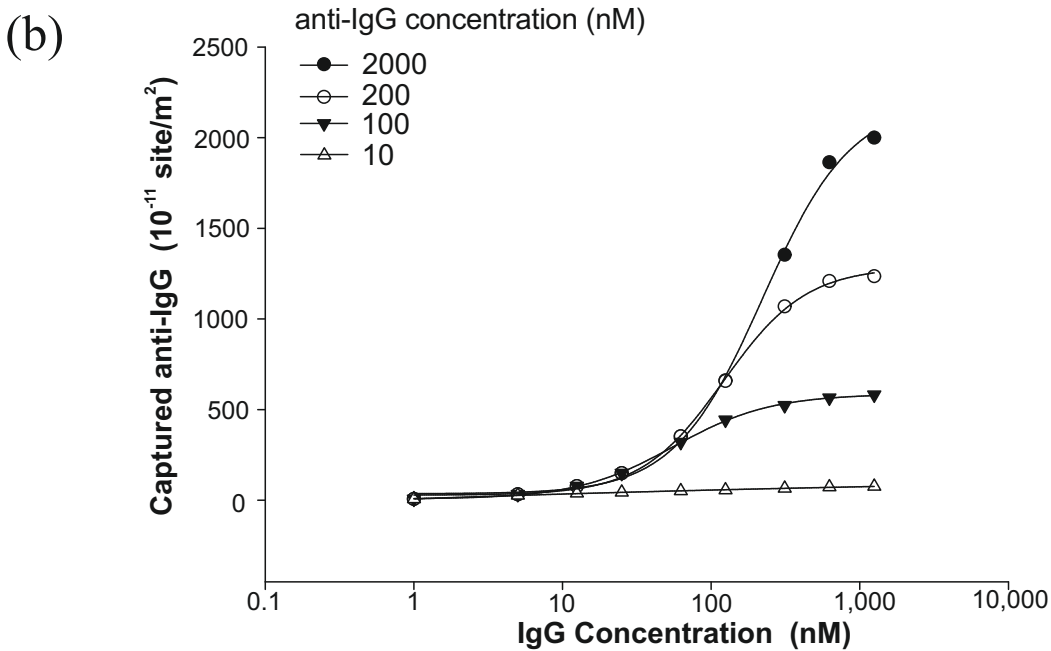
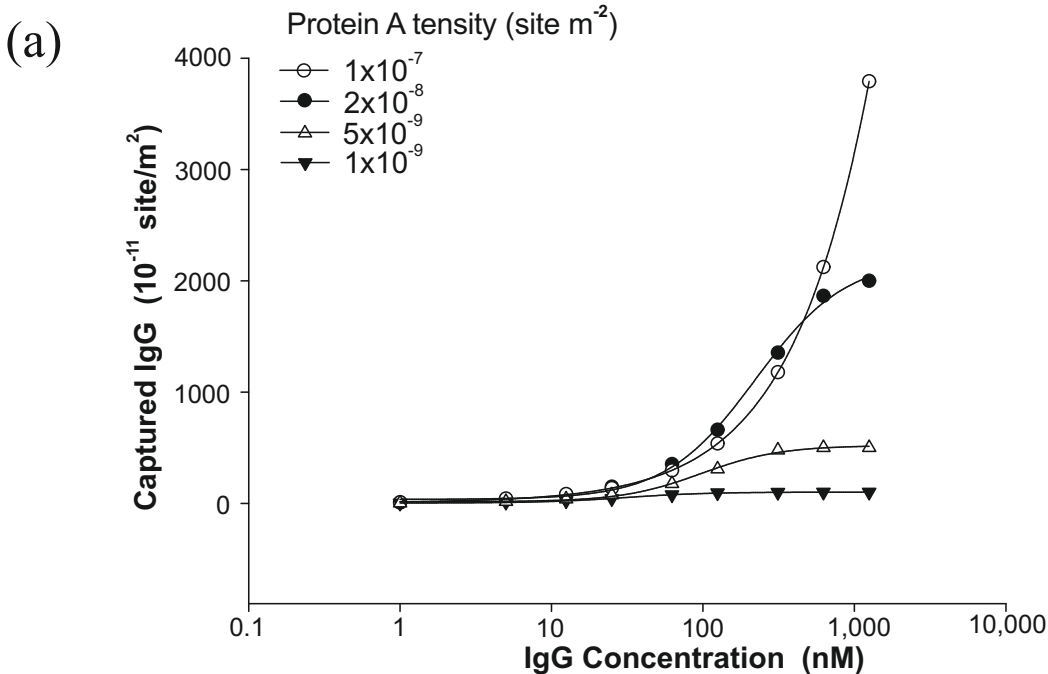
For most of the developed microfluidic immunoassay applications, the assay format is a heterogeneous assay with multiple reagents and reactions. In our previous study (Fig. 5.1.2), the heterogeneous indirect assay including three binding reactions. In order to investigate the influence of concentrations of assay reagents on the assay performance, simulations of this indirect hIgG assay in the microfluidic system were carried out with a finite volume of reagents (30 μ L) and the same residence time (20s) for each flow.

The density of initial binding sites in surface immunoassays usually plays an important role in defining the maximum number of analyte molecules that can be captured. The influence of the initial density of Protein A was investigated at the beginning of this section. Protein A surfaces with different densities (1×10^{-9} , 5×10^{-9} , 2×10^{-8} and 1×10^{-7} site/ m^2) were used to capture serial concentrations of hIgG reagents. The densities of captured hIgG were plotted against the hIgG concentrations, as shown in Fig 5.3.4a. It was demonstrated that increased density of Protein A binding sites dramatically enhanced sensitivity.

Based on the data in Fig 5.3.4a, the influence of concentration of secondary assay reagent on assay performance was investigated by simulation of the binding reaction between captured hIgG on the surface and anti-hIgG in solution. The simulation was carried out using the density of captured hIgG (Γ) as the surface density of binding (Γ_{\max}) for the secondary reaction. The density of captured hIgG (Γ) was determined from the first reaction with the Protein A with a density of 2×10^{-8} site/ m^2 as shown in Fig 5.3.4a. Additionally, varying concentrations of anti-hIgG solutions of 50, 100, 200 and 2000 nM, were applied in the secondary reaction. The densities of captured anti-hIgG on the microchannel surface were plotted against the hIgG concentrations in Fig 6.2.4b. The standard curve generated with the higher concentration of anti-hIgG shows the significantly increased sensitivity. This result indicates that the application of sufficient secondary reagent can provide an enhanced sensitivity to the assay through saturation the entire surface binding site which was generated from first reaction.

The reaction of the biotin labelled anti-hIgG and with the fluorescently labelled

NeutrAvidin dye relies on the biotin-NeutrAvidin binding, which exhibits the highest known affinity ($K_D=10^{15} \text{ M}^{-1}$) in the nature. Therefore, we did not take this reaction into account because it is generally not the limitation in immunoassays.



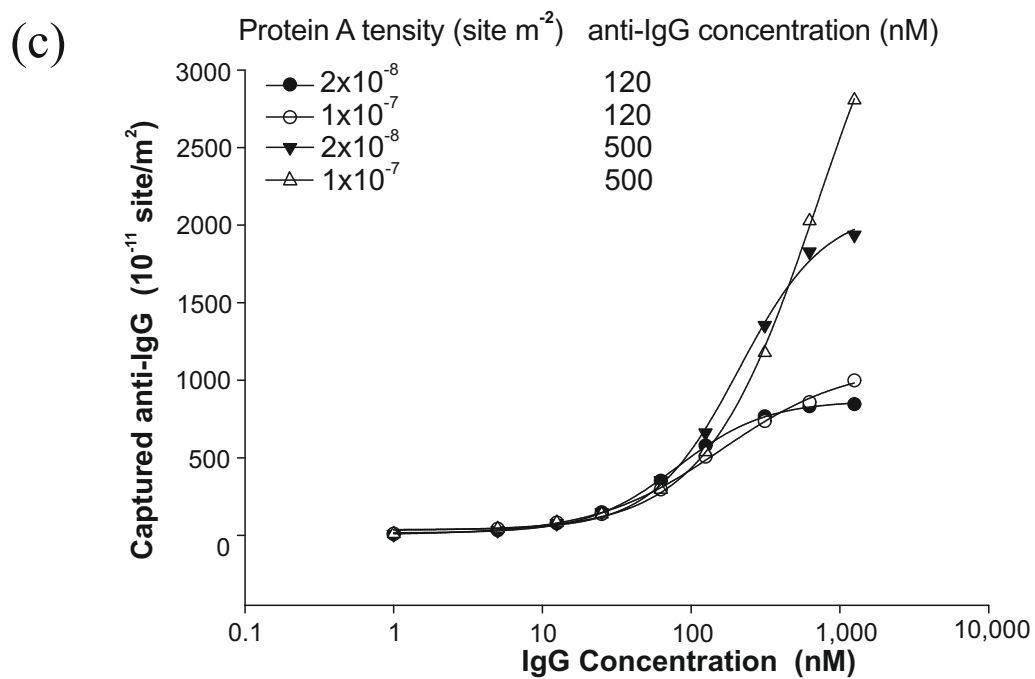


Figure 5.3.4 Influence of reagents concentrations on assay performance. (a) Optimisation of initial density of binding sites by comparing first-reaction performance. (b) Optimisation of anti-hIgG concentration by comparing second-reaction performance. (c) Optimisation of combination of assay reagents by analysis of assay performance with different reagent concentrations.

In Fig 6.2.4c, the standard curves of this hIgG indirect immunoassay in the microchannel with different concentrations of Protein A and anti-hIgG were compared. Both curves generated with 500 nM anti-hIgG reveals that 500 nM anti-hIgG is sufficient to saturate the captured-hIgG on the surfaces, where the concentrations of Protein A on the surface is 2×10^{-8} or 1×10^{-7} site/m². In contrast, the curves with 120 nM anti-hIgG shows dramatic reduction in assay sensitivity since it was not sufficient to saturate hIgG binding sites. For the curves generated with the high initial binding site numbers (1×10^{-7} site/m²), the superior binding rate presenting in first reaction can be eliminated by shortage of anti-hIgG (120 nM). However, it did not indicate that the assay with high concentrations of each reagent would provide the ideal performance. Comparing the two curves with 500 nM anti-hIgG and different Protein A densities, the curve generated with a Protein A of 2×10^{-8} site/m² possessed a better sensitivity than the curve with a Protein A of 1×10^{-7} site/m² during the range from 50 nM to 1000 nM, which was more accurate for detection of small amounts of analyte. Furthermore, the high sensitivity and extremely large working range presenting in the curve with a Protein A of 1×10^{-7} site/m², generally did not exist in practice due to limitations of active binding density and the detection technique.

5.4 Discussion

Microfluidic platforms offer several advantages over conventional microtiter plates where the assays are performed using much larger volumes and longer times. However, to take full advantage of microfluidic platforms, it is important to understand the influence of major parameters on the binding kinetics and identify the major parameters affecting assay performance in microfluidics. In previous studies, computational modeling was applied to investigate the influence of major parameters on the binding kinetics in the microchannel by simulating binding of the analytes with specific concentrations as a function of time (Zimmermann *et al.*, 2005; Parsa *et al.*, 2008). These simulated results show how a change of variable parameter affects the binding kinetics with regard to one specific concentration of analyte. It is not clear what the influence on the entire working range of analyte concentrations, This is essential for good design of a microfluidic sensor with outstanding binding kinetics and optimisation of the immunoassay thus providing good sensitivity across the entire working range.

In this study, we investigated the influence of the major parameters (flow velocity, channel height, capture area length and concentration of assay components) on assay performance (standard curves). For a defined volume of reagent, the variation in flow velocity or channel geometry can induce a change in fluid residence time, leading to a barrier for the analysis of the influence of these two factors on the assay performance. Hence, the study of flow velocity and channel geometry was performed under conditions of both finite and infinite volume of assay reagents.

The high flow velocity of reagents above the capture area can accelerate the binding process without considering reagent volume and time constraints. This viewpoint was proved by comparing the rate of analyte binding with different flow rates in Fu's study (Fu *et al.*, 2009). However, finite assay time and a large volume of reagent are not expected for the development of an ideal microfluidic system in practice.

There are several studies considering the effect of microchannel geometry on mass transport. Dutta's group investigated the effect of aspect ratio on solute dispersivity in pressure-driven flow systems for a fixed channel depth. They showed that the solute

dispersion coefficient decreased monotonically with an increase in the aspect ratio of the channel (Dutta *et al.*, 2006). Squires discussed the physical process of analyte transport within microchannels of various sizes by computing several dimensional parameters. In their study, it was theoretically proved that a smaller aspect ratio of the capture area could reduce analyte transport (Squires *et al.*, 2008). Our research analysed both the effect of height of microchannel on the standard curves and also precisely computed the criteria associated with microchannel height for our specific microfluidic system.

This study on the influence of capture area confirmed previous studies (Zimmermann *et al.*, 2005; Zhao *et al.*, 2010) that a smaller capture area can increase the rate of binding for microfluidic-based assay. Furthermore, we demonstrated the effect of the capture area on the sensitivity of the standard curve, which provided a direct guideline for design and optimization of the microfluidic system.

Using theoretical modeling, we investigated the effect of the varying flow velocity, channel height, and analyte-capture area length on the binding rate of analytes at different concentrations. This simulation revealed that depletion caused by mass-transport limitation is one of the key bottlenecks to the sensitivity of a solid-support based microfluidic assay. Without considering the constraints of reagent availability and assay time, this limitation can be reduced through faster flow velocity, reducing the size of the capture area, or optimising the channel height.

On the other hand, we examined the effect of these varying assay parameters on the capture of analytes at different concentrations under real-world operating conditions. Under the constraints of reagent and time, the simulations revealed trends that are not necessarily intuitive according to generic considerations of microfluidic advantages. For example, a 30 μL of sample with a high velocity resulted in a relatively low binding rate due to the fact that the contact time was reduced. In terms of producing guidelines for best practice, the simulation of the assay performance (e.g. standard curve) under real-world constraints was more convincing..

The influence of assay components on the performance of microfluidic system was investigated by simulation of the entire indirect assay in a microchannel. The simulated

data revealed the necessary amount of each reagent required for contributing to a sensitive assay. In addition, it was important for to optimise the concentrations of each of the assay components. Overall, this approach can provide very useful insights to aid in the optimisation of microfluidics-based immunoassays and can contribute to recent findings in the field (O’Kennedy, 2017)

CHAPTER 6

Overall Outcomes and Conclusions

The goals of the work presented in this thesis were to develop immunoassays and microfluidic systems for rapid detection of selected targets such as marine toxins and human IgG. The strategies employed involved the construction of a recombinant scFv library for the toxins and the isolation of high affinity scFv antibodies from the recombinant library. In addition, the techniques of microfluidics and SAF detection were applied for development of a rapid immunoassay system for IgG.

Chapter 3 described the production of a recombinant antibody against both STX and Neo groups of PSTs. Firstly, the anti-Neo-STX-KLH scFv library was constructed. Then phage display was employed to isolate STX-OVA-specific scFv from anti-Neo-STX-KLH scFv library via biopanning. After 4 rounds of bio-panning, recombinant antibodies, with high affinity to STXs, were not isolated. There are a variety of reasons to hinder the isolation of a recombinant antibody. The immunisation associated problems caused by the toxic nature of the immunogen and the size of the hapten and the quality of conjugation, may lead to poor immune responses in an animal (Campbell *et al.*, 2011). Amplification problems during the construction of the antibody library may lead to inefficient variable gene assembly and a poor diversity within the scFv library (Koohapitagtam *et al.*, 2010). The undesired loss of target-binding clones during biopanning was commonly reported (Barbas *et al.*, 2001). The main limitation to this project work was the scarcity and high price of purified toxin material. If a reliable, purified source of toxin material becomes available in the future, it may be possible to isolate the recombinant antibody to PSPs from the immune libraries generated during this project and this work is currently ongoing.

The development of a new immunoassay system for rapid quantification of hIgG, was described in chapter 4. In the initial part of this chapter a hIgG FLISA was successfully developed on a microtitre plate by optimizing the assay reagents' concentrations. Additionally, the application of mixture of anti-hIgG and DyLight gave this assay a reduced completion time and larger working range. This hIgG assay was then transferred onto a 'proof-of-concept' microfluidic system, with flow-cells, incorporating a number of optimized parameters: (1) use of a reduced volume

of assay reagents (from 100 μ L reduced to 30 μ L), (2) shortened assay-time (from one day to 20 minutes). (3) optimized surface chemistry for protein A immobilisation, and (5) a reduced number of assay steps. The study revealed that the immunoassay could be further developed by changing the addition sequence of assay reagents. In particular, it was initially demonstrated that premixing and pre-incubating of secondary antibody and detector reagents under ideal conditions was superior to sequentially adding reagents.

The ‘proof-of-concept’ microfluidic-flow-cells feature straight micro-channels molded in PMMA and PSA. The initial microfluidic design enabled 12 separate immunoassays to be performed simultaneously. However, manual loading was required for each immunoassay reagent. The SAF optical instrument was modified to specifically collect the fluorescence signals inside the microfluidic system from the immune-complexes and not from the bulk solution. The Zeonor[®] slide, was used both as a solid phase to support the formation of the reactive immune-complex and as an essential optical component in the SAF detection system. A calibration curve for the quantification of hIgG based on the ‘proof-of-concept’ microfluidic system was established. This microfluidic immunoassay is capable of detecting hIgG in the lower nanogram range. In addition, the assay had a dynamic range of quantification of approximately 2 logs with inter-day coefficients of variation of approximately 10%. This compares favorably to the conventional hIgG immunoassay. Furthermore, an industrial bioprocess sample was quantified using the microfluidic ‘flow-cell’ device. Both conventional and flow-cell methods yielded comparable results.

In the rest of chapter, two generations of microfluidic CDs were successfully developed for hIgG immunoassay. They are the ‘SAF-element’ CD and a ‘reagents delivery’ CD. These two CDs have improved design with three-dimensional (3D) microstructure and 3D microchannel networks. The ‘20-SAF-element’ CD contains 20 separate microfluidic units and incorporates the optical elements into each units. A new strategy for surface functionalization (PECVD) was introduced in surface preparation. It was demonstrated that PECVD-functionalisation using APTES generated better assay spot morphology and a more stable functionalised surface than

liquid-phase APTES depositions.

In the next iteration of microfluidic design, serial siphon valves were incorporated into the CD. The automatic hIgG FLISA on this 'reagents delivery' CD was realized through optimisations that included: (1) surface contact angle, (2) Tween-20[®] concentrations and (3) use of the serial siphon valving rotation protocol. A calibration curve for the hIgG immunoassay was successfully demonstrated using the serial siphon CD and the SAF prototype detector. The inter-day hIgG calibration curve exhibited an inter-day coefficient of variation (CV) of 2.2 % to 12.6 % across the entire hIgG concentration range tested. In contrast, the conventional FLISA displayed greater imprecision as the inter-day CV range was 5.9 % to 18.9 %. Furthermore, quantification of a bioprocess sample based on both calibration curves revealed comparable results.

A calibration curve for hIgG FLISA was optimised on 'reagents delivery' CDs, and a bioprocess sample was then quantified. Interestingly, comparison of both calibration curves revealed that microfluidic FLISA provides less inter-day CV. However, a shift in the range of the IgG assay was also observed. The conventional FLISA had a range of 0.08 – 10 µg/mL, in contrast, the microfluidic FLISA had a range of 0.8 – 50 µg/mL. This result was not unexpected as our device is a prototype system that contains not only an experimental protein capture surface but also experimental signal detection and reagent delivery systems. In contrast, conventional hIgG FLISA analysis was carried out with standard microtitre plates that have excellent protein binding properties as well as low autofluorescence levels. In addition, a commercially available microplate reader with high fluorescent sensitivity was used for sample analysis. Further optimisation of the microfluidic design, surface chemistry and the fluorescence detector has the potential to yield a lower IgG working range for the SAF-based microfluidic method. However, for our particular application the target analyte is in relative abundance. For example, bioprocess samples typically contain milligram amounts of IgG (Schepter *et al.*, 1999). Therefore, the shift in assay range was not undesirable, as it reduced the dilution needed to allow the sample to fall within the linear range of the calibration curve.

Modelling of the hIgG indirect immunoassay in a microchannel was described in chapter 5. Using theoretical modelling, several important parameters related to reaction binding rate were investigated. These included flow velocity, channel height, analyte-capture area length and reagent' concentration. This simulation revealed that depletion caused by mass-transport limitation above sensor area is one of the key bottlenecks to the sensitivity of solid-support-based microfluidic assays. Without considering the constraints of reagent availability and assay time, this limitation can be reduced through faster flow velocity, reducing the size of the capture area, or optimising the channel height. However, in practice, these real-world constraints have to be considered to develop a microfluidic system. Under the constraints of reagent and time, the simulations revealed trends that are not necessarily intuitive according to generic considerations of microfluidic advantages. For example, a 30 μL of sample with a high velocity resulted in a relatively low binding rate due to the fact that contact time was reduced. In terms of producing guidelines for best-practice, the simulation of the assay performance (e.g. standard curve) under real-world constraints was more convincing. In order to develop the microfluidic assay performance, the solutions place constraints on the operations. Therefore, the simulations have to be considered with some assay factors. In the rest of chapter 5, the influence of assay components on the performance of microfluidic system was investigated by simulation of the entire indirect assay in microchannel. The simulated data revealed the necessary amount of each reagent required for contributing to a sensitive assay. In addition, it was important to optimise the concentrations of each of the assay components.

The key outcomes from the study can be concluded as follows:

- (1) for the first time, SAF optical detection has been integrated with a centrifugal microfluidic platform, to enable surface-specific fluorescence detection in a heterogeneous immunoassay,
- (2) in addition, the SAF optical elements have been incorporated onto the microfluidic disc itself,
- (3) plasma technology was used to polymerise APTES onto the surface of the

SAF chip to mediate immobilisation of specific capture probes,

(4) a quantitative, surface-based, IgG immunoassay was developed and used to test this system,

(5) the concentration of Tween-20 in each of the assay reagents was optimised, so as to facilitate the function of the serial siphon and capillary valves,

(6) additionally, the hardware interface with such an integrated microfluidic platform was successfully developed,

(7) furthermore, modelling of the hIgG indirect microfluidic immunoassay was established and can be applied to optimise other similar microfluidics systems for further study.

CHAPTER 7

Bibliography

Abbas, A. K., Lichtman, A. H., & Pillai, S. (2012). Basic immunology: functions and disorders of the immune system. 4th Edition. Elsevier Health Sciences. St. Louis.

Absolom, D. R. & Van Oss, C. J. (1986). The nature of the antigen-antibody and factors affecting its association and dissociation, *CRC Crit. Rev. Immunology*, **6**,1-46.

Agarwal, V. (2010). Innate immunity. *Indian J. Rheumatol.*, **5**, 131–136.

Ait-Ali, I., Morin, P., Semet, V., Cabrera, M., & Ferrigno, R. (2012). High Precision Machining Strategy for the Integration of Electrochemical Cells in Cyclic Olefin Copolymer Microfluidic Devices. *Procedia Eng*, **47**, 450-453.

Akira, S., Takeda, K., & Kaisho, T. (2001). Toll-like receptors : critical proteins linking innate and acquired immunity. *Nat. Immunol.*, **2**(8), 675-680.

Akbari, S. & Pirbodaghi, T. (2014). A droplet-based heterogeneous immunoassay for screening single cells secreting antigen-specific antibodies. *Lab. Chip.*, **14**(17), 3275-3280.

Alberts, B. E. A. (2012). The Adaptive Immune System. *Immunol. Cell. Biol.*, **15**, 17283–17290.

Al-Mahdili, H. A. & Jones, G. R. (2010). High-dose hook effect in six automated human chorionic gonadotrophin assays. *Ann. Clin. Biochem.*, **47**(4), 383-385.

Almonte, L., Lopez-Elvira, E., & Baró, A. M. (2014). Surface charge differentiation of streptavidin and avidin by atomic force microscopy-force spectroscopy. *Chem. Phys. Chem.*, **15**(13), 2768-2773.

Angelini, E., Grassini, S., Rosalbino, F., Fracassi, F., Laera, S., & Palumbo, F. (2006). PECVD coatings : analysis of the interface with the metallic substrate. *Surf Interface Anal.*, **38**, 248-251.

Anderson, D. M. (1994,). Red Tides. *Sci. Am.*, **271**, 52–58.

- Armbruster, D. A. & Pry, T. (2008). Limit of blank, limit of detection and limit of quantitation. *Clin. Biochem. Rev.*, **29**, S49-52.
- Asp, T. N., Larsen, S., & Aune, T. (2004). Analysis of PSP toxins in Norwegian mussels by a post-column derivatization HPLC method. *Toxicon*, **43**(3), 319-327.
- Attia, U. M., Marson, S., & Alcock, J. R. (2009). Micro-injection moulding of polymer microfluidic devices. *Microfluid. Nanofluid.*, **7**, 1–28.
- Badley, R. A., Drake, R. A. L., Shanks, I. A., Smith, A. M., Stephenson, P. R., Thomas, J. D. R., & Thomas, J. D. R. (1987). Optical Biosensors for Immunoassays: The Fluorescence Capillary-Fill Device. *Phil. Trans. Roy. Soc. (Lond. B) Biol. Sci.*, **316**, 143-160.
- Badr, I. H., Johnson, R. D., Madou, M. J., & Bachas, L. G. (2002). Fluorescent ion-selective optode membranes incorporated onto a centrifugal microfluidics platform. *Anal. Chem.*, **74**(21), 5569-5575.
- Bange, A., Halsall, H. B., & Heineman, W. R. (2005). Microfluidic immunosensor systems. *Biosens. Bioelectron*, **20**(12), 2488–2503.
- Bartholomeusz, D. A., Boutté, R. W., & Andrade, J. D. (2005). Xurography: rapid prototyping of microstructures using a cutting plotter. *J. Microelectromech. S.*, **14**(6), 1364-1374.
- Becker H. & Gartner C. (2000). Polymer microfabrication methods for microfluidic analytical applications. *Electrophoresis*, **21**, 12-26.
- Berthier, J. & Silberzan, P. (2010). Microfluidics for biotechnology. 2nd Edition. Artech House, Boston.
- Bergeron, M., Peytavi, R., Kido, H., & Madou, M. (2008) Serial siphon valves for fluidic or microfluidic devices. Patent Application, WO/2008/106782.
- Bhagat, A. A. S., Hou, H. W., Li, L. D., Lim, C. T., & Han, J. (2011). Pinched flow

coupled shear-modulated inertial microfluidics for high-throughput rare blood cell separation. *Lab. Chip.*, **11**(11), 1870-1878.

Bier, F. F., Stöcklein, W., Böcher, M., Bilitewski, U., & Schmid, R. D. (1992). Use of a fibre optic immunosensor for the detection of pesticides. *Sens. Actuator B-Chem.*, **7**(1), 509-512.

Bigalke, B., Pötz, O., Kremmer, E., Geisler, T., Seizer, P., Puntmann, V. O., Phinikaridou, A., Chiribiri, A., Nagel, E., Botnar, R. M., Joos, T., & Gawaz, M. (2011). Sandwich immunoassay for soluble glycoprotein VI in patients with symptomatic coronary artery disease. *Clin. Chem.*, **57**(6), 898-904.

Bonwick, G. A. & Smith, C. J. (2004). Immunoassays: their history, development and current place in food science and technology. *Int. J. Food Sci. Tech.*, **39**, 817–827.

Botana, L. M. (Ed.). (2014). Seafood and Freshwater Toxins: pharmacology, physiology, and detection. 3rd Edition. CRC Press, Florida, USA.

Booy, E. P., Johar, D., Maddika, S., Pirzada, H., Sahib, M. M., Gehrke, I., & Loewen, S. (2006). Monoclonal and bispecific antibodies as novel therapeutics. *Arch. Immunol. Ther. Exp.*, **54**, 85–101.

Brown, L., Koerner, T., Horton, J. H., & Oleschuk, R. D. (2006). Fabrication and characterization of poly (methylmethacrylate) microfluidic devices bonded using surface modifications and solvents. *Lab. Chip.*, **6**(1), 66-73.

Branden, C. & Tooze, J. (1991). Introduction to Protein Structure (Vol. 2). New York: Garland.

Brenner, T., Glatzel, T., Zengerle, R., & Ducrée, J. (2004). Frequency-dependent transversal flow control in centrifugal microfluidics. *Lab. Chip.*, **5**(2), 146-150.

Bronzeau, S. & Pamme, N. (2008). Simultaneous bioassays in a microfluidic channel on plugs of different magnetic particles. *Anal. Chim. Acta*, **609**, 105-112.

Bratcher, A. R., Connell, L. B., & Millard, P. (2011). Portable biosensor detection of the harmful dinoflagellate *Alexandrium* using surface plasmon resonance and peptide nucleic acid probes. *In OCEANS 2011* (pp. 1-3). IEEE.

Buendia, R., Seoane, F., & Gil-Pita, R. (2010). A novel approach for removing the hook effect artefact from electrical bioimpedance spectroscopy measurements. In *J. Physics: Conference Series* (Vol. 224, No. 1, p. 012126). IOP publishing.

Carter, P. J. (2011). Introduction to current and future protein therapeutics: a protein engineering perspective. *Exp. Cell Res.*, **317**(9), 1261–1269.

Campbell, K., Rawn, D. F., Niedzwiadek, B., & Elliott, C. T. (2011). Paralytic shellfish poisoning (PSP) toxin binders for optical biosensor technology: problems and possibilities for the future: a review. *Food Addit. Contam.*, **28**(6), 711-725.

Campbell, K., Huet, A. C., Charlier, C., Higgins, C., Delahaut, P., & Elliott, C. T. (2009). Comparison of ELISA and SPR biosensor technology for the detection of paralytic shellfish poisoning toxins. *J. Chromatogr. B*, **877**(32), 4079-4089.

Campbell, K., Rawn, D. F., Niedzwiadek, B., & Elliott, C. T. (2011). Paralytic shellfish poisoning (PSP) toxin binders for optical biosensor technology: problems and possibilities for the future: a review. *Food Addit. Contam.*, **28**(6), 711-725.

Carter, P. (2006) Potent antibody therapeutics by design. *Nat. Rev. Immunol.*, **6**, 343–357.

Chehimi, M. M., Lamouri, A., Picot, M., & Pinson, J. (2014). Surface modification of polymers by reduction of diazonium salts: polymethylmethacrylate as an example. *J. Mater. Chem. C*, **2**(2), 356-363.

Chen, J., Huang, P., & Lin, M. (2008). Analysis and experiment of capillary valves for microfluidics on a rotating disk. *Microfluid. Nanofluid.*, **4**, 427–437.

Cho, H., Kim, H., Kang, J., & Kim, T. (2007). How the capillary burst microvalve works. *J. Colloid Interface Sci.*, **306**, 379–385.

Chang, H. C., Chen, Y. H., Lin, J. C., Hung, S. S., Li, C. H., Chang, I. N., & Chang, C. M. (2013). Detection of Real-Time Tannic Acid Concentration Based-on Quasi-Static Centrifugal-and-Fluorescence Microfluid Technology. *Adv. Sci. Lett.*, **19**(9), 2639-2642.

Chivers, C. E., Crozat, E., Chu, C., Moy, V. T., Sherratt, D. J., & Howarth, M. (2010). A streptavidin variant with slower biotin dissociation and increased mechanostability. *Nat. Methods*, **7**(5), 391-393.

Chang, L., Rissin, D. M., Fournier, D. R., Piech, T., Patel, P. P., Wilson, D. H., & Duffy, D. C. (2012). Single molecule enzyme-linked immunosorbent assays: theoretical considerations. *J. Immunol. Methods*, **378**(1-2), 102–115.

Cunningham, B. (2015). High sensitivity automated multiplexed Immunoassays using photonic crystal enhanced fluorescence microfluidic system. *Biosens. Bioelectron.*, **73**, 32-40.

Czugala, M., Gorkin III, R., Phelan, T., Gaughran, J., Curto, V. F., Ducrée, J., Diamond, D., & Benito-Lopez, F. (2012). Optical sensing system based on wireless paired emitter detector diode device and ionogels for lab-on-a-disc water quality analysis. *Lab. Chip.*, **12**(23), 5069-5078.

Dalton, C. & Kaler, K. V. I. S. (2007). A cost effective, re-configurable electrokinetic microfluidic chip platform. *Sens. Actuator B-Chem.*, **123**(1), 628–635.

Davies, D. R. & Chacko, S. (1993). Antibody structure. *Acc. Chem. Res.*, **26**, 421–427.

DeSilva, B., Smith, W., Weiner, R., Kelley, M., Smolec, J., Lee, B., Khan, M., Tacey, R., Hill, H., & Celniker, A. (2003). Recommendations for the bioanalytical method validation of ligand-binding assays to support pharmacokinetic assessments of macromolecules. *Pharmaceut. Res.*, **20**, 1885–1900.

Delves, P. J. & Roitt, I. M. (2000). Advances in Immunology: the immune system. *N. Engl. J. Med.*, **343**, 37-49.

DeSilva, B., Smith, W., Weiner, R., Kelley, M., Smolec, J., Lee, B., Khan, M., Tacey,

R., Hill, H., & Celniker, A. (2003) Recommendations for the bioanalytical method validation of ligand-binding assays to support pharmacokinetic assessments of macromolecules. *Pharm. Res.*, **20**,1885-1900.

Diamandis, E. P. & Christopoulos, T. K. (1991). The biotin-(strept) avidin system: principles and applications in biotechnology. *Clin. Chem.*,**37**(5), 625-636.

Dickey, R. W. (2000). Seafood and Freshwater toxins: pharmacology, physiology, and detection. (L. Botana, Ed.), Dekker, New York.

Dodig, S. (2009). Interferences in quantitative immunochemical methods. *Bioche. Med.*, **19**(1), 50-62.

Dungchai, W., Chailapakul, O., & Henry, C. S. (2011). A low-cost, simple, and rapid fabrication method for paper-based microfluidics using wax screen-printing. *Analyst*, **136**(1), 77-82.

Dudley, R. A., Edwards, P., Ekins, R. P., Finney D. J., Mckenzie, I. G., Raab, G. M., Rodbard, D., & Rodgers, R. P. (1985). Guidelines for immunoassay data processing. *Clin. Chem.*, **31**,1264-1271.

Enderlein, J., Ruckstuhl, T., & Seeger, S. (1999). Highly efficient optical detection of surface-generated fluorescence. *Appl Optic*, **38**, 724-732.

Etheridge, S. M. (2010). Paralytic shellfish poisoning: seafood safety and human health perspectives. *Toxicon*, **56**(2), 108-122.

Falconer, I. R. (2012). Algal toxins in seafood and drinking water. 1st Edition. Elsevier, New York, USA.

Findlay, J. W. A. & Dillard, R. F. (2007). Appropriate Calibration Curve Fitting in Ligand Binding Assays. *A. A. P. S.*, **9**(2): E260-E267.

Finney, D. J. & Phillips, P. (1977). The form and estimation of a variance function, with particular reference to radioimmunoassay. *Appl. Stat.*, **26**, 312-320.

Findlay, J. W. A., Smith, W. C., Lee, J. W., Nordblom, G. D., Das, I., DeSilva, B. S., Khan, M. N., & Bowsher, R. R. (2000). Validation of immunoassays for bioanalysis: a pharmaceutical industry perspective. *J. Pharmaceut. Biomed. Anal.*, **21**(6), 1249–1273.

Flamm, D. L. & Auciello, O. (2012). Plasma deposition, treatment, and etching of polymers: the treatment and etching of polymers. R. d'Agostino (Ed.). Elsevier. New York.

Fragoso, A., Latta, D., Laboria, N., von Germar, F., Hansen-Hagge, T. E., Kemmner, W., Gartner, C., Klemm, R., Drese, K.S., & O'Sullivan, C. K. (2011). Integrated microfluidic platform for the electrochemical detection of breast cancer markers in patient serum samples. *Lab. Chip.*, **11**(4), 625-631.

Fu, E., Nelson, K. E., Ramsey, S. a, Foley, J. O., Helton, K., & Yager, P. (2009). Modeling of a competitive microfluidic heterogeneous immunoassay: sensitivity of the assay response to varying system parameters. *Anal. Chem.*, **81**(9), 3407–3413.

Galusinski, C. & Vigneaux, P. (2008). On stability condition for bifluid flows with surface tension: Application to microfluidics. *J. Comput. Phy.*, **227**(12), 6140-6164.

Gandhiraman, R. P., Gubala, V., O'Mahony, C. C., Cummins, T., Raj, J., Eltayeb, A., Doyle, C., James, B., Daniels, S., & Williams, D. E. (2011). PECVD coatings for functionalization of point-of-care biosensor surfaces. *Vacuum 2012.*, **86**, 547-555.

Ganz, T., Olbina, G., Girelli, D., Nemeth, E., & Westerman, M. (2008). Immunoassay for human serum hepcidin. *Blood*, **112**(10), 4292-4297.

Garber, E. A. (2008). Detection of melamine using commercial enzyme-linked immunosorbent assay technology. *J. Food. Prot.*, **71**(3), 590-594.

Geng, D., Shankar, G., Schantz, A., Rajadhyaksha, M., Davis, H., & Wagner, C. (2005). Validation of immunoassays used to assess immunogenicity to therapeutic monoclonal antibodies. *J. Pharmaceut. Biomed. Anal.*, **39**(3-4), 364–375.

Gervais, T. & Jensen, K. F. (2006). Mass transport and surface reactions in microfluidic systems. *Chem. Eng. Sci.*, **61**(4), 1102–1121.

Giordano, B. C., Burgi, D. S., Hart, S. J., & Terray, A. (2012). On-line sample pre-concentration in microfluidic devices: A review. *Anal. Chim. Acta.*, **718**, 11-24.

Gossett, D. R., Weaver, W. M., Mach, A. J., Hur, S. C., Tse, H. T. K., Lee, W., Amini, H., & Di Carlo, D. (2010). Label-free cell separation and sorting in microfluidic systems. *Anal. Bioanal. Chem.*, **397**(8), 3249-3267.

Gómez-Hens, A. & Aguilar-Caballeros, M. P. (2010). Trends in immunoassay techniques. *Encyclopedia of Analytical Chemistry*. , John Wiley and Sons Ltd. Chichester, UK.

Gorkin, R. A. (2010). Enabling technologies for nucleic acid 'sample-to-answer' centrifugal microfluidics. University of California, Irvine, USA.

Gorkin, R., Soroori, S., Southard, W., Clime, L., Veres, T., Kido, H., Kulinaky, L., & Madou, M. (2012). Suction-enhanced siphon valves for centrifugal microfluidic platforms. *Microfluid. Nanofluid.*, **12**(1-4), 345-354.

Godino, N., Gorkin, R., Bourke, K., & Ducrée, J. (2012). Fabricating electrodes for amperometric detection in hybrid paper/polymer lab-on-a-chip devices. *Lab. Chip.*, **12**(18), 3281-3284.

Guo, M. T., Rotem, A., Heyman, J. A., & Weitz, D. A. (2012). Droplet microfluidics for high-throughput biological assays. *Lab. Chip.*, **12**(12), 2146-2155.

Gubala, V., Siegrist, J., Monaghan, R., O'Reilly, B., Gandhiraman, R. P., Daniels, S., & Ducrée, J. (2013). Simple approach to study biomolecule adsorption in polymeric microfluidic channels. *Anal. Chim. Acta.*, **760**, 75-82.

Gubala, V., Gandhiraman, R. P., Volcke, C., Doyle, C., Coyle, C., James, B., Daniels, S., & Williams D. E. (2010). Functionalization of cycloolefin polymer surfaces by plasma-enhanced chemical vapour deposition: comprehensive characterization and analysis of the contact surface and the bulk of aminosiloxane coatings. *The Analyst*, **135**, 1375–

Haeberle, S. & Zengerle, R. (2007). Microfluidic platforms for lab-on-a-chip applications. *Lab. Chip*, **7**, 1094–1110.

Haeberle, S. & Zengerle, R. (2007). Microfluidic platforms for lab-on-a-chip applications. *Lab. Chip*, **7**(9), 1094–1110.

Hachem, R. Y., Kontoyiannis, D. P., Chemaly, R. F., Jiang, Y., Reitzel, R., & Raad, I. (2009). Utility of galactomannan enzyme immunoassay and (1, 3) β -d-glucan in diagnosis of invasive fungal infections: low sensitivity for *Aspergillus fumigatus* infection in hematologic malignancy patients. *J. Clin. Microbiol.*, **47**(1), 129–133.

Han, X. X., Chen, L., Ji, W., Xie, Y., Zhao, B., & Ozaki, Y. (2011). Label-Free indirect immunoassay using an avidin-induced surface-enhanced raman scattering substrate. *Small*, **7**(3), 316–320.

Haven, M. C., Orsulak, P. J., Arnold, L. L., & Crowley, G. (1987). Data-reduction methods for immunoradiometric assays of thyrotropin compared. *Clin. Chem.*, **33**, 1207–1210.

Hamrle, J. & MacCraith, B. D. (2000). Theory of the radiation of dipoles placed within a multilayer system. *Appl. Optics*, **39**, 3968–3977.

Hartwell, S. K. & Grudpan, K. (2010). Flow-based immuno/bioassay and trends in micro-immuno/biosensors. *Microchim. Acta*, **169**, 201–220.

Hellen, E. H. & Axelrod, D. (1987). Fluorescence emission at dielectric and metal-film interfaces. *J. O. S. A. B.*, **4**(3), 337–350.

Henares, T. G., Mizutani, F., & Hisamoto, H. (2008). Current development in microfluidic immunosensing chip. *Anal. Chim. Acta*, **611**(1), 17–30.

Hemmilä, I. (1985). Fluoroimmunoassays and immunofluorometric assays. *Clin. Chem.*, **31**(3), 359–370.

- Henares, T. G., Mizutani, F., & Hisamoto, H. (2008). Current development in microfluidic immunosensing chip. *Anal. Chim. Acta*, **611**(1), 17–30.
- Hoogenboom, H. R. (2002). Overview of antibody phage-display technology and its applications. *Meth. Mol. Biol. (Clifton, N.J.)*, **178**, 1–37.
- Howarter, J. & Youngblood, J. P. (2006). Optimization of silica silanization by 3-aminopropyltriethoxysilane. *Langmuir : J. Surfaces & Coll.*, **22**, 142–170.
- Howarter, J. A. and Youngblood, J. P. (2006). Optimization of silica silanization by 3-aminopropyltriethoxysilane. *Langmuir*, **22**(26), 11142-11147.
- Hudson, P. J. (1999). Recombinant antibody constructs in cancer therapy. *Curr. Opin. Allergy (Clin. Immunol.)*, 548–557.
- Humpage, A. R., Magalhaes, V. F., & Froscio, S. M. (2010). Comparison of analytical tools and biological assays for detection of paralytic shellfish poisoning toxins. *Anal. Bioanal. Chem.*, **397**(5), 1655-1671.
- Hu, G., Gao, Y., & Li, D. (2007). Modeling micropatterned antigen–antibody binding kinetics in a microfluidic chip. *Biosens. Bioelectron.*, **22**(7), 1403-1409.
- Irawan, R., Tjin, S. C., Fang, X., & Fu, C. Y. (2007). Integration of optical fiber light guide, fluorescence detection system, and multichannel disposable microfluidic chip. *Biomed Microdevices*, **9**(3), 413-419.
- Jain, E. & Kumar, A. (2008) Upstream processes in antibody production – evaluation of critical parameters. *Biotechnol. Adv.*, **26**, 46–72.
- Jefferis, R. (2009) Glycosylation as a strategy to improve antibody-based therapeutics. *Nature (Lond.)*, **8**, 226–234.
- Jeon, J. K., Lee, J. S., Shim, W. J., Aarakawa, O., Takatani, T., Honda, S., & Noguchi, T. (2008). Changes in activity of hepatic xenobiotic-metabolizing enzymes of tiger puffer (*Takifugu rubripes*) exposed to paralytic shellfish poisoning toxins. *J. Environ. Biol.*, **29**,

599–603.

Jena, R. K., Yue, C. Y., & Anand, L. (2011). Improvement of thermal bond strength and surface properties of Cyclic Olefin Copolymer (COC) based microfluidic device using the photo-grafting technique. *Sens. Actuator B Chem.*, **157**(2), 518-526.

Jia, G., Ma, K. S., Kim, J., Zoval, J. V., Peytavi, R., Bergeron, M. G., & Madou, M. J. (2006). Dynamic automated DNA hybridization on a CD (compact disc) fluidic platform. *Sens. Actuators B-Chem.*, **114**, 173-181.

Johnson, S. W., Kanatani, M., Humphries, R. M., & Uslan, D. Z. (2013). Clinical impact of switching conventional enzyme immunoassay with nucleic acid amplification test for suspected *Clostridium difficile*-associated diarrhea. *Am. J. Infect. Control.*, **41**(4), 373-375.

Juan-García, A., Font, G., & Picó, Y. (2005). Determination of organic contaminants in food by capillary electrophoresis. *J. Sep. Sci.*, **28**(9-10), 793-812.

Karle, M., Miwa, J., Czilwik, G., Auwärter, V., Roth, G., Zengerle, R., & von Stetten, F. (2010). Continuous microfluidic DNA extraction using phase-transfer magnetophoresis. *Lab. Chip.*, **10**(23), 3284-3290.

Kawatsu, K., Hamano, Y., Sugiyama, A., Hashizume, K., & Noguchi, T. (2002). Development and application of an enzyme immunoassay based on a monoclonal antibody against gonyautoxin components of paralytic shellfish poisoning toxins. *J. Food Prot.*, **65**(8), 1304-1308.

Karpinski, K. F. (1990). Optimality assessment in the enzyme-linked immunosorbent assay (ELISA). *Biometrics.* **46**, 381-390.

Kantak, C., Zhu, Q., Beyer, S., Bansal, T., & Trau, D. (2012). Utilizing microfluidics to synthesize polyethylene glycol microbeads for Förster resonance energy transfer based glucose sensing. *Biomicrofluidics*, **6**(2), 022006.

Kelley, B. (2007) Very large-scale monoclonal antibody purification – the case for

conventional unit operations. *Biotechnol. Prog.*, **23**, 995– 1008.

Kelley, B. (2009) Industrialization of mAb production technology– the bioprocessing industry at a crossroads. *MAbs.*, **1**, 1–10.

Killard, A. J., Deasy, B., Kennedy, R. O., & Smyth, R. (1995). Antibodies : production , functions and applications in biosensors. *Trends Anal Chem.* **14**, 257–266.

Kipriyanov, S. M., & Little, M. (1999). Generation of recombinant antibodies. *Mol Biotechnol*, **12**, 173–201.

Kim, D., Wu, X., Young, A. T., & Haynes, C. L. (2014). Microfluidics-Based in Vivo Mimetic Systems for the Study of Cellular Biology. *Acc. Chem. Res.*, **47**(4), 1165-1173.

Kim, T. H., Abi-Samra, K., Sunkara, V., Park, D. K., Amasia, M., Kim, N., Madou, M., & Cho, Y. K. (2013). Flow-enhanced electrochemical immunosensors on centrifugal microfluidic platforms. *Lab. Chip.*, **13**(18), 3747-3754.

Kirby, D., Siegrist, J., Zavattoni, L., Burger, R., & Ducrée, J. (2012) *Centrifugomagnetophoretic particle separation. Microfluid. Nanofluid.*, **13**, 899-908.

Knopp, D. (2006). Immunoassay development for environmental analysis. *Anal. Bioanal. Chem.*, **385**, 425–427.

Kozlowski, S. & Swann, P. (2006). Current and future issues in the manufacturing and development of monoclonal antibodies. *Adv. Drug. Deliv. Rev.*, **58**, 707-722.

Kreisig, T., Hoffmann, R., & Zuchner, T. (2011). Homogeneous fluorescence-based immunoassay detects antigens within 90 seconds. *Anal Chem*, **83**, 4281–4287.

Kurzbuch, D., Bakker, J., Melin, J., Jönsson, C., Ruckstuhl, T., & MacCraith, B. D. (2009). A biochip reader using super critical angle fluorescence. *Sens. Actuators B-Chem*, **137**(1), 1-6.

Lawrence, J. F., Niedzwiadek, B., & Menard, C. (2005). Quantitative determination of paralytic shellfish poisoning toxins in shellfish using prechromatographic oxidation and

liquid chromatography with fluorescence detection: collaborative study. *J. AOAC Int.*, **88**(6), 1714-1732.

Lai, S., Wang, S., Luo, J., Lee, L. J., Yang, S.-T., & Madou, M. J. (2004). Design of a compact disk-like microfluidic platform for enzyme-linked immunosorbent assay. *Anal. Chem.*, **76**, 1832–7.

Lagos, N., Onodera, H., Zagatto, P. A., & Oshima, Y. (1999). The first evidence of paralytic shellfish toxins in the freshwater cyanobacterium *Cylindrospermopsis raciborskii*, isolated from Brazil. *Toxicon.*, **37**, 1359–1373.

Lee, C. Y., Chang, C. L., Wang, Y. N., & Fu, L. M. (2011). Microfluidic mixing: a review. *Int. J. Mol. Sci.*, **12**(5), 3263-3287.

Lenshof, A. & Laurell, T. (2010). Continuous separation of cells and particles in microfluidic systems. *Chem. Soc. Rev.*, **39**(3), 1203-1217.

Le, N. C. H., Gubala, V., Gandhiraman, R. P., Daniels, S., & Williams, D. E. (2011). Evaluation of different non-specific binding blocking agents deposited inside poly (methylmethacrylate) (PMMA) microfluidic flow-cells. *Langmuir*, **27**(14), 9043-9051.

Lesch, H. P., Kaikkonen, M. U., Pikkarainen, J. T., & Ylä-Herttuala, S. (2010). Avidin-biotin technology in targeted therapy. *Expert Opin. Drug. Deliv.*, **7**(5), 551-564.

Lin, S. W., Chang, C. H., & Lin, C. H. (2011). High-throughput fluorescence detections in microfluidic systems. *GMBHS*, **3**(1), 27-38.

Li, Z., Woo, C. J., Iglesias-Ussel, M. D., Ronai, D., & Scharff, M. D. (2004). The generation of antibody diversity through somatic hypermutation and class switch recombination. *Genes & Dev.*, **18**, 1–11.

Little, M., Dübel, S., Kipriyanov, S., & Breitling, F. (1998). Recent developments in antibody engineering. *Methods in Molec. Med.*, **13**, 555–580.

Lindsley, M. D., Mekha, N., Baggett, H. C., Surinthong, Y., Autthateinchai, R.,

Sawatwong, P., & Poonwan, N. (2011). Evaluation of a newly developed lateral flow immunoassay for the diagnosis of cryptococcosis. *Clin. Infect. Dis.*, **53**(4), 321-325.

Li, J. & Zhu, Z. (2010). Research and development of next generation of antibody-based therapeutics. *Acta Pharmacologica Sinica*, **31**, 1198–207.

Lutz, S., Weber, P., Focke, M., Faltin, B., Hoffmann, J., Müller, C., Mark, D., & Roth, G. (2010). Microfluidic Lab-on-a-Foil for Nucleic Acid Analysis based on Isothermal Recombinase Polymerase Amplification (RPA). *Lab. Chip.*, **10**, 887-893.

Livnah, O., Bayer, E. A., Wilchek, M., & Sussman, J. L. (1993). Three-dimensional structures of avidin and the avidin-biotin complex. *Proc. Nati. Acad. Sci.*, **90**(11), 5076-5080.

Lionello, A., Josserand, J., Jensen, H., & Girault, H. H. (2005). Protein adsorption in static microsystems: effect of the surface to volume ratio. *Lab. Chip.*, **5**(3), 254-260.

Liu, X., Huo, Q. (2009). A washing-free and amplification-free one-step homogeneous assay for protein detection using gold nanoparticle probes and dynamic light scattering. *J. Immunol. Methods*, **349**(1), 38-44.

Lindsley, M. D., Mekha, N., Baggett, H. C., Surinthong, Y., Autthateinchai, R., Sawatwong, P., Harris, J. R., Park, B. J., Chiller, T., B, S. A., Poonwan, N. (2011). Evaluation of a newly developed lateral flow immunoassay for the diagnosis of cryptococcosis. *Clin. Infect. Dis.*, **53**, 321-325.

Liu, M., Ning, B., Qu, L., Peng, Y., Dong, J., Gao, N., Liu, L., & Gao, Z. (2012). Development of indirect competitive immunoassay for highly sensitive determination of ractopamine in pork liver samples based on surface plasmon resonance sensor. *Sens. Actuator B Chem.*, **161**(1), 124-130.

Liu, L., Kong, D., Xing, C., Zhang, X., Kuang, H., & Xu, C. (2014). Sandwich immunoassay for lactoferrin detection in milk powder. *Anal. Methods.*, **6**(13), 4742-4745.

Liu, J. L., Zabetakis, D., Walper, S. A., Goldman, E. R., & Anderson, G. P. (2014).

Bioconjugates of rhizavidin with single domain antibodies as bifunctional immunoreagents. *J. Immunol. Methods.* **411**, 37-42.

Liang, Y., Huang, J., Zang, P., Kim, J. and Hu, W. (2014). Molecular layer deposition of APTES on silicon nanowire biosensors: Surface characterization, stability and pH response. *Appl. Surf. Sci.* **322**, 202-208.

Lapin, N.A. and Chabal, Y.J. (2009). Infrared characterization of biotinylated silicon oxide surfaces, surface stability, and specific attachment of streptavidin. *J. Phys. Chem. B.* **113**(25), 8776-8783.

Li, H., Zhao, M., Liu, W., Chu, W. and Guo, Y. (2016). Polydimethylsiloxane microfluidic chemiluminescence immunodevice with the signal amplification strategy for sensitive detection of human immunoglobulin G. *Talanta.* **147**, 430-436.

Madou, M., Zoval, J., Jia, G., Kido, H., Kim, J., & Kim, N. (2006). Lab on a CD. *Ann. Rev. Biomed. Eng.*, **8**, 601–28.

Mark, D., Weber, P., Lutz, S., Focke, M., Zengerle, R., & von Stetten, F. (2011). Aliquoting on the centrifugal microfluidic platform based on centrifugo-pneumatic valves. *Microfluid. Nanofluid.*, **10**(6), 1279-1288.

Mark, D., Haeberle, S., Roth, G., von Stetten, F., & Zengerle, R. (2010). Microfluidic lab-on-a-chip platforms: requirements, characteristics and applications. *Chem. Soc. Rev.*, **39**(3), 1153–82.

Mayilo, S., Ehlers, B., Wunderlich, M., Klar, T. a, Josel, H.-P., Heindl, D., & Nichtl, A. (2009). Competitive homogeneous digoxigenin immunoassay based on fluorescence quenching by gold nanoparticles. *Anal. Chim. Acta*, **646**(1-2), 119–22.

Mark, D., Haeberle, S., Roth, G., von Stetten, F., & Zengerle, R. (2010). Microfluidic lab-on-a-chip platforms: requirements, characteristics and applications. *Chem. Soc. Rev.*, **39**(3), 1153-1182.

Marose, S., Lindemann, C., & Scheper, T. (2008). Two-Dimensional Fluorescence

Spectroscopy: A New Tool for On-Line Bioprocess Monitoring. *Biotechnol. Progr.*, **14**, 63-74.

Madou, M. J. (2002). Fundamentals of microfabrication: the science of miniaturization. 2nd edition. CRC Press, Washington, DC.

McCafferty, J., Griffiths, A. D., Winter, G., & Chiswell, D. J. (1990). Phage antibodies: filamentous phage displaying antibody variable domains. *Nature*. **348**, 552–554.

McNeely, M. (1999). Sample Processing with Hydrophobic Microfluidics. *J. Assoc. Lab. Auto.*, **4**(4), 30–33.

Mihali, T. K., Kellmann, R., & Neilan, B. A. (2009). Characterisation of the paralytic shellfish toxin biosynthesis gene clusters in *Anabaena circinalis* AWQC131C and *Aphanizomenon* sp. NH-5. *BMC biochem.*, **10**(1), 8.

Miller, O. J., El Harrak, A., Mangeat, T., Baret, J. C., Frenz, L., El Debs, B., Mayot, E., Samuels, M. L., Ronney, E. K., Dieu, P., Galvan, M., Link, D. R., & Galvan, M. (2012). High-resolution dose-response screening using droplet-based microfluidics. *Proc. Natl. Acad. Sci.*, **109**(2), 378-383.

Miller, K. J., Bowsher, R. R., Celniker, A., Gibbons, J., Gupta, S., & Lee, J. W. (2001). Workshop on bioanalytical methods validation for macromolecules: summary report. *Pharm. Res.*, **18**, 1373-1383.

Moutel, S., El Marjou, A., Vielemeyer, O., Nizak, C., Benaroch, P., Dübel, S., & Perez, F. (2009). A multi-Fc-species system for recombinant antibody production. *BMC Biotechnol.*, **9**(1), 14.

Mukundan, H., Kumar, S., Price, D. N., Ray, S. M., Lee, Y. J., Min, S., & Anderson, A. S. (2012). Rapid detection of *Mycobacterium tuberculosis* biomarkers in a sandwich immunoassay format using a waveguide-based optical biosensor. *Tuberculosis*, **92**(5), 407-416.

Murphy, K. (2011). Janeway's immunobiology. 8th Edition. Garland Science. New York.

- Muto, A., Tashiro, S., Nakajima, O., & Hoshino, H. (2004). The transcriptional programme of antibody class switching involves the repressor Bach. *Nature*, **429**, 566-571.
- Ng, A. H., Choi, K., Luoma, R. P., Robinson, J. M., & Wheeler, A. R. (2012). Digital microfluidic magnetic separation for particle-based immunoassays. *Anal. Chem.*, **84**(20), 8805-8812.
- Ng, A. H. C., Uddayasankar, U., & Wheeler, A. R. (2010). Immunoassays in microfluidic systems. *Anal. Bioanal. Chem.*, **397**(3), 991–1007.
- Nguyen, T. T., Sly, K. L., & Conboy, J. C. (2011). Comparison of the energetics of avidin, streptavidin, neutrAvidin, and anti-biotin antibody binding to biotinylated lipid bilayer examined by second-harmonic generation. *Anal. Chem.*, **84**(1), 201-208.
- Niederberger, V., Niggemann, B., Kraft, D., Spitzauer, S., & Valenta, R. (2002). Evolution of IgM, IgE and IgG(1-4) antibody responses in early childhood monitored with recombinant allergen components: implications for class switch mechanisms. *Eur. J. Immunol.*, **32**(2), 576–84.
- Nieri, P., Donadio, D., Rossi, S., Adinolfi, B., & Podesta, A. (2009). Antibodies for therapy.
- Norderhaug, L., Olafsen, T., Michaelsen, T. E., & Sandlie, I. (1997). Versatile vectors for transient and stable expression of recombinant antibody molecules in mammalian cells. *J. Immunol. Meth.*, **204**, 77–87.
- Nunes, P. S., Ohlsson, P. D., Ordeig, O., & Kutter, J. P. (2010). Cyclic olefin polymers: emerging materials for lab-on-a-chip applications. *Microfluid. Nanofluid.*, **9**(2-3), 145-161.
- Nwankire, C. E., Chan, D. S. S., Gaughran, J., Burger, R., Gorkin, R., & Ducrée, J. (2013). Fluidic automation of nitrate and nitrite bioassays in whole blood by dissolvable-film based centrifugo-pneumatic actuation. *Sensors*, **13**(9), 11336-11349.

Nwankire, C. E., Donohoe, G. G., Zhang, X., Siegrist, J., Somers, M., Kurzbuch, D., Monaghan, R., Kitsara, M., Burger, R., Hearty, S., Murrell, J., Martin, C., Rook, M., Barrett, L., Daniels, S., McDonagh, C., O’Kennedy, R., & Ducreé, J. (2013). At-line bioprocess monitoring by immunoassay with rotationally controlled serial siphoning and integrated supercritical angle fluorescence optics. *Anal. Chim. Acta.*, **781**, 54-62.

peutic uses and the evolution of biotechniques. *Curr. Med. Chem.*, **16**(6), 753-779.

Ofek, G., Guenaga, F. J., Schief, W. R., Skinner, J., Baker, D., Wyatt, R., & Kwong, P. D. (2010). Elicitation of structure-specific antibodies by epitope scaffolds. *Proc. Natl. Acad. Sci.*, **107**(42), 17880-17887.

O’ Kennedy, R. (2017) Antibodies – Natures Analytical Masterpieces IN *Methods* 116, 1-3.

O’ Toole, M., Lau, K. T., Shepherd, R., Slater, C., & Diamond, D. (2007). Determination of phosphate using a highly sensitive paired emitter-detector diode photometric flow detector. *Anal. Chim. Acta.*, **597**, 290-294.

Parsa, H., Chin, C. D., Mongkolwisetwara, P., Lee, B. W., Wang, J. J., & Sia, S. K. (2008). Effect of volume- and time-based constraints on capture of analytes in microfluidic heterogeneous immunoassays. *Lab. Chip.*, **8**(12), 2062–2070.

Pancer, Z. & Cooper, M. D. (2006). The evolution of adaptive immunity. *Ann. Rev. Immunol.*, **24**, 497–518.

Pande, J., Szewczyk, M. M., & Grover, A. K. (2010). Phage display: concept, innovations, applications and future. *Biotechnol. Adv.*, **28**(6), 849-858.

Pansri, P., Jaruseranee, N., Rangnoi, K., Kristensen, P., & Yamabhai, M. (2009). A compact phage display human scFv library for selection of antibodies to a wide variety of antigens. *BMC Biotechnol.*, **9**(1), 6.

Park, D. L., Adams, W. N., Graham, S. L., & Jackson, R. C. (1985). Variability of mouse bioassay for determination of paralytic shellfish poisoning toxins. *J. Assoc. Off. Anal. Chem.*, **69**(3), 547-550.

- Parra, J., Mercader, J. V., Agulló, C., Abad-Somovilla, A., & Abad-Fuentes, A. (2012). Generation of anti-azoxystrobin monoclonal antibodies from regioisomeric haptens functionalized at selected sites and development of indirect competitive immunoassays. *Anal. Chim. Acta.*, **715**, 105-112.
- Pereira, A. T., Novo, P., Prazeres, D. M. F., Chu, V., & Conde, J. P. (2011). Heterogeneous immunoassays in microfluidic format using fluorescence detection with integrated amorphous silicon photodiodes. *Biomicrofluidics*, **5**(1), 14102.
- Qi, H., Lu, H., Qiu, H. J., Petrenko, V., & Liu, A. (2012). Phagemid vectors for phage display: properties, characteristics and construction. *J. Mol. Bio.*, **417**(3), 129-143.
- Raj, J., Herzog, G., Manning, M., Volcke, C., MacCraith, B. D., Ballantyne, S., & Thompson, M. (2009). Surface immobilisation of antibody on cyclic olefin copolymer for sandwich immunoassay. *Biosens. Bioelectron.*, **24**(8), 2654–2658.
- Rawn, D. F., Niedzwadek, B., Campbell, K., Higgins, H. C., & Elliott, C. T. (2009). Evaluation of surface plasmon resonance relative to high pressure liquid chromatography for the determination of paralytic shellfish toxins. *J. Agric. Food Chem.*, **57**(21), 10022-10031.
- Ramakrishna Matte, H. S. S., Subrahmanyam, K. S., Venkata Rao, K., George, S. J., & Rao, C. N. R. (2011). Quenching of fluorescence of aromatic molecules by graphene due to electron transfer. *Chem. Phys. Lett.*, **506**(4), 260-264.
- Selmi, M., Khemiri, R., Echouchene, F. and Belmabrouk, H. (2016). Electrothermal effect on the immunoassay in a microchannel of a biosensor with asymmetrical interdigitated electrodes. *Appl. Therm. Eng.* **105**. 77-84.
- Reichert, J. M., Rosensweig, C. J., Faden, L. B., & Dewitz, M. C. (2005). Monoclonal antibody successes in the clinic. *Nat. Biotechnol.*, **23**(9), 1073-1078.
- Reichert, J. M., & Valge-Archer, V. E. (2007). Development trends for monoclonal antibody cancer therapeutics. *Nat. Rev. Drug Discovety*, **6**(5), 349-356.

Reverberi, R. & Reverberi, L. (2007). Factors affecting the antigen-antibody reaction. *Acta. Appl. Math.*, **5**, 227–40.

Rodbard, D., Frazier, G. R. (1975). Statistical analysis of radioligand assay data. *Meth. Enzymol.*, **37**, 3-22.

Rodbard, D. & Frazier, G. R. (1975). Statistical analysis of radioligand assay data. *Meth. Enzymol.*, **37**, 3-22.

Roy, S., Yue, C. Y., Lam, Y. C., Wang, Z. Y., & Hu, H. (2010). Surface analysis, hydrophilic enhancement, ageing behavior and flow in plasma modified cyclic olefin copolymer (COC)-based microfluidic devices. *Sens. Actuator B Chem.*, **150**(2), 537-549.

Rockberg, J., Löfblom, J., Hjelm, B., Uhlén, M., & Stahl, S. (2008). Epitope mapping of antibodies using bacterial surface display. *Nat. Methods*, **5**(12), 1039-1045.

Rocke, D. M. & Jones, G. (1997). Optimal Design for ELBA and Other Forms of Immunoassay. *Technometrics*, **39**(2), 162-170.

Ruuls, S. R., Lammerts van Bueren, J. J., van de Winkel, J. G., & Parren, P. W. (2008). Novel human antibody therapeutics: the age of the Umabs. *Biotechnol. J.*, **3**(9-10), 1157-1171.

Ruckstuhl, T., Rankl, M., & Seeger, S. (2003). Highly sensitive biosensing using a supercritical angle fluorescence (SAF) instrument. *Biosens. Bioelectron.*, **18**, 1193.

Saha, K., Bender, F., & Gizeli, E. (2003). Comparative study of IgG binding to proteins G and A: nonequilibrium kinetic and binding constant determination with the acoustic waveguide device. *Anal. Chem.*, **75**(4), 835–842.

Shah, V. P., Midha, K. K., Findlay, J. W., Hill, H. M., Hulse, J. D., McGilveray, I. J., & McKay, G. (2000). Bioanalytical method validation--a revisit with a decade of progress. *Pharmaceut. Res.*, **17**, 1551–1557.

Shanker, A. (2010). Adaptive control of innate immunity. *Immunol. Lett.*, **131**, 107–122.

Shukla, A. A., Hubbard, B., Tressel, T., Guhan, S., & Low, D. (2007). Downstream processing of monoclonal antibodies—application of platform approaches. *J. Chrom. B.*, **848**, 28-39.

Shukla, A. A. & Thömmes, J. (2010). Recent advances in large-scale production of monoclonal antibodies and related proteins. *Trends Biotechnol.*, **28**, 253–261.

Siegrist, J., Peytavi, R., & Madou, M. (2009). Microfluidics for biological analysis: Triumphs and hurdles of CD platforms. *IVD Technology*, 111–127.

Siegrist, J., Burger, R., Kirby, D., Zavattoni, L., Kijanka, G., & Ducrée, J. (2011). Stress-free centrifugo-magnetic 2D-separation of cancer cells in a stopped-flow mode. *μ TAS.*, 1915-1917.

Siegrist, J., Gorkin, R., Clime, L., Roy, E., Peytavi, R., Kido, H., Bergeron, M., Veres, T., & Madou, M. (2010). Serial siphon valving for centrifugal microfluidic platforms. *Microfluid. Nanofluid.*, **9**(1), 55-63.

Skinner, J. P., Gayda, S., & Tetin, S. Y. (2014). Use of Cyclic Olefin Polymer in Single Molecule Total Internal Reflection Fluorescence Microscopy. *Biophys. J.*, **106**(2), 197a.

Song, K. C., Lee, K. J., Yu, H. S., Mok, J. S., Kim, J. H., Lim, K. S., & Lee, M. (2013). Paralytic Shellfish Poisoning (PSP) Analysis using Liquid Chromatography-Tandem Mass Spectrometry. *Korean J. Fish. Aquat. Sci.*, **46**(2), 154-159

Squires, T. M., Messinger, R. J., & Manalis, S. R. (2008). Making it stick: convection, reaction and diffusion in surface-based biosensors. *Nat. Biotechnol.*, **26**(4), 417–426.

Squires, T. & Quake, S. (2005). Microfluidics: Fluid physics at the nanoliter scale. *Rev. Mod. Phys.*, **77**(3), 977–1026.

Stein, P. D., Janjua, M., Matta, F., Pathak, P. K., Jaweesh, F., Alrifai, A., & Chughtai, H.

L. (2011). Prognosis based on creatine kinase isoenzyme MB, cardiac troponin I, and right ventricular size in stable patients with acute pulmonary embolism. *Am. J. Cardiol.*, **107**(5), 774-777.

Suzuki, H. & Machii, K. (2013). Effects of injection speed of test samples on the mouse bioassay for paralytic shellfish poisoning toxins. *Ital. J. Food Saf.*, **2**(2), e21.

Tan, C., Gajovic-Eichelmann, N., Stöcklein, W. F., Polzius, R., & Bier, F. F. (2010). Direct detection of Δ^9 -tetrahydrocannabinol in saliva using a novel homogeneous competitive immunoassay with fluorescence quenching. *Anal. Chim. Acta.*, **658**(2), 187-192.

Tatters, A. O., Flewelling, L. J., Fu, F., Granholm, A. A., & Hutchins, D. A. (2013). High CO₂ promotes the production of paralytic shellfish poisoning toxins by *Alexandrium catenella* from Southern California waters. *Harmful Algae*, **30**, 37-43.

Tabeling, P. (2010). Introduction to microfluidics. 1st Edition. Oxford University Press. Oxford.

Tachi, T., Kaji, N., Tokeshi, M., & Baba, Y. (2009). Simultaneous separation, metering, and dilution of plasma from human whole blood in a microfluidic system. *Anal. Chem.*, **81**(8), 3194-3198.

Tang, S. & Hewlett, I. (2010). Nanoparticle-based immunoassays for sensitive and early detection of HIV-1 capsid (p24) antigen. *J. Infect. Dis.*, **201**(Supplement 1), 59-64.

Tennico, Y. H., Koesdjojo, M. T., Kondo, S., Mandrell, D. T., & Remcho, V. T. (2010). Surface modification-assisted bonding of polymer-based microfluidic devices. *Sens. Actuator B-Chem.*, **143**(2), 799-804.

Tiller, T., Meffre, E., Yurasov, S., Tsuiji, M., Nussenzweig, M. C., & Wardemann, H. (2008). Efficient generation of monoclonal antibodies from single human B cells by single cell RT-PCR and expression vector cloning. *J. Immunol. Methods.*, **329**(1), 112-124.

Tomizaki, K. Y., Usui, K., & Mihara, H. (2010). Protein-protein interactions and selection: array-based techniques for screening disease-associated biomarkers in predictive/early diagnosis. *FEBS J.*, **277**(9), 1996-2005.

Tsougeni, K., Papageorgiou, D., Tserepi, A., & Gogolides, E. (2010). “Smart” polymeric microfluidics fabricated by plasma processing: controlled wetting, capillary filling and hydrophobic valving. *Lab. Chip.*, **10**(4), 462-469.

Turner, A. D., Dhanji-Rapkova, M., Algoet, M., Suarez-Isla, B. A., Cordova, M., Caceres, C., & Lees, D. N. (2012). Investigations into matrix components affecting the performance of the official bioassay reference method for quantitation of paralytic shellfish poisoning toxins in oysters. *Toxicon*, **59**(2), 215-230.

Turvey, S. E. & Broide, D. H. (2010). Innate immunity. *J. Allergy Clin. Immunol.*, **125**, 24–32.

Usleber, E., Dietrich, R., Bürk, C., Schneider, E., & Märklbauer, E. (2001). Immunoassay methods for paralytic shellfish poisoning toxins. *J. AOAC Int.*, **84**, 1649–1656.

Valeur, B. & Berberan-Santos, M. N. (2012). Molecular fluorescence: principles and applications. 2nd Edition. John Wiley & Sons, London.

Viswanathan, C. T., Bansal, S., Booth, B., DeStefano, A. J., Rose, M. J., Sailstad, J., & Weiner, R. (2007). Quantitative bioanalytical methods validation and implementation: best practices for chromatographic and ligand binding assays. *Pharmaceut. Res.*, **24**, 1962-1973.

Volcke, C., Gandhiraman, R. P., Gubala, V., Raj, J., Cummins, T., Fonder, G., Nooney, R.I., Mekhalif, Z., Herzog, G., Daniels, S., Arrigan, D.W.M., Cafolla, A.A., & Williams, D. E. (2010). Reactive amine surfaces for biosensor applications, prepared by plasma-enhanced chemical vapour modification of polyolefin materials. *Biosens. Bioelectron.*, **25**(8), 1875-1880.

Walczak, R. (2011). Fluorescence detection by miniaturized instrumentation based on

non-cooled CCD minicamera and dedicated for lab-on-a-chip applications. *Biochip. J.*, **5**(3), 271-279.

Wang, H., Li, G., Wu, Y., Yuan, F., & Chen, Y. (2014). Development of an indirect competitive immunoassay for walnut protein component in food. *Food chem*, **147**, 106-110.

Wang, Z., Luo, P., Cheng, L., Zhang, S., & Shen, J. (2011). Hapten–antibody recognition studies in competitive immunoassay of α -zearalanol analogs by computational chemistry and Pearson Correlation analysis. *J. Mol. Recognit.*, **24**(5), 815-823.

Wang, X. & Kaplan, D. L. (2011). Functionalization of silk fibroin with NeutrAvidin and biotin. *Macromol. Biosci.*, **11**(1), 100-110.

Weiner, L. (2006) Fully human therapeutic monoclonal antibodies. *J. Immunother.*, **29**, 1–9.

Werner, R. G. (1998). The value of contract manufacturing. *Pharmaceut. Tech. Eur.*, **10**, 60-71.

Werner, R. G. (2004). Economic aspects of commercial manufacture of biopharmaceuticals. *J. Biotechnol.*, **113**, 171–82.

Whitesides, G. M. (2006). The origins and the future of microfluidics. *Nature*, **442** (7101), 368-373.

Wild, D. (2001). The immunoassay handbook. 2nd Edition. Nature Publishing Group, New York, USA.

Xiaolin, W. (2009) Potential aggregation-prone regions in biotherapeutics. *MAbs.*, **1**, 254–267.

Yang, J. & Kwok, D. Y. (2004). Analytical treatment of electrokinetic microfluidics in hydrophobic microchannels. *Anal. Chim. Acta.*, **507**, 39–53.

Yalow, R. S. & Berson, S. A. (1959) Assay of plasma insulin in human subjects by immunological methods. *Nat.*, **21**,1648–1649.

Yager, P., Edwards, T., Fu, E., Helton, K., Nelson, K., Tam, M. R., & Weigl, B. H. (2006). Microfluidic diagnostic technologies for global public health. *Nature (Lond.)*. **442**, 412-418.

Yue, M., Stachowiak, J. C., Lin, H., Datar, R., Cote, R., & Majumdar, A. (2008). Label-free protein recognition two-dimensional array using nanomechanical sensors. *Nano. lett.*, **8**(2), 520-524.

Zhang, Z., Yu, L., Xu, L., Hu, X., Li, P., Zhang, Q., & Feng, X. (2014). Biotxin sensing in food and environment via microchip. *Electrophoresis*, **35**(11), 1547-1559.

Zhou, J., Ellis, A. V., & Voelcker, N. H. (2010). Recent developments in PDMS surface modification for microfluidic devices. *Electrophoresis*, **31**(1), 2-16.

Zimmermann, M., Delamarche, E., Wolf, M., & Hunziker, P. (2005). Modeling and optimization of high-sensitivity, low-volume microfluidic-based surface immunoassays. *Biomed. Microdevices.*, **7**(2), 99–110.

Zourob, M., Elwary, S., & Turner, A. P. (2008). Principles of Bacterial Detection: Biosensors, Recognition Receptors and Microsystems: Biosensors, Recognition Receptors, and Microsystems. 1st Edition. Springer, New York, USA.

United States Pat., US20100243914, 2010.

[1] <http://www.andor.com/scientific-cameras/ixon-emccd-camera-series/ixon3-885>

[2]http://www.tillphotonics.com/Support/files/Polychrome%20V_data%20sheet.pdf

CHAPTER 8

Appendix

Computer program for simulation of hIgG immunoassay in microchannel

```

clc;          % Clear Command Window Screen
clear all;    % Clear Matlab Memory
close all;    % Clear all figures

% Configuration for simulation
make_video = 0;          % 0: do not make video clip; 1: make video
clip.

% Advection-Diffusion Equation Variables -----
D      = 4*(10^-11);      % Diffusivity
C0      = 6*(10^-6);      % Bulk concentration
k_on    = 2.5*(10^3);      % Constant of hybridization.
k_off   = 5*10^-3;        % Constant of desorption.
gamma0  = 2*10^8;         % Initial concentration in available
hybridization sites.
v_mean  = 3.75*10^-4;      % Mean velocity (m/s)

% Temporal Variables -----
ts      = 0;              % Start Time (s)
t_off   = 3000;           % Time to turn off the flow (s) - 1 minute =
60s
tf      = 5000;           % Final Time (s)
tw      = 4000;           % Time to finish washing
dt      = 1;              % Time Step, Delta T (s)

% Spatial Variables -----
xs      = 0;              % Start x-location (m)
xf      = 10*10^-3;       % Final x-location (m)
ys      = 0;              % Start y-location (m)
yf      = 10*10^-6;       % Final y-location (m)

discretisationx = 400;    % No of points per mm
discretisationy = 40;     % No of points per mm
dy = (yf-ys)/discretisationy;% Delta x (m)
dx = (xf-xs)/discretisationx;% Delta y (m)
Nx = (xf-xs)/dx+1;        % Number of Nodes
Ny = (yf-ys)/dy+1;        % Number of Nodes
N   = Nx*Ny;
x   = [xs:dx:xf]';        % Store X values for each node of the
solution
y   = [ys:dy:yf]';        % Store Y values for each node of the
solution

C_matrix = sparse(Ny,Nx);  % The unknown matrix
C_array  = reshape(C_matrix,N,1); % Turn the matrix into array - to form
A*x = b

x_chip_s = 4*10^-3; x_chip_s_index = floor(x_chip_s/dx)+1; % start x-
location of the Biochip
x_chip_f = 5*10^-3; x_chip_f_index = floor(x_chip_f/dx)+1; % end x-
location of the Biochip
x_chip   = x_chip_s:dx:x_chip_f;
x_chip_index = x_chip_s_index:x_chip_f_index;

```

```

v = 3/2*v_mean*(1-(2*(y-(yf-ys)/2)/(yf-ys)).^2);

%*****
%                               BUILD SYSTEM OF LINEAR EQUATIONS
%*****

% Build LHS and RHS Coefficients -----
L1 = -D/2/dx^2;
L2 = -D/2/dy^2;
L3 = D/dx^2 + D/dy^2 + 1/dt;
R1 = -L1;
R2 = -L2;
R3 = -D/dx^2 - D/dy^2 + 1/dt;

% Build "A" Matrix -----
A = sparse(N,N);           % Define a sparse nxn Matrix "A"
B = sparse(N,N);           % Define a sparse nxn Matrix "B"
c = zeros(N,1);
d = zeros(N,1);
gamma = zeros(Nx,1);       % Define Gamma on the BIOCHIP

for ct1 = 1:Ny              % Set Boundary Conditon for the "inlet" -
surface 1
    A(ct1,ct1) = 1;
    d(ct1) = C0;
end

for ct1 = N-Ny+1:N         % Set Boundary Conditon for the "outlet" -
surface 3
    A(ct1,ct1) = 1;
    A(ct1,ct1-1) = -1;
end

for ct1 = Ny+1:N-Ny        % Loop through Inner Matrix & set values
    y_index = mod(ct1,Ny);
    x_index = floor(ct1/Ny);

    if y_index == 1        % Set Boundary Conditon for the lower surface
(surface 2)
        A(ct1,ct1) = 1;
        A(ct1,ct1+1)=-1;
    elseif y_index == 0    % Set Boundary Conditon for the upper surface
(surface 4)
        A(ct1,ct1) = 1;
        A(ct1,ct1-1)=-1;
    else
        v_inst = v(y_index);
        A(ct1,ct1-1) = L2;
        A(ct1,ct1) = L3 + v_inst/dx;
        A(ct1,ct1+1) = L2;
        A(ct1,ct1-Ny)= L1 - v_inst/dx;
        A(ct1,ct1+Ny)= L1;

        B(ct1,ct1-1) = R2;
        B(ct1,ct1) = R3;
        B(ct1,ct1+1) = R2;
        B(ct1,ct1-Ny)= R1;
        B(ct1,ct1+Ny)= R1;
    end
end

```

```

end
end

%*****
%
%                               RUN SIMULATION
%*****
t_index = 0; figure;
t_array = [];
for t = ts+dt:dt:tf          % Loop through time (dt increment)
    t_array = [t_array; t];
    if mod(t_index,1000) == 0
        fprintf('Simulation is running at t = %d\n',t_index);
    end

    if t > t_off              % Turn off the flow
        v = zeros(Ny,1);

        % Change the boundary condition for the "inlet" surface
        for ct1 = 1:Ny
            A(ct1,ct1) = 1;
            A(ct1,ct1+1) = -1;
            d(ct1) = 0;
        end
    end

    if t > tw
        v = 3/2*v_mean*(1-(2*(y-(yf-ys)/2)/(yf-ys)).^2);

        for ct1 = 1:Ny          % Set Boundary Condition for the
            "inlet" - surface 1
                A(ct1,ct1) = 1;
                A(ct1,ct1+1) = 0;
                d(ct1) = 0;
            end
        end

        % Update value of gamma
        t_index = t_index + 1;
        C_mat = reshape(c,Ny,Nx);
        for ct1 = 1:Nx
            if (ct1 >= x_chip_s_index) && (ct1 <= x_chip_f_index)
                gamma(ct1) = (k_on*C_mat(1,ct1)*(gamma0-gamma(ct1)) -
                k_off*gamma(ct1))*dt + gamma(ct1);
                gamma(ct1) = (gamma(ct1) + k_on*C_mat(1,ct1)*gamma0*dt)/(1 +
                (k_on*C_mat(1,ct1)+k_off)*dt);
                if ct1 == x_chip_s_index
                    gamma_store(t_index) = mean(gamma(ct1:ct1+x_chip_f_index-
                    x_chip_s_index));
                end
            end
        end

        for ct1 = Ny+1:N-Ny      % Loop through Inner Matrix & set values
            y_index = mod(ct1,Ny);
            x_index = floor(ct1/Ny);

            % Set Boundary Condition for the surface containing the BIOCHIP
            if y_index == 1 && (x_index >= x_chip_s_index) && (x_index <=

```

```

x_chip_f_index)
    A(ct1,ct1)    = -D/2/dy - k_on*(gamma0 - gamma(x_index));
    A(ct1,ct1+1) =  D/2/dy;
    B(ct1,ct1)    =  D/2/dy;
    B(ct1,ct1+1) = -D/2/dy;
    d(ct1)        = -k_off*gamma(x_index);
end
end

C_mat = reshape(c,Ny,Nx);
CNEW = A\ (B*c+d);      % Solve for Cj+1
c = CNEW;                % Store Cj+1 as Cj for next time step

% Plot Solution
C_mat = flipud(C_mat);
imagesc(x,y,C_mat);
colorbar;
title(strrep(strcat('Simulation is running at t
=: ',num2str(t_index*dt,'%10.1f'),'s'),' ',' '));
if make_video == 1 && mod(t_index*dt,1) == 0
    frame(t_index) = getframe;      % Generate a movie clip
end
end

figure;
plot(t_array,gamma_store/gamma0);    % Plot the Kinetic Curves
xlabel('Time (s)');                  % Set x label of the figure
ylabel('Gamma/Gamma0');              % Set y label of the figure
title('Kinetics Curve');             % Set title of the figure

if make_video == 1
    movie(frame);                    % Play video clip
    movie2avi(frame,'demo');         % Save the video clip
%
%     writerObj = VideoWriter('Demo.mp4','MPEG-4');
%     open(writerObj);
%     f = im2frame(frame);
%     writeVideo(writerObj,f);
end

```